UNIVERSITÀ
DEGLI STUDI
FIRENZE

DOTTORATO DI RICERCA IN
SCIENZE CHIMICHE

CICLO XXIX

COORDINATORE Prof. PIERO BAGLIONI

Molecular aspects of iron-sulfur protein maturation

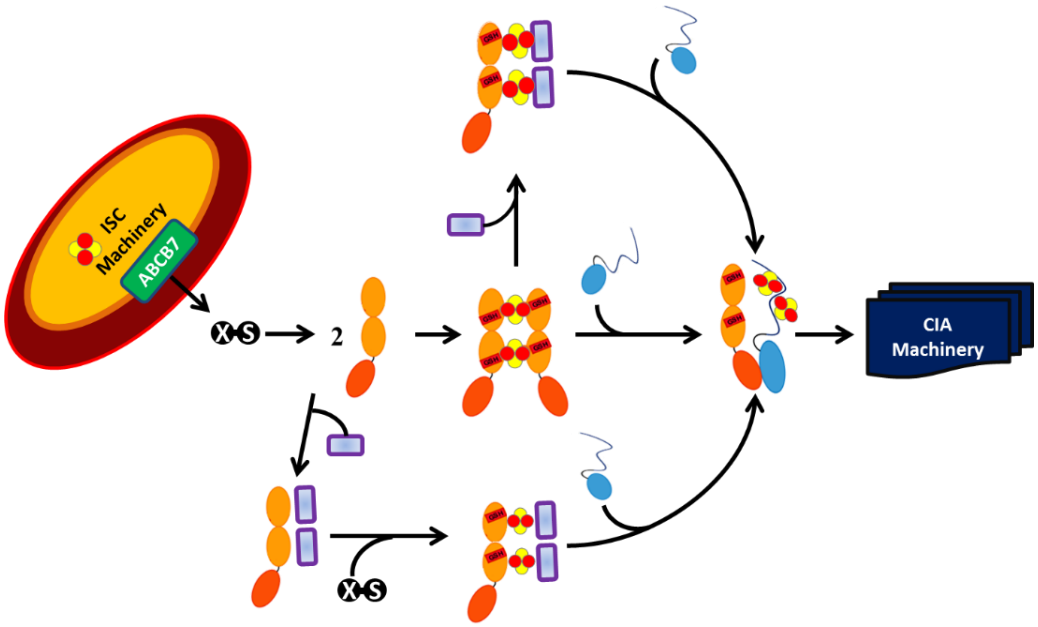

Dottorando
Dott. Riccardo Muzzioli

Tutore
Prof. Simone Ciofi Baffoni

UNIVERSITÀ
DEGLI STUDI
FIRENZE

DOTTORATO DI RICERCA IN
SCIENZE CHIMICHE

CICLO XXIX

COORDINATORE Prof. PIERO BAGLIONI

Molecular aspects of iron-sulfur protein maturation

Settore Scientifico Disciplinare CHIM/03

Dottorando
Dott. Riccardo Muzzioli

_____
(firma)

Tutore
Prof. Simone Ciofi Baffoni

_____
(firma)

Coordinatore
Prof. Piero Baglioni

_____
(firma)

Anni 2013/2016

Index

-Chapter 1-

INTRODUCTION

1.1. The role of iron in biological systems

Of the more than 100 chemical elements known to scientists today, only a relatively small number of these elements are found in the human body. In fact, only 24 different elements are thought to be essential for humans. The largest elemental components of the body, by mass, are oxygen (65%), carbon (18%), hydrogen (10%), and nitrogen (3%).[1] The other elements in the body, such as calcium, phosphorus, iron, copper, and others, are known to physiologists as trace elements. Some of this trace elements, which are vital to the body's proper functioning, must be present in the proper amounts, and their cellular concentrations must be continuously controls to prevent adverse/toxic reactions.

Metals are involved in a wide range of biochemical processes in all living organisms. They are “key” players in different function like:

- Structural : Zn
- Lewis catalysis: Zn, Fe, Ni, Mn
- Electron transfer: Fe, Cu, Mo
- Group transfer (like: CH_3, O, S): V, Fe, Co, Ni, Cu, Mo, W
- Redox processes: Fe, Cu, Ni, Co, W, V, Mn

The use of metals in living organisms is, indeed, important mainly due to their redox properties and to the feasibility of metal ion transfer in different locations or compartments of the cell. Metalloprotein is a generic term for a protein that contains a metal ion cofactor. Indeed, about one quarter to one third of all proteins require metals to carry out their functions.[2,3,4] The metal ion is usually coordinated by nitrogen, oxygen or sulfur atoms and could by directly coordinated to amino acids in the polypeptide chain or are present

inside a macrocyclic ligand incorporated into the protein. The presence of the metal ion inside a protein molecule, change the chemical proprieties of the molecules itself, providing functions that cannot easily be performed by only amino acids present in the chain. Metalloproteins can bind one or, if is necessary, more metals ion to maintain the function and the structure of the protein. Also in the word of DNA maintenance/repairs and RNA stabilization, metalloproteins are very important for function and structure of the genetic material. [5,6]

One of the most abundant essential trace elements in the human body is iron. Healthy adults possess from 4 to 6 g of iron, which approximately comprises only 0,008% of the body mass (75 kg).[7,8] Nevertheless it is necessary for our survival. In the human body, we have a lot of proteins that bind iron in a different way and we find these metalloproteins with different function. The major class of iron-proteins have an electron transfer function, but we can find iron-proteins also in transport, catalytic and DNA interaction/maintenance function. The bulk of iron is bound to hemoglobin in the red blood corpuscles, which is necessary for oxygen transport in the blood. In humans, the hemoglobin molecule is an assembly of four globular protein subunits. Each subunit is composed of a protein chain tightly associated with a non-protein protoporfiniricIX group. This cofactor contain iron as the central atom of the heme group, a metal complex that binds molecular oxygen (O_2) in the lungs and carries it to all the other cells in the body that need oxygen to perform their activities (e.g., muscle cells). In addition to hemoglobin**,** other important proteins in the body that contain heme groups (and therefore contain iron) include myoglobin**,** which takes oxygen from hemoglobin and allows the oxygen to diffuse throughout the muscle cells, and the cytochromes**,** that are crucial in the electron transfer reaction.[7,9] An important class of electron-transfer proteins utilizes iron–sulfur clusters (Fe-S) as redox centers (**Fig. 1**).

These proteins are characterized by the presence of iron-sulfur (Fe-S) clusters containing sulfide-linked di-, tri-, and tetra-iron centers in variable oxidation states. Fe-S clusters are found in a variety of metalloproteins, such as the ferredoxins, as well as NADH dehydrogenase, hydrogenases, Coenzyme Q - cytochrome c reductase, Succinate - coenzyme Q reductase and nitrogenase. (Fe-S) clusters are best known for their role in the oxidation-reduction reactions of mitochondrial electron transport. Both Complex I and Complex II of oxidative phosphorylation have multiple (Fe-S) clusters. They have many other functions including catalysis as illustrated by aconitase, generation of radicals as illustrated by SAM-dependent enzymes, and as sulfur donors in the biosynthesis of lipoic acid and biotin. Additionally some (Fe-S) proteins regulate gene expression.

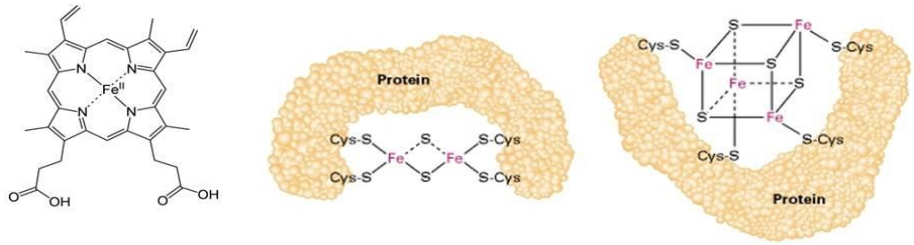

Figure 1. Examples of protein cofactors containing iron. From left to right; HEME group, [2Fe2S] cluster, [4Fe4S] cluster

Other proteins, such as those needed for DNA repair or DNA replication and cell division, also require on iron. Furthermore, iron is used to help to produce the connective tissues in our body, some of the neurotransmitters in our brain, and to maintain the immune system. Iron (Z=26) is one of the

major element on earth and present two different oxidation state with different spectroscopical characteristics:

- Ferric (Fe^{3+}): d^5 with electronic state ^6S, electronic configuration t_{2g}^3 e_g^2, fundamental state in octhaedrical geometry ^6A and is a paramagnetic ion
- Ferrous (Fe^{2+}): d^6 with electronic state ^5D, electronic configuration t_{2g}^4 e_g^2, fundamental state in octhaedrical geometry ^5T_g and is a paramagnetic ion

Iron have generally a coordination number of 4 with tetrahedric geometry, 5 (heme group without O_2) or 6 with octhaedrical geometry. Iron is an essential element for metabolic processes intrinsic to life, and yet the properties that make iron a necessity also make it potentially deleterious. The biological importance of iron is largely attributable to its chemical properties as a transition metal. It readily engages in one-electron oxidation-reduction reactions between its ferric (Fe^{3+}) and ferrous (Fe^{2+}) states and have a redox potential between -300mV and +700mM. However, the same chemical property explains why an excess of "free," reactive iron is toxic. In the cytoplasm, a significant fraction of iron(III) is reduced to iron(II) by a molecule of hydrogen peroxide, forming a hydroperoxyl radical and a proton. Iron(II) is oxidized by hydrogen peroxide to iron(III), forming a hydroxyl radical and a hydroxide ion in the process. The net effect is a disproportionation of hydrogen peroxide to create two different oxygen-radical species, with water as a byproduct.

$$Fe^{2+} + H_2O_2 \rightarrow Fe^{3+} + OH\cdot + OH^-$$

$$Fe^{3+} + H_2O_2 \rightarrow Fe^{2+} + OOH\cdot + H^+$$

The ability to change the oxidation state changing of iron Fe^{3+} in Fe^{2+} allows the iron to be part of the "Fenton-type" redox chemistry; the highly reactive hydroxyl radical (OH•) and the hydroperoxyl radical (OOH·) can damage lipid membranes, proteins, and nucleic acids inside the cell. To avoid this kind of reaction, iron homeostasis is strictly controlled in all the phase from iron transport, to storage and regulatory proteins. That allows the cells to use the benefits of iron, but also limits its ability to do harm.[10,11]

1.2. Iron metabolism and its cellular uptake

The common oxidation state for the iron is the Fe^{3+}; iron uptake is tightly regulated by the human body, which has no pathway of iron excretion. Only small amounts of iron are lost daily due to mucosal and skin epithelial cell sloughing, desquamation of skin and urinary cells, blood loss, or sweat. To compensate this loss only about 1-2 mg of dietary iron per day is absorbed by duodenal enterocytes. This amount of iron compared to the amount ingested is typically low. The efficiency with which iron is absorbed varies largely depending on the source. Generally the best absorbed forms of iron come from animal products,[8,12] we can also absorbed the vegetable iron but in a less amount. Like most mineral nutrients, the majority of the iron absorbed from digested food or supplements is absorbed in the duodenum by enterocytes of the duodenal lining. These cells have special molecules that allow them to move iron into the body. To be absorbed, dietary iron can be absorbed as part of a protein such as heme protein or iron must be in its ferrous Fe^{2+} form. Iron absorption from diet is enhanced in the presence of vitamin C and diminished by excess calcium, zinc, or manganese. A ferric reductase enzyme, reduces ferric Fe^{3+} to Fe^{2+}. A protein called divalent metal transporter 1 (DMT1), which can transport several divalent metals across the

plasma membrane, then transports iron across the enterocyte's cell membrane into the cell. Iron is released directly into the blood stream by ferroportin which is located at the basolateral membrane of duodenal enterocytes. It is oxidized to the Fe^{3+} form and binds to transferrin (Tf). Tf-$2Fe^{3+}$ complexes circulate in the plasma, and deliver iron to all the tissues (**Fig. 2**). Most of the iron is incorporated into hemoglobin, in erythroid precursors and mature red blood cells (approx. 1800 mg). Approximately 400 mg is present in the other tissues (in enzymes and cytochromes) and muscle fibers (in myoglobin). Liver (parenchymal cells) and reticuloendothelial macrophages are responsible for iron storage (approx. 1600 mg). The macrophages provide most of the usable iron by degrading hemoglobin in aged or damaged erythrocytes and reloading ferric iron into transferrin for delivery to cells, because the amount of plasma iron is just around 10% (approx. 3mg) of the amount used daily, which means that plasma iron is turned over many times each day (**Fig. 2**).

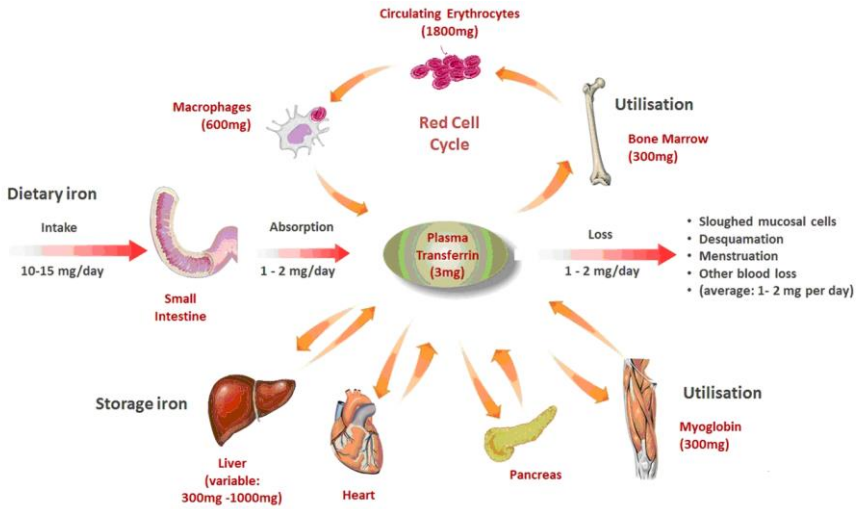

Figure 2. Circulation of iron in human body.

Most cell types take up iron primarily through receptor-mediated endocytosis via transferrin receptor 1 (TFR1), transferrin receptor 2 (TFR2). Transferrin-bound ferric iron is recognized by these transferrin receptors, triggering a conformational change that causes endocytosis. A proton pump decreases the pH within the endosomes, leading to conformational changes in the transferin that result in the release of iron into the cytoplasm from the endosome via the divalent metal transporter 1 (DMT1) after being reduced to its ferrous state by a STEAP family reductase. In the cytoplasm, ferrous iron is found in a soluble, chelatable state which constitutes the labile iron pool (~0.001 mM). In this pool, iron is thought to be bound to low-mass compounds such as peptides, carboxylates and phosphates, although some might be in a free, hydrated form (aqua ions). Alternatively, iron ions might be conservated in a non-toxic form the ferritin. Iron from this pool can be taken up by mitochondria via mitoferrin to synthesize (Fe-S) clusters and heme groups (**Fig. 3**). Meanwhile, transferrin (Apo-Tf) and transferrin receptor are recycled to the cell surface, where each can be used for further cycles of iron binding and iron uptake.[5,10,13]

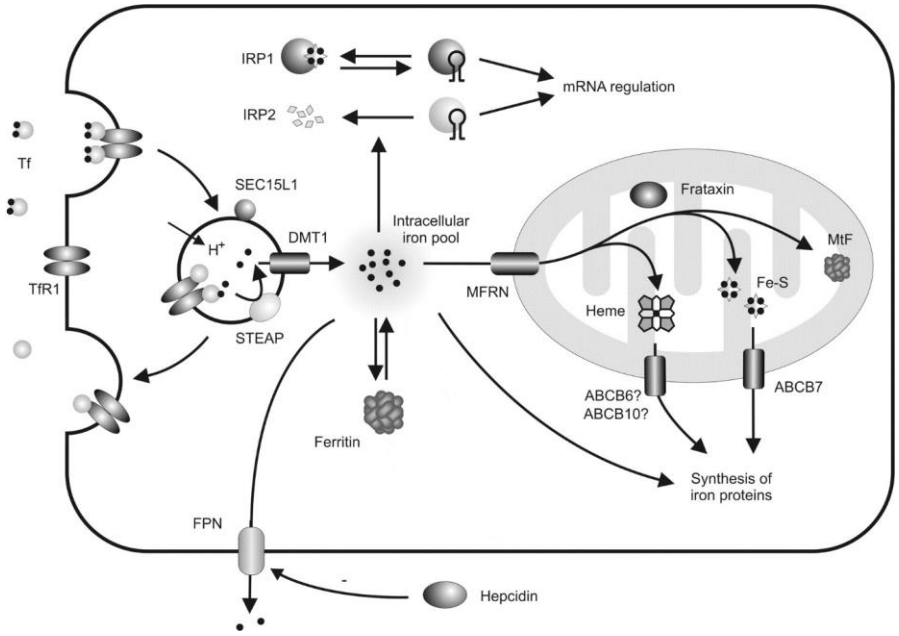

Figure 3. Transferrin bound to two iron atoms (Tf-[Fe(III)$_2$) binds to TfR1 on the cell surface where the Tf-[Fe(III)$_2$–TfR1 complex is endocytosed. Acidification of the endosome causes the release of Fe(III) from Tf where it is reduced to Fe(II) by the STEAP3 oxidoreductase before export by DMT1 (divalent metal transporter 1). ApoTf/TfR1 complex is returned to the cell surface where it dissociates and initiates another round of iron uptake.

Disruptions in iron homeostasis from both iron deficiency and overload account for some of the most common human diseases (e.g. hemoglobin and iron deficiency anemia or hemochromatosis). That is why cells developed mechanisms for sensing their own need of iron. Iron metabolism is maintained by two regulatory systems:

- the first one functions systemically and relies on the hormone hepcidin that directly inhibits ferroportin. By inhibiting ferroportin, hepcidin prevents enterocytes of the intestine and macrophages of the

reticuloendothelial system from secreting iron into the blood stream, thereby functionally reducing the iron level.

- the second one predominantly controls the cellular iron metabolism through iron-regulatory proteins (IRP1 and IRP2). When the iron level in the cell is low IRPs bind to iron-responsive elements in regulated messenger RNAs of the transferrin receptors and ferritin. The binding of IRPs to iron responsive elements (IREs) in the 5'-untranslated regions (UTRs) of mRNA blocks the translation (e.g. of ferritin), while IRP binding to the IRE in the 3'-UTR stabilizes the mRNA (e.g. of transferrin receptor). When the iron concentration in the cell is high IRP1 binds an [4Fe-4S] cluster (and acts like aconitase) and IRP2 degrades with the result that they can no longer bind to mRNA. This liberates the IRE in the 5'-untranslated region of Ferritin mRNA and directs the cell to produce more storage molecules. On the other hand the free IRE at the 3'-UTR of transferrin receptors accelerates its mRNA degradation resulting in decreased protein expression.[14,15]

1.3. The role of iron in mitochondrial processes

Mitochondria are well known for their fundamental role in the cellular metabolism. The mitochondrion (**Fig. 4**) is an eukaryotic cellular organelle that contains outer and inner membranes composed of phospholipid bilayers and proteins.[20,17]

Because of this double-membraned organization, there are five distinct compartments:

- the outer mitochondrial membrane,
- the intermembrane space (IMS): space between the outer and inner membranes
- the inner mitochondrial membrane
- the cristae space (formed by infoldings of the inner membrane),
- and the matrix (space within the inner membrane). Main place for iron utilization.

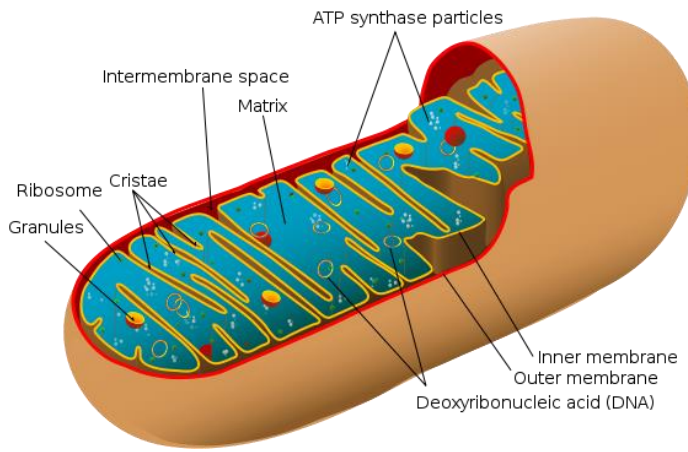

Figure 4. Schematic representation of the mitochondrion structure.

The main function of this organella is synthesis of ATP, the energetic molecule of our cells. The overall process of oxidizing glucose to carbon dioxide is known as cellular respiration. ATP can be produced via:

- glycolysis, citric acid cycle (TCA or Krebs cycles) and oxidative phosphorylation, both components of cellular respiration.
- beta-oxidation of fatty acids

All this kind of reaction takes place in the mitochondria, in the matrix and on the internal membrane. During all the reaction in these pathway, we can have the direct formation of ATP or the production of high energetic molecules (in a reduced form) that can be uses for the synthesis of ATP after ri-oxidation in the respiratory chain. This is the last part of the cellular respiration and is formed by a large number of electron transport protein in order to convert the electron flow in ATP. Iron is directly involved in the ATP synthesis, because several protein present cytochromes or iron sulfur cluster (Fe-S) as cofactor to catalyze the electron transport. So the mitochondria require iron and this transport inside the mitochondria is a crucial step; once iron is transported into the mitochondrion it can then be used for heme synthesis, ISC synthesis, or stored in mitochondrial ferritin (Ftmt). It is essential that mitochondrial iron is maintained in a safe form to prevent oxidative damage, as mitochondria are a major source of cytotoxic ROS. This kind of import require iron in a reduced (ferrous) form and a membrane potential. Import is facilitated by two mitochondrial transporter proteins Mitoferrin1/2, but further iron transporters may be identified. [16,17,18,19,89]

1.4. The role and types of (Fe-S) cluster

(Fe-S) clusters are ubiquitous protein cofactors highly conserved from bacteria to human. Practically, they play a crucial and essential role in every living cell. Initially, the biophysical properties of (Fe-S) cluster proteins were used by the earliest forms of life to perform fundamental metabolic processes (amino acid metabolism), when the earth's atmosphere was a reducing and anaerobic environment (billion years ago).

Reducing environment:

$K_{ps}(Fe(OH)_2) = 4.9 \times 10^{-17}$ $[Fe(II)] = 5.0 \times 10^{-3}$

To maintain these cofactors after transformation of the atmosphere into an oxidative and aerobic one (which does not support the formation, neither the stability of (Fe-S) the organism evolved a whole set of proteins to coordinate and solubilize the Fe(III) in a safe, efficient and specific biogenesis system for these fundamental cofactors.

Oxidative environment: $Fe(II) \longrightarrow Fe(III)$

$K_{ps}(Fe(OH)_3) = 2.6 \times 10^{-39}$ $[Fe(III)] = 2.6 \times 10^{-18}$

Another reason why biosynthesis of ISCs has to be strictly controlled is their potential toxicity. Improper biogenesis and maintaining of the iron and the clusters may fuel the Fenton chemistry, which produces highly toxic reactive oxygen species (ROS).[19,21,22] The (Fe-S) clusters contain iron in oxidation state Fe^{2+} or Fe^{3+} and sulfide ion S^{2-}, and the most common (Fe-S) cluster types are[2]:

1. $[(RS)_4 2Fe\text{-}2S]^{2-/3-}$: is the first and simple cluster, it's call also diamond (**Fig. 5 A**). This cluster has a potential of E°'= -150/-450mV with a coordinative motif like Cys-X-X-Cys-X_n-Cys-X-Cys. We can also find one or two histidine substituting one or two cys ligands $[(Cys)_2(His)_2 2Fe\text{-}2S]^{0/-}$, and with this change of ligand we have a more positive potential of E°'= -100/400mV (**Fig. 5 B**).

2. $[(RS)_4 4Fe\text{-}4S]^{-/2-//2-/3-}$: cluster with the four irons linked with four sulfide ions (**Fig.5 B**). The common name of this cluster is cubane and present a potential of E°'= 100/400mV. A different form of this cluster is the $[(RS)_3 3Fe\text{-}4S]^{2-/3-}$ in this modification an iron atom is lost from the cubane (**Fig. 5 C**).

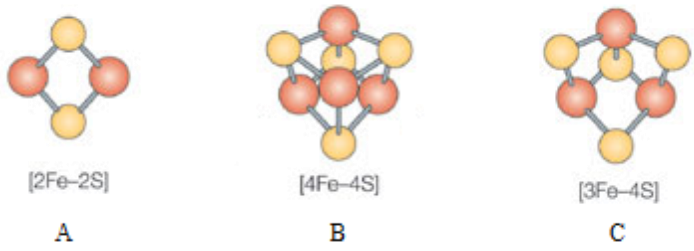

Figure 5. type of iron sulfur clusters

Fe-S are indispensable for life because of the ability of the iron to accept or donate electrons, formally altering between the ferrous (Fe^{2+}) and ferric (Fe^{3+}) oxidation states. The ability of the iron to change the oxidation state, plus the present of the sulfide ions and the effect of the external ligands, has allowed to expand the range of reduction potentials (–700 mV to 400 mV) and are among the most important electron carriers in nature.[23] Much is known about the electronic structure of iron–sulfur clusters in their various oxidation states. For example, in [2Fe-2S] systems, addition of one electron to the diferric cluster results in the localized reduction of one of the two iron ions, the other one remaining ferric. On the other hand, reduction of the all-ferric $[3Fe\text{-}4S]^{+}$ cluster results in the extra electron being delocalized onto a pair of iron ions having a 2.5+oxidation state (the so-called mixed-valence

pair), while the third iron ion remains ferric. Similarly, $[4Fe\text{-}4S]^{3+}$ clusters consist of a mixed-valence pair and a ferric pair, $[4Fe\text{-}4S]^{2+}$ clusters contain all mixed-valence irons, and $[4Fe\text{-}4S]^{+}$ clusters have a mixed valence and a ferrous pair. This variation in the distribution of oxidation number is the result of specific ferro- and antiferromagnetic coupling between the Fe ions. When the Fe ions are all oxidized, only antiferromagnetic coupling occurs. By considering a pair of Fe(III) ions, the five unpaired electrons with an $S = {}^{5}/_{2}$ ground state on each ion sense those on the neighbor Fe through the sulfur bridges in such a way as to provide a total ground state with S'= 0 (i.e., with all the electrons paired). In the case of different oxidation states, the five electrons of Fe(III) with a total spin $S = {}^{5}/_{2}$ and the six electrons of Fe(II) with a total spin $S = 2$ provide a total ground state $S' = {}^{5}/_{2} - 2 = {}^{1}/_{2}$ in the case of antiferromagnetic coupling. However, if the Fe(III)–Fe(II) pair interacts strongly, the electron can be considered fully delocalized between the two metal centers and the oxidation state for each Fe is 2.5+. In this case, the ground state has nine unpaired electrons. The result is the same as that obtained when there is ferromagnetic coupling and the two S values of ${}^{5}/_{2}$ and 2 sum to $S' = {}^{9}/_{2}$. In this case, we say that a mixed-valence pair occurs. In polymetallic systems, a mixed-valence pair with $S = {}^{9}/_{2}$ may couple in an antiferromagnetic fashion with either a single Fe ion or another pair of Fe ions[1,2,3]. In the resulting cluster, the spin takes the smallest possible value. The situation for iron–sulfur clusters is summarized in **Fig. 6** and the resulting global and local spin states are summarized in **Table 1**.

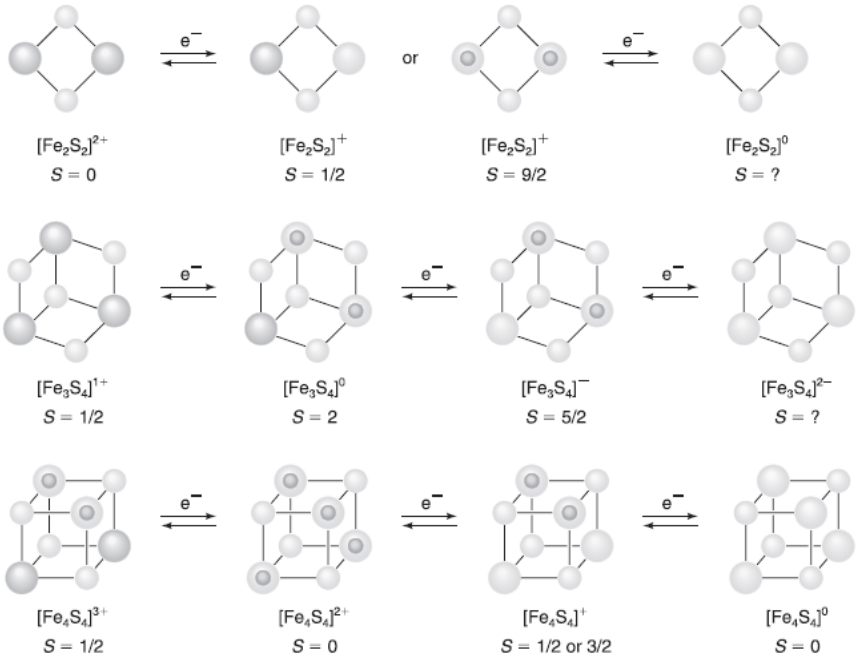

Figure 6. Total spin of the cluster and individual redox states of the iron ions in various iron–sulfur clusters as a function of the cluster oxidation state. Filled circles indicate Fe(III) ions, empty circles Fe(II) ions, and partially filled circles iron ions with a 2.5+ oxidation state.

Cluster	Individual Spin	Subspins[a]	Total *S*
$[Fe_2S_2]^{2+}$	5/2, 5/2	5/2, 5/2	0
$[Fe_2S_2]^{+}$	2, 5/2	2, 5/2	1/2
$[Fe_3S_4]^{0}$	2, 5/2, 5/2	9/2*, 5/2	2
$[Fe_3S_4]^{+}$	5/2, 5/2, 5/2	2, 5/2 (3, 5/2)	1/2
$[Fe_4S_4]^{0}$	2, 2, 2, 2	0, 0 (?)	0
$[Fe_4S_4]^{+}$	2, 2, 2, 5/2	9/2*, 4 (?)	1/2
$[Fe_4S_4]^{2+}$	2, 2, 5/2, 5/2	9/2*, 9/2* (?)	0
$[Fe_4S_4]^{3+}$	2, 5/2, 5/2, 5/2	9/2*, 4 (7/2*, 3) (9/2*, 4 + 7/2*, 4)	1/2

[a] Subspin related to mixed-valence pairs within the polymetallic center are marked with an asterisks. Alternate ground states are reported in parentheses.

Table 1. Spin Distribution within Iron–Sulfur Clusters

The spectra of iron–sulfur proteins in the visible and near-ultraviolet (UV) range show a broad absorption envelope resulting from several overlapping absorption bands deriving from transitions with predominant S → Fe(III) charge-transfer character, where S can be either the Cys or the inorganic sulfur. Circular dichroism (CD) and magnetic circular dichroism (MCD) spectra partially resolve this complex envelope thanks to the different selection rules and the appearance of both positive and negative bands. (Fe-S) clusters contain high-spin Fe(III) and Fe(II): while the former has no spin-allowed d–d transition high-spin Fe(II) has spin-allowed transitions of the type $d_z^2 \rightarrow d_{xz}$ and $d_z^2 \rightarrow d_{yx}$ ($e \rightarrow t_2$ in a tetrahedral environment). Bands attributable to these d–d transitions have been detected in CD spectra.

The (Fe-S) clusters proteins play a central role in different processes like:

Function	Type of Cluster	Protein
Electron transfer	[2Fe-2S] [3Fe-4S] [4Fe-4S]	Ferredoxins High-potential iron–sulfur
Catalysis of a nonredox reaction	[4Fe-4S]	Aconitase
Catalysis of redox reactions	[4Fe-4S]	Sulfite reductase
Stabilization of protein structure for DNA repair	[4Fe-4S]	Endonuclease III, MutY
Sensing and regulation: (i) Oxygen sensors: loss of original cluster and of Activity	[4Fe-4S] [4Fe-4S]/[2Fe-2S] [4Fe-4S]/[3Fe-3S]	Aconitase
(ii) Sensor of O2 and NO: redox-regulated control of transcription	[2Fe-2S]	SoxR protein
(iii) Iron sensor: posttranscriptional regulation	[4Fe-4S]	Iron regulatory protein aconitase
Redox-mediated generation of free radicals	[4Fe-4S]	Biotin synthase

1.5. Biogenesis of (Fe-S) clusters

The biosynthesis of the (Fe-S) clusters has been well studied in the last years.[27,28,29,90] The most extensive studies were focused on bacteria (*Escherichia coli* and *Azetobacter vinelandii*) and yeast *Saccharomyces cerevisiae*. Three different systems were identified for the biogenesis of bacterial (Fe-S) proteins: the NIF system, for specific maturation of nitrogenase in azototrophic bacteria; the ISC assembly and SUF systems, for the generation of housekeeping (Fe-S) proteins under normal and oxidative-stress conditions, respectively. The yeast *S. cerevisiae* has served as an excellent model organism to establish the first details of the complex biosynthesis pathways in eukaryotes. Recent investigations in human cell culture and other model systems have demonstrated that the entire process is highly conserved from yeast to human. The synthesis of (Fe-S) clusters and their insertion into apo proteins requires almost 30 proteins in the mitochondria and cytosol of eukaryotic cells. Three distinct protein machineries are required in the (non-plant) eukaryotic cells for the biogenesis of the (Fe-S) clusters; the ISC assembly machinery in mitochondria (inherited from bacteria during evolution), the ISC export machinery located in the mitochondrial inter membrane space, and the cytosolic ISC assembly machinery (CIA) (**Fig. 7**). ISC export and CIA machineries are specifically involved in the maturation of cytosolic and nuclear ISC proteins, whereas the mitochondrial ISC assembly machinery is required for the generation of all cellular (Fe-S) proteins.[30,31,32,91,92]

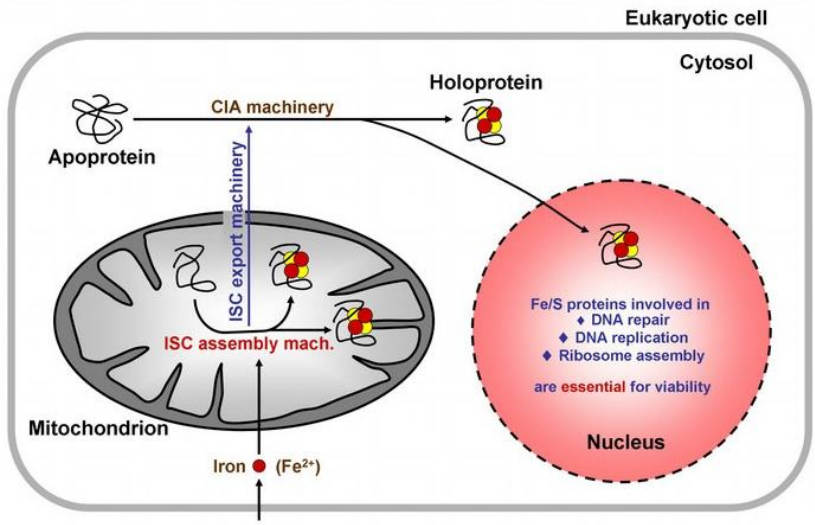

Figure 7. Schematic representation of (Fe-S) cluster assembly in eukaryotic cell

1.5.1. Mitochondrial (Fe-S) cluster assembly machinery

Mitochondria perform crucial roles in many biochemical processes. They generate ATP by oxidative phosphorylation and participate in numerous metabolic pathways such as citric acid cycle, fatty acid degradation, urea cycle, and the biosynthesis of lipids and amino acids. Moreover, the organelles are involved in the bio-synthesis of various protein cofactors such as heme, biotin, lipoic acid, and, last but not least, iron–sulfur (Fe-S) clusters. The mitochondrial (Fe-S) cluster (ISC) assembly machinery consists of 17 proteins that operate in three major steps of the maturation process:

1. Core ISC assembly: Nfs1–Isd11 as the sulfur donor cooperates with ferredoxin–ferredoxin reductase acting as an electron transfer chain, and frataxin to synthesize an [2Fe–2S] cluster on the scaffold protein Isu1.

2. ISC factors involved in cluster transfer: in this part, the cluster is released from Isu1 and transferred toward apoproteins with the help of a dedicated Hsp70 chaperone system and the glutaredoxin Grx5.
3. Late actins ISC targeting factor: Various specialized ISC components assist in the generation of [4Fe–4S] clusters and cluster insertion into specific target apoproteins.

Each of these steps involves the participation of several proteins and cofactors, which execute specific biosynthetic partial reactions.[33,90,93] The mitochondrial components required for (Fe-S) cluster formation in higher organisms are similar to the bacterial ISC proteins and apparently were inherited from a prokaryotic progenitor.[34] The central component of the mitochondrial ISC assembly machinery (ISC *core*) is the scaffold protein Isu1 (human ISCU) on which *de novo* assembly of a [2Fe-2S] cluster takes place. Isu1 is one of the most conserved proteins in evolution and is found in many bacteria, and virtually in all eukaryotes. It has three cysteine residues which are necessary for the cluster synthesis.[35,36,37] To accomplish *de novo* cluster formation, sources of iron and sulfur are necessary. Iron is imported from the cytosol into mitochondria through the innermembrane transporters Mitoferrin1/2 (Mrfn1/2) in its ferrous (Fe^{2+}) form, and is delivered to the scaffold by Frataxin which was shown to interact with Isu1 *in vivo* and *in vitro* in an iron stimulated fashion.[38, 39, 40] The free cysteine is the source of the sulfur; which is released and delivered to Isu1 by the complex of cysteine desulfurase Nfs-Isd11 (human NFS1 and ISD11). As an intermediate, a persulfide is formed on a conserved cysteine residue of the enzyme, and is then transferred to the scaffold protein. Although isolated Isu1 has the enzymatic activity (as a cysteine desulfurase) *in vitro,* the Nfs1–Isd11 complex is the functional entity for sulfur transfer from Nfs1 to Isu1 *in vivo*.[41,42,] This reaction is aided by direct interaction between Nfs1 and Isu1.

Before the assembly reaction on Isu1 is accomplished the sulfur is reduced by the electron transfer chain composed of ferredoxin and ferredoxin reductase which receives the electron from NADH (**Fig. 8**).

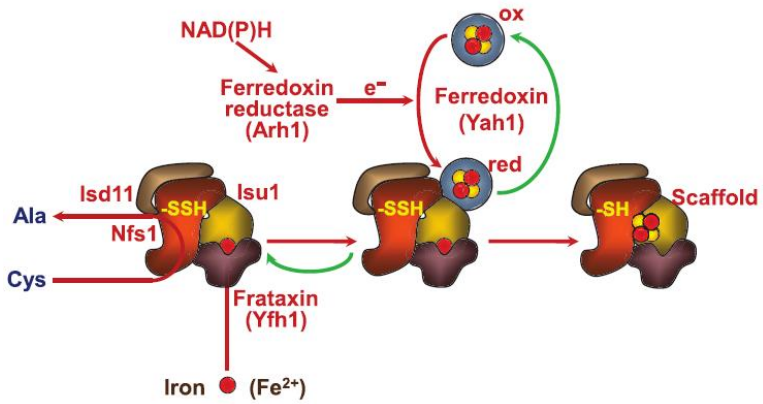

Figure 8. First step of ISC biosynthesis process in mitochondria - assembly of (Fe-S)cluster on Isu1.

The second major step performed by late components of the ISC assembly machinery is the release of the (Fe-S) cluster from Isu1 and its transfer and incorporation into recipient apo-proteins. The first interaction is between Isu1 and Jaq1 (human HSC20) this interaction open the access to Ssq1 (human GRP75). This protein is able to interact with both pre two previous protein and contain a Hsp70 ATPase domain; the hydrolysis of ATP induce a conformational change into the complex and reduce the binding strength of the cluster on Isu1. ADP is exchanged for ATP by the exchange factor Mge1 (human GRLP1/2) which triggers a conformational change of the peptide binding domain of Ssq1 from the closed to an open state thus leading to

disassembly of the Ssq1–Isu1 complex (**Fig. 9**) and the cluster is transfer to glutaredoxin 5 Grx5 (human GRLX5).

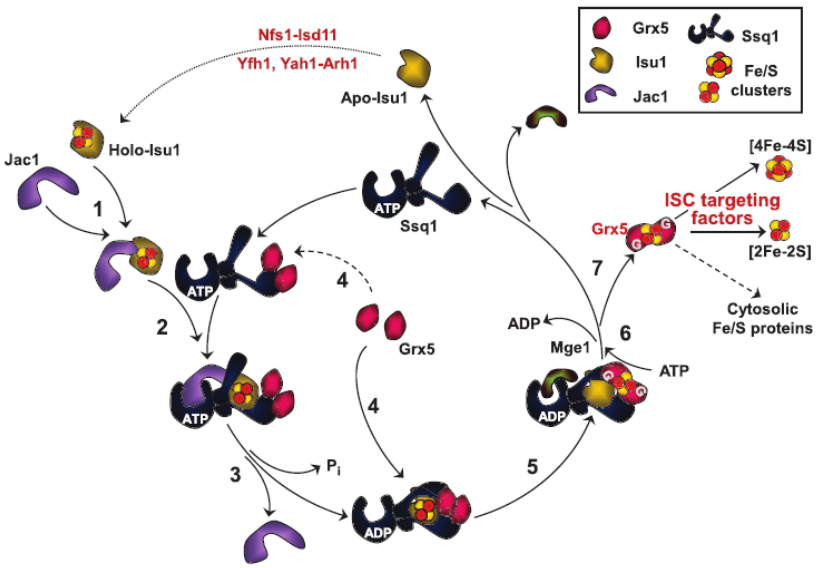

Figure 9. Chaperon cycle from Isu1 to Grx5

The monothiol glutaredoxin Grx5 then helps to transfer the (Fe-S) cluster toward apo proteins, presumably via transient binding of the (Fe-S) cluster in a glutathione-containing complex (GSH). Afterwards the delivery of the assembled (Fe-S) on Grx5, several other proteins can receive the cluster, combine two [2Fe-2S] clusters to form a [4Fe-4S] cluster and driving the cluster to the correct apo target. Isa1/Isa2 (Human ISCA1/2[93]) and IBA57[94] are fundamentals to the assembly of the [4Fe-4S] cluster, Ind1 (Human IND1) is necessary for cluster incorporation into respiratory Complex I of oxidative phosphorylation in mitochondria, Nfu1 (human NUF1), Aim1 (Human BolA3) are all proteins that help the targeting of cluster in a apo protein like lipoate sinthase (**Fig. 10**).[44,45,46,] The biogenesis of cytosolic and

nuclear (Fe-S) proteins requires the close cooperation between the mitochondrial ISC machineries and the CIA system. The central constituent of the mitochondrial ISC export apparatus is the ATP binding cassette (ABC) transporter Atm1 (Human ABCB7) located in the mitochondrial inner membrane. The mitochondrion produce a sulfur rich still unknown molecule (X-S), that can be exported to the cytosol by the transporter.

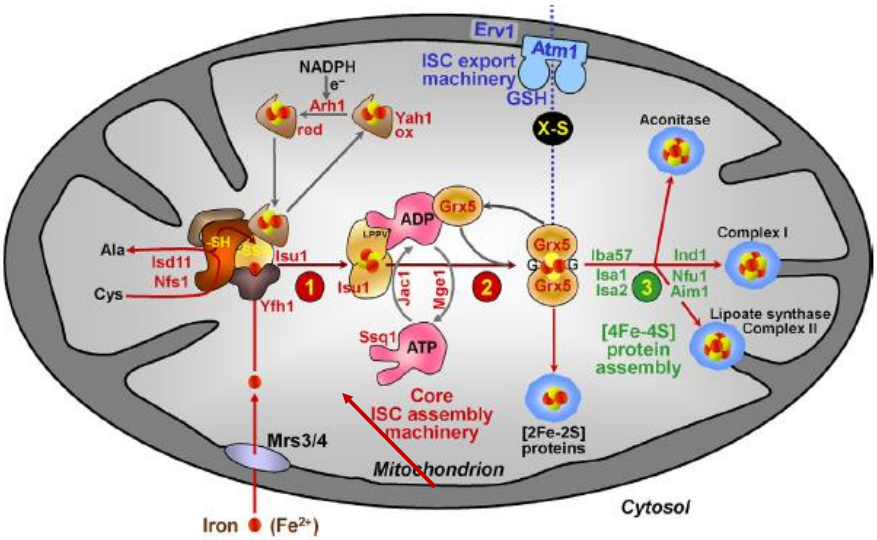

Figure 10. Mitochondrial ISC assembly machinery components and pathway.

1.5.2. Mitochondrial (Fe-S) cluster export machinery

The necessity of mitochondrial ISC assembly for cytosolic (Fe-S) protein maturation was previously explained by the export of ready, preassembled clusters. This idea was abandoned when the ISC export system was discovered. The export machinery consists of three components; the inner

mitochondrial membrane ABC transporter - ABCB7, the intermembrane space protein - ALR and three peptide glutathione GSH (**Fig. 11**). Downregulation or depletion experiments of latter proteins in yeast and human cell lines lead to defective cytosolic and nucleus (Fe-S) proteins due to improper maturation and increased iron uptake in the cell and mitochondrial iron overload.[48,49] It was shown *in vitro* that ATPase activity of the yeast homologue of ABCB7 (the yeast homologue is called Atm1) is stimulated by the sulfhydryl groups (e.g. cysteine residues).[50] Because the ATPase of ABC transporters is usually stimulated by their physiological substrates, this may indicate that the substrate X transported from the mitochondria contains a sulfhydryl group in a peptidic environment. Moreover, the further step of the export process is performed by the ALR, which has sulfhydryl oxidase activity and is located in the mitochondrial intermembrane space. ALR has also been shown to assist incorporation of disulfide bonds by Mia40 into substrate proteins during protein import and trapping in the IMS.[51,52,53] The last component of the ISC export machinery is the glutathione (GSH). This is a reducing agent, existing at a concentration of approximately 5mM in animal cells. Glutathione reduces disulfide bonds formed within cytoplasmic proteins to cysteines by serving as an electron donor. In summary, all known components of the ISC export machinery deal with sulfhydryl chemistry, but identification of their specific function will depend on the identification of the exported moiety.[19,26]

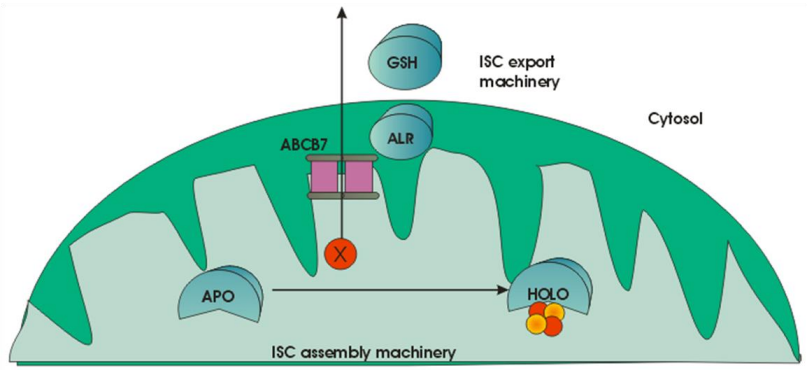

Figure 11. Mitochondrial ISC export machinery.

1.5.3. CIA - cytosolic iron-sulfur cluster assembly machinery

The maturation of cytosolic and nucleus (Fe-S) proteins requires not only the functionality of the mitochondrial ISC assembly machinery but also a dedicated cytoplasmic system (CIA). The overall process can be subdivided into two steps[96] (**Fig.12**):

1. (Fe-S) scaffold system; An initial step of cytosolic (Fe–S) protein biogenesis is the assembly and transient binding of a [4Fe–4S] cluster on the cytosolic scaffold
2. CIA targeting complex; The second major step of cytosolic (Fe–S) protein biogenesis involves the transfer of the newly assembled and transiently bound [4Fe–4S] cluster and its subsequent insertion into dedicated apoproteins

Till now several proteins were identified to play a crucial role in this process;

- Cfd1 and Nbp35 (Human Nubp2 and Nubp1 respectively) both P-loop NTPases that form a tetrameric complex where *de novo* [4Fe-4S] cluster formation takes place

- Nar1 (Human IOP1) is required for [4Fe-4S] cluster transfer to the targeting complex system,
- Cia2B (Human FAM96B or Mip18) and MMS19 compose the scaffold for the targeting process to the final apo protein.
- Cia1 (Human CIAO1) that mediates protein-protein interaction between MMS19 and Nar1,
- Dre2/Tah18 (Human Anamorsin and Ndor1, respectively) that are fundamental for the electron transfer process on the tetramer
- Cia2A (Human Fam96A) necessary for the maturation of IRP1.

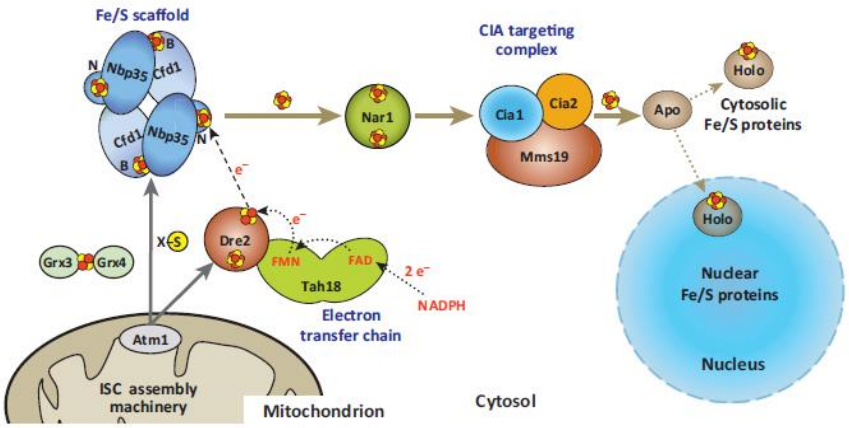

Figure 12. Components of cytosolic ISC assembly machinery.

The assembly process can be dissected into two different steps. First, a [4Fe–4S] clusters are assembled on the Cfd1–Nbp35 heterotetrameric scaffold complex. This reaction requires a sulfur source (X–S) generated by the mitochondrial ISC assembly and exported by the ABCB7 transporter.

Generation of the functionally essential N-terminal (Fe-S) cluster (N) of Nubp1 depends on the flavoprotein Ndor1 and the (Fe-S) protein anamorsin, which serve as an NADPH-dependent electron transfer chain. Second, the bridging (Fe-S) clusters are released from Cfd1–Nbp35 and transferred to apoproteins (Apo), a reaction mediated by the (Fe-S) protein IOP1 and the CIA targeting complex Cia1-Cia2B-MMS19. The latter three proteins interact in different parts of the scaffold complex with target (apo) proteins, and assure specific (Fe-S) cluster insertion. All the components of the CIA machinery are defined by having a primary location in the cytoplasm and they act just in the cytosolic (not the mitochondrial) (Fe-S) cluster protein maturation. This distinguishes CIA proteins from ISC factors that are important for both mitochondrial and cytosolic (Fe-S) cluster biogenesis and ISC export proteins that are required for cytosolic cluster biogenesis but are located only within the mitochondria. The cytosolic (Fe-S) maturation machinery is functionally conserved from yeast to humans and is linked with the iron regulation via Cia2A protein, that can interact with Nar1 or Cia1 and transfer the cluster to IRP1, protein related to the regulation of iron uptake (**Fig.13**).

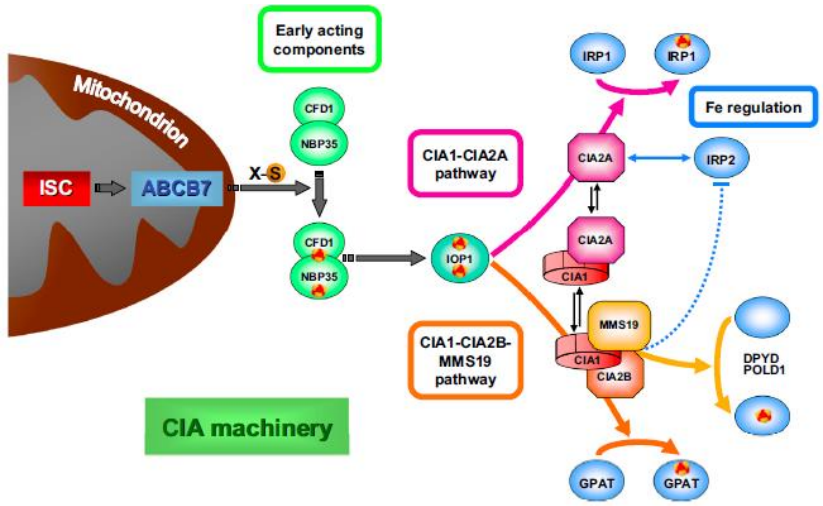

Figure 13. Summary of the CIA machinery

Depletion experiments of single CIA factors in yeast and human cell lines lead to a massive reduction in growth rates, malfunction of iron homeostasis (impaired maturation of IRP1) and decrease of cytosolic (Fe-S) protein activities, with preserved activity of mitochondrial (Fe-S) proteins. This suggests that the cytosolic ISC assembly system works downstream of the ISC assembly machinery in mitochondria.[57,96,58] Identification of factor X, necessary for cytosolic cluster formation, produced by the ISC assembly machinery and exported by the ISC export machinery will give a new insight into the overall cellular maturation process, and will help to fully understand the connection between these three distinct machineries.

1.6 Biogenesis of (Fe-S) cluster and human diseases

Maturation of (Fe-S) clusters strictly depends on the two mitochondrial ISC systems and the CIA machinery providing a tight link between mitochondrial function and cytosolic protein translation. Most of the ISC and CIA components are essential for the viability of the human cells. (Fe-S) clusters are essential cofactors of many proteins so the disruption of their biosynthesis leads to dysfunction of many fundamental cellular processes[95]. The central importance of (Fe-S)-protein biogenesis in mammal's is impressively documented in numerous diseases associated with defects in (Fe-S) protein biogenesis components or Fe-S proteins. Depletion of frataxin, the putative iron donor for (Fe-S) cluster formation on Isu1, causes the neurodegenerative disease Friedreich's ataxia (FRDA)[59-64], which is associated with (Fe-S) protein activity defects and iron accumulation. In FRDA, a progressive degeneration manifests in the central and peripheral nervous system in addition to hypertrophic cardiomyopathy. Defects in the glutaredoxin Grx5, is associated with diseases exhibiting mainly haematological phenotypes, like the sideroblastic anaemia. A splicing defect in the ISCU gene in humans results in a myopathy with exercise intolerance and intracellular iron overload. Mutations in the mitochondrial inner membrane ABC transporter ABCB7 result in X-linked sideroblastic anemia[66,65,91] with cerebellar ataxia. The manifestations of this disorder include an early onset, nonprogressive spinocerebellar ataxia with severe, selective cerebellar hypoplasia, accompanied by a mild hypochromic, microcytic anemi.a Mutations in the genes IBA57, NFU1, and BOLA3 may severely impair diverse mitochondrial metabolic pathways and interfere with

energy production. Hence, these diseases have been designated as multiple mitochondrial dysfunction syndromes (MMDS)[91] which may be fatal at perinatal stages. Affected individuals present with hypotonia, respiratory insufficiency, encephalopathy, brain malformations, and neurological regression. At the biochemical level, patients exhibit metabolic acidosis, hyperglycinemia, and severely increased concentrations of lactate and ketoacids. Also mutation in mitochondrial and cytosolic (Fe-S) final targets proteins are related to many disease. Genetic mutations in LIAS (Lipoyl synthase), an enzyme in the matrix of mitochondria that catalyze the formation of lipoyl cofactor, have been identified as a cause of glycine encephalopathy[91,95,98], also known as nonketotic hyperglycemia, a rare autosomal recessive disorder of the glycine cleavage system in which deficient enzyme activity leads to glycine accumulation in body tissues. Symptoms usually present at birth and early infancy and are marked by mental retardation and seizures, involuntary muscle movement, coma, and death. Mutations in the putative human (Fe-S) proteins XPD and FANCJ cause multiple disease phenotypes including xeroderma pigmentosum and Fanconi anaemia. In conclusion, understanding both the physiological functions of Fe-S proteins and how (Fe-S) clusters are formed will undoubtedly enhance our ability to identify and treat known disorders of (Fe-S) cluster biogenesis and to recognize hitherto undescribed (Fe-S) cluster-related diseases.

References

1. J. Emsley *The Element, 3rd ed.* (Oxford: Clarendon Press: 1998).

2. Bertini, I.;Sigel, A.; Sigel, H. Handbook on Metalloproteins. *Journal of the American Chemical Society* **123**, 12748 (2001).

3. Finney, L.A. & O'Halloran, T.V. Transition Metal Speciation in the Cell: Insights from the Chemistry of Metal Ion Receptors. *Science* **300**, 931-936 (2003).

4. Bidlack, W.R. Metal Ions in Biological System, Volume 36: Interrelations Between Free Radicals and Metal Ions in Life Processes. *J Am Coll Nutr* **18**, 368-369 (1999).

5. Hentze, M.W., Muckenthaler, M.U., Galy, B. & Camaschella, C. Two to Tango: Regulation of Mammalian Iron Metabolism. *Cell* **142**, 24-38 (2010).

6. Bidlack, W.R. Metal Ions in Biological Systems. Vol. 35: Iron Transport and Storage in Microorganisms, Plants and Animals. *J Am Coll Nutr* **18**, 95 (1999).

7. Andrews, N.C. Disorders of iron metabolism. *N. Engl. J. Med* **341**, 1986-1995 (1999).

8. Beard, J.L., Dawson, H. & Piñero, D.J. Iron Metabolism: A Comprehensive Review. *Nutrition Reviews* **54**, 295-317 (1996).

9. Lippard, S.J. & Berg, J.M. *Principles of bioinorganic chemistry*. (University Science Books: 1994).

10. Hentze, M.W., Muckenthaler, M.U. & Andrews, N.C. Balancing Acts: Molecular Control of Mammalian Iron Metabolism. *Cell* **117**, 285-297 (2004).

11. Letelier, M.E., Sánchez-Jofré, S., Peredo-Silva, L., Cortés-Troncoso, J. & Aracena-Parks, P. Mechanisms underlying iron and copper ions toxicity in biological systems: Pro-oxidant activity and protein-binding effects. *Chem Biol Interact* (2010).doi:10.1016/j.cbi.2010.06.013

12. Dunn, L., Rahmanto, Y. & Richardson, D. Iron uptake and metabolism in the new millennium. *Trends in Cell Biology* **17**, 93-100 (2007).

13. Andrews, N.C. Forging a field: the golden age of iron biology. *Blood* **112**, 219-230 (2008).

14. Rouault, T.A. The role of iron regulatory proteins in mammalian iron homeostasis and disease. *Nat Chem Biol* **2**, 406-414 (2006).

15. Cairo, G. & Recalcati, S. Iron-regulatory proteins: molecular biology and pathophysiological implications. *Expert Rev Mol Med* **9**, 1-13 (2007).

16. Lill, R. et al. The essential role of mitochondria in the biogenesis of cellular iron-sulfur proteins. *Biol. Chem* **380**, 1157-1166 (1999).

17. McBride, H.M., Neuspiel, M. & Wasiak, S. Mitochondria: More Than Just a Powerhouse. *Current Biology* **16**, R551-R560 (2006).

18. Richardson, D.R. et al. Mitochondrial iron trafficking and the integration of iron metabolism between the mitochondrion and cytosol. *Proceedings of the National Academy of Sciences* **107**, 10775 -10782 (2010).

19. Lill, R. & Mühlenhoff, U. Maturation of iron-sulfur proteins in eukaryotes: mechanisms, connected processes, and diseases. *Annu. Rev.*

Biochem **77**, 669-700 (2008).

20. Henze, K. & Martin, W. Evolutionary biology: essence of mitochondria. *Nature* **426**, 127-128 (2003).

21. Py, B. & Barras, F. Building Fe–S proteins: bacterial strategies. *Nat Rev Micro* **8**, 436-446 (2010).

22. Xu, X.M. & Møller, S.G. Iron-Sulfur Clusters: Biogenesis, Molecular Mechanisms and Their Functional Significance. *Antioxid Redox Signal* (2010).doi:10.1089/ars.2010.3259

23. Rouault, T.A. & Tong, W. Iron-sulphur cluster biogenesis and mitochondrial iron homeostasis. *Nat Rev Mol Cell Biol* **6**, 345-351 (2005).

24. Rudolf, J., Makrantoni, V., Ingledew, W.J., Stark, M.J.R. & White, M.F. The DNA repair helicases XPD and FancJ have essential iron-sulfur domains. *Mol. Cell* **23**, 801-808 (2006).

25. Rouault, T.A. & Tong, W.H. Iron-sulfur cluster biogenesis and human disease. *Trends Genet* **24**, 398-407 (2008).

26. Lill, R. et al. Mechanisms of iron-sulfur protein maturation in mitochondria, cytosol and nucleus of eukaryotes. *Biochim. Biophys. Acta* **1763**, 652-667 (2006).

27. Johnson, D.C., Dean, D.R., Smith, A.D. & Johnson, M.K. STRUCTURE, FUNCTION, AND FORMATION OF BIOLOGICAL IRON-SULFUR CLUSTERS. *Annu. Rev. Biochem.* **74**, 247-281 (2005).

28. Johnson, M.K. & Smith, A.D. Iron-Sulfur Proteins. *Encyclopedia of Inorganic Chemistry* (2006).at

<http://onlinelibrary.wiley.com/doi/10.1002/0470862106.ia116/full>

29. Lill, R. & Mühlenhoff, U. Iron-sulfur-protein biogenesis in eukaryotes. *Trends Biochem. Sci* **30**, 133-141 (2005).

30. Fosset, C. et al. RNA silencing of mitochondrial m-Nfs1 reduces Fe-S enzyme activity both in mitochondria and cytosol of mammalian cells. *J. Biol. Chem* **281**, 25398-25406 (2006).

31. Hausmann, A., Samans, B., Lill, R. & Mühlenhoff, U. Cellular and Mitochondrial Remodeling upon Defects in Iron-Sulfur Protein Biogenesis. *Journal of Biological Chemistry* **283**, 8318 -8330 (2008).

32. Martelli, A. et al. Frataxin is essential for extramitochondrial Fe–S cluster proteins in mammalian tissues. *Human Molecular Genetics* **16**, 2651 -2658 (2007).

33. Lill, R. Function and biogenesis of iron-sulphur proteins. *Nature* **460**, 831-838 (2009).

34. Tokumoto, U., Kitamura, S., Fukuyama, K. & Takahashi, Y. Interchangeability and distinct properties of bacterial Fe-S cluster assembly systems: functional replacement of the isc and suf operons in Escherichia coli with the nifSU-like operon from Helicobacter pylori. *J. Biochem* **136**, 199-209 (2004).

35. Agar, J.N., Zheng, L., Cash, V.L., Dean, D.R. & Johnson, M.K. Role of the IscU Protein in Iron−Sulfur Cluster Biosynthesis: IscS-mediated Assembly of a [Fe2S2] Cluster in IscU. *Journal of the American Chemical Society* **122**, 2136-2137 (2000).

36. Chandramouli, K. et al. Formation and Properties of [4Fe-4S] Clusters

on the IscU Scaffold Protein†. *Biochemistry* **46**, 6804-6811 (2007).

37. Agar, J.N. et al. IscU as a scaffold for iron-sulfur cluster biosynthesis: sequential assembly of [2Fe-2S] and [4Fe-4S] clusters in IscU. *Biochemistry* **39**, 7856-7862 (2000).

38. Gerber, J., Mühlenhoff, U. & Lill, R. An interaction between frataxin and Isu1/Nfs1 that is crucial for Fe-S cluster synthesis on Isu1. *EMBO Rep* **4**, 906-911 (2003).

39. Leidgens, S., De Smet, S. & Foury, F. Frataxin interacts with Isu1 through a conserved tryptophan in its beta-sheet. *Hum. Mol. Genet* **19**, 276-286 (2010).

40. Foury, F., Pastore, A. & Trincal, M. Acidic residues of yeast frataxin have an essential role in Fe-S cluster assembly. *EMBO Rep* **8**, 194-199 (2007).

41. Adam, A.C., Bornhovd, C., Prokisch, H., Neupert, W. & Hell, K. The Nfs1 interacting protein Isd11 has an essential role in Fe-S cluster biogenesis in mitochondria. *EMBO J* **25**, 174-183 (2006).

42. Biederbick, A. et al. Role of human mitochondrial Nfs1 in cytosolic iron-sulfur protein biogenesis and iron regulation. *Mol. Cell. Biol* **26**, 5675-5687 (2006).

43. Bonomi, F., Iametti, S., Morleo, A., Ta, D. & Vickery, L.E. Studies on the mechanism of catalysis of iron-sulfur cluster transfer from IscU[2Fe2S] by HscA/HscB chaperones. *Biochemistry* **47**, 12795-12801 (2008).

44. Rodríguez-Manzaneque, M.T., Tamarit, J., Bellí, G., Ros, J. & Herrero,

E. Grx5 is a mitochondrial glutaredoxin required for the activity of iron/sulfur enzymes. *Mol. Biol. Cell* **13**, 1109-1121 (2002).

45. Dutkiewicz, R. et al. Sequence-specific interaction between mitochondrial Fe-S scaffold protein Isu and Hsp70 Ssq1 is essential for their in vivo function. *J. Biol. Chem* **279**, 29167-29174 (2004).

46. Andrew, A.J., Dutkiewicz, R., Knieszner, H., Craig, E.A. & Marszalek, J. Characterization of the interaction between the J-protein Jac1p and the scaffold for Fe-S cluster biogenesis, Isu1p. *J. Biol. Chem* **281**, 14580-14587 (2006).

47. Sheftel, A.D. et al. Human ind1, an iron-sulfur cluster assembly factor for respiratory complex I. *Mol. Cell. Biol* **29**, 6059-6073 (2009).

48. Sharma, A.K., Pallesen, L.J., Spang, R.J. & Walden, W.E. Cytosolic iron-sulfur cluster assembly (CIA) system: factors, mechanism, and relevance to cellular iron regulation. *J. Biol. Chem* **285**, 26745-26751 (2010).

49. Cavadini, P. et al. RNA silencing of the mitochondrial ABCB7 transporter in HeLa cells causes an iron-deficient phenotype with mitochondrial iron overload. *Blood* **109**, 3552-3559 (2007).

50. Kuhnke, G., Neumann, K., Mühlenhoff, U. & Lill, R. Stimulation of the ATPase activity of the yeast mitochondrial ABC transporter Atm1p by thiol compounds. *Mol. Membr. Biol* **23**, 173-184 (2006).

51. Hell, K. The Erv1-Mia40 disulfide relay system in the intermembrane space of mitochondria. *Biochim. Biophys. Acta* **1783**, 601-609 (2008).

52. Bihlmaier, K., Mesecke, N., Kloeppel, C. & Herrmann, J.M. The

disulfide relay of the intermembrane space of mitochondria: an oxygen-sensing system? *Ann. N. Y. Acad. Sci* **1147**, 293-302 (2008).

53. Banci, L. et al. MIA40 is an oxidoreductase that catalyzes oxidative protein folding in mitochondria. *Nat. Struct. Mol. Biol* **16**, 198-206 (2009).

54. Zhang, Y. et al. Dre2, a conserved eukaryotic Fe-S cluster protein, functions in cytosolic Fe-S protein biogenesis. *Mol. Cell. Biol* **28**, 5569-5582 (2008).

55. Vernis, L. et al. A newly identified essential complex, Dre2-Tah18, controls mitochondria integrity and cell death after oxidative stress in yeast. *PLoS ONE* **4**, e4376 (2009).

56. Netz, D.J.A. et al. Tah18 transfers electrons to Dre2 in cytosolic iron-sulfur protein biogenesis. *Nat Chem Biol* (2010).doi:10.1038/nchembio.432

57. Song, D. & Lee, F.S. A Role for IOP1 in Mammalian Cytosolic Iron-Sulfur Protein Biogenesis. *Journal of Biological Chemistry* **283**, 9231 - 9238 (2008).

58. Stehling, O. et al. Human Nbp35 Is Essential for both Cytosolic Iron-Sulfur Protein Assembly and Iron Homeostasis. *Mol. Cell. Biol.* **28**, 5517-5528 (2008).

59. Puccio, H. & Koenig, M. Friedreich ataxia: a paradigm for mitochondrial diseases. *Curr. Opin. Genet. Dev* **12**, 272-277 (2002).

60. Babady, N.E. et al. Advancements in the pathophysiology of Friedreich's Ataxia and new prospects for treatments. *Molecular Genetics and*

Metabolism **92**, 23-35

61. Campuzano, V. et al. Friedreich's Ataxia: Autosomal Recessive Disease Caused by an Intronic GAA Triplet Repeat Expansion. *Science* **271**, 1423-1427 (1996).

62. Condò, I. et al. In vivo maturation of human frataxin. *Human Molecular Genetics* **16**, 1534 -1540 (2007).

63. Pandolfo, M. Iron and Friedreich ataxia. *J. Neural Transm. Suppl* 143-146 (2006).

64. Allikmets, R. et al. Mutation of a Putative Mitochondrial Iron Transporter Gene (ABC7) in X-Linked Sideroblastic Anemia and Ataxia (XLSA/A). *Human Molecular Genetics* **8**, 743 -749 (1999).

65. Pondarré, C. et al. The mitochondrial ATP-binding cassette transporter Abcb7 is essential in mice and participates in cytosolic iron-sulfur cluster biogenesis. *Hum. Mol. Genet* **15**, 953-964 (2006).

66. Pondarre, C. et al. Abcb7, the gene responsible for X-linked sideroblastic anemia with ataxia, is essential for hematopoiesis. *Blood* **109**, 3567-3569 (2007).

67. Ye, H. et al. Glutaredoxin 5 deficiency causes sideroblastic anemia by specifically impairing heme biosynthesis and depleting cytosolic iron in human erythroblasts. *J. Clin. Invest* **120**, 1749-1761 (2010).

68. Mochel, F. et al. Splice Mutation in the Iron-Sulfur Cluster Scaffold Protein ISCU Causes Myopathy with Exercise Intolerance. *Am J Hum Genet* **82**, 652-660 (2008).

69. Gottlieb, E., King, A. & Selak, M.A. Succinate dehydrogenase and

fumarate hydratase: linking mitochondrial dysfunction and cancer. (2006).at <http://eprints.gla.ac.uk/23549/>

70. Rudolf, J., Makrantoni, V., Ingledew, W.J., Stark, M.J. & White, M.F. The DNA Repair Helicases XPD and FancJ Have Essential Iron-Sulfur Domains. *Molecular Cell* **23**, 801-808 (2006).

83. Li, X. et al. A new apoptosis inhibitor, CIAPIN1 (cytokine-induced apoptosis inhibitor 1), mediates multidrug resistance in leukemia cells by regulating MDR-1, Bcl-2, and Bax. *Biochem. Cell Biol* **85**, 741-750 (2007).

84. Wang, Y., Qi, H., Li, X., Chen, X. & Liu, J. [CIAPIN1 expression in human lung cancer tissues and inhibitory effects of the gene on human pulmonary carcinoma NCI-H446 cells]. *Xi Bao Yu Fen Zi Mian Yi Xue Za Zhi* **24**, 434-437 (2008).

85. Shizusawa, T. et al. The expression of anamorsin in diffuse large B cell lymphoma: possible prognostic biomarker for low IPI patients. *Leuk. Lymphoma* **49**, 113-121 (2008).

86. Kim, K., Chung, W., Kim, H., Lee, K. & Roe, J. Monothiol glutaredoxin Grx5 interacts with Fe-S scaffold proteins Isa1 and Isa2 and supports Fe-S assembly and DNA integrity in mitochondria of fission yeast. *Biochem. Biophys. Res. Commun* **392**, 467-472 (2010).

87. Stemmler, T.L., Lesuisse, E., Pain, D. & Dancis, A. Frataxin and Mitochondrial FeS Cluster Biogenesis. *Journal of Biological Chemistry* **285**, 26737 -26743 (2010).

88. Wiedemann, N. et al. Essential role of Isd11 in mitochondrial iron-sulfur cluster synthesis on Isu scaffold proteins. *EMBO J* **25**, 184-195 (2006).

89. Richardson, D.R., Lane, D.J., Becker, E.M., Huang, M.L., Whitnall, M., Suryo Rahmanto, Y., Sheftel, A.D., Ponka, P., 2010. Mitochondrial iron trafficking and the integration of iron metabolism between the mitochondrion and cytosol. Proc. Natl. Acad. Sci. U. S. A. 107, 10775–10782.

90. Lill, R., Uzarska, M.A., Wohlschlegel, J.A., 2014b. Eukaryotic iron–sulfur cluster biogenesis and its role in maintaining genome stability. In: Rouault, T. (Ed.), Iron–Sulfur Clusters in Chemistry and Biology. Walter de Gruyter GmbH, Berlin/Boston, pp. 541–598

91. Lill, R., Muhlenhoff, U., 2008. Maturation of iron–sulfur proteins in eukaryotes: mechanisms, connected processes, and diseases. Annu. Rev. Biochem 77, 669–700.

92.Lill, R., Srinivasan, V., Muhlenhoff, U., 2014a. The role of mitochondria in cytosolic-nuclear iron–sulfur protein biogenesis and in cellular iron regulation. Curr. Opin. Microbiol. 22C, 111–119.

93. Brancaccio D, Gallo A, Mikolajczyk M, Zovo K, Palumaa P, Novellino E, Piccioli M, Ciofi-Baffoni S, Banci L. Formation of [4Fe-4S] clusters in the mitochondrial iron-sulfur cluster assembly machinery. J Am Chem Soc. 2014 Nov 19;136(46):16240-50. doi: 10.1021/ja507822j. Epub 2014 Nov 7.

94. Sheftel, Alex D, et al. The human mitochondrial ISCA1, ISCA2, and IBA57 proteins are required for [4Fe-4S] protein maturation. Molecular biology of the cell. 23 (1157-1166) 2012

95. Sheftel A, Stehling O, Lill R. Iron-sulfur proteins in health and disease. Trends Endocrinol Metab. 2010 May;21(5):302-14.

96. Netz DJ,et al. Maturation of cytosolic and nuclear iron-sulfur proteins. Trends Cell Biol. 2014 May;24(5):303-12.

97. Stehling O, Wilbrecht C, Lill R. Mitochondrial iron-sulfur protein biogenesis and human disease. Biochimie. 2014 May;100:61-77.

98. Landgraf BJ, McCarthy EL, Booker SJ. Radical S-Adenosylmethionine Enzymes in Human Health and Disease. Annu Rev Biochem. 2016 Jun 2;85:485-514.

-Chapter 2-

AIMS OF THE RESEARCH

2.1. Topics of the research

During the three years of my PhD course I worked on recombinant protein production of human proteins involved in iron-sulfur protein biogenesis, and on its biochemical and structural characterization, with the final aim of investigating at an atomic level the functional role of these proteins within the (Fe-S) protein biogenesis pathways. In my research, I used a multidisciplinary approach exploiting several techniques and disciplines ranging from bioinformatics, molecular cloning, cell culture, protein purification, NMR, EPR, CD, UV-vis spectroscopies, and mass spectrometry. Specific target proteins part of the human CIA machinery were selected and recombinantly produced in E. coli cells to investigate their molecular interactions with protein targets, in such a way to define the cellular pathway of the CIA machinery at the molecular level. In the last period of my PhD program, a final target of the mitochondrial ISC assembly machinery, i.e. the human lipoyl synthase, was recombinantly produced since genetic mutations in this mitochondrial enzyme have been identified as a cause of a rare autosomal recessive disorder of the glycine cleavage system in which deficient enzyme activity leads to glycine accumulation in body tissues. Symptoms of this disease usually present at birth and early infancy and are marked by mental retardation and seizures, involuntary muscle movement, coma, and death.

A general overview of the three projects developed during my PhD thesis are reported in the following sections.

2.2. Glutaredoxin 3 (GRX3 or PICOT) / Anamorsin (CIAPIN1) pathway

In eukaryotes, both cytosolic and mitochondrial monothiol glutaredoxin proteins bind [2Fe-2S] clusters in the same way, i.e., via the formation of a [2Fe-2S]-bridged homodimer[1,2]. However, though the molecular function of mitochondrial monothiol glutaredoxins in assisting (Fe-S) protein maturation by acting as [2Fe-2S] cluster donors toward partner apo proteins has been demonstrated in the last few years[3–6], the question of whether cytosolic monothiol glutaredoxins can perform the same function in the cytosol still remains unsolved. In contrast, the [2Fe-2S] cluster–bound form of cytosolic monothiol glutaredoxins has been recently proposed to be implicated, together with other protein candidates[7], in cytosolic iron trafficking, playing a crucial part in iron delivery from the cytosolic labile iron pool to virtually all iron-binding proteins in the cell[8,9]. Recently, it has been also shown that, in Saccharomyces cerevisiae, the cytosolic monothiol glutaredoxin-3 can transfer the cluster to the iron-responsive transcription factor Aft2 in a way that deactivates the iron regulon for iron uptake, but cluster transfer occurs only when GRX3 is complexed with the BolA-like protein Fra2 (Human BOLA2). to form a $[2Fe\text{-}2S]^{2+}$ bridged heterodimer complex[10-13].

The human proteome contains only one monothiol glutaredoxin (Grx) in the cytosol, GRX3 (also commonly named GLRX3 and PICOT). GRX3 is a protein of 335 amino acids formed by three domains: one N-terminal thioredoxin (Trx) domain with no Trx-related enzymatic role[8,14] and two Grx domains, call GrxA and GrxB, each able to bind a glutathione-coordinated [2Fe-2S] cluster via protein dimerization with the cysteine of a conserved CGFS motif present in each domain. Recently, multiple high-throughput

yeast two-hybrid19 and affinity-capture MS (BioGRID interaction 1077826) screens have shown that GRX3 binds anamorsin (also commonly named CIAPIN1), a [2Fe-2S] cluster–binding protein involved in the maturation of cytosolic Fe-S proteins, in vivo[16,17]. However, the interaction mode and functional role of this interaction have not yet been defined. Anamorsin contains two domains: an N-terminal well-folded domain (N domain, hereafter) comprising 172 residues and a largely unstructured C-terminal domain of 90 residues named cytokine-induced apoptosis inhibitor 1 (CIAPIN1 domain), which contains two highly conserved cysteine-rich motifs able to independently bind a [2Fe-2S] cluster[16,17]. These two domains are connected by a long flexible linker of 50 residues. Anamorsin is an appropriate target to investigate a potential functional role of GRX3 in transferring [2Fe-2S] clusters as it interacts with GRX3 in vivo. The final goal of this research project is to investigate the ability of GRX3 to transfer [2Fe-2S] clusters to final target proteins by studying its interaction with anamorsin. Through this work, I will be able to define whether GRX3 is an active component of the CIA machinery.

2.3. BOLA2 modulation in the Anamorsin maturation pathway

The functional role of eukaryotic monothiol glutaredoxins (Grx) has been largely studied in Saccharomyces cerevisiae, which encodes three CysGlyPheSer(CGPS)-type monothiol Grx homologues, Grx3/Grx4 and Grx5.[18-20] Grx5 is a single domain protein, located in the mitochondrial matrix, Grx3 and Grx4 are located in the cytoplasm, and each consists of a N-terminal thioredoxin (Trx) domain, with no Trx-related activity,[21,22] and

of a glutaredoxin domain capable of binding a [2Fe-2S] cluster through protein dimerization and glutathione binding,[23]. Grx3 and Grx4 have been linked to iron regulation through their binding to the transcriptional activator Aft1/2, which regulates iron uptake in yeast.[25-26] Specifically, to perform this regulatory function, Grx3 (or Grx4) needs to be complexed with the BolA-like protein Fra2 (Human BOLA2), forming a [2Fe-2S]-bridged hetero complex,[23,27] which, can transfer the cluster to the iron-responsive transcription factor Aft2[28]. Starting from this information on yeast and from the acquired knowledge on the anamorsin maturation pathway investigated in the previous project, I overexpressed the human BOLA2, studied its interaction with GRX3, and characterized the GRX3-BOLA2 driven maturation pathway of anamorsin at the molecular level..

2.4. LIAS (lipoyl synthase)

Lipoyl cofactors are essential for living organisms and are produced by the insertion of two sulfur atoms into the relatively unreactive C–H bonds of an octanoyl substrate. This reaction requires lipoyl synthase, a member of the radical S-adenosylmethionine (SAM) enzyme superfamily. LIAS contains two [4Fe–4S] clusters, which are both essential in catalysis[29]. One cluster is bound by cysteines in a canonical Cx3Cx2C RS motif and participates in the reductive cleavage of SAM, whereas a second cluster, bound by cysteines in an N-terminal Cx4Cx5C motif as well as a serine residue in a conserved C-terminal RSSY motif[29,30], is the source of the inserted sulfur atoms and is degraded during turnover[31,32]. To this date, four mutations in the LIAS gene that result in severe disease states have been described in patients[33-35]. Genetic mutations in LIAS have been identified as a cause of glycine

encephalopathy, also known as nonketotic hyperglycemia. Due to the critical role of LIAS in several diseases, I overexpressed and purified this protein in order to solve the structure of this protein and to characterize its spectroscopic and structural properties. These information will allow to evaluate how pathogenic mutation can affect the enzyme functionality and thus thay will provide the structural basis of the disease states related to the genetic mutations in the LIAS gene.

References

1. Banci, L. et al. [2Fe-2S] cluster transfer in iron-sulfur protein biogenesis. Proc. Natl. Acad. Sci. USA 111, 6203–6208 (2014).

2. Haunhorst, P., Berndt, C., Eitner, S., Godoy, J.R. & Lillig, C.H. Characterization of the human monothiol glutaredoxin 3 (PICOT) as iron-sulfur protein. Biochem. Biophys. Res. Commun. 394,

3. Lill, R. et al. The role of mitochondria in cellular iron-sulfur protein biogenesis and iron metabolism. Biochim. Biophys. Acta 1823, 1491–1508 (2012).4. Bidlack, W.R. Metal Ions in Biological System, Volume 36: Interrelations Between Free Radicals and Metal Ions in Life Processes. *J Am Coll Nutr* **18**, 368-369 (1999).

4. Uzarska, M.A., Dutkiewicz, R., Freibert, S.A., Lill, R. & Muhlenhoff, U.

The mitochondrial Hsp70 chaperone Ssq1 facilitates Fe/S cluster transfer

from Isu1 to Grx5 by complex formation. Mol. Biol. Cell 24, 1830–1841 (2013).

5. Mapolelo, D.T. et al. Monothiol glutaredoxins and A-type proteins: partners in Fe-S cluster trafficking. Dalton Trans. 42, 3107–3115 (2013).

6. Shakamuri, P., Zhang, B. & Johnson, M.K. Monothiol glutaredoxins function in storing and transporting [Fe2S2] clusters assembled on IscU scaffold proteins. J. Am. Chem. Soc. 134, 15213–15216 (2012).

7. Philpott, C.C. Coming into view: eukaryotic iron chaperones and intracellular iron delivery. J. Biol. Chem. 287, 13518–13523 (2012).

8. Mühlenhoff, U. et al. Cytosolic monothiol glutaredoxins function in intracellular iron sensing and trafficking via their bound iron-sulfur cluster. Cell Metab. 12, 373–385 (2010).

9. Haunhorst, P. et al. Crucial function of vertebrate glutaredoxin 3 (PICOT) in iron homeostasis and hemoglobin maturation. Mol. Biol. Cell 24, 1895–1903 (2013).

10. Yamaguchi-Iwai, Y., Stearman, R., Dancis, A. & Klausner, R.D. Iron-regulated DNA binding by the AFT1 protein controls the iron regulon in yeast. EMBO J. 15, 3377–3384 (1996).

11. Rutherford, J.C., Jaron, S., Ray, E., Brown, P.O. & Winge, D.R. A second iron-regulatory system in yeast independent of Aft1p. Proc. Natl. Acad. Sci. USA 98, 14322–14327 (2001).

12. Blaiseau, P.L., Lesuisse, E. & Camadro, J.M. Aft2p, a novel iron-regulated transcription activator that modulates, with Aft1p, intracellular iron use and resistance to oxidative stress in yeast. J. Biol. Chem. 276, 34221–34226 (2001).

13. Ojeda, L. et al. Role of glutaredoxin-3 and glutaredoxin-4 in the iron regulation of the Aft1 transcriptional activator in Saccharomyces cerevisiae. J. Biol. Chem. 281, 17661–17669 (2006).

14. Hoffmann, B. et al. The multidomain thioredoxin-monothiol glutaredoxins represent a distinct functional group. Antioxid. Redox Signal. 15, 19–30 (2011).

15. Banci, L. et al. Molecular view of an electron transfer process essential for iron-sulfur protein biogenesis. Proc. Natl. Acad. Sci. USA 110, 7136–7141 (2013).

16. Netz, D.J. et al. Tah18 transfers electrons to Dre2 in cytosolic iron-sulfur protein biogenesis. Nat. Chem. Biol. 6, 758–765 (2010).

17. Banci, L. et al. Anamorsin is a [2Fe-2S] cluster–containing substrate of the Mia40-dependent mitochondrial protein-trapping machinery. Chem. Biol. 18, 794–804 (2011).

18. Herrero, E.; de la Torre-Ruiz, M. A. Cell. Mol. Life Sci. 2007, 64,1518−1530.

19. Couturier, J.; Przybyla-Toscano, J.; Roret, T.; Didierjean, C.;Rouhier, N. Biochim. Biophys. Acta, Mol. Cell Res. 2015, 1853, 1513−1527.

20. Rouhier, N.; Couturier, J.; Johnson, M. K.; Jacquot, J. P. Trends Biochem. Sci. 2010, 35, 43−52.

21. Muhlenhoff, U.; Molik, S.; Godoy, J. R.; Uzarska, M. A.; Richter, N.; Seubert, A.; Zhang, Y.; Stubbe, J.; Pierrel, F.; Herrero, E.; Lillig, C. H.; Lill, R. Cell Metab. 2010, 12, 373−385.

22. Hoffmann, B.; Uzarska, M. A.; Berndt, C.; Godoy, J. R.;Haunhorst, P.; Lillig, C. H.; Lill, R.; Muhlenhoff, U. Antioxid. Redox Signaling 2011, 15, 19−30.

23. Li, H.; Mapolelo, D. T.; Dingra, N. N.; Naik, S. G.; Lees, N. S.; Hoffman, B. M.; Riggs-Gelasco, P. J.; Huynh, B. H.; Johnson, M. K.; Outten, C. E. Biochemistry 2009, 48, 9569−9581.

24. Ojeda, L.; Keller, G.; Muhlenhoff, U.; Rutherford, J. C.; Lill, R.; Winge, D. R. J. Biol. Chem. 2006, 281, 17661−17669.

25. Pujol-Carrion, N.; Belli, G.; Herrero, E.; Nogues, A.; de la Torre-Ruiz, M. A. J. Cell Sci. 2006, 119, 4554−4564.

26. Kumanovics, A.; Chen, O. S.; Li, L.; Bagley, D.; Adkins, E. M.; Lin, H.; Dingra, N. N.; Outten, C. E.; Keller, G.; Winge, D.; Ward, D. M.; Kaplan, J. J. Biol. Chem. 2008, 283, 10276−10286.

27. Li, H.; Mapolelo, D. T.; Dingra, N. N.; Keller, G.; Riggs-Gelasco, P. J.; Winge, D. R.; Johnson, M. K.; Outten, C. E. J. Biol. Chem. 2011, 286, 867−876.

28. Poor, C. B.; Wegner, S. V.; Li, H.; Dlouhy, A. C.; Schuermann, J. P.; Sanishvili, R.; Hinshaw, J. R.; Riggs-Gelasco, P. J.; Outten, C. E.; He, C. Proc. Natl. Acad. Sci. U. S. A. 2014, 111, 4043−4048.

29. Cicchillo RM, Lee K-H, Baleanu-Gogonea C, Nesbitt NM, Krebs C, Booker SJ. 2004. Escherichia coli lipoyl synthase binds two distinct [4Fe-4S] clusters per polypeptide. Biochemistry 43:11770–81

30. Harmer JE, Hiscox MJ, Dinis PC, Fox SJ, Lliopoulos A, et al. 2014. Structures of lipoyl synthase reveal a compact active site for controlling sequential sulfur insertion reactions. Biochem. J. 464:123–33

31. Cicchillo RM, Booker SJ. 2005. Mechanistic investigations of lipoic acid biosynthesis in Escherichia coli: Both sulfur atoms in lipoic acid are contributed by the same lipoyl synthase polypeptide. J. Am. Chem. Soc. 127:2860–61

32. Lanz ND, Pandelia ME, Kakar ES, Lee K-H, Krebs C, Booker SJ. 2014. Evidence for a catalytically and kinetically competent enzyme-substrate cross-linked intermediate in catalysis by lipoyl synthase. Biochemistry 53:4557–72

33. Baker PR 2nd, Friederich MW, Swanson MA, Shaikh T, Bhattacharya K, et al. 2014. Variant nonketotic hyperglycinemia is caused by mutations

in LIAS, BOLA3 and the novel gene GLRX5. Brain 137:366–79

34. Mayr JA, Feichtinger RG, Tort F, Ribes A, SperlW. 2014. Lipoic acid biosynthesis defects. J. Inherit. Metab. Dis. 37:553–63

35. Tsurusaki Y, Tanaka R, Shimada S, Shimojima K, ShiinaM, et al. 2015. Novel compound heterozygous LIAS mutations cause glycine encephalopathy. J. Hum. Genet. 60:631–35

36. Rouault TA, Tong WH. 2008. Iron–sulfur cluster biogenesis and human disease. Trends Genet. 24:398–407

37. StehlingO,WilbrechtC, Lill R. 2014. Mitochondrial iron-sulfur protein biogenesis and human disease. Biochimie 100:61–77

-Chapter 3-

MATERIALS AND METHODS

3.1. Genome browsing

One of the main challenges facing the molecular biology community today is to make sense of the wealth of data that has been produced by the genome sequencing projects. In t3.1he past decade, bioinformatics has become an integral part of research and development in the biomedical sciences. Bioinformatics now has an essential role both in deciphering genomic, transcriptomic and proteomic data, generated by high-throughput experimental technologies, and in organizing information gathered from traditional biology. It is an interdisciplinary research area at the interface between the biological and computational science. The ultimate goal of bioinformatics is to uncover the biological information hidden in the mass of data and obtain a clearer insight into the fundamental biology of organisms. Genome browsing is the first and crucial step for the expression and characterization of a recombinant protein. In this step, bioinformatics tools are necessary to analyse the nucleotide and amino acid sequences and obtain information useful for the choice of the protein target. A number of data banks are available and provide the scientific community tools for searching gene banks, for the analysis of protein sequences, for the prediction of a variety of protein properties. Primary databases contain information and annotations of DNA and protein sequences, DNA and protein structures and protein expression profiles. Some available databases for genome browsing are:

- **NCBI** (www.ncbi.nlm.nih.gov/Entrez/) - This web site integrates information from several databases (Swissprot, EMBL, all geneBank, etc...)
- **UniProt** (http://www.uniprot.org/) - A database for all the proteins

- **PDB** (www.rcsb.org/pdb) - A 3-D biological macromolecular structure database
- **Pfam** (http://pfam.sanger.ac.uk/) - A collection of different protein families organized in terms of different domains as obtained from multiple alignments.[1]

Secondary or derived databases are so called because they contain the results of analysis of the primary resource including information on sequence patterns or motifs, variants and mutations and evolutionary relationships. Once all biological data is stored, the requirement is to provide bioinformatic tools for extracting the meaningful information. The most used programs for genome browsing are:

- **BLAST** (www.ncbi.nlm.nih.gov/BLAST/): Standard BLAST (Basic Local Alignment Search Tool) is a set of similarity search programs designed to explore all of the available sequence databases regardless of whether the query is protein or DNA. PHIBLAST is designed to search for proteins that contain a pattern specified by the user, and simultaneously are similar to the query sequence.
- **CLUSTALW** (www.ebi.ac.uk/clustalw/) is a general purpose multiple sequence alignment program for DNA or proteins. It produces biologically meaningful multiple sequence alignments of divergent sequences. It calculates the best match for the selected sequences, and lines them up so that the identities, similarities and differences can be seen. Evolutionary relationships can be seen via viewing Cladograms or Phylograms
- **PROSITE** (www.expasy.org/prosite/) SCANPROSITE allows to scan a protein sequence, provided by the user, for the occurrence of patterns and profiles stored in the PROSITE database, or to search in protein databases all sequences with a user entered pattern.

- **STRING** (http://string.embl.de/) STRING is a database of predicted functional associations among genes/proteins. Genes of similar function tend to be maintained in close neighbourhood and tend to be present or absent together.[2]

3.2. Construct design

Once the target protein is chosen, it is subjected to further bioinformatics investigations in order to predict important features like stability, solubility, hydrophobicity, secondary and tertiary structures. In this crucial step other bioinformatic tools can be used.

- Several tools can be used in order to predict if the target is a fully soluble, transmembrane protein, or a protein containing both soluble and transmembrane domains;
  http://www.sbc.su.se/~miklos/DAS/,
  http://www.cbs.dtu.dk/services/TMHMM-2.0/,
  http://www.ch.embnet.org/software/TMPRED/form.html;
- The presence in the sequence of subcellular targeting signals can be confirmed by the tools from servers like: SignalP, TargetP and PSORT.org;[3,4,5]
  http://www.cbs.dtu.dk/services/TargetP/,
  http://www.cbs.dtu.dk/services/SignalP/,
  http://www.psort.org/;
- Topological and structural predictions can help in the identification of intrinsically unstructured regions and the prediction of secondary and tertiary structures; [6,7,8,9]
  http://iupred.enzim.hu/,
  http://bip.weizmann.ac.il/fldbin/findex/,

http://www.sbg.bio.ic.ac.uk/~3dpssm/,
http://pbil.univ-lyon1.fr/;

- The construct should be designed with respect to the N-end rules;[10]

These tools applied for each target protein, domain or construct selected for expression, can increase the probability of obtaining a soluble and well-folded protein.

3.3. Gene cloning

In order to get high yield of soluble proteins, many factors have to be taken in consideration, such as the choice of the vector, of the cloning strategy, and of culture conditions. Of course, the knowledge of the protein characteristics will help in this choice, thus increasing the chance of success. In the last years several eukaryotic expression systems were optimized, such as mammalian, yeast and insect cell expression. Cell-free protein synthesis has also a great potential, in particular with membrane proteins. [11,12,13] However, especially for NMR which requires high yields of labelled ^{15}N,^{13}C and ^{2}H samples, the *E.coli* expression system is nowadays the most widely used. That is why many efforts were focused on the optimization of this expression system. The gene cloning is the first part of the heterologous protein expression and consists into the creation of an expression vector. This vector can present different fusion tag to exploit the gene fusion technology. Gene fusion technology can facilitate purification, enhance protein expression and solubility, chaperone proper folding, reduce protein degradation, and in some cases, generate proteins with a native N-terminus. Factors such as reduced temperature, changes the *E.coli* expression strain, use different promoters or induction conditions and co-expression of molecular chaperones and folding modulators have all been examined and, in some specific cases, they lead to

enhancements of soluble protein production. Nevertheless, protein expression remains an arduous task that involves a complex decision tree. To date, no technology or reagent is a panacea. Thus, establishing tools and optimal conditions for each protein remains an empirical exercise.[14] The best way to maximize the probability of obtaining a soluble and correctly folded target protein is to proceed with a parallel cloning and expression of it with a high number of fusion partners.

There are different way to clone a gene into different plasmid with different fusion partner:

- Classical cloning: digestion of gene and plasmid with a restriction enzyme and ligase reaction
- Ligase independent cloning (LIC)
- Gateway technology®

Classical cloning, using restriction enzymes, typically can't be adapted to high-throughput approaches, due to the complication of selecting compatible and appropriate restriction enzymes for each cloning procedure and to its multistep process. Also LIC approach is not used for the cloning screening. High-throughput cloning therefore requires procedures which can help to screen a broad range of conditions in less time, for these reasons new cloning technologies have been developed in recent years. Landy and coworkers have described a universal cloning method (Gateway technology®) based on the site-specific recombination of bacteriophage lambda, which facilitates the integration of lambda into *E.coli* chromosome and the switch between the lytic and lysogenic cycle.[15] By this technology (developed by Invitrogen) it is possible to clone a target gene into different expression vectors, after the creation of the enrty clone, eliminating the time consuming work with restriction enzymes and ligase (**Fig.14**).

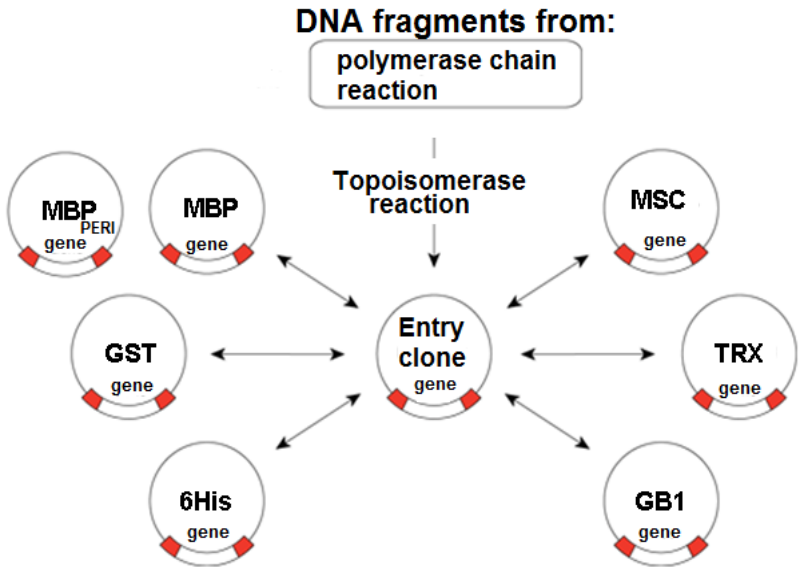

Figure 14. The two reaction of the Gateway: a PCR reaction and the recombination in differents expression vectror.

Gateway technology allows one-step cloning in the pENTR vector, and by site-specific recombination the target gene can be inserted in different expression vectors. The entry vector is obtained via recombination reaction of the pENTR/TOPO vector with our gene (PCR fragment); the reaction is catalyzed by the Topoisomerase I. After isolation of the entry vector, the second step is to generate an expression construct by performing an LR recombination reaction between the entry clone and a Gateway destination vector of choice. This cloning method is faster due to the higher reaction efficiency and to the fact that only sequencing of the entry clone is required, and most of all, the destination vector are compatible with one single entry clone making the parallel approach easier. Moreover, using different destination vectors allows expressing a chosen protein with different fusions or tags, which can increase solubility, yield and make the purification of the target much easier. However, the main function of an expression vector is to

yield the product of a gene (usually the more product the better). Therefore, expression vectors are ordinarily equipped with very strong promoters; the rationale is that the more mRNA that is produced, the more protein product will be made. The ideal promoter is strong, has a low basal expression level, is easy to induce and is independent from the common components of culturing media. The most used promoter system for the bacterial expression of recombinant proteins is the T7/lac promoter.[16] Genes under the control of T7/lac promoter can be transcribed by T7 RNA polymerase, in presence of lactose. Since *E.coli* cells do not produce this type of RNA polymerase, in order to use this promoter system they have to be genetically modified by incorporation of the genes encoding the T7 RNA polymerase, the lac promoter and the lac operator into their genome. The repressor is displaced from the lac operator when lactose or a similar molecule like Isopropyl β-D-1-thiogalactopyranoside (IPTG), is added to the culture (**Fig.15**). IPTG activates genes encoding the T7 RNA polymerase and the target protein in the plasmid, because lac operators are located upstream in the bacterial genome.

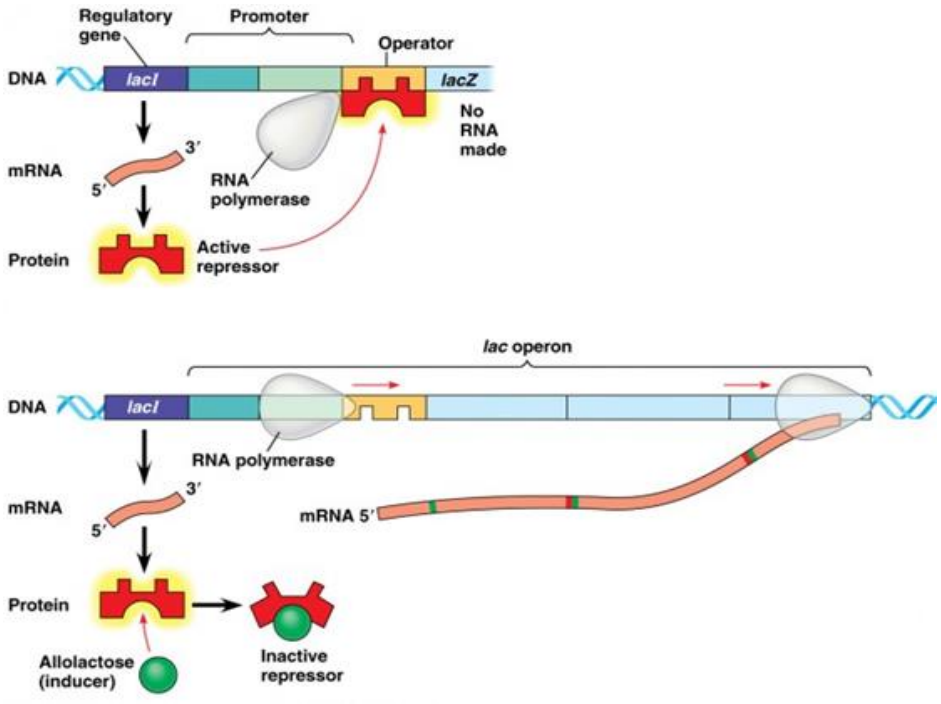

Figure 15.. Function of the *lacI* operator; operative way of the repressor and conformational modification of the repressor in the present of the inductor.

Because of the high selectivity of the T7 RNA polymerase, almost all of the cell's resources are converted to target gene expression and the amount of desired product can reach up to 50% of the total cell protein in few hours after induction. In some cases, (e.g. toxic or membrane proteins) the basal expression of the recombinant protein has to be reduced. In order to achieve this, host strains containing the pLysS or pLysE vectors that express T7 lysozyme (natural inhibitor of T7 RNA polymerase) should be used.

3.4. Protein expression

After bio-informatic characterization and choice of the cloning strategy several conditions for the target protein expression have to be tested in order

to obtain a high yield of soluble protein. The variables which affect the expression of a recombinant protein are: host strain, growth medium and induction parameters (temperature, IPTG concentration and duration of induction step). A preliminary expression test is performed in a small-volume scale using at least:

- different E.coli strains (e.g.: Bl21(DE3), Bl21(DE3) Ripl codon+ hight expression of tRNA ,Bl21(DE3)pLysS a protease deficient strain, Bl21(DE3) Rosetta for rare codons containing genes and Origami(DE3) for disulphide containing proteins);
- different expression vectors (containing different tags and/or fusion partners);
- three expression temperatures (37-25-17°C);
- different inducer (IPTG) concentrations and different induction times (4-6-16h).

Expression results are checked on SDS polyacrylamide gels (SDS-PAGE). This kind of approach allows to explore a large set of expression conditions and to evaluate which one gives the best level of expression and yield of soluble protein. A second expression test is performed to better refine the expression conditions before the scale-up. On the basis of these preliminary results, the expression protocol can be optimised and, in case of negative results, it is possible to try the expression of mutants, change the cloning strategy, the construct or the expression system. With such an approach it is possible to find good expression conditions for many proteins. Anyway some proteins can be difficult to obtain, since *E.coli* is a prokaryote and lacks intracellular organelles, such as the endoplasmic reticulum and the Golgi apparatus, which are responsible for post-translation modifications of the produced proteins. In case of negative results, variables like bacterial strain,

induction time, the kind of vectors and expression promoters can be modified. If the main fraction of the protein is produced in the insoluble fraction, another approach is to try an *in vitro* refolding screening with different additives in order to get a folded and soluble protein. The last choices are to redesign the expressed domains or to switch to other expression system.[17]

In dependence of the spectroscopic technique of choice, protein expression is performed in differently composed media. In fact, when large amounts of proteins must be isolated for techniques that do not require isotopic labelling, the culture is usually performed in a rich media. Rich media contain water soluble extracts of plant or animal tissue (e.g., enzymatically digested animal proteins such as peptone and tryptone), and for this reason are rich in nutrients and minerals, assuring a fast bacterial growth and a high expression level. Their exact composition is unknown and this can impair the reproducibility of cultures. Chemically defined (or minimal) media are composed of pure ingredients in measured concentrations, dissolved in milliQ water; in this way the exact chemical composition of the medium is known, allowing high reproducibility of protein yields and grade and type of interferents. Typically, this class of media is composed of a buffering agent to maintain culture pH around physiological values, a carbon and energy source like a simple sugar (glucose) or glycerol, an inorganic nitrogen source, usually an ammonium inorganic salt and some other components in a define concentration such as metals and vitamins. In dependence of the bacterial strain and of the expressed proteins various mineral salts can be added and, if necessary, growth factors such as purified amino acids, purines and pyrimidines. Chemically defined media are easier to isotopically enrich, simply using ^{15}N and ^{13}C enriched nitrogen and carbon sources in its composition, even if isotopically enriched complex media are also

commercially available.

3.5 Protein purification

Basically, protein purification is a series of processes intended to isolate a single type of protein from a complex mixture. Protein purification is vital for the characterization of the function, structure and interactions of the protein of interest. Separation of one protein from all others is typically the most laborious aspect of protein purification. Separation steps exploit differences in protein size, physico-chemical properties and binding affinity. The location of expressed protein within the host will affect the choice of methods for its isolation and purification. Bacterial host may secrete the protein into the growth media, transport it to the periplasmic space, express a cytosolic protein or store it as insoluble inclusion bodies (IBs) inside the cistoplasm. For insoluble proteins, the first purification step is the extraction from inclusion bodies. Indeed, most of the bacterial proteins are removed by different extraction steps with native buffer conditions, while the recombinant protein is extracted from inclusion bodies with a denaturing buffer. One of the most popular techniques of purification, which can be adopted for denatured and native state proteins, is immobilized metal ion affinity chromatography (IMAC). It is based on the specific coordinate covalent bond of amino acids, particularly histidine, to metals. This common technique involves engineering the sequence in such a way that 6 to 12 histidines are added to the N- or C-terminus of the protein. The polyhistidine binds strongly to divalent metal ions such as nickel. The protein can be passed through a column containing immobilized nickel ions, which binds the polyhistidine tag. All untagged proteins pass through the column. The protein can be eluted with imidazole, which competes with the polyhistidine tag for binding to the column, or by a decrease in pH (typically to 4.5),

which decreases the affinity of the tag for the resin (**Fig.16**).

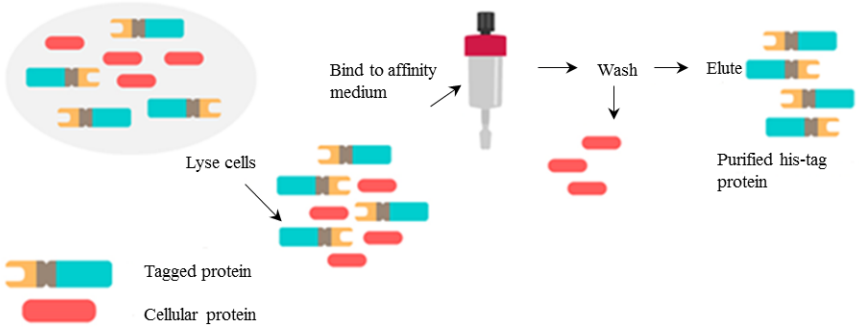

Figure 16. General purification procedure of a typical His-tagged proteins

After the affinity purification, the fusion-tag must be removed from the recombinant protein. Indeed many expression vectors are engineered to express a protease clevage site between the fusion-tag and the protein. Tobacco Etch Virus (TEV), Factor Xa, Thrombin, Prescission Protease, recombinant Enterokinase are some examples of proteases that are normally used for the cleavage of tags. A second IMAC is generally performed in order to separate the fusion from the target native protein. However, if the fused protein is expressed in inclusion bodies, it must be refolded before performing the tag cleavage to avoid the sfolding of the protease dude to the denaturant agent.

This is not always possible, since fusion tags may interfere with protein refoldind and hide the cleavage site of the protease. Gel filtration (GF) chromatography is the most common used purification step if the protein, after affinity chromatography, is not pure enough. GF is the simplest and mildest of all the chromatographic techniques; the support for gel filtration chromatography is composed of beads which contain holes, called "pores," of given sizes. Larger molecules, which can't penetrate the pores, move around the beads and migrate through the spaces which separate the beads faster than the smaller molecules, which may penetrate the pores. Size

exclusion can be performed on a “rough” level, separating the components of a sample in major groups to remove for example high or low molecular weight contaminants or to exchange buffers, while high resolution fractionation of bio- molecules allows to isolate one or more components of a protein mixture, to separate monomers from aggregates and last but not least to determine molecular weights or to perform a molecular weight distribution analysis, provided that suitable standards are available.

3.6. Protein characterization

3.6.1. Metals content determination by ICP

Inductively Coupled Plasma (ICP) is an analytical technique used for the detection of trace metals and allows multi-elemental, simultaneous analysis of elements in the periodic table in a mass range of 7 to 250 (from Li to U), with excellent sensitivity (one part in 10^{15}, part of quadrillion ppq). The analytical principle used is optical emission spectroscopy, triggered by plasma ionization. The liquid sample is introduced in the pre-chamber, usually by means of a peristaltic pump, then nebulized and entrained in the flow of plasma support gas, which is typically Argon (**Fig.17**). Making the plasma from argon, instead of other gases, has several advantages. First, argon is abundant (in the atmosphere, as a result of the radioactive decay of potassium) and also has a higher first ionization potential than all other elements. Because of this high ionization energy, the reaction ($Ar^+ + e^- \rightarrow Ar$) is less energetically favorable than the reaction

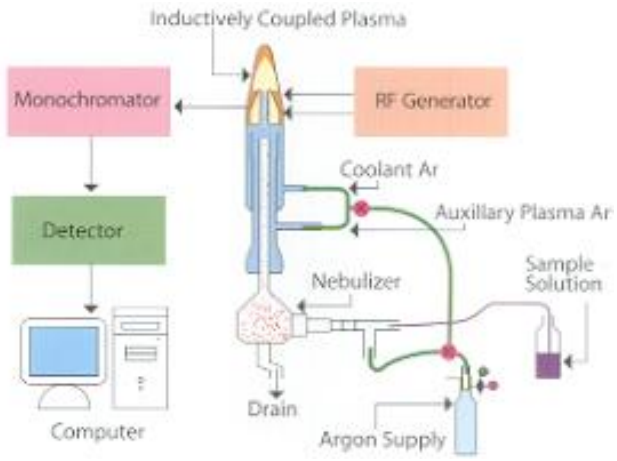

Figure 17. General scheme of an ICP instrument

The analytes are excited into a state of radiated light emission by the plasma vapour and the emitted radiation is converted to an electrical signal that can be measured quantitatively by resolving the light into its component radiation (almost always by means of a diffraction grating). The light intensity is measured, at the specific wavelength for each element line, with a CCD (*charge coupled device*, basically an array of tiny, light-sensitive diodes) which converts it to electrical signals. The electron signal intensity is then compared to previously measured intensities of standard solutions of the target elements, and a concentration is computed. This spectroscopic technique is very suitable for the protein's metal content determination, since it requires very small amounts of sample, and is not perturbed by the polypeptidic matrix.

3.6.2. Electron Paramagnetic Resonance (EPR)

Electron paramagnetic resonance (EPR) or Electron spin resonance (ESR) spectroscopy is a very powerful and sensitive method for the characterization of the electronic structures of materials with unpaired electrons. There is a

variety of ESR techniques, each with its own advantages. In continuous wave ESR (CW-ESR), the sample is subjected to a continuous beam of microwave irradiation of fixed frequency and the magnetic field is swept[29]. Different microwave frequencies may be used and they are denoted as S-band (3.5 GHz), X-band (9.25 GHz), K-band (20 GHz), Q-band (35 GHz) and W-band (95 GHz). EPR is a technique for studying chemical species that have one or more unpaired electrons, such as organic and inorganic free radicals or inorganic complexes possessing a transition metal ion. Electron paramagnetic resonance is a magnetic resonance technique, based on the interaction of unpaired electron spins with an external magnetic field. The essential aspects of EPR may be illustrated by considering the hypothetical case of a single isolated electron. This electron is characterized by the quantum number S = 1/2 and possesses a magnetic moment:

$$\vec{\mu} = -g_e \cdot \beta_e \cdot \vec{S}$$

with g_e=2.0023 is the electron g-factor or Landé-factor, β_e=9.42·10^{-24} J.T^{-1}, the electronic Bohr magneton and $\vec{S}$ the dimensionless electron spin vector. In a magnetic field, B_0, there are two energy states for this electron, as illustrated in **Fig.18**. This interaction, known as the Zeeman interaction, is expressed by the following Hamiltonian:

$$\overline{H_{ZI}} = -\mu_e \cdot \overline{B} = g_e \cdot \beta_e \cdot B_0 \cdot S_z$$

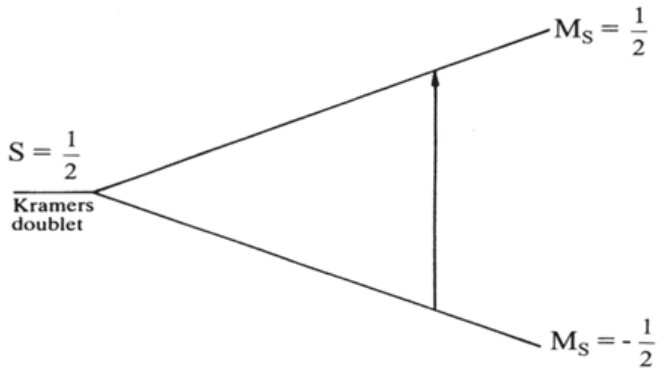

Figure 18. Splitting of the energy levels of an electron spin subjected to a magnetic field.

In ESR spectroscopy, the magnetic component of a microwave energy, which is perpendicular to the magnetic field B_0, induces microwave energy absorption subject to the resonance condition:

$$\Delta E = h \cdot \nu = g_e \cdot \beta_e \cdot B_0$$

where ν is the microware frequency. In a typical experiment the sample is placed in a resonant cavity which has a high sensitivity at a fixed microwave frequency, the magnetic field B_o is varied until resonance occurs at the value B given by the equation above[29]. By observing spectral line width and intensity, it is possible to obtain information about the spin environment. Electron spin exchange between identical and non-identical molecules, chemical exchange between the paramagnetic molecule and its environment, and the interaction of nearby molecules having unpaired spins are some examples of environmental effects which can influence line width and intensity in the EPR spectrum. Moreover, an observed spectrum can split in several lines referred to as hyperfine structure, arising from the electrons interacting with surrounding nuclear spins. This last property becomes very useful when investigating biological molecules that contain transition metal ions in their structure, since it can be exploited to characterize their

coordination environment in dependence of their intrinsic geometry.

3.6.3. Mass spectrometry

Mass Spectrometry is a powerful technique for identifying unknowns, studying molecular structure and reaction, and probing the fundamental principles of chemistry[30]. For large samples such as biomolecules, molecular masses can be measured with an accuracy of 0.01% of the total molecular mass of the sample. Mass spectrometry can be used for different types of characterization:

- Accurate molecular weight measurements, to determine the purity of a sample, to verify amino acid substitutions, to detect post-translational modifications, to calculate the number of disulphide bridges;
- Reaction monitoring: monitor enzyme reactions, chemical modification, protein digestion;
- Amino acid sequencing: sequence confirmation, characterisation of peptides, identification of proteins by databases from proteolytic fragmentation;
- Protein structure: protein folding monitored by H/D exchange, protein-ligand complex formation under physiological conditions, macromolecular structure determination.

Mass spectrometers can be divided into three fundamental parts: the ionization source, the analyzer and the detector (**Fig.19**).

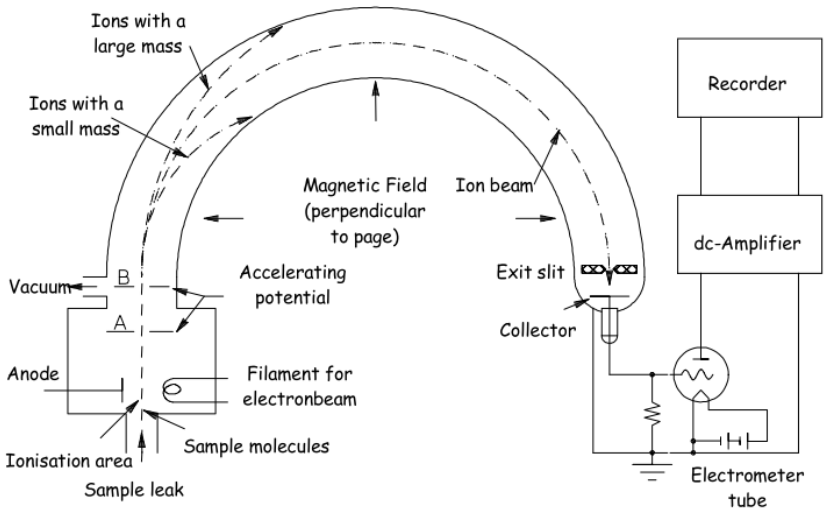

Figure 19. schematic reproduction of a mass-spectrometer

Sample molecules are ionized in the ionization source; these ions are extracted into the analyzer region of the mass spectrometer where they are separated according to their mass (m)-to-charge (z) ratios (m/z). The separated ions are detected and this signal sent to a data system where the m/z ratios are stored together with their relative abundance for presentation in the format of a m/z spectrum. Many ionization methods are available, each with its own advantages and disadvantages, and the choice depend on the type of sample under investigation and the mass spectrometer available. The ionization methods used for the majority of biochemical analyses are:

- Electrospray Ionization[31] (ESI): is produced by applying a strong electric field, under atmospheric pressure,to a liquid passing through a capillary tube with a weak flux (normally 1–10μlmin−1). The electric field is obtained by applying a potential difference of 3–6kV between this capillary and the counter-electrode, separated by 0.3–2 cm, producing electric fields of the order of 10^6V m^{-1} (**Fig.20**).

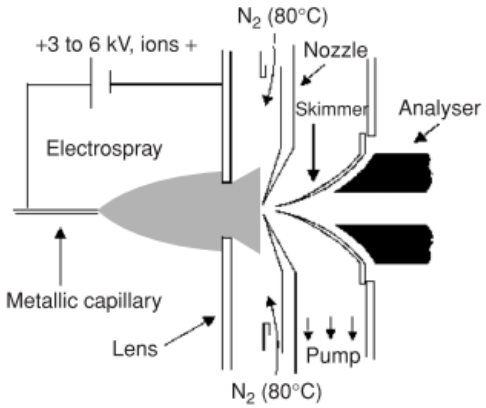

Figure 20. ESI injector

- Matrix Assisted Laser Desorption Ionization[31] (MALDI): it's a widespread and powerful source for the production of intact gas-phase ions from a broad range of large, non-volatile and thermally labile compounds such as proteins, oligonucleotides, synthetic polymers and large inorganic compounds. MALDI[20] is achieved in two steps. In the first step, the compound to be analyzed is dissolved in a solvent called the matrix; the second step involves ablation of bulk portions of this solid solution by intense laser (**Fig.21**).

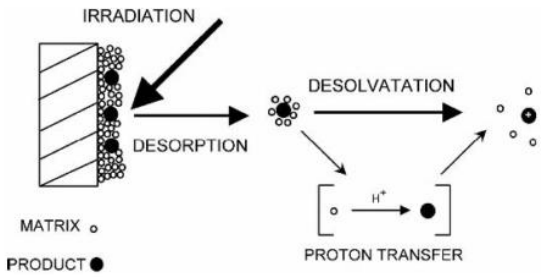

Figure 21. MALDI method.

The main function of the mass analyzer is to separate, or resolve, the ions formed in the ionization source of the mass spectrometer according to their

mass-to-charge (m/z) ratios. There are a number of mass analyzers currently available, including quadrupoles, time-of-flight (TOF)[21] analyzers**,** magnetic sectors, both Fourier transform and quadrupole ion traps, and Orbitrap. These mass analyzers have different features, including the m/z range that can be covered, the mass accuracy, and the achievable resolution. The detector monitors the ion current, amplifies it and the signal is then transmitted to the data system where it is recorded as mass spectra. The m/z values of the ions are plotted against their intensities to show the number of components in the sample, the molecular mass of each component, and the relative abundance of the various components in the sample. The time-of-flight (TOF) analyzer separates ions according to their mass (m)-to-charge (z) (m/z) ratios, by measuring the time it takes for ions to travel through a field free region known as the flight tube. The heavier ions are slower than the lighter ones. In negative ionization mode, the deprotonated molecular ions (M^-) are usually the most abundant species, accompanied by some salt adducts and possibly traces of dimeric or doubly charged materials. Negative ionization can be used for the analysis of oligonucleotides and oligosaccharides. In positive ionization mode, the protonated molecular ions (M^+) are usually the dominant species, although they can be accompanied by salt adducts, a trace of the doubly charged molecular ion at approximately half the m/z value, and/or a trace of a dimeric species at approximately twice the m/z value. Positive ionization is used in general for protein and peptide analyses.[21] In Orbitrap[22] ions are electrostatically trapped in an orbit around a central, spindle shaped electrode. The electrode confines the ions so that they both orbit around the central electrode and oscillate back and forth along the central electrode's long axis. This oscillation generates an image current in the detector plates which is recorded by the instrument. The frequencies of these image currents depend on the mass to charge ratios of the ions. Mass spectra are obtained by Fourier

transformation of the recorded image currents. Orbitraps have a high mass accuracy, high sensitivity and a good dynamic range.[22]

3.6.4. Circular dichroism (CD)

Circular dichroism (CD) spectroscopy is a spectroscopic technique where the CD of molecules is measured over a range of wavelengths. CD spectroscopy is used extensively to study chiral molecules of all types and sizes, but it is in the study of large biological molecules where it finds its most important applications. A primary use is in analysing the secondary structure or conformation of macromolecules, particularly proteins as secondary structure is sensitive to its environment, temperature or pH, circular dichroism can be used to observe how secondary structure changes with environmental conditions or on interaction with other molecules. Structural, kinetic and thermodynamic information about macromolecules can be derived from circular. Plane polarised light can be viewed as being made up of 2 circularly polarised components of equal magnitude (**Fig.22 AI**), one rotating counter-clockwise (left handed, L) and the other clockwise (right handed, R). Circular dichroism (CD) refers to the differential absorption of these 2 components. If, after passage through the sample being examined, the L and R components are not absorbed or are absorbed to equal extents, the recombination of L and R would regenerate radiation polarised in the original plane (**Fig.22 AII**). However, if L and R are absorbed to different extents, the resulting radiation would be said to possess elliptical polarisation (**Fig. 22 AII**). A CD signal will be observed when a chromophore is chiral (optically active) for one of the following reasons:

- it is intrinsically chiral because of its structure,
- it is covalently linked to a chiral centre in the molecule

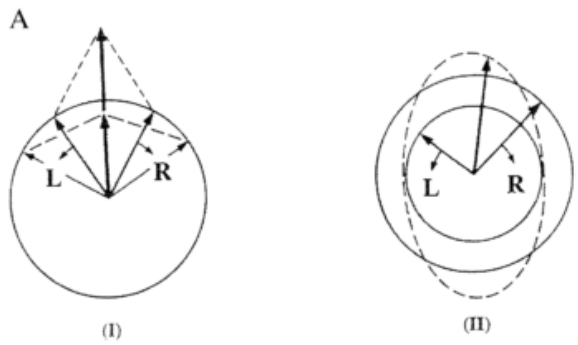

Figure 22. (AI) the two components of the polarization light L and R; (AII) elliptical polarisation generate from different absorption of the two component L and R.

We can have two different signals in a CD spectrum (**Fig.22 B**): positive if the L component is absorbed more than the R component or negative if the R component is absorbed more than L component[32].

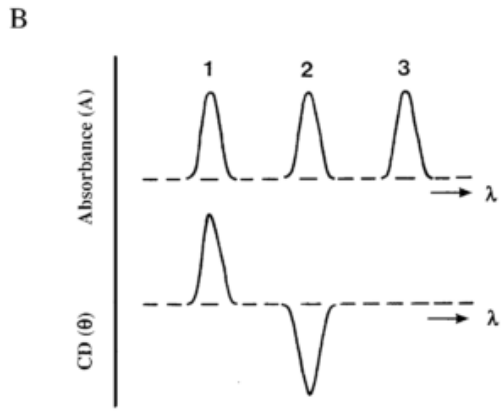

Figure 22 B: peak positive in 1 due to a L major absorption, negative peak in 2 create by a major absorption of R respect to L and a non-chiral molecules in 3

In proteins the major optically active groups are the amide bonds of the peptide backbone, typically disposed in highly ordered arrays such as α-helices, β-pleated sheets or random coli. In proteins, the chromophores of

interest include the peptide bond (absorption below 240 nm), aromatic amino acid side chains (absorption in the range 260 to 320 nm) and disulphide bonds (weak broad absorption bands centred around 260 nm). In addition, non-protein cofactors can absorb over a wide spectral range. Absorption in the region of 240 nm is due principally to the peptide bond; there is a weak but broad $n \rightarrow \pi^*$ transition centred around 220 nm and a more intense $\pi \rightarrow \pi^*$ transition around 190 nm. Each secondary structure presents a characteristic CD spectrum, so the CD spectroscopy in particular good to study the protein folding[33]. The tertiary folding of the polypeptide chain can place these side chains in chiral environments, thus giving rise to CD spectra which can serve as characteristic fingerprints of the native structure. CD in the near UV, visible and near IR can give a great deal of information on the environments of cofactors (which play an integral role in the biological activity of the protein) or of other non- covalently bound ligands. Typically, the free ligand or cofactor has little or no CD signal; the observed CD signals in the complex therefore indicate that the binding site of ligand or cofactor confers chirality.

Circular dichroism spectroscopy is particularly good to:

- Determine whether a protein is folded, and if so characterizing its secondary structure;
- Compare the structures of a protein obtained from different sources (e.g. species or expression systems) or comparing structures for different mutants of the same protein;
- Study the conformational stability of a protein under stress (thermal stability, pH stability, and stability to denaturants) and how this stability is altered by buffer composition or addition of stabilizers;

- Determine whether protein-protein interactions alter the conformation of the protein.

3.6.5. NMR – protein structural characterization

Discovering the tertiary structure of a protein, or the quaternary structure of a protein or a complexes, can provide important clues about how the protein performs its function. Nuclear Magnetic Resonance (NMR) is an experimental method of structure determination that can produce information at atomic resolution[23]. NMR experiments are able to provide information from which a subset of distances between pairs of atoms can be estimated, and the final possible conformations for a protein are determined by solving a distance geometry problem. Moreover, NMR spectroscopy is unique among the methods available for three-dimensional structure determination of proteins at atomic resolution, since the NMR data can be recorded in solution[24,25]. Considering that body fluids such as blood, stomach liquid and saliva are protein solutions where these molecules perform their physiological functions, knowledge of the molecular structures in solution is highly relevant. Furthermore, in addition to protein structure determination, NMR applications include investigations of dynamic features of the molecular structures, as well as studies of structural, thermodynamic and kinetic aspects of interactions between proteins and other solution components, which may either be other proteins or low molecular weight ligands.[23,24] The NMR phenomenon is based on the fact that nuclei of atoms have magnetic properties that can be utilized to yield chemical information. Quantum mechanically subatomic particles (protons, neutrons and electrons) have spin. A spinning nucleus acts as a tiny bar magnet

oriented along the spin rotation axis (**Fig.23**).

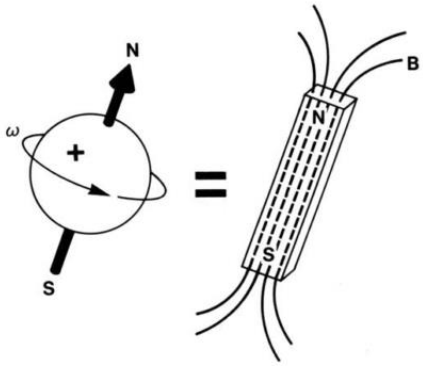

Figure 23 The charged nucleus (e.g., ^{1}H) rotating with angular frequency ω (ω = 2πν) creates a magnetic field B and is equivalent to a small bar magnet whose axis is coincident with the spin rotation axis.

This tiny magnet is often called a nuclear spin. In some atoms (^{12}C, ^{16}O, ^{32}S) these spins are paired and cancel each other out so that the nucleus of the atom has no overall spin. However, in many atoms (^{1}H,^{13}C, ^{31}P, ^{15}N, ^{19}F etc) the nucleus possess an overall spin that is different to zero (I = 1/2 for the previous nuclei). When there is no external or applied magnetic field (B_0), the nuclear spins orient randomly; however, when there is an applied magnetic field, the nuclei orient themselves with or against the larger applied field. The α-spin state is parallel to the applied force and has lower energy than the β-spin state that is antiparallel to the applied force (**Fig.24**)

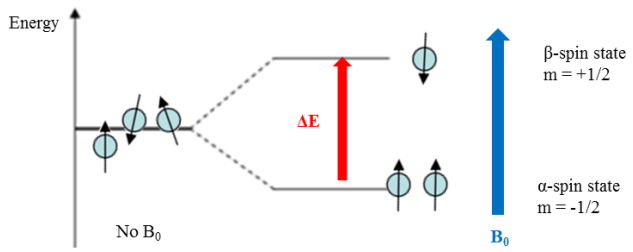

Figure 24. Proton spin states in a present of a mangnetic field

The small nuclear magnet may spontaneously "flip" from one orientation (energy state) to the other as the nucleus sits in the large magnetic field. However, if energy equal to the difference in energies (ΔE) of the two nuclear spin orientations is applied to the nucleus (or more realistically, group of nuclei), much more flipping between energy levels is induced. The irradiation energy is in the RF range is typically applied as a short (milliseconds or microseconds) pulse. The absorption of energy by the nuclear spins causes transitions from higher to lower energy as well as from lower to higher energy. This two-way flipping is a hallmark of the resonance process. The energy required to induce flipping and obtain an NMR signal is just the energy difference:

$$\Delta E = \gamma h B_0 / 2\pi$$

where h is Planck's constant ($6.62607004 \times 10^{-34}$ joule·second). The Bohr condition ($\Delta E = h\nu$) enables the frequency ν_0 of the nuclear transition to be written as:

$$\nu_0 = \gamma B_0 / 2\pi$$

this last eqaution is often referred to as the Larmor equation, and $\omega_0 = 2\pi \nu_0$ is the angular Larmor resonance frequency. The gyromagnetic ratio γ is a constant for any particular type of nucleus and is directly proportional to the strength of the tiny nuclear magnet. So the energy required to induce flipping and obtain an NMR signal is just the energy difference between the two nuclear orientations and is shown in Fig. ddd, and depend on the strength of the magnetic field B_0 in which the nucleus is placed. The energy absorbed by the nuclear spins induces a voltage that can be detected by a suitably tuned coil of wire, amplified, and the signal displayed as a free induction decay (FID) in the time domain; Fourier transformation of the FID, convert the signal in the frequency domain spectrum. What we obtain is a spectra compose by different signal at different frequency, this different are related

to the chemical shift effects. Electrons are negatively charged particles that surround nuclei within a molecule. We know that moving charged particles will generate a magnetic field. So the electrons around nuclei in a molecule generate their own magnetic field that run in the opposite direction as the lines of force generated by the external magnetic field B_0. This electronic magnetic field effect will cause protons with different chemical environments to yield resonance frequencies perturbed from the frequency defined by the applied external field B_0. Differences in the electronic environments cause the protons to experience slightly different applied magnetic fields owing to the shielding/deshielding effect of the induced electronic magnetic fields. In a large molecule such as a protein, the large number of protons create a lot of signal and linked to the different chemical environment, generate at the end a large one dimensional spectra (^{1}H-1D) with a extended overlap. For this reason, protein NMR spectra cannot be resolved in a conventional one-dimensional spectra (1D) and multi-dimensional nuclear magnetic resonance spectroscopy is required to correlate the frequencies of different nuclei. Multi-dimensional NMR spectra provide both, increased resolution and correlations which are easy to analyse.

The preparation of the protein sample is a crucial step of this process, since a highly purified protein sample is required. Inhomogeneous preparation and/or aggregation of the protein as well as low molecular weight impurities may severely harm the structure determination. Since the NMR technique exploits the property that magnetic nuclei, with an uneven spin quantum number such as the isotopes ^{1}H, ^{2}H, ^{13}C, ^{15}N, the protein need isotope labeling is necessary for NMR analysis because not all atoms are magnetically active.

There are different types of experiments that can detect through-bonds and through-space nucleus/nucleus interactions. With unlabeled protein the usual

procedure is to record a set of two dimensional homonuclear (^{1}H-^{1}H) NMR experiments starting with homonuclear thought bond (J-coupling) correlation method like:

- Correlation spectroscopy (COSY): used to identify spins which are coupled to each other, we obtain cross peak for each pair of coupling nuclei.
- Total correlation spectroscopy (TOCSY): similar to the COSY experiment, in that cross peaks of coupled protons are observed. However, cross peaks are observed not only for nuclei which are directly coupled, but also between nuclei which are connected by a chain of couplings. This makes it useful for identifying the larger interconnected networks of spin couplings.

We can also detect the homonuclear correlation thought space with methods that establish correlations between nuclei which are physically close to each other regardless of whether there is a bond between them. The most use experiment is:

- Nuclear overhauser effect spectroscopy (NOESY): we obtain a spectrum similar to COSY, with diagonal peaks and cross peaks, however the cross peaks connect resonances from nuclei that are close in space.[25,26]

Homonuclear NMR is usually restricted to small proteins or peptides because of the signal overlap problem in the case of bigger proteins. The process of structure determination starts with this experiment, but we must know other correlation for solve a structure. For this reason, we need other experiment to correlate nitrogen, carbon and hydrogen atoms. For that experiment we need an isotope enrich sample (^{15}N,^{13}C and ^{2}H)[25,26].
The ^{1}H-^{15}N HSQC (Heteronuclear Single Quantum Correlation) experiment

is probably the first and the most frequently recorded experiment in protein NMR. In this experiment we have the correlation between the proton and the nitrogen. During the condensation reaction between the amino acids, the carboxyl group (-COOH) react with the amino group ($-NH_2$) to form the peptide bond (-CO-NH) with the release of a water molecule.
Each residue of the protein (except proline and the NH_2 of the last amino acid at the C-terminal) has an amide proton attached to nitrogen in the peptide bond, so with the ^{1}H-^{15}N HSQC experiment we can correlate the proton with the nitrogen of the amide group. If the protein is folded, the peaks are usually well dispersed in the proton/nitrogen dimension, and most of the individual peaks can be distinguished. The number of peaks in the spectrum should match the number of residues in the protein (though side chains with nitrogen-bound protons will add additional peaks). It will probably be difficult to solve the structure of the protein if this is not the case. The process of structure determination is usually not undertaken until a good HSQC spectrum is obtained. In order to analyze the nuclear magnetic resonance data, it is important to get a resonance assignment for the protein. That is to find out which chemical shift corresponds to which atom. This is typically achieved by sequential walking using information derived from several different types of NMR experiment. This barrier can be overcome with 3D NMR techniques and uniformly ^{13}C and ^{15}N labelled proteins. In the case of labelled proteins, it is possible to record an experiment that transfers magnetization over the peptide bond, and thus connects different spin systems through bonds. The 3D experiments exclusively correlate the resonances of the protein backbone, and the experiments used are: HNCA, HNCACB, HN(CO)CA, HN(CO)CACB, HNCO and HN(CA)CO.
In the case of proteins with a molecular weight larger than 30 kDa we have to use experiment that help us to reduce the problems created by the larger

molecular weight; one of that is the TROSY (Transverse Relaxation Optimized Spectroscopy) experiment. The TROSY technique benefits from a variety of triple resonance NMR experiments as the 3D HNCA and HN(CO)CA.

After the backbone assign, we can use 3D experiment like H(C)CH-TOCSY and (H)CCH-TOCSY to link the side chain spin systems to the backbone assignments.[27,28]

Another field in the NMR of proteins is the paramagnetic NMR of metalloproteins. This kind of experiments are different respect to the classical diamagnetic system, in fact the present of a paramagnetic center modify the proprieties of the proteins in solution (major line broadening and major relaxation). We have now several NMR sequence to obtain the proton distance (respect to the paramagnetic center) and dihedral angle.

Protein NMR techniques are continually being used and developed. Improvements in NMR hardware (magnetic field strength, cryoprobes) and NMR methodology, combined with the availability of molecular biology and biochemical methods for preparation and isotope labeling of recombinant proteins, have dramatically increased the use of NMR for the characterization of structure and dynamics of biological molecules in solution.

References

1. Finn, R.D. et al. The Pfam protein families database. *Nucleic Acids Research* **38**, D211-D222 (2009).
2. Jensen, L.J. et al. STRING 8--a global view on proteins and their functional interactions in 630 organisms. *Nucleic Acids Res* **37**, D412-416 (2009).
3. Schneider, G. & Fechner, U. Advances in the prediction of protein targeting signals. *Proteomics* **4**, 1571-1580 (2004).
4. Emanuelsson, O., Brunak, S., von Heijne, G. & Nielsen, H. Locating proteins in the cell using TargetP, SignalP and related tools. *Nat. Protocols* **2**, 953-971 (2007).
5. Emanuelsson, O. Predicting protein subcellular localisation from amino acid sequence information. *Brief. Bioinformatics* **3**, 361-376 (2002).
6. Dosztányi, Z., Csizmok, V., Tompa, P. & Simon, I. IUPred: web server for the prediction of intrinsically unstructured regions of proteins based on estimated energy content. *Bioinformatics* **21**, 3433-3434 (2005).
7. Prilusky, J. et al. FoldIndex©: a simple tool to predict whether a given protein sequence is intrinsically unfolded. *Bioinformatics* **21**, 3435 -3438
8. Kelley, L.A. & Sternberg, M.J.E. Protein structure prediction on the Web: a case study using the Phyre server. *Nat. Protocols* **4**, 363-371 (2009).
9. Perrière, G. et al. Integrated databanks access and sequence/structure analysis services at the PBIL. *Nucleic Acids Research* **31**, 3393 -3399 (2003).
10. Varshavsky, A. The N-end rule: functions, mysteries, uses. *Proceedings of the National Academy of Sciences of the United States of America* **93**,

12142 -12149 (1996).

11. Boettner, M., Prinz, B., Holz, C., Stahl, U. & Lang, C. High-throughput screening for expression of heterologous proteins in the yeast Pichia pastoris. *Journal of Biotechnology* **99**, 51-62 (2002).
12. Ozawa, K., Wu, P.S.C., Dixon, N.E. & Otting, G. N-Labelled proteins by cell-free protein synthesis. Strategies for high-throughput NMR studies of proteins and protein-ligand complexes. *FEBS J* **273**, 4154-4159 (2006).
13. Ozawa, K., Dixon, N.E. & Otting, G. Cell-free synthesis of 15N-labeled proteins for NMR studies. *IUBMB Life* **57**, 615-622 (2005).
14. John P. Hall Applying Fusion Protein Technology to E. Coli. (2006).a <http://biopharminternational.findpharma.com/biopharm/article/articleDetail.jsp?id=301977&sk=&date=&pageID=5>
15. Landy, A. Dynamic, structural, and regulatory aspects of lambda site-specific recombination. *Annu. Rev. Biochem* **58**, 913-949 (1989).
16. Dubendorff, J.W. & Studier, F.W. Controlling basal expression in an inducible T7 expression system by blocking the target T7 promoter with lac repressor. *J. Mol. Biol* **219**, 45-59 (1991).
17. Miroux, B. & Walker, J.E. Over-production of proteins in Escherichia coli: mutant hosts that allow synthesis of some membrane proteins and globular proteins at high levels. *J. Mol. Biol* **260**, 289-298 (1996).
18. Tsumoto, K., Ejima, D., Kumagai, I. & Arakawa, T. Practical considerations in refolding proteins from inclusion bodies. *Protein Expression and Purification* **28**, 1-8 (2003).
19. Tsumoto, K. et al. Role of Arginine in Protein Refolding, Solubilization, and Purification. *Biotechnol. Prog.* **20**, 1301-1308 (2004).
20. Tanaka, K. et al. Protein and polymer analyses up tom/z 100 000 by laser ionization time-of-flight mass spectrometry. *Rapid Commun. Mass*

Spectrom. **2**, 151-153 (1988).

21. Wollnik, H. Time-of-flight mass analyzers. *Mass Spectrom. Rev.* **12**, 89-114 (1993).
22. Hu, Q. et al. The Orbitrap: a new mass spectrometer. *J Mass Spectrom* **40**, 430-443 (2005).
23. Dyson, H.J. & Wright, P.E. Insights into protein folding from NMR. *Annu Rev Phys Chem* **47**, 369-395 (1996).
24. Wüthrich, K. NMR Studies of Structure and Function of Biological Macromolecules. *Biosci Rep* **23**, 119-168 (2003).
25. Wider, G., Macura, S., Kumar, A., Ernst, R.R. & Wüthrich, K. Homonuclear two-dimensional 1H NMR of proteins. Experimental procedures. *Journal of Magnetic Resonance (1969)* **56**, 207-234 (1984).
26. Bax, A. & Lerner, L. Two-dimensional nuclear magnetic resonance spectroscopy. *Science* **232**, 960-967 (1986).
27. Bax, A. & Ikura, M. An efficient 3D NMR technique for correlating the proton and 15N backbone amide resonances with the alpha-carbon of the preceding residue in uniformly 15N/13C enriched proteins. *J. Biomol. NMR* **1**, 99-104 (1991).
28. Kay, L.E., Ikura, M., Tschudin, R. & Bax, A. Three-dimensional triple-resonance NMR spectroscopy of isotopically enriched proteins. *Journal of Magnetic Resonance (1969)* **89**, 496-514 (1990).
29. Bert M.Weckhuysen, Ralf Heidler, Robert A. Schoonheydt,. Electron Spin Resonance Spectroscopy Mol. Sieves (2004) 4: 295–335
30. Scott E. Van Bramer, An Introduction to Mass Spectrometry
31. Edmond de Hoffmann,Vincent Stroobant. Mass Spectrometry (Third Edition) Copyright C® 2007 John Wiley & Sons Ltd,
32. Sharon M. Kelly, Thomas J. Jess, Nicholas C. Price. How to study

proteins by circular dichroism. Biochimica et Biophysica Acta 1751 (2005) 119 – 139

33. Sharon M. Kelly, Nicholas C. Price. The Use of Circular Dichroism in the Investigation of Protein Structure and Function. Current Protein and Peptide Science, 2000, 1, 349-384

-Chapter 4-

EXPERIMENTAL SECTION

4.1. Glutaredoxin 3 (Grx3): protein production

The cDNA coding for human GRX3 (UniProtKB/Swiss-Prot: O76003) was acquired from Source BioScience LiefeScience. Four different constructs (full-length 1-335 aa, Trx domain 1-119 aa, Trx/Grx 1-236 aa, GrxA 120-236 aa, GrxA-GrxB 130-335 aa), were amplified by PCR and subsequently inserted into the pETG20 A vector modified with Trx-Histag using the Gateway technology (Invitrogen). The Cys to Ala substitutions in GRX3 were obtained using the QuikChange® Site-Directed mutagenesis kit from Stratagene (La Jolla, CA). BL21-CodonPlus (DE3)-RIPL Competent *E.coli* Cells (Stratagene, La Jolla, CA) were transformed with the desired constructs, and cells were grown in LB or minimal media (with $(^{15}NH_4)_2SO_4$ and/or [^{13}C]-glucose) containing 1 mM ampicillin and chloramphenicol at 37° C under vigorous shaking until the OD at 600 nm reached 0.6. For expression of holo GRX3 constructs, cells were grown in the presence of 250 µM FeCl3. Protein expression was induced by adding 0.5 mM IPTG and expression was performed over night at 17°C. Cells were harvested by centrifugation at 7500 x g and resuspended in degassed lysis buffer (50 mM Tris-HCl pH 8 containing 500 mM NaCl, 5 mM imidazole and 5 mM DTT, DNAase 0.01mg/ml, lysozyme 0.01 mg/ml and $MgSO_4$ 1mM. For the Trx/Grx, GrxA and full-length constructs, 5 mM GSH was added. Cell disruption was performed on ice by sonication alternating 30 seconds of sonication and 5 minutes of resting for 10 times. Except for the Trx domain construct, the following purification steps were performed under anaerobic conditions. The soluble extract, obtained by ultracentrifugation at 40000 x g, was loaded on a HiTrap chelating HP column (GE Healthcare) and the recombinant proteins were eluted with 50 mM Tris-HCl pH 8, 500 mM NaCl and 500 mM imidazole. 5 mM DTT and 5 mM GSH were added to the

protein-containing fractions (except for the Trx domain construct). The proteins were then concentrated with an Amicon Ultra-15 Centrifugal Filter Units with a MWCO of 10 kDa (Millipore). Cleavage of the tags was performed by TEV protease in 50 mM Tris-HCl pH 8, 500 mM NaCl, 5 mM imidazole, 0.3 mM EDTA, 5 mM GSH and 2 mM DTT overnight at room temperature. Than the protein solution was loaded again on the His Trap column to separate the digested proteins from the tags. Size exclusion chromatography was performed as the final purification step using a HiLoad Superdex75 16/60 column (GE Healthcare) and degassed 50 mM phosphate buffer pH 7, 5 mM GSH, 5 mM DTT as running buffer. Apo proteins were obtained by treatment of the protein (purified in presence of oxygen and without adding GSH or DTT into the buffers) with 100 mM EDTA and 20 mM $K_4[Fe(CN)_6]$. Full-length, Trx/Grx, GrxA and GrxA-GrxB constructs were chemically reconstituted by incubating the purified apo proteins in degassed 50 mM Tris, 100 mM NaCl, 5 mM DTT, 5 mM GSH at pH 8 with 1 mM $FeCl_3$ and 1 mM Na_2S over night at room temperature. Iron concentration was determined by inductively coupled plasma mass spectrometry (ICP-MS). To estimate the iron content a standard procedure has been followed with few modifications (Zhang, et al., 2008). 350µL of each sample dilution were treated with 50µl of 5% SDS for 5 minutes and then reduced with 50µl of 10mM sodium dithionite followed by addition of 50µl of 10mM bathophenanthrolinedisulfonic acid disodium salt (BPS) to chelate iron(II). Samples were
incubated in the dark for 20 minutes, mixed and centrifuged for 5 minutes at 12000 x g.
Absorbance at 515nm was measured and the concentration was estimated through standard

curve analysis using $NH_4Fe(SO_4)_2$. To estimate the sulfide content, a standard procedure has been followed with few modifications (Siegel, 1965). Samples (600µl) were treated with 50µl of 6% NaOH and incubated for 5 minutes. Samples were mixed with 125µl of 0.1% DPD (N,N-dimethyl-pphenylenediamine dihydrochloride, Sigma-Aldrich) followed by addition of 50µl of 11.5 mM $FeCl_3$ and incubated for 30 minutes at room temperature. Sulfide concentration was estimated at 670nm through standard curve analysis using sodium sulfide Na_2S.

4.1.1. Analytical gel filtration

The aggregation state of the apo and holo forms of GRX3 WT plus all the contruscts or the mixture of GRX3 and anamorsin was analyzed using analytical gel filtration. Purified samples were loaded on a SuperdexTM 75 HR 10/30 analytical column (Amersham Bioscience) or Superdext 200 increase 10/300 GL (GE Healthacare). Degassed 50 mM phosphate buffer pH 7, 5 mM GSH, 5mM DTT was used as an eluent.

4.1.2. UV/vis and EPR spectroscopy

UV-visible spectra of holo GRX3, holo GrxA, holo GrxA-GrxB, holo Trx-GrxA and holo anamorsin in degassed 50 mM phosphate buffer pH 7, 5 mM GSH and 5 mM DTT were performed on a Cary 50 Eclipse spectrophotometer. EPR spectra of holo GRX3 full-length plus all the holo different constructs and holo anamorsin with the [2Fe-2S] cluster in the reduced state were recorded in 50 mM phosphate buffer pH 7, 5mM GSH, 5 mM DTT and 10% glycerol with a Bruker Elexsys E500 spectrometer equipped with a X-band microwave bridge (microwave frequency, 9.45 GHz) and an ER 4131 VT (unit for temperature control). EPR parameters were the following: sample temperature 45 K, microwave frequency 9.45

GHz; microwave power 5 mW; modulation frequency 9,387691 GHz; modulation amplitude 2500 G, time constant 167 ms. To reduce the cluster, sodium dithionite was added, in a 1:1 protein/dithionite ratio, under anaerobic conditions and the sample was immediately frozen.

4.1.3. Structural characterization of GRX3 by NMR spectroscopy

Standard 1H-detected triple-resonance NMR experiments for backbone resonance assignment were recorded on 0.5 to 1 mM ^{13}C, ^{15}N-labeled samples (apo forms of GRX3 Trx/Grx, Trx and GrxA domain) at 298 K, using a Bruker AVANCE 500 MHz (GRX3 Trx/Grx and GrxA domains) or 700 MHz (Trx domain) spectrometer. To identify backbone amide resonances affected by paramagnetic relaxation effects, ^{1}H-^{15}N HSQC, edited by a 1H inversion recovery and observed in the antiphase component (IR-HSQC-AP), were collected, at 700 MHz and 311 K, using a 512 × 100 data point matrix, collected over a 25 × 40 ppm spectral region. A total of 2,048 scans per fid were acquired, using inversion recovery, inept transfer, and recycle delays of 50 ms, 0.83 ms, and 55 ms, respectively. All NMR data were processed using the Topspin software package and were analyzed with the program CARA[3,4]. Secondary structure analysis has been performed by TALOS+[1]and the webserver PECAN[2]. ^{15}N longitudinal (R^1) and transverse (R^2) relaxation rates and steady-state heteronuclear NOE measurements were performed at 14.1 T (600MHz) using the standard pulse sequences on ^{15}N-labeled samples. The overall rotational correlation times were estimated from the R^2/R^1 ratio, using the program QUADRATIC_DIFFUSION, excluding relaxation data of NHs having an exchange contribution to the R^2 value or exhibiting large-amplitude internal motions.

1D ^{1}H paramagnetic NMR spectra of 0.5 mM holo GRX3 (in D_2O, 50 mM phosphate buffer, pH 7, 5 mM GSH and 5 mM DTT) were recorded at 298 K

on a Bruker Avance 600 MHz spectrometer, equipped with a selective ^{1}H probe head (SEL ^{1}H 5 mm), to detect H_{α} and H_{β} signals of the iron ligands. These spectra were acquired by means of the super-WEFT sequence with a recycle time of 50 ms.

4.1.4. Cluster transfer and interaction between GRX3 and anamorsin

To monitor cluster transfer, holo GRX3 full-length was incubated with the His12-tag apo form of anamorsin (protein ratio ~ 1:2) in 50 mM phosphate buffer pH 7, 5 mM GSH and 5 mM DTT and, after separating the two proteins through affinity chromatography, UV-visible, EPR spectra and paramagnetic NMR spectra were recorded as described above. The same experiment was performed for holo anamorsin and apo GRX3 full-length.
Cluster transfer and interaction between GRX3 and anamorsin was followed by NMR titrating ^{15}N-labeled holo GRX3 (Trx-domain, Trx/Grx) with unlabeld full-length anamorsin in 50 mM phosphate buffer pH 7, 5 mM GSH and 5 mM DTT containing 10% (v/v) D_2O at 298K and monitoring chemical shift changes by ^{1}H-^{15}N HSQC spectra.
Protein-protein interaction between ^{15}N-labeled apo GRX3 (Trx-domain, Trx/Grx, GrxA, GrxA-GrxB, full-length) and unlabeled apo anamorsin (N-terminal domain, C-terminal domain, full-length) and ^{15}N-labeled apo anamorsin (full-length, N-terminal domain) and unlabeled apo GRX3 (Trx-domain, Trx/Grx, GrxA, full-length) in 50 mM phosphate buffer pH 7, 5 mM GSH and 5 mM DTT containing 10% (v/v) D_2O at 298K was investigated by NMR monitoring chemical shift changes by ^{1}H-^{15}N HSQC spectra after addition of increasing amounts of the unlabeled partner.

4.2. Anamorsin: protein production

The cDNA coding for the human full-length anamorsin (UniProtKB/Swiss-Prot: Q6FI81, Genbank Accession No. BC024196) was commercially acquired from Imagenes (ORF Shuttle Clone IOH4051) and after amplification by PCR inserted into the Gateway® pEntr-TEV-dTopo vector (Invitrogen^{TM}). The N-terminal domain and the C-terminally truncated (1-270aa) construct were PCR-amplified from the pEntr-TEV-D-Topo vector containing full-length anamorsin and then re-inserted into the same vector. For recombinant expression, all the three constructs were cloned via the Gateway® technology (InvitrogenTM) into the expression vector pCold-DEST 12His-tag. This vector is based on the pColdI (Takara Bio Inc, Japan) and has been modified by us to make it suitable for the Gateway® system. According to the vector construction all proteins are expressed with an N-terminal His12 tag and, for the release from it, a sequence coding for the specific recognition site of the TEV protease was located at the 5' end of the codifying sequences. All the recombinant proteins contain four additional amino acids, GSFT, at the N-terminus. BL21-CodonPlus (DE3)-RIPL Competent Cells (Stratagene, La Jolla, CA) were transformed with the anamorsin/pCOLD-DEST construct for the protein expression. The cultures were grown at 37°C under vigorous shaking overnight, diluted 1:100 into LB medium or minimal medium containing 100 µg/ml ampicillin and 34 µg/ml chloramphenicol and grown further at 37°C until OD at 600 nm reached 0.8-1. The culture was transferred to 25°C and protein expression was induced by addition of IPTG to a final concentration of 0.5 mM and the incubation was continued for 3 h (rich media) or 4 h (minimal media). The full-length anamorsin and C-terminally truncated construct were expressed in the presence of 125 µM FeCl3. Subsequently, the cells were harvested by

centrifugation (7500 x g, 15 min, 4°C) and the pellets were stored at -20°C. The frozen cell pellets were re-suspended in degassed lysis buffer (Tris-HCl 50mM, NaCl 500mM, glycerol 5%, imidazole 20mM, pH 8) containing lysozyme (0.01mg/ml), DNA-se I (0.01mg/ml) and MgSO4 (1mM). Cells were incubated on ice for 30 min with gentle shaking and subsequently, disrupted on ice by sonication alternating 30 seconds of sonication and 5 minutes of resting for 10 times. The resulting cell lysate was centrifuged (400000 x g, 40 min, 4°C). All the proteins were purified by immobilized metal ion affinity chromatography, under anaerobic conditions in a glove box for the full-length protein and the C-terminally truncated construct and under aerobic conditions for the N-terminal domain. The supernatant was applied to a nickel-charged HiTrap chelating HP column (GE Healthcare) and the proteins were eluted with degassed elution buffer (50mM Tris-HCl, 500mM NaCl, 500 mM imidazole, 5% glycerol, pH 8) and concentrated in presence of 3mM DTT with an Amicon Ultra-15 Centrifugal Filter Units with a MWC of 10 kDa (Millipore). The His-tag was cleaved from the recombinant proteins by incubation overnight with TEV protease (3µl TEV/1mg anamorsin) and used for reverse Ni(II) affinity chromatography in order to remove the cleaved His-Tag. Size exclusion chromatography was performed as the final purification step using a HiLoad 16/60 Superdex 75 pg column (GE Healthcare) and degassed 50mM Tris-HCl, 500mM NaCl, 2mM DTT, 5% glycerol, pH 8 as a running buffer. The proteins were used directly for analysis or frozen in liquid nitrogen and stored at -80°C.

4.3. BOLA2: protein production

The cDNA coding for human BOLA2 (UniProtKB/Swiss-Prot: Q9H3K6) was acquired from Life technologies. BOLA2 gene were amplified by PCR and subsequently inserted into the pET21a vector using the restriction enzymes NdeI and BanH I. BL21(DE3)gold competent E. coli cells (Stratagene, La Jolla, CA) were transformed with the obtained plasmid, and cells were grown in LB or minimal media (with $(^{15}NH_4)_2SO_4$ and/or [^{13}C]-glucose) containing 1 mM ampicillin at 37° C under vigorous shaking until the OD at 600 nm reached 0.6. Protein expression was induced by adding 0.5 mM IPTG and cells were grown 4 hours at 25°C. Cells were harvested by centrifugation at 7500 x g and resuspended in lysis buffer (25 mM MES pH 6 containing 0.01 mg/ml DNAase, 0.01 mg/ml lysozyme, 1 mM $MgSO_4$, 0.5 mM EDTA and 5 mM DTT). Cell disruption was performed on ice by sonication and the soluble extract, obtained by ultracentrifugation at 40000 x g, was loaded on HiTrap SP FF column (GE Healthcare) and BOLA2 protein was eluted with 25 mM MES pH 6, 1 M NaCl and 5 mM DTT. The protein was then concentrated with an Amicon Ultra-15 Centrifugal Filter Units with a MWCO of 3 kDa (Millipore) and then the buffer was exchanged by PD10 desalting column in 50 mM phosphate buffer pH 7, 5 mM DTT and 5 mM GSH.

4.3.1. Biochemical and UV/vis, CD, EPR spectroscopic methods

The aggregation state of isolated apo and holo proteins and of protein mixtures was analyzed in air using analytical gel filtration (superdext 75 HR 10/30 and superdext 200 10/300 increase columns (Amersham Bioscience and GE Healthcare) calibrated with gel filtration marker calibration kit, 6500-66000 Da (Sigma Aldrich)). Purified samples were loaded on the

column pre-equilibrated with degassed 50 mM phosphate buffer pH 7, 5 mM GSH, 5 mM DTT. Elution profiles were recorded at 280 nm with a flow rate of 0.5 or 0.75 mL/min. UV/vis and CD spectra were anaerobically acquired on a Cary 50 Eclipse spectrophotometer and JASCO J-810 spectropolarimeter, respectively, in degassed 50 mM phosphate buffer pH 7, 5 mM GSH and 5 mM DTT. EPR spectrum of the 1:4 $[2Fe\text{-}2S]_2$ $GRX3_2$ and apo BOLA2 was recorded after the stoichiometric addition, inside an anaerobic chamber, of a degassed sodium dithionite solution to reduce the cluster and the obtained protein solution was immediately frozen. The EPR spectrum was acquired in degassed 50 mM phosphate buffer pH 7, 5 mM GSH, 5 mM DTT and 10% glycerol at 45 K using a Bruker Elexsys E500 spectrometer working at a microwave frequency of ca. 9.45 GHz and equipped with a SHQ cavity and a continuous flow He cryostat (ESR900, Oxford instruments) for temperature control. Acquisition parameters were as following: microwave frequency, 9.640928 GHz; microwave power, 5 mW; modulation frequency, 100 KHz; modulation amplitude, 2.0 G; acquisition time constant, 163.84 ms; number of points 1024; number of scans 8; field range 2300-4300 G or 2800-3800 G.

4.3.2. NMR spectroscopy

Standard 1H-detected triple-resonance NMR experiments for backbone resonance assignment were recorded on 1 mM ^{13}C, ^{15}N labeled samples (apo forms of GRX3(GrxA/B) and BOLA2) in degassed 50 mM phosphate buffer pH 7, 5 mM DTT and 5 mM GSH at 298 K, using Bruker AVANCE 500 MHz and 700 MHz spectrometers. 15N heteronuclear relaxation experiments performed on ^{15}N-labeled apo BOLA2 and on 15N-labeled apo GRX3(GrxA/B) in presence and in the absence of two equivalents of unlabeled apo BOLA2 were collected to measure ^{15}N backbone longitudinal

(R_1) and transverse (R_2) relaxation rates and heteronuclear $^{15}N\{1H\}$ NOEs. All NMR data were processed using the Topspin software package and were analysed with the program CARA.

4.3.3. Cluster transfer and protein-protein interaction between GRX3 and BOLA2

$[2Fe\text{-}2S]_2$-$GRX3_2$ was incubated under anaerobic conditions with apo BOLA2 at increasing BOLA2 concentrations up to a 1:4 protein ratio in degassed 50 mM phosphate buffer pH 7, 5 mM GSH and 5 mM DTT. Then, UV/vis and CD spectra were recorded on the final protein mixture as described above. Protein-protein interaction between ^{15}N labeled apo or holo forms of GRX3 or GRX3(GrxA/B) and unlabeled apo BOLA2, between ^{15}N labeled apo BOLA2 and unlabeled apo or holo forms of GRX3 or GRX3(GrxA/B) in degassed 50 mM phosphate buffer pH 7, 5 mM GSH and 5 mM DTT containing 10% (v/v) D_2O at 298K was investigated by ^{1}H-^{15}N HSQC NMR spectra monitoring spectral changes after addition of increasing amounts of the unlabeled partner. Spectral changes were analysed with CARA program and plotted following standard procedures.

4.3.4. Cluster transfer and protein-protein interaction between $[2Fe\text{-}2S]_2$ GRX3-$BOLA2_2$ and anamorsin

The chemically reconstituted $[2Fe\text{-}2S]_2$ GRX3-$BOLA2_2$ complex was titrated under anaerobic conditions with increasing concentrations of apo anamorsin up to a 1:1 protein ratio in degassed 50 mM phosphate buffer pH 7, 5 mM GSH, and 5 mM DTT. Cluster transfer and the protein−protein interaction were followed by UV−vis and CD spectroscopy and analytical gel filtration chromatography, respectively.

4.4. LIAS: protein production

The cDNA coding for human LIAS (UniProtKB/Swiss-Prot: O43766) was acquired from Life technologies after optimization in a pENTR-like plasmid and insert in a pDEST-His MBP expression vector. BL21(DE3)Rosetta Plyss competent E. coli cells (Novagen) were transformed with the obtained plasmid, and cells were grown in LB or minimal media (with $(^{15}NH_4)_2SO_4$ and/or [^{13}C]-glucose) containing 1 mM ampicillin and 1mM chloramphenicol at 37° C under vigorous shaking until the OD at 600 nm reached 0.6. Protein expression was induced by adding 0.5 mM IPTG and cells were grown over night at 25 °C. Cells were harvested by centrifugation at 7500 x g and resuspended in lysis buffer (50 mM Tris-HCl pH 8, 0.5M NaCl, 5mM imidazole containing 0.01 mg/ml DNAase, 0.01 mg/ml lysozyme, 1 mM $MgSO_4$, 0.5 mM EDTA and 5 mM DTT). Cell disruption was performed on ice by sonication and the soluble extract, obtained by ultracentrifugation at 40000 x g, was loaded, inside an anaerobic chamber, on a HiTrap chelating HP column (GE Healthcare) and the recombinant proteins were eluted with 50 mM Tris-HCl pH 8, 500 mM NaCl and 500 mM imidazole. 5 mM DTT was added to the protein-containing fractions The proteins were then concentrated with an Amicon Ultra-15 Centrifugal Filter Units with a MWCO of 10 kDa (Millipore). Cleavage of the tags was performed by TEV protease in 50 mM Tris-HCl pH 8, 500 mM NaCl, 5 mM imidazole, 0.2 mM EDTA and 2 mM DTT overnight at room temperature. Than the protein solution was loaded again on the His Trap column to separate the digested proteins from the tags. Size exclusion chromatography was performed as the final purification step using a HiLoad Superdex75

16/60 column (GE Healthcare) and degassed 50 mM phosphate buffer pH 7, 5 mM DTT as running buffer.
We performed the mutagenesis reaction on the expression vector using the QuikChange Site-Directed Mutagenesis Kits (Agilent)

4.4.1. Biochemical and UV/vis, CD, EPR spectroscopic methods

The aggregation state of isolated protein was analysed in air using analytical gel filtration (superdext 200 10/300 increase columns (Amersham Bioscience and GE Healthcare) calibrated with gel filtration marker calibration kit, 6500-66000 Da (Sigma Aldrich)). Purified samples were loaded on the column pre-equilibrated with degassed 50 mM phosphate buffer pH 7 and 5 mM DTT. Elution profiles were recorded at 280 nm with a flow rate of 0.75 mL/min. UV/vis and CD spectra were anaerobically acquired on a Cary 50 Eclipse spectrophotometer and JASCO J-810 spectropolarimeter, respectively, in degassed 50 mM phosphate buffer pH 7 and 5 mM DTT. EPR spectrum of the LIAS protein was recorded after the stoichiometric addition, inside an anaerobic chamber, of a degassed sodium dithionite solution to reduce the cluster and the obtained protein solution was immediately frozen. The EPR spectrum was acquired in degassed 50 mM phosphate buffer pH 7, 5 mM DTT and 10% glycerol at 45 K using a Bruker Elexsys E500 spectrometer working at a microwave frequency of ca. 9.45 GHz and equipped with a SHQ cavity and a continuous flow He cryostat (ESR900, Oxford instruments) for temperature control. Acquisition parameters were as following: microwave frequency, 9.640928 GHz; microwave power, 5 mW; modulation frequency, 100 KHz; modulation amplitude, 2.0 G; acquisition time constant, 163.84 ms; number of points 1024; number of scans 8; field range 2300-4300 G or 2800-3800 G.

4.4.2 NMR spectroscopy

Standard ^{1}H-detected and ^{1}H-^{15}N HSQC NMR experiments were recorded on 0.7 or 1 mM ^{15}N labeled samples in degassed 50 mM phosphate buffer pH 7, 5 mM DTT and at 298 K, using Bruker AVANCE 700 MHz spectrometers. ^{1}H monodimensional paramagnetic spectra were acquire using Bruker 400M Hz equipped with a selective probe for ^{1}H (Sel ^{1}H 5mm probe).

References

1. Yang Shen, Frank Delaglio, Gabriel Cornilescu, and Ad Bax,. TALOS+: A hybrid method for predicting protein backbone torsion angles from NMR chemical shifts J. Biomol. NMR, 44, 213-223 (2009)
2. Eghbalnia HR, Wang L, Bahrami A, Assadi A, Markley JL. Protein energetic conformational analysis from NMR chemical shifts (PECAN) and its use in determining secondary structural elements. J Biomol NMR. 2005 May;32(1):71-81.

3. Rochus Keller, The Computer Aided Resonance Assignment Tutorial.

4.Rochus' PhD thesis, Diss. ETH Nr. 15947

-Chapter 5-

RESULTS

5.1. The GRX3-Anamorsin maturation pathway[18]

To investigate Fe-S cluster transfer from GRX3 to anamorsin, several GRX3 constructs were prepared: (i) full-length GRX3 (fGRX3), (ii) a construct lacking the C-terminal Grx domain (GRX3(Trx-GrxA)), (iii) a construct containing only the Trx domain (GRX3(Trx)) and (iv) a two-domain construct containing both Grx domains (GRX3(GrxA/B)). All the GRX3 constructs were monomeric in their apo form, as determined by analytical gel filtration and by ^{15}N NMR relaxation data, which provided overall reorientational correlation times consistent with monomeric protein states (GRX3(Trx-GrxA) 13.6 ± 1.0 ns, GRX3(Trx) 8.7 ± 0.4 ns and GRX3(GrxA/B) 12.0 ± 1.2 ns; in which errors represent s.d.). The Trx domain did not interact with the Grx domains, as indicated by the complete superimposition of the ^{1}H-^{15}N HSQC map of GRX3(Trx) with the signals of the Trx domain in the ^{1}H-^{15}N HSQC maps of apo-fGRX3 and apo-GRX3(Trx-GrxA) (**Fig.25**).

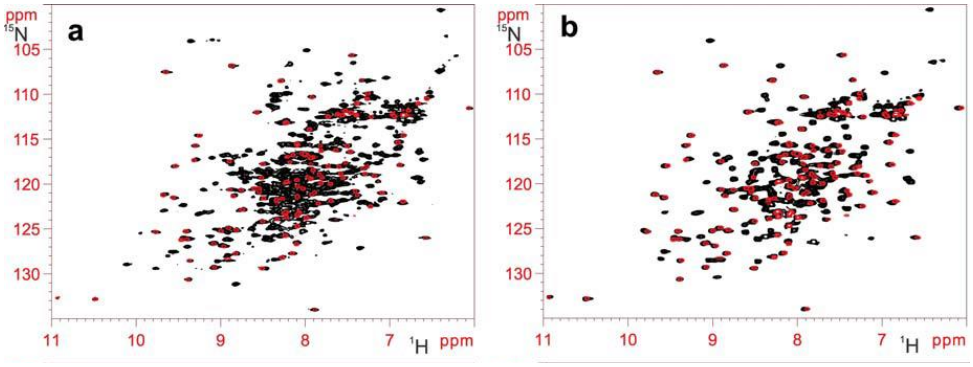

Figure 25. Monitoring the intra- and inter-subunit interactions of the Trx domain of f GRX3 with the Trx and Grx domains. (a) Overlay of ^{1}H-^{15}N HSQC spectra of ^{15}N labeled GRX3(Trx) (red) and of ^{15}N labeled apo fGRX3 (black) recored at 900MHz. (b) Overlay of ^{1}H-^{15}N HSQC spectra of ^{15}N labeled GRX3(Trx) (red) and of ^{15}N labeled apo GRX3 (Trx-GrxA) (black) recored at 900MHz.

Once they were chemically reconstituted, fGRX3, GRX3(Trx-GrxA) and GRX3(GrxA/B) dimerized through their Grx domains, with each domain bridging a [2Fe-2S] cluster in the oxidized state, as assessed by UV-visible (UV-vis) and EPR spectroscopy and analytical gel filtration data (**Fig.26**) and by determining the Fe/S/protein ratio.

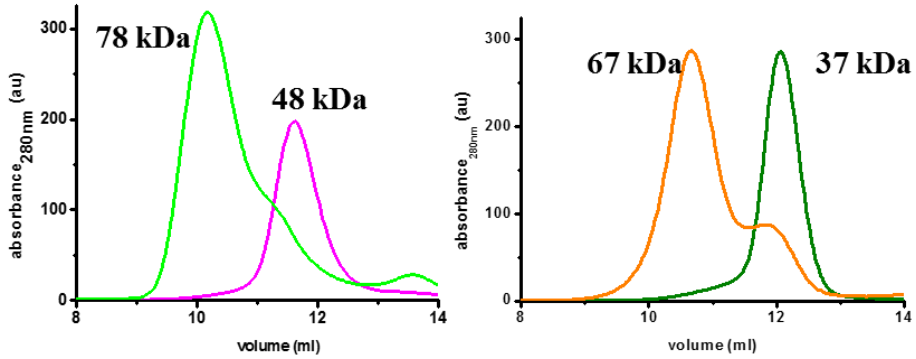

Figure 26. Analytical gel filtration chromatograms of isolated proteins in their apo and holo state. Purple line: apo fGRX3; green line: $[2Fe\text{-}2S]_2$-$fGRX3_2$; dark green line: apo GRX3(GrxA/B); orange line: $[2Fe\text{-}2S]_2$-$GRX3(GrxA/B)_2$

Specifically, all holo proteins exhibited UV-vis spectra typical of oxidized $[2Fe\text{-}2S]^{2+}$ protein-bound clusters (**Fig.27 b**) and were EPR silent, as expected for the presence of a S = 0 ground state of an oxidized $[2Fe\text{-}2S]^{2+}$ cluster. Upon chemical reduction with sodium dithionite, EPR signals of reduced $[2Fe\text{-}2S]^{+}$ protein-bound clusters were observed (**Fig.27 c**). According to analytical gel filtration data and Fe/S/protein ratio quantification performed on the chemically reconstituted samples, the species $[2Fe\text{-}2S]_2$-$fGRX3_2$, [2Fe-2S]-$GRX3(Trx\text{-}GrxA)_2$ and $[2Fe\text{-}2S]_2$-$GRX3(GrxA/B)_2$ (**Fig.27 a**) resulted in the major species present in solution. In all of the dimeric holo-GRX3 constructs, the Trx domain did not have intra- and intersubunit interactions with the Grx domains or with the Trx domain of the other monomer, as demonstrated from the complete superimposition of the $^{1}H\text{-}^{15}N$ HSQC map of GRX3(Trx) with the signals of the Trx domain in the $^{1}H\text{-}^{15}N$ HSQC maps of $[2Fe\text{-}2S]_2$-$fGRX3_2$ and [2Fe-2S]-$GRX3(Trx\text{-}GrxA)_2$. Cluster transfer occurred from either $[2Fe\text{-}2S]_2$-$fGRX3_2$ or [2Fe-2S]-$GRX3(Trx\text{-}GrxA)_2$ to apo-anamorsin, as observed

by UV-vis and EPR spectroscopy. Once the two proteins were mixed, the absorbance peaks typical of the oxidized $[2Fe\text{-}2S]^{2+}$ cluster of $[2Fe\text{-}2S]_2$-$fGRX3_2$ and [2Fe-2S]-$GRX3(Trx\text{-}GrxA)_2$ disappeared, and the absorbance peaks typical of the oxidized $[2Fe\text{-}2S]^{2+}$ cluster–bound forms of anamorsin ([2Fe-2S]-anamorsin) appeared (**Fig.27 b /c**).

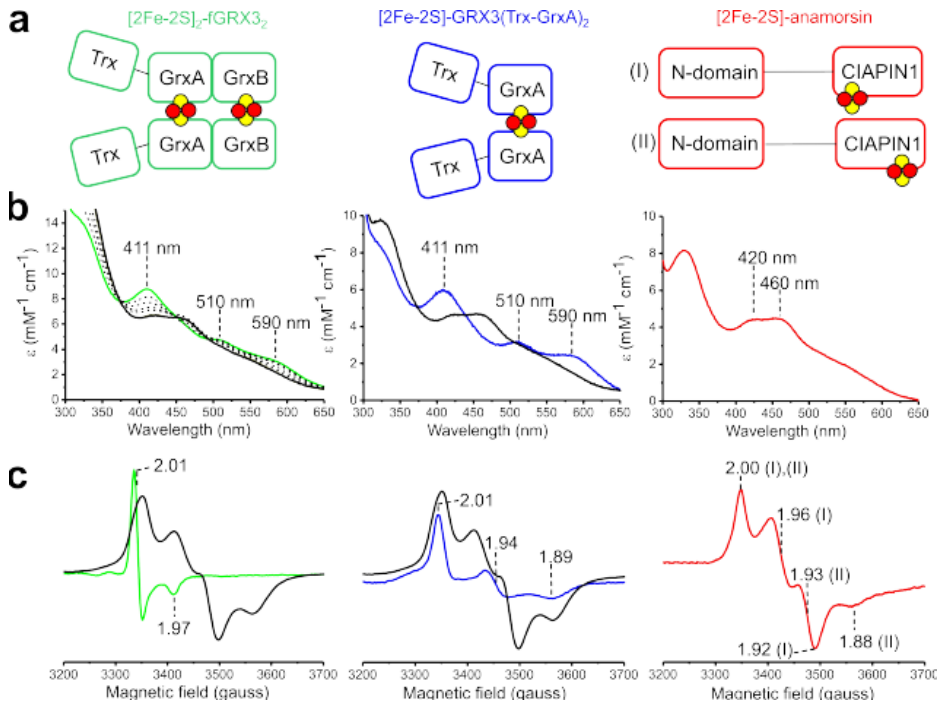

Figure 27. Schematic representation of GRX3 constructs and anamorsin in their [2Fe-2S] cluster–bound forms. (I) and (II) indicate the two cluster-bound species of [2Fe-2S]-anamorsin[2]. Fe and S atoms are represented by red and yellow circles, respectively. (**b**,**c**) UV-vis (**b**) and EPR (**c**) spectra of the isolated proteins and protein mixtures of the cluster transfer experiments. Green line, $[2Fe\text{-}2S]_2$-$fGRX3_2$; blue line, [2Fe-2S]-$GRX3(Trx\text{-}GrxA)_2$; red line, [2Fe-2S]-anamorsin; black line, 1:1 mixtures of $[2Fe\text{-}2S]_2$-$fGRX3_2$ or [2Fe-2S]-$GRX3(Trx\text{-}GrxA)_2$ with apo-anamorsin; dashed line, UV-vis spectra of mixtures of $[2Fe\text{-}2S]_2$-$fGRX3_2$ and apo-anamorsin at increasing anamorsin concentrations up to a 1:1 protein/protein ratio. The EPR *g* values and UV-vis absorbance maxima typical of the [2Fe-2S] cluster–bound forms of anamorsin and GRX3 are reported.

Both anamorsin and GRX3 protein mixtures were EPR silent, in agreement with the presence of the typical S = 0 ground state of an oxidized $[2Fe\text{-}2S]^{2+}$ cluster. Upon chemical reduction with sodium dithionite, only EPR signals typical of the reduced $[2Fe\text{-}2S]^{+}$ clusters of [2Fe-2S]-anamorsin were observed (**Fig.27 c**), showing that the clusters were transferred from GRX3 to anamorsin. Incubation of [2Fe-2S]-anamorsin with apo-GRX3(Trx-GrxA), even in excess, did not result in any changes of the UV-vis spectrum, indicating that the transfer was unidirectional. Finally, the UV-vis results showed no efficient cluster transfer (<10%) when $[2Fe\text{-}2S]_2$-GRX3(GrxA/B)$_2$ was mixed with apo-anamorsin (**Fig.27**).

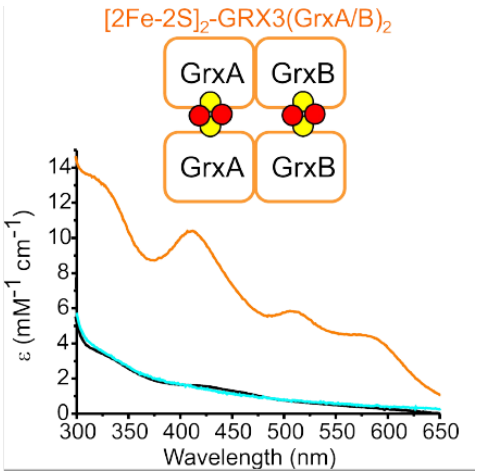

Figure 27. Schematic representation of $[2Fe\text{-}2S]_2$-GRX3(GrxA/B)$_2$ .UV-vis spectra of $[2Fe\text{-}2S]_2$-GRX3(GrxA/B)$_2$ (orange) and of His-tagged apo-anamorsin recorded before (cyan) and after (black) incubation in a ~1:1 protein-protein ratio with $[2Fe\text{-}2S]_2$-GRX3(GrxA/B)$_2$ and its separation through nickel-affinity chromatography.

Altogether, these data demonstrated that $[2Fe\text{-}2S]^{2+}$ clusters were transferred from fGRX3 to anamorsin and that the Trx domain of GRX3 was essential to efficiently drive this process. To understand why the Trx domain of GRX3, which has no cluster-binding properties, drives the observed cluster transfer

process, we studied the interaction between the two partner proteins by NMR. In the first step, each ^{15}N-labeled GRX3 construct in its apo form, i.e., fGRX3, GRX3(Trx-GrxA), GRX3(Trx) and GRX3(GrxA/B), was titrated with unlabeled apo-anamorsin. Although no effects were observed in the ^{1}H-^{15}N HSQC maps when GRX3(GrxA/B) was mixed with anamorsin, chemical shift variations and signal broadening effects were observed in the ^{1}H-^{15}N HSQC maps of fGRX3, GRX3(Trx-GrxA) and GRX3(Trx) when increasing amounts of anamorsin were added. Chemical shift changes were limited to the Trx domain signals only, with similar chemical shifts of the Trx domain in the ^{1}H-^{15}N HSQC maps of the three final mixtures (**Fig.28**)

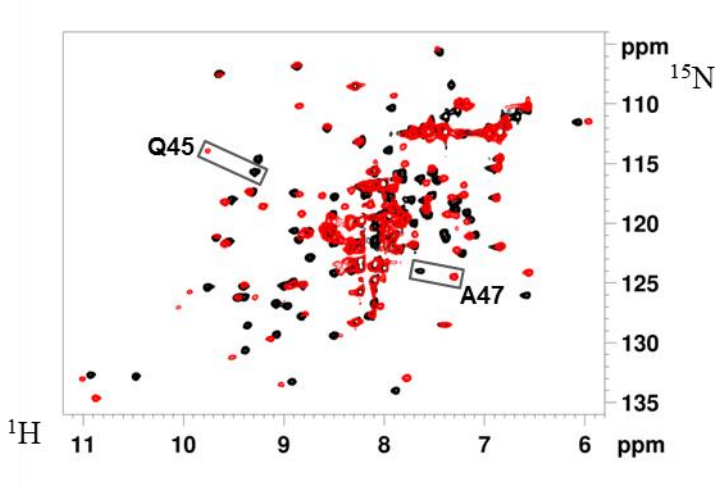

Figure 28. overlay of ^{1}H-^{15}N HSQC spectra of ^{15}N-labeled apo-GRX3(Trx) before (black) and after (red) the addition of 1 eq. of apo-anamorsin.

Therefore, the NMR data indicated that a heterocomplex at a 1:1 ratio between the two proteins in all three protein mixtures was formed, that the Trx domain was essential for the formation of this heterocomplex and that the Grx domains did not interact with anamorsin in the complex. To define the interaction site of apo-anamorsin with the Trx domain of apo-GRX3, we performed NMR titrations by recording ^{1}H-^{15}N HSQC experiments. In the

first titration, ^{15}N-labeled GRX3(Trx) was mixed with the apo-CIAPIN1 domain, and then unlabeled anamorsin N domain was added. In the second, ^{15}N-labeled apo-anamorsin was mixed with unlabeled GRX3(Trx) or fGRX3. No spectral changes were observed upon the addition of unlabeled apo-CIAPIN1 domain in the first titration, indicating that the CIAPIN1 domain does not interact with the Trx domain of GRX3, whereas spectral changes were observed upon addition of the unlabeled N domain of anamorsin to the GRX3(Trx)-CIAPIN1 domain mixture. Overall, these data showed that apo-GRX3 and apo-anamorsin form a 1:1 heterodimeric complex through their N-terminal domains and that the CIAPIN1 domain of anamorsin and the Grx domains of GRX3 are not involved in any permanent interaction in this complex. Molecular recognition between the N-terminal domains was therefore the crucial factor in determining complex formation between the two proteins. When ^{15}N-labeled GRX3(Trx) was titrated with the unlabeled N domain of anamorsin, nine signals broadened beyond detection in the ^{1}H-^{15}N HSQC spectra, and ten signals experienced a small chemical shift variation with sizable signal broadening. When detecting the ^{15}N-labeled N domain of anamorsin, 15 NH signals broadened beyond detection in the ^{1}H-^{15}N HSQC spectra, and 22 NH signals experienced chemical shift variation with sizable signal broadening (**Fig.29**).

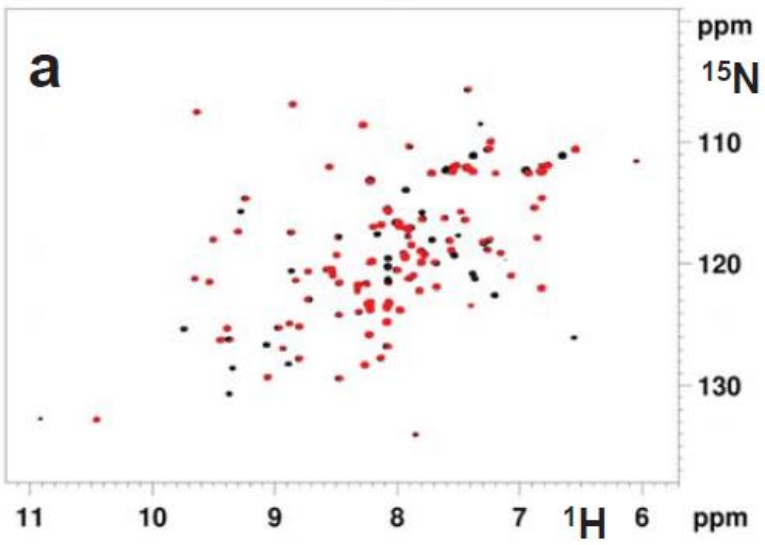

Figure 29 Overlay of ^{1}H-^{15}N HSQC spectra of ^{15}N labeled GRX3(Trx) (black) after (red) incubation with 1 eq. of the N-domain of anamorsin

A structural model of the complex, based on these NMR titration data, was calculated with HADDOCK[1]. Specifically, the 'active' residues (defined in Online Methods) engaged in the protein-protein interaction were Gln45, Ala47, Gln48, Glu51, Val52, Glu55, Glu59, Ala103, His104, Ala105, Glu107, Thr109 and Lys110 in GRX3(Trx) and Gln52, Ala54, His55, Glu57, Glu78, Arg85, Ser117 and Leu121 in the N domain of anamorsin. The statistics of the final docking calculation are reported in **Table 2**.

HADDOCK score	-75.1 ± 1.5
Cluster size	200
RMSD from the overall lowest-energy structure	0.5 ± 0.3
Van der Waals energy	-33.5 ± 1.7
Electrostatic energy	-430.9 ± 39.3
Desolvation energy	39.6 ± 6.2
Restraints violation energy	51.0 ± 3.6
Buried Surface Area	1454.0 ± 24.2
Z-Score	0.0

Table 2 Parameters of the data-driven docking model of the complex between GRX3(Trx) and the N-domain of anamorsin.

The residues involved in the protein-protein interaction were located in α-helices 2 and 4 of GRX3(Trx) and in α-helices 2, 3 and 4 and the loop between helix α2 and strand β3 of the N domain of anamorsin (Fig.30).

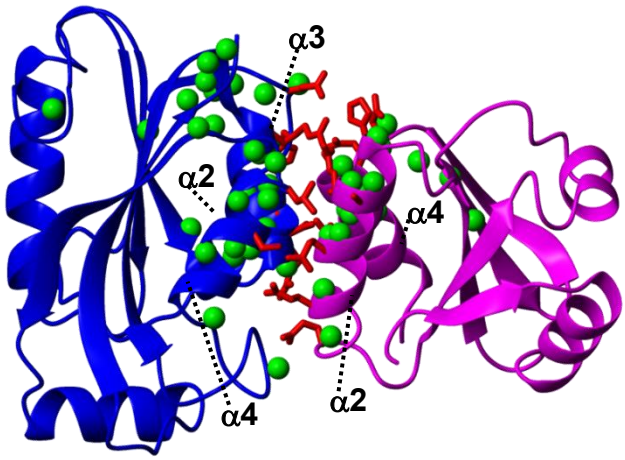

Figure 30. Backbone NHs (green spheres) experiencing reliable spectral changes in the ^{1}H-^{15}N HSQC spectra upon formation of a 1:1 complex between GRX3(Trx) and the N domain of anamorsin or between apo-fGRX3 and apo-anamorsin are mapped on the docking model of the GRX3(Trx)–anamorsin N domain complex. GRX3(Trx) is shown in magenta, and the anamorsin N domain is in blue

As the CIAPIN1 domain of anamorsin did not interact with the Trx domain of GRX3, these additional observed shifts were necessarily due to the interaction between the unstructured linker region of anamorsin and the Trx domain of GRX3. This additional interacting region is fundamental to stabilize the complex. The first part of the anamorsin linker is rich in positively charged lysines (Lys175, Lys180, Lys181 and Lys187) that could electrostatically interact with the glutamic acid–rich region of the Trx domain of GRX3 (**Fig.31**).

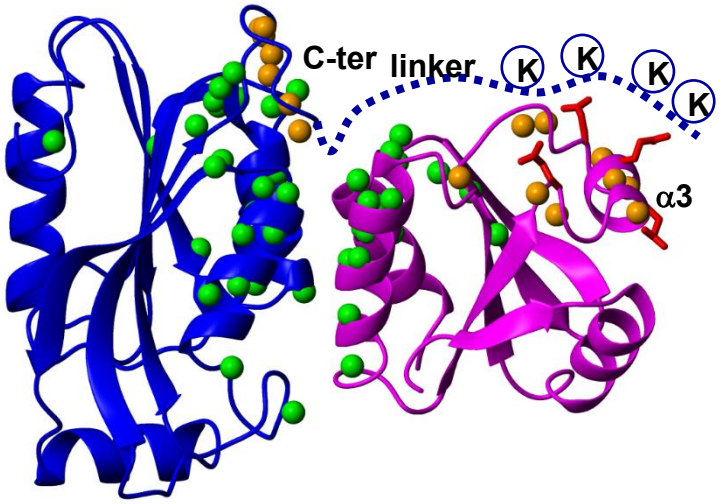

Figure 31. docking model of the GRX3(Trx)–anamorsin N domain complex. GRX3(Trx) is shown in magenta, and the anamorsin N domain is in blue. Orange spheres identify residues influenced by the interaction between full-length proteins in addition to those (green spheres) observed in the GRX3(Trx)–N domain complex. Side chains of the solvent-exposed glutamic acid residues on helix α3 of GRX3(Trx) are shown as red sticks, and the first part of the unstructured linker of anamorsin is shown as a dashed blue line with lysine residues marked with blue circles

To address whether the GRX3–anamorsin complex was still intact once the beafore mentioned cluster transfer had occurred between $[2Fe\text{-}2S]_2$-$fGRX3_2$ or [2Fe-2S]-$GRX3(Trx\text{-}GrxA)_2$ and apo-anamorsin, we performed $^{1}H\text{-}^{15}N$ HSQC NMR spectroscopy and analytical gel filtration on mixtures of

1. ^{15}N-labeled $[2Fe\text{-}2S]_2$-$fGRX3_2$ and unlabeled apo-anamorsin
2. ^{15}N-labeled [2Fe-2S]-$GRX3(Trx\text{-}GrxA)_2$ and unlabeled apo-anamorsin at a 1:1 protein/protein ratio (considering the monomeric protein concentration for the holo-GRX3 constructs).

It resulted that the $^{1}H\text{-}^{15}N$ HSQC maps of the analyzed constructs of GRX3 in these mixtures were well superimposable with those of the corresponding apo mixtures and that gel filtration chromatography showed the presence of a 1:1 heterodimeric complex.

These data indicated that, in both mixtures, the GRX3 molecule of the 1:1 heterodimeric complex was in the apo state, being thus the [2Fe-2S] cluster (or clusters) bound to the anamorsin in the complex, and that the N-terminal domains (Trx of GRX3 and N domain of anamorsin) interacted in the complex, whereas the C-terminal cluster-binding domains (Grx and CIAPIN1 domains) were not involved in the protein-protein interaction, like what was observed in the apo–apo complexes. Additionally, the EPR spectra of the two mixtures (**Fig.27 c**), acquired upon chemical reduction with sodium dithionite, and the paramagnetic IR ^{15}N-HSQC-AP NMR spectra[3] of the 1:1 mixture of ^{15}N-labeled apo-anamorsin and unlabeled [2Fe-2S]- $GRX3(Trx\text{-}GrxA)_2$ (**Fig.32**) showed EPR parameters and paramagnetic NMR signals typical of the [2Fe-2S]- anamorsin species that binds the clusters through its two-conserved cysteine-rich motifs[2]. This indicated that the [2Fe-2S] cluster transfer occurred from both the GrxA and GrxB cluster–loaded domains of fGRX3 or from the GrxA cluster–loaded

domain of GRX3(Trx-GrxA) to both cluster-binding sites of the anamorsin CIAPIN1 domain.

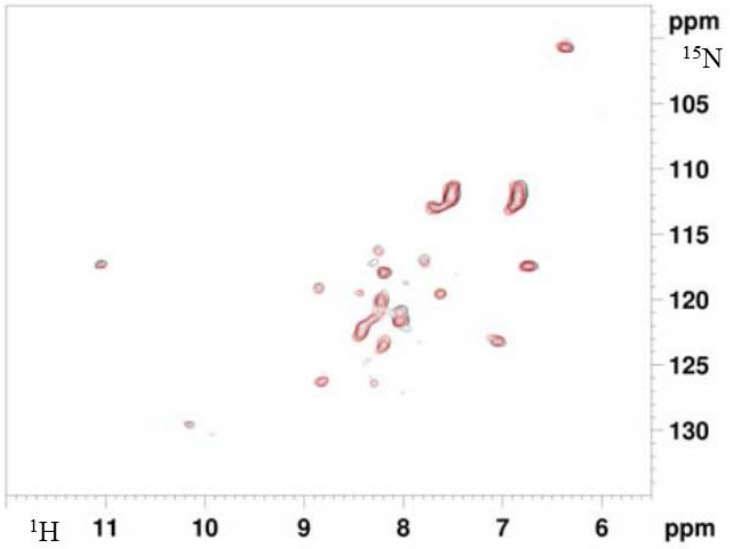

Figure 32.. Paramagnetic NMR spectra to monitor cluster transfer from [2Fe-2S]-GRX3(Trx-GrxA)$_2$ to apo anamorsin. Overlay of paramagnetic IR-^{15}N-HSQC-AP spectra of a ~1:1 apo anamorsin/[2Fe-2S]- GRX3(Trx-GrxA)$_2$ mixture (black) and of [2Fe-2S]- anamorsin (red) recorded at 700MHz and 311K.

We have shown at the molecular level that GRX3 can have a functional role in cytosolic [2Fe-2S] cluster trafficking by transferring two [2Fe-2S] clusters to its protein partner anamorsin. The transfer mechanism was dependent on the formation of a protein-protein complex between the N-terminal domains of GRX3 and of anamorsin. Their interaction was indeed the fundamental requisite to observe [2Fe-2S] cluster transfer from GRX3 to the CIAPIN1 domain of anamorsin (**Fig.33**). We suggest that the protein-protein interaction between the N-terminal domains puts the cluster-binding domains, i.e., the Grx donors and the CAPIN1 acceptor, in the optimal reciprocal orientation for the cluster transfer to occur.

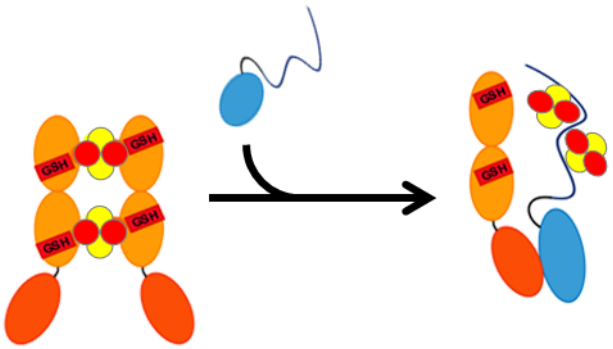

Figure 33. Working model for the functional role of cluster transfer from GRX3 to anamorsin in iron metabolism. GRX3 dimerized upon binding two [2Fe-2S] clusters through its GrxA and GrxB domains (orange), with each domain containing a GSH ligand (red). Specific protein-protein recognition between the N-terminal domains of $[2Fe\text{-}2S]_2$-$fGRX3_2$ and apo-anamorsin (in dark orange and blue, respectively) drives the transfer of the two [2Fe-2S] clusters bound to fGRX3 to the two cysteine-rich motifs of the CIAPIN1 domain of anamorsin

ARTICLE
PUBLISHED ONLINE: 24 AUGUST 2015 | DOI: 10.1038/NCHEMBIO.1892

N-terminal domains mediate [2Fe-2S] cluster transfer from glutaredoxin-3 to anamorsin

Lucia Banci[1,2]*, Simone Ciofi-Baffoni[1,2]*, Karolina Gajda[1], Riccardo Muzzioli[1,2], Riccardo Peruzzini[1] & Julia Winkelmann[1]

In eukaryotes, cytosolic monothiol glutaredoxins are proteins implicated in intracellular iron trafficking and sensing via their bound [2Fe-2S] clusters. We define a new role of human cytosolic monothiol glutaredoxin-3 (GRX3) in transferring its [2Fe-2S] clusters to human anamorsin, a physical and functional protein partner of GRX3 in the cytosol, whose [2Fe-2S] cluster–bound form is involved in the biogenesis of cytosolic and nuclear Fe-S proteins. Specific protein recognition between the N-terminal domains of the two proteins is the mandatory requisite to promote the [2Fe-2S] cluster transfer from GRX3 to anamorsin.

In eukaryotes, both cytosolic and mitochondrial monothiol glutaredoxin proteins bind [2Fe-2S] clusters in the same way, i.e., via the formation of a [2Fe-2S]-bridged homodimer[1,2]. However, though the molecular function of mitochondrial monothiol glutaredoxins in assisting Fe-S protein maturation by acting as [2Fe-2S] cluster donors toward partner apo proteins has been demonstrated in the last few years[1,3–6], the question of whether cytosolic monothiol glutaredoxins can perform the same function in the cytosol still remains unsolved. In contrast, the [2Fe-2S] cluster–bound form of cytosolic monothiol glutaredoxins has been recently proposed to be implicated, together with other protein candidates[7], in cytosolic iron trafficking, playing a crucial part in iron delivery from the cytosolic labile iron pool to virtually all iron-binding proteins in the cell[8,9]. Recently, it has been also shown that, in *Saccharomyces cerevisiae*, the cytosolic monothiol glutaredoxin-3 can transfer the cluster to the iron-responsive transcription factor Aft2 (ref. 10) in a way that deactivates the iron regulon for iron uptake, but cluster transfer occurs only when GRX3 is complexed with the BolA-like protein Fra2 to form a $[2Fe\text{-}2S]^{2+}$-bridged heterodimer complex[11–14]. Monothiol cytosolic glutaredoxins in cooperation with BolA-like proteins therefore have a key role in regulating iron homeostasis in *S. cerevisiae*. However, this function is not conserved in humans as cellular iron homeostasis is regulated at the RNA level by the iron regulatory proteins 1 and 2 (ref. 15). Yeast glutaredoxin-3 alone also can bind a $[2Fe\text{-}2S]^{2+}$ cluster in a homodimeric form, with the cluster coordinated by the cysteine residue of the conserved CGFS motif of each monomer and by two glutathione (GSH) molecules[16]. However, unlike the heterodimeric species formed between glutaredoxin-3 and Fra2, the $[2Fe\text{-}2S]^{2+}$ cluster–bound form of yeast glutaredoxin-3 is unable to transfer the cluster to Aft2 (ref. 10). Thus, despite what it has been observed for mitochondrial monothiol glutaredoxins[1], evidence showing that the homodimeric [2Fe-2S] cluster–bound form of cytosolic monothiol glutaredoxins can be involved in Fe-S protein maturation via a [2Fe-2S] cluster transfer process from their homodimeric holo states to partner apo proteins is still lacking.

The human proteome contains only one monothiol glutaredoxin (Grx) in the cytosol, GRX3 (also commonly named GLRX3 and PICOT). GRX3 consists of three domains: one N-terminal thioredoxin (Trx) domain with no Trx-related enzymatic role[8,17] and two Grx domains each able to bind a glutathione-coordinated [2Fe-2S] cluster via protein dimerization[2,18]. Although the specific function of the *in vivo* indispensable[17] Trx domain is still unknown, the Grx domains of the yeast homologs of GRX3, i.e., Grx3 and Grx4, which can bind one [2Fe-2S] cluster each, are absolutely required for the trafficking of iron in the cytosol and for the regulation of cellular iron homeostasis[8,14,17]. Recently, multiple high-throughput yeast two-hybrid[19] and affinity-capture MS (BioGRID interaction 1077826) screens have shown that GRX3 binds anamorsin (also commonly named CIAPIN1), a [2Fe-2S] cluster–binding protein involved in the maturation of cytosolic Fe-S proteins, *in vivo*[20,21]. A specific yeast two-hybrid assay was also performed to identify anamorsin-interacting molecules using mouse anamorsin cDNA as bait and a cDNA library produced from mouse testis[22]. Results from that study showed that GRX3 preferentially binds anamorsin in cells. Furthermore, either GRX3-deficient (*Glrx3*$^{-/-}$ or anamorsin-deficient (*Ciapin1*$^{-/-}$) mice are both embryonic lethal. Deletion of the anamorsin gene results in embryonic lethality in late gestation (the rate of dead *Ciapin1*$^{-/-}$ embryos is 18.8% at embryonic day 14.5) because of a defect in definitive hematopoiesis in the fetal liver[23,24], whereas 100% of *Glrx3*$^{-/-}$ mice are dead at embryonic day 14.5 (ref. 25), although no defects in fetal hematopoiesis are observed in *Glrx3*$^{-/-}$ embryos. Finally, a high-throughput protein-protein interaction screen showed that the yeast homolog of anamorsin, Dre2, is found in complexes with Grx3 and Grx4 (ref. 26), and Fe-S cluster insertion into Dre2 is decreased three-fold upon Grx4 depletion; still, Dre2 levels are comparable to those detected in wild-type cells[8]. Taken together, these data provide *in vivo* evidence that GRX3 and anamorsin are physical and functional protein partners involved in the Fe-S cluster assembly process. However, the interaction mode and functional role of this interaction have not yet been defined.

Anamorsin contains two domains: an N-terminal well-folded domain (N domain, hereafter) comprising 172 residues and a largely unstructured C-terminal domain of 90 residues named cytokine-induced apoptosis inhibitor 1 (CIAPIN1, hereafter), which contains two highly conserved cysteine-rich motifs able to independently bind a [2Fe-2S] cluster[20,27]. These two domains are connected by a long flexible linker of 50 residues[27]. Anamorsin is an appropriate target to investigate a potential functional role of GRX3 in transferring [2Fe-2S] clusters as (i) it interacts with GRX3 (ref. 22); (ii) the insertion of the Fe-S cluster into the yeast homolog of anamorsin,

[1]Magnetic Resonance Center CERM, University of Florence, Florence, Italy. [2]Department of Chemistry, University of Florence, Florence, Italy.
*e-mail: banci@cerm.unifi.it or ciofi@cerm.unifi.it

Dre2, depends on Grx3 and Grx4, the two cytosolic and functionally redundant yeast homologs of GRX3 (refs. 8,14); and (iii) Fe-S cluster loading on Dre2 is independent of the cytosolic Fe-S protein assembly machinery[21].

In this work, we investigated the ability of GRX3 to transfer [2Fe-2S] clusters to final target proteins by studying its interaction with anamorsin. Protein-protein interaction and cluster transfer were studied *in vitro* by a set of spectroscopic techniques. We found that GRX3 transfers two [2Fe-2S] clusters to anamorsin and that the transfer mechanism was dependent on the formation of a specific protein-protein complex between the N-terminal domains of GRX3 and of anamorsin. Their interaction was indeed the fundamental requisite to observe cluster transfer from Grx domains of GRX3 to the CIAPIN1 domain of anamorsin. These findings provide an advanced view of the functional role of GRX3 in iron metabolism.

RESULTS

GRX3 transfers $[2Fe\text{-}2S]^{2+}$ clusters to anamorsin

To investigate Fe-S cluster transfer from GRX3 to anamorsin, a number of GRX3 constructs were prepared: (i) full-length GRX3 (fGRX3), (ii) a construct lacking the C-terminal Grx domain (GRX3(Trx-GrxA)) with a resemblance to the topological organization of yeast Grx3 and Grx4, (iii) a construct containing only the Trx domain (GRX3(Trx)) and (iv) a two-domain construct containing both Grx domains (GRX3(GrxA/B)) (**Fig. 1a** and **Supplementary Results**, **Supplementary Fig. 1**). All of the GRX3 constructs were monomeric in their apo form, as determined by analytical gel filtration (**Supplementary Fig. 1**) and/or by ^{15}N NMR relaxation data, which provided overall reorientational correlation times consistent with monomeric protein states (GRX3(Trx-GrxA) 13.6 ± 1.0 ns, GRX3(Trx) 8.7 ± 0.4 ns and GRX3(GrxA/B) 12.0 ± 1.2 ns; in which errors represent s.d.). The Trx domain did not interact with the Grx domains, as indicated by the complete superimposition of the ^{1}H-^{15}N HSQC map of GRX3(Trx) with the signals of the Trx domain in the ^{1}H-^{15}N HSQC maps of apo-fGRX3 and apo-GRX3(Trx-GrxA) (**Supplementary Fig. 2**). Once they were chemically reconstituted, fGRX3, GRX3(Trx-GrxA) and GRX3(GrxA/B) dimerized through their Grx domains, with each domain bridging a [2Fe-2S] cluster in the oxidized state, as assessed by UV-visible (UV-vis) and EPR spectroscopy and analytical gel filtration data and by determining the Fe/S/protein ratio. Specifically, all holo proteins exhibited UV-vis spectra typical of oxidized $[2Fe\text{-}2S]^{2+}$ protein-bound clusters (**Fig. 1b**) and were EPR silent, as expected for the presence of a S = 0 ground state of an oxidized $[2Fe\text{-}2S]^{2+}$ cluster. Upon chemical reduction with sodium dithionite, EPR signals of reduced $[2Fe\text{-}2S]^{+}$ protein-bound clusters were observed (**Fig. 1c**). According to gel filtration data and Fe/S/protein ratio quantification performed on the chemically reconstituted samples (**Supplementary Fig. 1** and **Supplementary Table 1**), the species $[2Fe\text{-}2S]_2$-fGRX3$_2$, $[2Fe\text{-}2S]$-GRX3(Trx-GrxA)$_2$ and $[2Fe\text{-}2S]_2$-GRX3(GrxA/B)$_2$ (**Fig. 1a**) resulted in the major species present in solution. These data on fGRX3 and GRX3(GrxA/B) are in agreement with previously reported studies[2,28]. In all of the dimeric holo-GRX3 constructs, the Trx domain did not have intra- and intersubunit interactions with the Grx domains or with the Trx domain of the other monomer, as demonstrated from the complete superimposition of the ^{1}H-^{15}N HSQC map of GRX3(Trx) with the signals of the Trx domain in the ^{1}H-^{15}N HSQC maps of $[2Fe\text{-}2S]_2$-fGRX3$_2$ and $[2Fe\text{-}2S]$-GRX3(Trx-GrxA)$_2$ (**Supplementary Fig. 2**).

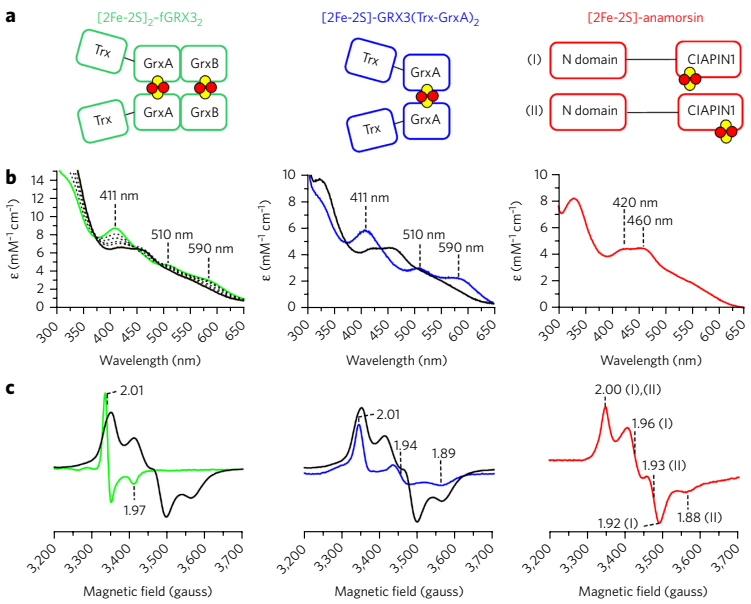

Figure 1 | Cluster transfer from GRX3 to anamorsin. (**a**) Schematic representation of GRX3 constructs and anamorsin in their [2Fe-2S] cluster–bound forms. (I) and (II) indicate the two cluster-bound species of [2Fe-2S]-anamorsin previously described in ref. 29. Fe and S atoms are represented by red and yellow circles, respectively. (**b**,**c**) UV-vis (**b**) and EPR (**c**) spectra of the isolated proteins and protein mixtures of the cluster transfer experiments. Green line, $[2Fe\text{-}2S]_2$-fGRX3$_2$; blue line, $[2Fe\text{-}2S]$-GRX3(Trx-GrxA)$_2$; red line, [2Fe-2S]-anamorsin; black line, 1:1 mixtures of $[2Fe\text{-}2S]_2$-fGRX3$_2$ or $[2Fe\text{-}2S]$-GRX3(Trx-GrxA)$_2$ with apo-anamorsin; dashed line, UV-vis spectra of mixtures of $[2Fe\text{-}2S]_2$-fGRX3$_2$ and apo-anamorsin at increasing anamorsin concentrations up to a 1:1 protein/protein ratio. The EPR *g* values and UV-vis absorbance maxima typical of the [2Fe-2S] cluster–bound forms of anamorsin and GRX3 are reported. In the EPR spectrum of [2Fe-2S]-anamorsin, the *g* values of the two clusters, each bound to one of the two cysteine-rich motifs of the anamorsin CIAPIN1 domain, are reported[29].

Cluster transfer occurred from either $[2Fe\text{-}2S]_2$-fGRX3$_2$ or $[2Fe\text{-}2S]$-GRX3(Trx-GrxA)$_2$ to apo-anamorsin, as observed by UV-vis and EPR spectroscopy. Once the two proteins were mixed, the absorbance peaks typical of the oxidized $[2Fe\text{-}2S]^{2+}$ cluster of $[2Fe\text{-}2S]_2$-fGRX3$_2$ and $[2Fe\text{-}2S]$-GRX3(Trx-GrxA)$_2$ disappeared, and the absorbance peaks typical of the oxidized $[2Fe\text{-}2S]^{2+}$ cluster–bound forms of anamorsin ([2Fe-2S]-anamorsin)[27,29] appeared (**Fig. 1b**). Both anamorsin and GRX3 protein mixtures were EPR silent, in agreement with the presence of the typical S = 0 ground state of an oxidized $[2Fe\text{-}2S]^{2+}$ cluster. Upon chemical reduction with sodium dithionite, only EPR signals typical of the reduced $[2Fe\text{-}2S]^{+}$ clusters of [2Fe-2S]-anamorsin were observed (**Fig. 1c**), showing that the clusters were transferred from GRX3 to anamorsin. Incubation of [2Fe-2S]-anamorsin with apo-GRX3(Trx-GrxA), even in excess, did not result in any changes of the UV-vis spectrum, indicating that the transfer was unidirectional. Finally, the UV-vis results showed no efficient cluster transfer (<10%) when $[2Fe\text{-}2S]_2$-GRX3(GrxA/B)$_2$ was mixed with apo-anamorsin (**Fig. 2a**). Altogether, these data demonstrated that $[2Fe\text{-}2S]^{2+}$ clusters were transferred from fGRX3 to anamorsin and that the Trx domain of GRX3 was essential to efficiently drive this process.

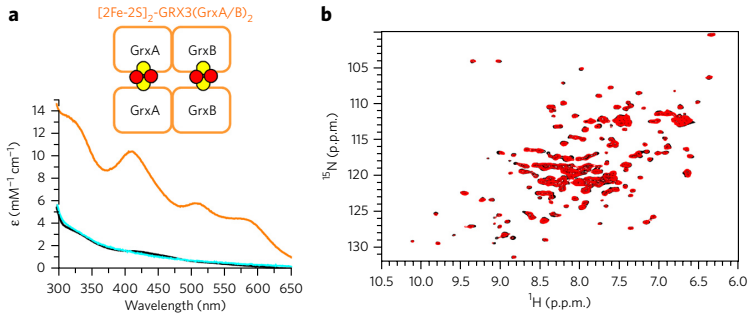

Figure 2 | Impaired cluster transfer and no protein-protein interaction between GRX3(GrxA/B) and anamorsin. (**a**) Schematic representation of $[2Fe\text{-}2S]_2$-GRX3(GrxA/B)$_2$. UV-vis spectra of $[2Fe\text{-}2S]_2$-GRX3(GrxA/B)$_2$ (orange) and of His-tagged apo-anamorsin recorded before (cyan) and after (black) incubation in a ~1:1 protein-protein ratio with $[2Fe\text{-}2S]_2$-GRX3(GrxA/B)$_2$ and its separation through nickel-affinity chromatography. (**b**) The overlay of ^{1}H-^{15}N HSQC spectra of ^{15}N-labeled apo-GRX3(GrxA/B) before (black) and after (red) the addition of 1 eq. apo-anamorsin is shown.

GRX3-anamorsin interaction promotes cluster transfer

To understand why the Trx domain of GRX3, which has no cluster-binding properties, drives the observed cluster transfer process, we studied the interaction between the two partner proteins by NMR. In the first step, each ^{15}N-labeled GRX3 construct in its apo form, i.e., fGRX3, GRX3(Trx-GrxA), GRX3(Trx) and GRX3(GrxA/B), was titrated with unlabeled apo-anamorsin. Although no effects were observed in the ^{1}H-^{15}N HSQC maps when GRX3(GrxA/B) was mixed with anamorsin (**Fig. 2b**), chemical shift variations and signal broadening effects were observed in the ^{1}H-^{15}N HSQC maps of fGRX3, GRX3(Trx-GrxA) and GRX3(Trx) when increasing amounts of anamorsin were added (**Fig. 3a** and **Supplementary Fig. 3**). In particular, chemical shift changes were limited to the Trx domain signals only, with similar chemical shifts of the Trx domain in the ^{1}H-^{15}N HSQC maps of the three final mixtures (**Fig. 3b** and **Supplementary Fig. 4**). Two nonoverlapping NH cross-peaks (assigned to Gln45 and Ala47) in the ^{1}H-^{15}N HSQC map of ^{15}N-labeled apo-GRX3(Trx), whose chemical shifts were largely affected by the protein-protein interaction, were selected to estimate the stoichiometry of the binding. Specifically, the intensity of these two cross-peaks decreased upon addition of unlabeled apo-anamorsin, and the formation of two new cross-peaks assigned to the two corresponding NHs of apo-GRX3(Trx) bound to apo-anamorsin was observed, with their intensities increasing with the addition of unlabeled partner. The two NH resonances of each residue are therefore representative of the free and bound states of GRX3(Trx), respectively. Using their intensity ratios in the ^{1}H-^{15}N HSQC maps along the results from titration, the molar fraction of the two species was determined and plotted against the GRX3(Trx)/anamorsin protein concentration ratio (**Fig. 3a**). From the analysis of these NMR titration data, it resulted that (i) spectral changes were complete at a 1:1 protein/protein ratio and that (ii) the NH signals of the Trx domain were affected, whereas those of the Grx domains in fGRX3 and GRX3(Trx-GrxA) were not. In the final protein mixtures, line broadening was observed for all backbone NH signals of the ^{15}N-labeled protein, even for those with no chemical shift variations, indicating a sizable increase in the molecular weight of the observed species. Therefore, the NMR data indicated that a heterocomplex at a 1:1 ratio between the two proteins in all three protein mixtures was formed, that the Trx domain was essential for the formation of this heterocomplex and that the Grx domains did not interact with anamorsin in the complex. Data from gel filtration experiments performed on the fGRX3-anamorsin protein mixture (**Supplementary Fig. 1**) showed that the heterocomplex is a heterodimer.

To define the interaction site of apo-anamorsin with the Trx domain of apo-GRX3, we performed NMR titrations by recording ^{1}H-^{15}N HSQC experiments. In the first titration, ^{15}N-labeled GRX3(Trx) was mixed with the apo-CIAPIN1 domain, and then unlabeled anamorsin N domain was added. In the second, ^{15}N-labeled apo-anamorsin was mixed with unlabeled GRX3(Trx) or fGRX3. No spectral changes were observed upon the addition of unlabeled apo-CIAPIN1 domain in the first titration, indicating that the CIAPIN1 domain does not interact with the Trx domain of GRX3, whereas spectral changes were observed upon addition of the unlabeled N domain of anamorsin to the GRX3(Trx)-CIAPIN1 domain mixture (**Supplementary Fig. 5**).

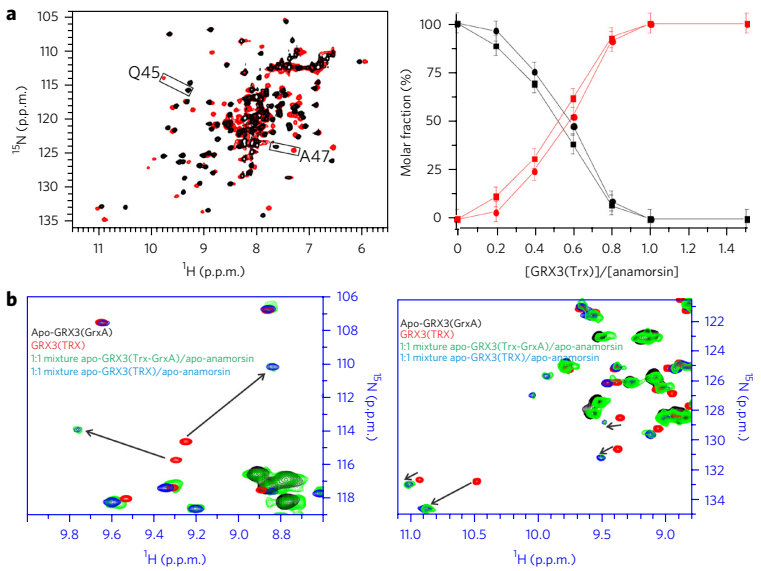

Figure 3 | Apo-GRX3 and apo-anamorsin specifically recognize each other via their N-terminal domains. (**a**) Left panel, overlay of ^{1}H-^{15}N HSQC spectra of ^{15}N-labeled apo-GRX3(Trx) before (black) and after (red) the addition of 1 eq. of apo-anamorsin. Right panel, stoichiometric formation of the GRX3-anamorsin complex at a 1:1 protein ratio, as determined by integrating two not-overlapping NH cross-peaks of the free (black) and bound (red) state of apo-GRX3(Trx). Gln45 (●) and Ala47 (■) are indicated with rectangles in the ^{1}H-^{15}N HSQC spectra. Data represent mean values ± s.d. ($n \geq 3$). (**b**) Overlay of ^{1}H-^{15}N HSQC spectral regions of ^{15}N-labeled apo-GRX3(GrxA) (black) and GRX3(Trx) (red) with 1:1 mixtures between ^{15}N-labeled apo-GRX3(Trx-GrxA) and unlabeled apo-anamorsin (green) and between ^{15}N-labeled apo-GRX3(Trx) and unlabeled apo-anamorsin (cyan). Arrows indicate chemical shift changes of NHs belonging to the Trx domain, whereas NHs of GrxA domain remain essentially unperturbed.

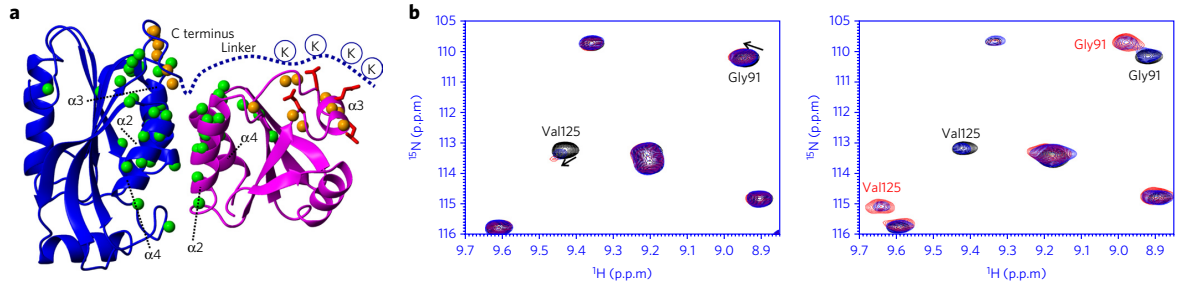

Figure 4 | N domains of apo-GRX3 and of apo-anamorsin form a heterodimer stabilized through the unstructured linker of anamorsin. (**a**) Backbone NHs (green spheres) experiencing reliable spectral changes in the ^{1}H-^{15}N HSQC spectra upon formation of a 1:1 complex between GRX3(Trx) and the N domain of anamorsin or between apo-fGRX3 and apo-anamorsin are mapped on the docking model of the GRX3(Trx)–anamorsin N domain complex. GRX3(Trx) is shown in magenta, and the anamorsin N domain is in blue. Orange spheres identify residues influenced by the interaction between full-length proteins in addition to those (green spheres) observed in the GRX3(Trx)–N domain complex. Side chains of the solvent-exposed glutamic acid residues on helix α3 of GRX3(Trx) are shown as red sticks, and the first part of the unstructured linker of anamorsin is shown as a dashed blue line with lysine residues marked with blue circles. (**b**) Overlay of ^{1}H-^{15}N HSQC spectral regions of the ^{15}N-labeled N domain of anamorsin before (black) and after the addition of 0.5 eq. (blue) and 1 eq. (red) of GRX3(Trx) (left panel) or of apo-fGRX3 (right panel). In the left panel, arrows illustrate chemical shift deviations of Gly91 and Val125 upon addition of GRX3(Trx), which occur on a fast or intermediate exchange regime on the NMR timescale. In the right panel, NH chemical shifts of Gly91 and Val125 switch to a slow exchange regime on the NMR timescale upon addition of apo-fGRX3. The NH resonances of Gly91 and Val125 showing the presence of free and fGRX3-bound states of the N domain of anamorsin are shown in black and red, respectively.

These data showed that anamorsin recognizes the Trx domain of GRX3 through its N domain. In agreement with this, in the second titration, spectral changes were observed in the ^{1}H-^{15}N HSQC spectra of apo-anamorsin for the backbone NHs of the N domain of anamorsin (**Supplementary Fig. 5**).

Overall, these data showed that apo-GRX3 and apo-anamorsin form a 1:1 heterodimeric complex through their N-terminal domains and that the CIAPIN1 domain of anamorsin and the Grx domains of GRX3 are not involved in any permanent interaction in this complex. Molecular recognition between the N-terminal domains was therefore the crucial factor in determining complex formation between the two proteins.

Anamorsin linker stabilizes the interaction with GRX3

When ^{15}N-labeled GRX3(Trx) was titrated with the unlabeled N domain of anamorsin, nine signals broadened beyond detection in the ^{1}H-^{15}N HSQC spectra, and ten signals experienced a small chemical shift variation with sizable signal broadening (**Supplementary Fig. 6**). When detecting the ^{15}N-labeled N domain of anamorsin, 15 NH signals broadened beyond detection in the ^{1}H-^{15}N HSQC spectra, and 22 NH signals experienced chemical shift variation with sizable signal broadening (**Supplementary Fig. 6**). A structural model of the complex (**Fig. 4a**), based on these NMR titration data, was calculated with HADDOCK[30]. Specifically, the 'active' residues (defined in Online Methods) engaged in the protein-protein interaction were Gln45, Ala47, Gln48, Glu51, Val52, Glu55, Glu59, Ala103, His104, Ala105, Glu107, Thr109 and Lys110 in GRX3(Trx) and Gln52, Ala54, His55, Glu57, Glu78, Arg85, Ser117 and Leu121 in the N domain of anamorsin. The statistics of the final docking calculation are reported in **Supplementary Table 2**. The residues involved in the protein-protein interaction were located in α-helices 2 and 4 of GRX3(Trx) and in α-helices 2, 3 and 4 and the loop between helix α2 and strand β3 of the N domain of anamorsin (**Fig. 4a**). This recognition mode between the Trx domain of GRX3 and the N domain of anamorsin was conserved when the two full-length proteins were made to interact, as shown by the fact that the same interacting regions, comprising α-helices 2 and 4 of the Trx domain of GRX3, were identified when ^{15}N-labeled apo-fGRX3 was titrated with unlabeled apo-anamorsin (**Fig. 4a**). However, additional NH signals of the Trx domain of GRX3, located in a negatively charged, glutamic acid–rich region (Glu71, Glu75, Glu78 and Glu81) adjacent to the interaction surface, experienced chemical shift changes (**Fig. 4a**). As the CIAPIN1 domain of anamorsin did not interact with the Trx domain of GRX3 (**Supplementary Fig. 5**), these additional observed shifts were necessarily due to the interaction between the unstructured linker region of anamorsin and the Trx domain of GRX3. This additional interacting region is fundamental to stabilize the complex. Indeed, on the NMR timescale, the exchange between the free and the bound proteins switched from fast or intermediate, when the N-terminal domains of GRX3(Trx) and of anamorsin interacted, to slow, when the N domain of GRX3(Trx) interacted with full-length anamorsin (**Fig. 4b**), suggesting that protein-protein affinity is increased when the linker is present[31]. According to the structural model of the complex, the C terminus of the N domain of anamorsin (where the linker begins) is located near the interaction region (**Fig. 4a**). The first part of the anamorsin linker is rich in positively charged lysines (Lys175, Lys180, Lys181 and Lys187) that could electrostatically interact with the glutamic acid–rich region of the Trx domain of GRX3. The presence of this additional protein-protein interaction region was further supported by the disappearance of signals in the unstructured and flexible C-terminal tail of the N domain of anamorsin (from Phe166 to Arg172) in the ^{1}H-^{15}N HSQC NMR spectrum of anamorsin upon complex formation (**Fig. 4a**). In conclusion, the NMR and biomolecular docking data described here defined how the N domains of the two proteins recognize each other and identified a role of the linker of anamorsin in stabilizing the protein-protein interaction.

Anamorsin–GRX3 complex binds two [2Fe-2S]$^{2+}$ clusters

To address whether the GRX3–anamorsin complex was still intact once the aforementioned cluster transfer had occurred between $[2Fe\text{-}2S]_2$-fGRX3$_2$ or [2Fe-2S]-GRX3(Trx-GrxA)$_2$ and apo-anamorsin, we performed ^{1}H-^{15}N HSQC NMR spectroscopy and analytical gel filtration on mixtures of (i) ^{15}N-labeled $[2Fe\text{-}2S]_2$-fGRX3$_2$ and unlabeled apo-anamorsin and (ii) ^{15}N-labeled [2Fe-2S]-GRX3(Trx-GrxA)$_2$ and unlabeled apo-anamorsin at a 1:1 protein/protein ratio (considering the monomeric protein concentration for the holo-GRX3 constructs). It resulted that the ^{1}H-^{15}N HSQC maps of the analyzed constructs of GRX3 in these mixtures were well superimposable with those of the corresponding apo mixtures

(**Supplementary Fig. 7**) and that gel filtration chromatography showed the presence of a 1:1 heterodimeric complex (**Supplementary Fig. 1**). These data indicated that, in both mixtures, the GRX3 molecule of the 1:1 heterodimeric complex was in the apo state, being thus the [2Fe-2S] cluster (or clusters) bound to the anamorsin in the complex, and that the N-terminal domains (Trx of GRX3 and N domain of anamorsin) interacted in the complex, whereas the C-terminal cluster-binding domains (Grx and CIAPIN1 domains) were not involved in the protein-protein interaction, similar to what was observed in the apo–apo complexes. Additionally, the EPR spectra of the two mixtures (**Fig. 1c**), acquired upon chemical reduction with sodium dithionite, and the paramagnetic IR ^{15}N-HSQC-AP NMR spectra[32] of the 1:1 mixture of ^{15}N-labeled apo-anamorsin and unlabeled [2Fe-2S]-GRX3(Trx-GrxA)$_2$ (**Supplementary Fig. 8**) showed EPR parameters and paramagnetic NMR signals typical of the [2Fe-2S]-anamorsin species that binds the clusters through its two conserved cysteine-rich motifs[29]. This indicated that the [2Fe-2S] cluster transfer occurred from both the GrxA and GrxB cluster–loaded domains of fGRX3 or from the GrxA cluster–loaded domain of GRX3(Trx-GrxA) to both cluster-binding sites of the anamorsin CIAPIN1 domain. Finally, to define whether both metal binding sites of anamorsin in the complex with fGRX3 were fully occupied after the transfer, we quantified the Fe/S ratio before and after [2Fe-2S]$_2$-fGRX3$_2$ was mixed with apo-anamorsin in a 1:1 ratio (Online Methods). It resulted that this ratio was unaltered (**Supplementary Table 1**), indicating that anamorsin received two [2Fe-2S] clusters from [2Fe-2S]$_2$-fGRX3$_2$, and therefore, two [2Fe-2S] clusters were bound per protein molecule of anamorsin (**Fig. 5a**). As we were never able to chemically reconstitute anamorsin with both [2Fe-2S] clusters bound at stoichiometric levels[20,27,29], the specific protein-protein interaction between fGRX3 and anamorsin was essential to achieve complete cluster incorporation into anamorsin.

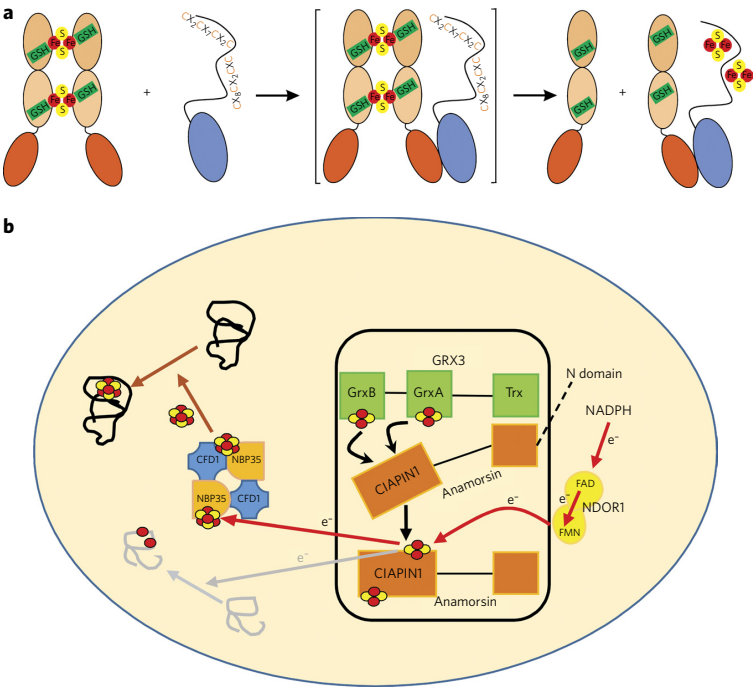

Figure 5 | Working model for the functional role of cluster transfer from GRX3 to anamorsin in iron metabolism. (**a**) GRX3 dimerized upon binding two [2Fe-2S] clusters through its GrxA and GrxB domains (coral), with each domain containing a GSH ligand (green)[28]. Specific protein-protein recognition between the N-terminal domains of [2Fe-2S]$_2$-fGRX3$_2$ and apo-anamorsin (in orange and blue, respectively) drives the transfer of the two [2Fe-2S] clusters bound to fGRX3 to the two cysteine-rich motifs of the CIAPIN1 domain of anamorsin. On this basis, a protein-protein adduct, depicted in square brackets, can be assumed as the low-population intermediate required to modulate the cluster transfer process. One molecule of fGRX3 is then released from this intermediate, whereas the other remains in a complex with anamorsin through the interacting N-terminal domains. The latter complex represents an intermediate product in the cellular environment as it is expected to terminate, allowing anamorsin to perform its electron transfer function in the CIA machinery. (**b**) The GRX3-dependent maturation process of holo-anamorsin (black box) can affect all of the cellular processes involving cytosolic and nuclear [4Fe-4S]-dependent proteins as holo-anamorsin, once complexed with NDOR1, is part of a cytosolic electron transfer chain (red arrows) responsible for the maturation of cytosolic or nuclear [4Fe-4S] cluster-binding proteins (brown arrows)[21,36]. In yeast, Dre2 complexed with Tah18 functions as a source of reducing equivalent for the assembly of di-iron centers of cytosolic enzymes (light gray arrows)[34]. Thus, deficiency in the GRX3-dependent maturation process of anamorsin might affect di-iron cofactor biosynthesis, as observed in yeast[8].

DISCUSSION

We have shown at the molecular level that GRX3 can have a functional role in cytosolic [2Fe-2S] cluster trafficking by transferring two [2Fe-2S] clusters to its protein partner anamorsin (**Fig. 5a**). The transfer mechanism was dependent on the formation of a protein-protein complex between the N-terminal domains of GRX3 and of anamorsin. Their interaction was indeed the fundamental requisite to observe [2Fe-2S] cluster transfer from GRX3 to the CIAPIN1 domain of anamorsin (**Fig. 5a**). We suggest that the protein-protein interaction between the N-terminal domains puts the cluster-binding domains, i.e., the Grx donors and the CAPIN1 acceptor, in the optimal reciprocal orientation for the cluster transfer to occur. Therefore, it seems that the transfer process from GRX3 to anamorsin is a thermodynamically favored process under kinetic control. This mechanism also guarantees that two [2Fe-2S] clusters are concomitantly transferred in a single molecular event to the target protein requiring two [2Fe-2S] clusters.

Once the cluster transfer has occurred, the complex between the two proteins (**Fig. 5a**) then needs to be terminated in the cell so that the functional process (or processes) performed by the matured form of anamorsin can proceed. It has already been shown that holo-anamorsin is essential for cytosolic and nuclear [4Fe-4S] protein assembly and that it is an early step component of the cytosolic Fe-S protein assembly (CIA) machinery. Specifically, the matured holo form of anamorsin forms a stable complex with the diflavin reductase NDOR1 in the cell[20,21]. This complex, which receives electrons from NADPH, has been proposed to act as a source of reducing equivalents for the assembly of target but not scaffold Fe-S cytosolic proteins[21]. It is possible that, once anamorsin has received the clusters from GRX3, it favors the interaction with NDOR1, thus terminating the interaction with GRX3. Recently, we found that the unstructured linker is the only region of anamorsin that tightly interacts with NDOR1, inducing the formation of a specific and stable protein complex[20]. Indeed, the N-terminal domain of anamorsin

was not involved in protein-protein recognition, and the C-terminal CIAPIN1 domain of anamorsin, containing the [2Fe-2S] redox center, only transiently interacts, through complementary charged residues, with the flavin mononucleotide (FMN)-binding domain of NDOR1 to perform the electron transfer reaction[20]. Considering these previous observations and the fact that this study showed that the anamorsin linker was also involved in the interaction with GRX3, we suggest that, upon interaction of the GRX3–anamorsin complex with NDOR1, the linker might weaken its interaction with GRX3 while favoring the interaction with NDOR1. As the stabilizing effect of the linker on GRX3-anamorsin interaction is then weakened, the binding affinity of the N-terminal domain of GRX3 with that of anamorsin might be decreased, and, as a consequence, the complex between GRX3 and anamorsin might switch to the complex between anamorsin and NDOR1. The linker interaction is therefore responsible for modulating the formation and release of the various protein-protein complexes needed to induce the redox-competent state in anamorsin, rendering it able to receive electrons from NDOR1. That this linker has multiple functional interactions is consistent with its high flexibility, which enables its interaction with multiple partners, as commonly observed for intrinsically disordered proteins or regions[33]. This mechanism of action can also explain how the interaction between the holo forms of anamorsin and GRX3 is avoided in the cell, as the stable interaction between holo-anamorsin and NDOR1 will be favored with respect to the interaction of holo-anamorsin with holo-GRX3.

Our study contributes to the mechanistic understanding of Fe-S protein biogenesis in the cytosol, opening a new molecular view for the cellular function of GRX3 in humans. Our finding, showing that GRX3 has a key role in maturing anamorsin, indirectly links GRX3 to all of the anamorsin-dependent cellular processes (**Fig. 5b**). *In vivo* data showed that silencing of human GRX3 expression in HeLa cells decreases the activities of the cytosolic Fe-S proteins IRP1 and GPAT[9]. This behavior can be a consequence of an impairment of the GRX3-dependent anamorsin maturation process, which therefore makes the CIA machinery unable to function, i.e., to assemble the [4Fe-4S] clusters of IRP1 and GPAT. Similarly, in the functionally homologous yeast system[8], *in vivo* data showed a decrease of Fe-S cluster insertion into two cytosolic Fe-S protein targets, the [4Fe-4S] proteins Rli1 and Nar1, upon Grx4 depletion as well as a defect in the di-iron cluster assembly of the cytosolic ribonucleotide reductase, which, similarly to the CIA machinery, depends on the Dre2-anamorsin electron transfer chain[34,35]. By demonstrating this and showing how GRX3 is able to mature anamorsin, our findings suggest a new molecular interpretation of the available *in vivo* data on GRX3 (refs. 8,9,34), thus moving forward the existing functional information on GRX3 from a limited, intracellular iron trafficking protein toward a new, more complex functional role.

Received 10 March 2015; accepted 1 July 2015;
published online 24 August 2015

METHODS

Methods and any associated references are available in the online version of the paper.

References

1. Banci, L. *et al.* [2Fe-2S] cluster transfer in iron-sulfur protein biogenesis. *Proc. Natl. Acad. Sci. USA* **111**, 6203–6208 (2014).
2. Haunhorst, P., Berndt, C., Eitner, S., Godoy, J.R. & Lillig, C.H. Characterization of the human monothiol glutaredoxin 3 (PICOT) as iron-sulfur protein. *Biochem. Biophys. Res. Commun.* **394**, 372–376 (2010).
3. Lill, R. *et al.* The role of mitochondria in cellular iron-sulfur protein biogenesis and iron metabolism. *Biochim. Biophys. Acta* **1823**, 1491–1508 (2012).
4. Uzarska, M.A., Dutkiewicz, R., Freibert, S.A., Lill, R. & Muhlenhoff, U. The mitochondrial Hsp70 chaperone Ssq1 facilitates Fe/S cluster transfer from Isu1 to Grx5 by complex formation. *Mol. Biol. Cell* **24**, 1830–1841 (2013).
5. Mapolelo, D.T. *et al.* Monothiol glutaredoxins and A-type proteins: partners in Fe-S cluster trafficking. *Dalton Trans.* **42**, 3107–3115 (2013).
6. Shakamuri, P., Zhang, B. & Johnson, M.K. Monothiol glutaredoxins function in storing and transporting $[Fe_2S_2]$ clusters assembled on IscU scaffold proteins. *J. Am. Chem. Soc.* **134**, 15213–15216 (2012).
7. Philpott, C.C. Coming into view: eukaryotic iron chaperones and intracellular iron delivery. *J. Biol. Chem.* **287**, 13518–13523 (2012).
8. Mühlenhoff, U. *et al.* Cytosolic monothiol glutaredoxins function in intracellular iron sensing and trafficking via their bound iron-sulfur cluster. *Cell Metab.* **12**, 373–385 (2010).
9. Haunhorst, P. *et al.* Crucial function of vertebrate glutaredoxin 3 (PICOT) in iron homeostasis and hemoglobin maturation. *Mol. Biol. Cell* **24**, 1895–1903 (2013).
10. Poor, C.B. *et al.* Molecular mechanism and structure of the *Saccharomyces cerevisiae* iron regulator Aft2. *Proc. Natl. Acad. Sci. USA* **111**, 4043–4048 (2014).
11. Yamaguchi-Iwai, Y., Stearman, R., Dancis, A. & Klausner, R.D. Iron-regulated DNA binding by the AFT1 protein controls the iron regulon in yeast. *EMBO J.* **15**, 3377–3384 (1996).
12. Rutherford, J.C., Jaron, S., Ray, E., Brown, P.O. & Winge, D.R. A second iron-regulatory system in yeast independent of Aft1p. *Proc. Natl. Acad. Sci. USA* **98**, 14322–14327 (2001).
13. Blaiseau, P.L., Lesuisse, E. & Camadro, J.M. Aft2p, a novel iron-regulated transcription activator that modulates, with Aft1p, intracellular iron use and resistance to oxidative stress in yeast. *J. Biol. Chem.* **276**, 34221–34226 (2001).
14. Ojeda, L. *et al.* Role of glutaredoxin-3 and glutaredoxin-4 in the iron regulation of the Aft1 transcriptional activator in *Saccharomyces cerevisiae*. *J. Biol. Chem.* **281**, 17661–17669 (2006).
15. Anderson, C.P., Shen, M., Eisenstein, R.S. & Leibold, E.A. Mammalian iron metabolism and its control by iron regulatory proteins. *Biochim. Biophys. Acta* **1823**, 1468–1483 (2012).
16. Li, H. *et al.* The yeast iron regulatory proteins Grx3/4 and Fra2 form heterodimeric complexes containing a [2Fe-2S] cluster with cysteinyl and histidyl ligation. *Biochemistry* **48**, 9569–9581 (2009).
17. Hoffmann, B. *et al.* The multidomain thioredoxin-monothiol glutaredoxins represent a distinct functional group. *Antioxid. Redox Signal.* **15**, 19–30 (2011).
18. Li, H. & Outten, C.E. Monothiol CGFS glutaredoxins and BolA-like proteins: [2Fe-2S] binding partners in iron homeostasis. *Biochemistry* **51**, 4377–4389 (2012).
19. Rual, J.F. *et al.* Towards a proteome-scale map of the human protein-protein interaction network. *Nature* **437**, 1173–1178 (2005).
20. Banci, L. *et al.* Molecular view of an electron transfer process essential for iron-sulfur protein biogenesis. *Proc. Natl. Acad. Sci. USA* **110**, 7136–7141 (2013).
21. Netz, D.J. *et al.* Tah18 transfers electrons to Dre2 in cytosolic iron-sulfur protein biogenesis. *Nat. Chem. Biol.* **6**, 758–765 (2010).
22. Saito, Y. *et al.* PICOT is a molecule which binds to anamorsin. *Biochem. Biophys. Res. Commun.* **408**, 329–333 (2011).
23. Shibayama, H. *et al.* Identification of a cytokine-induced antiapoptotic molecule anamorsin essential for definitive hematopoiesis. *J. Exp. Med.* **199**, 581–592 (2004).
24. Tanimura, A. *et al.* The anti-apoptotic gene *Anamorsin* is essential for both autonomous and extrinsic regulation of murine fetal liver hematopoiesis. *Exp. Hematol.* **42**, 410–422 (2014).
25. Cha, H. *et al.* PICOT is a critical regulator of cardiac hypertrophy and cardiomyocyte contractility. *J. Mol. Cell. Cardiol.* **45**, 796–803 (2008).
26. Tarassov, K. *et al.* An *in vivo* map of the yeast protein interactome. *Science* **320**, 1465–1470 (2008).
27. Banci, L. *et al.* Anamorsin is a [2Fe-2S] cluster–containing substrate of the Mia40-dependent mitochondrial protein-trapping machinery. *Chem. Biol.* **18**, 794–804 (2011).
28. Li, H., Mapolelo, D.T., Randeniya, S., Johnson, M.K. & Outten, C.E. Human glutaredoxin 3 forms [2Fe-2S]-bridged complexes with human BolA2. *Biochemistry* **51**, 1687–1696 (2012).
29. Banci, L. *et al.* Human anamorsin binds [2Fe-2S] clusters with unique electronic properties. *J. Biol. Inorg. Chem.* **18**, 883–893 (2013).
30. Dominguez, C., Boelens, R. & Bonvin, A.M. HADDOCK: a protein-protein docking approach based on biochemical or biophysical information. *J. Am. Chem. Soc.* **125**, 1731–1737 (2003).
31. Zuiderweg, E.R. Mapping protein-protein interactions in solution by NMR spectroscopy. *Biochemistry* **41**, 1–7 (2002).
32. Ciofi-Baffoni, S., Gallo, A., Muzzioli, R. & Piccioli, M. The IR-^{15}N-HSQC-AP experiment: a new tool for NMR spectroscopy of paramagnetic molecules. *J. Biomol. NMR* **58**, 123–128 (2014).

33. Oldfield, C.J. & Dunker, A.K. Intrinsically disordered proteins and intrinsically disordered protein regions. *Annu. Rev. Biochem.* **83**, 553–584 (2014).
34. Zhang, Y. *et al.* Conserved electron donor complex Dre2-Tah18 is required for ribonucleotide reductase metallocofactor assembly and DNA synthesis. *Proc. Natl. Acad. Sci. USA* **111**, E1695–E1704 (2014).
35. Zhang, Y. *et al.* Investigation of *in vivo* diferric tyrosyl radical formation in *Saccharomyces cerevisiae* Rnr2 protein: requirement of Rnr4 and contribution of Grx3/4 AND Dre2 proteins. *J. Biol. Chem.* **286**, 41499–41509 (2011).
36. Netz, D.J., Pierik, A.J., Stumpfig, M., Muhlenhoff, U. & Lill, R. The Cfd1-Nbp35 complex acts as a scaffold for iron-sulfur protein assembly in the yeast cytosol. *Nat. Chem. Biol.* **3**, 278–286 (2007).

Acknowledgments

We thank A. Gallo (CERM) for assistance in recording the EPR spectra. This work was supported by Ente Cassa di Risparmio (Grant ID no. 2013/7101); the Ministero dell'Istruzione, dell'Università e della Ricerca (Grant ID number: CTN01_00177_962865); the European Integrated Structural Biology Infrastructure (INSTRUCT), which is part of the European Strategy Forum on Research Infrastructures; and national member subscriptions.

Author contributions

The work plan was conceived and designed by L.B. and S.C.-B.; R.M. and K.G. produced protein constructs of anamorsin and GRX3; L.B. and S.C.-B. planned the experiments; J.W. and R.P. performed and analyzed NMR data; K.G., J.W. and R.M. performed and analyzed EPR and UV-vis experiments. The manuscript was drafted by L.B. and S.C.-B. and revised by all authors.

Competing financial interests

The authors declare no competing financial interests.

Additional information

Supplementary information is available in the online version of the paper. Reprints and permissions information is available online at http://www.nature.com/reprints/index.html. Correspondence and requests for materials should be addressed to L.B. or S.C.-B.

ONLINE METHODS

Protein production. The cDNA coding for human GRX3 (UniProtKB/Swiss-Prot: O76003) was acquired from Source BioScience. Five different constructs (fGRX3 residues 1–335, GRX3(Trx) residues 1–117, GRX3(Trx-GrxA) residues 1–236, GRX3(GrxA/B) residues 130–335, GRX3(GrxA) residues 120–236) were amplified by PCR and subsequently inserted into the pETG20A vector using the Gateway technology (Invitrogen). BL21-CodonPlus (DE3)-RIPL Competent *E. coli* cells (Stratagene, La Jolla, CA) were transformed with the obtained plasmids, and cells were grown in LB or minimal medium (with $(^{15}NH_4)_2SO_4$ and/or [^{13}C]glucose) containing 1 mM ampicillin, 1 mM chloramphenicol and 250 μM $FeCl_3$ at 37 °C under vigorous shaking until the $OD_{600\ nm}$ reached 0.6. Protein expression was induced by adding 0.5 mM IPTG, and cells were grown overnight at 17 °C. Cells were harvested by centrifugation at 7,500*g* and resuspended in lysis buffer (50 mM Tris-HCl (pH 8) containing 500 mM NaCl, 5 mM imidazole, 0.01 mg/ml DNAase, 0.01 mg/ml lysozyme, 1 mM $MgSO_4$, 5 mM GSH and 5 mM DTT). Cell disruption was performed on ice by sonication, and the soluble extract, obtained by ultracentrifugation at 40,000*g*, was loaded on a HiTrap chelating HP column (GE Healthcare), and the recombinant proteins were eluted with 50 mM Tris-HCl (pH 8) 500 mM NaCl and 500 mM imidazole, 5 mM DTT and 5 mM GSH. The proteins were then concentrated with an Amicon Ultra-15 Centrifugal Filter Units with a MWCO of 10 kDa (Millipore). Cleavage of the tag was performed by TEV protease in 50 mM Tris-HCl (pH 8) 500 mM NaCl, 5 mM imidazole and 3 mM DTT overnight at room temperature. The protein solution was then loaded on the His-Trap column to separate the digested protein from the tag. Size-exclusion chromatography was performed as final purification step using a HiLoad Superdex75 16/60 column (GE Healthcare) and degassed 50 mM phosphate buffer (pH 7), 5 mM GSH and 5 mM DTT as running buffer. Apo proteins were obtained by addition of 100 mM EDTA and 20 mM $K_4[Fe(CN)_6]$, followed by a gel filtration desalting column. fGRX3, GRX3(Trx-GrxA) and GRX3(GrxA/B) were chemically reconstituted inside an anaerobic chamber (O_2, <5 p.p.m.) by incubating the purified proteins in degassed 50 mM Tris, 100 mM NaCl, 5 mM DTT and 5 mM GSH at pH 8 with 1 mM $FeCl_3$ and 1 mM Na_2S overnight at room temperature. To prevent the possible interference in the cluster transfer experiments of free [2Fe-2S] clusters, formed in solution in the reconstitution process, desalting with a gel filtration column was performed. Iron and acid-labile sulfide content were determined by colorimetric assays as described in ref. 27.

Human anamorsin (full-length protein and the N domain and CIAPIN1 domains) in its apo and [2Fe-2S]-bound form was obtained following previously reported procedures[20,27,29].

The aggregation state of isolated apo and holo proteins and of protein mixtures was analyzed in air using analytical gel filtration. Purified samples were loaded on a SuperdexTM 75 HR 10/30 analytical column (Amersham Bioscience) pre-equilibrated with 50 mM phosphate buffer (pH 7), 5 mM GSH and 5 mM DTT and calibrated with the Low Molecular Weight Gel Filtration Calibration kit (GE Healthcare). The buffer was bubbled with N_2 overnight to minimize dissolved O_2 levels. Elution profiles were recorded at 280 nm with a flow rate of 0.5 mL/min.

Protein concentration was determined using a Bradford assay[37] with BSA as the calibration standard and by UV-vis absorbance using extinction coefficient predicted by amino acid protein sequence for the apo protein. The results from each determination were in good agreement.

UV-vis and EPR spectroscopy. UV-vis spectra were anaerobically acquired on a Cary 50 Eclipse spectrophotometer in degassed 50 mM phosphate buffer (pH 7), 5 mM GSH and 5 mM DTT. EPR spectra of $[2Fe\text{-}2S]_2$-$fGRX3_2$, [2Fe-2S]-GRX3(Trx-GrxA)$_2$ and [2Fe-2S]-anamorsin and of the protein mixtures between $[2Fe\text{-}2S]_2$-$fGRX3_2$ or [2Fe-2S]-GRX3(Trx-GrxA)$_2$ and apo-anamorsin were recorded after the addition of a degassed sodium dithionite solution inside an anaerobic chamber to reduce the cluster, and the obtained protein solutions were immediately frozen. The EPR spectra were acquired in degassed 50 mM phosphate buffer (pH 7), 5 mM GSH, 5 mM DTT and 10% glycerol at 45 K using a Bruker Elexsys E500 spectrometer working at a microwave frequency of ~9.45 GHz and equipped with a SHQ cavity and a continuous flow He cryostat (ESR900, Oxford Instruments) for temperature control. Acquisition parameters were as following: microwave frequency, 9.640928 GHz; microwave power, 5 mW; modulation frequency, 100 KHz; modulation amplitude, 2.0 G; acquisition time constant, 163.84 ms; number of points, 1,024; number of scans, 8; field range 2,300–4,300 G or 2,800–3,800 G.

NMR spectroscopy. Standard ^{1}H-detected triple-resonance NMR experiments for backbone resonance assignment were recorded on 0.5–1 mM ^{13}C,^{15}N–labeled samples (apo forms of GRX3(Trx-GrxA), GRX3(Trx) and GRX3(GrxA)) in degassed 50 mM phosphate buffer (pH 7), 5 mM DTT at 298 K, using Bruker AVANCE 500-MHz and 700-MHz spectrometers. To identify backbone amide resonances affected by paramagnetic relaxation effects, ^{1}H-^{15}N HSQC edited by a ^{1}H inversion recovery and observed in the antiphase component (IR-^{15}N-HSQC-AP) were collected at 700 MHz and 298 K on apo-anamorsin/[2Fe-2S]-GRX3(Trx-GrxA)$_2$ mixture and [2Fe-2S]-anamorsin, prepared in an anaerobic chamber with degassed 50 mM phosphate buffer (pH 7), 5 mM GSH, 5 mM DTT[32]. Resonance assignment of apo- and [2Fe-2S]-anamorsin was already available[20,27]. All NMR data were processed using the Topspin software package and were analyzed with the program CARA.

Cluster transfer and interaction between GRX3 and anamorsin. To monitor cluster transfer, $[2Fe\text{-}2S]_2$-$fGRX3_2$ and [2Fe-2S]-GRX3(Trx-GrxA)$_2$ were incubated under anaerobic conditions for 30 min with the apo form of anamorsin at increasing anamorsin concentrations up to a 1:1 protein/protein ratio (considering the monomeric protein concentration for the holo-GRX3 constructs) in degassed 50 mM phosphate buffer (pH 7), 5 mM GSH and 5 mM DTT. Then, UV-vis, EPR and analytical gel filtration were recorded as described above. The same experiment was performed under anaerobic conditions incubating, at a 1:1 protein ratio, [2Fe-2S]-anamorsin and apo-fGRX3 and $[2Fe\text{-}2S]_2$-GRX3(GrxA/B)$_2$ and His_{12}-tagged apo-anamorsin.

The protein-protein interaction between ^{15}N-labeled apo forms of fGRX3, GRX3(Trx-GrxA), GRX3(GrxA/B) and GRX3(Trx); unlabeled apo-anamorsin (full-length, N domain, CIAPIN1 domain); ^{15}N-labeled apo-anamorsin (full-length, N domain); and unlabeled apo-GRX3(Trx) and fGRX3 in degassed 50 mM phosphate buffer (pH 7) and 5 mM DTT containing 10% (v/v) D_2O at 298K was investigated by ^{1}H-^{15}N HSQC NMR spectrometry monitoring spectral changes after addition of increasing amounts of the unlabeled partner. To follow both protein-protein interaction and cluster transfer processes in the same experiment, ^{15}N-labeled $[2Fe\text{-}2S]_2$-$fGRX3_2$ or [2Fe-2S]-GRX3(Trx-GrxA)$_2$ was titrated under anaerobic conditions with unlabeled anamorsin and with ^{15}N-labeled apo-anamorsin with unlabeled [2Fe-2S]-GRX3(Trx-GrxA)$_2$ in degassed 50 mM phosphate buffer (pH 7), 5 mM GSH and 5 mM DTT containing 10% (v/v) D_2O at 298 K, and the spectral changes were monitored by both ^{1}H-^{15}N HSQC and IR-^{15}N-HSQC-AP NMR spectra[32].

The structural docking model of the complex between GRX3(Trx) and the N domain of anamorsin was obtained using the HADDOCK program and protocol[38] from the WeNMR portal[39]. In the HADDOCK calculations, the active residues engaged in the protein-protein interaction are those with a high solvent accessibility in the free form of the protein (>50% relative accessibility as calculated with NACCESS) and (i) experiencing reliable backbone NH chemical shift perturbation upon complex formation (the threshold to define significant chemical shift perturbations was taken for each protein as the average over all the Δδ values plus 1 σ (s.d.))[30] or (ii) whose NH cross-peaks in ^{1}H-^{15}N HSQC NMR spectra disappeared upon complex formation.

Fe-S cluster quantification. The level of cluster transferred from $[2Fe\text{-}2S]_2$-$fGRX3_2$ to apo-anamorsin was quantified through the following procedure: (i) $[2Fe\text{-}2S]_2$-$fGRX3_2$ was titrated under anaerobic conditions with apo-anamorsin to up to ~1 eq. in degassed 50 mM phosphate buffer (pH 7), 5 mM GSH and 5 mM DTT. The complete transfer of the [2Fe-2S] cluster from fGRX3 to anamorsin was observed by UV-vis experiments. (ii) On the starting material $[2Fe\text{-}2S]_2$-$fGRX3_2$ and on the final mixture, the iron and acid-labile sulfur content and the protein concentration were estimated following the chemical assays described above. The analysis of these data is reported in **Supplementary Table 1**.

37. Bradford, M.M. Rapid and sensitive method for the quantitation of microgram quantities of protein utilizing the principle of protein-dye binding. *Anal. Biochem.* **72**, 248–254 (1976).
38. de Vries, S.J., van Dijk, M. & Bonvin, A.M. The HADDOCK web server for data-driven biomolecular docking. *Nat. Protoc.* **5**, 883–897 (2010).
39. Wassenaar, T.A. *et al.* WeNMR: structural biology on the grid. *J. Grid Computing* **10**, 743–767 (2012).

Supplementary Information

N-terminal domains mediate [2Fe-2S] cluster transfer from glutaredoxin-3 to anamorsin

Lucia Banci[1,2,*], Simone Ciofi-Baffoni[1,2,*], Karolina Gajda[1], Riccardo Muzzioli[1,2], Riccardo Peruzzini[1], Julia Winkelmann[1]

[1]Magnetic Resonance Center CERM, University of Florence, Via Luigi Sacconi 6, 50019, Sesto Fiorentino, Florence, Italy

[2]Department of Chemistry, University of Florence, Via della Lastruccia 3, 50019 Sesto Fiorentino, Florence, Italy

Supplementary Results

Supplementary Table 1. Iron, and acid-labile sulfide analyses of fGRX3, GRX3(Trx-GrxA), GRX3(GrxA/B), anamorsin and of fGRX3/anamorsin 1:1 hetero-complex.

Sample	Fe[a]	S[a]
Chemically reconstituted [2Fe-2S] fGRX3	4.2 ± 0.1	4.1 ± 0.1
Chemically reconstituted [2Fe-2S] GRX3(Trx-GrxA)	1.8 ± 0.1	1.9 ± 0.1
Chemically reconstituted [2Fe-2S] GRX3(GrxA/B)	4.0 ± 0.1	4.1 ± 0.1
[2Fe-2S] anamorsin	2.1 ± 0.1	2.0 ± 0.1
[2Fe-2S] fGRX3 - apo anamorsin 1:1 complex	3.9 ± 0.1	4.3 ± 0.1

[a]Fe and acid-labile S measurements are reported as mol Fe or S per mol of complex (homodimer or heterodimer) and of anamorsin. Fe and S measurements are obtained from two independent samples. Data represent mean values ± s.d.

Supplementary Table 2. Parameters of the data-driven docking model of the complex between GRX3(Trx) and the N-domain of anamorsin. Data represent mean values ± s.d. obtained from 200 structures clustered in 1 cluster.

HADDOCK score	-75.1 ± 1.5
Cluster size	200
RMSD from the overall lowest-energy structure	0.5 ± 0.3
Van der Waals energy	-33.5 ± 1.7
Electrostatic energy	-430.9 ± 39.3
Desolvation energy	39.6 ± 6.2
Restraints violation energy	51.0 ± 3.6
Buried Surface Area	1454.0 ± 24.2
Z-Score	0.0

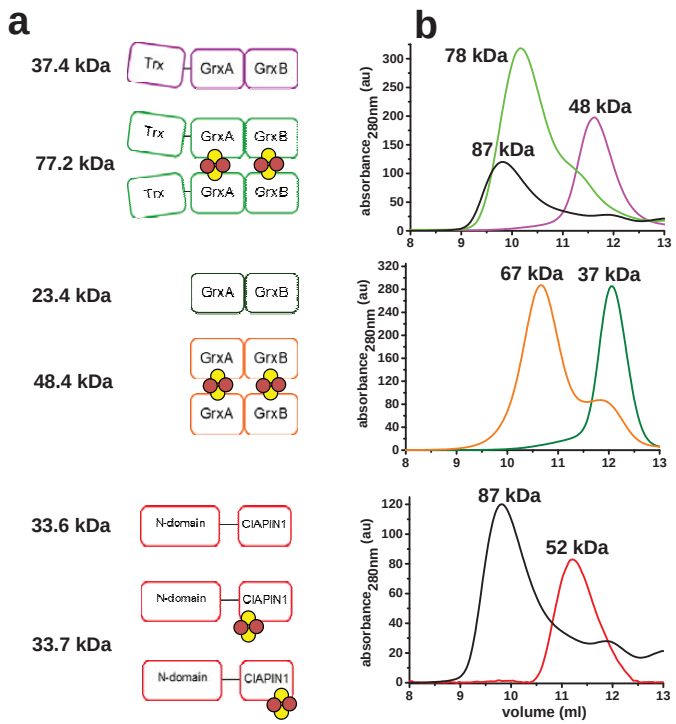

Supplementary Fig. 1. Spectoscopic and aggregation properties of apo/holo forms of GRX3 and anamorsin before and after their interaction. (**a**) Schematic representation of fGRX3, GRX3(GrxA/B) and anamorsin in their apo and [2Fe-2S] cluster bound forms with their corresponding theoretical masses reported on the left. Fe and S atoms are represented by red and yellow circles, respectively. (**b**) Analytical gel filtration chromatograms of isolated proteins in their apo and holo states and of the protein mixtures analyzed in this study. Purple line: apo fGRX3; green line: $[2Fe\text{-}2S]_2$-$fGRX3_2$; dark green line: apo GRX3(GrxA/B); orange line: $[2Fe\text{-}2S]_2$-$GRX3(GrxA/B)_2$; red line: apo or [2Fe-2S]-anamorsin; black line: 1:1 mixture of apo or $[2Fe\text{-}2S]_2$-$fGRX3_2$ with apo anamorsin. The experimental masses reported at the top of each chromatographic peak derive from analytical gel filtration analysis.

Supplementary Fig. 2. Monitoring by NMR the intra- and inter-subunit interactions of the Trx domain of fGRX3 with the Trx and Grx domains. (**a**) Overlay of ^{1}H-^{15}N HSQC spectra of ^{15}N labeled GRX3(Trx) (red) and of ^{15}N labeled apo fGRX3 (black) recored at 900MHz. (**b**) Overlay of ^{1}H-^{15}N HSQC spectra of ^{15}N labeled GRX3(Trx) (red) and of ^{15}N labeled apo GRX3(Trx-GrxA) (black) recored at 900MHz. (**c**) Overlay of ^{1}H-^{15}N HSQC spectra of ^{15}N labeled GRX3(Trx) (red) and of ^{15}N labeled [2Fe-2S]$_2$-fGRX3$_2$ (black) recored at 900MHz. (**d**) Overlay of ^{1}H-^{15}N HSQC spectra of ^{15}N labeled GRX3(Trx) (red) and of ^{15}N labeled [2Fe-2S]-GRX3(Trx-GrxA)$_2$ (black) recored at 900MHz.

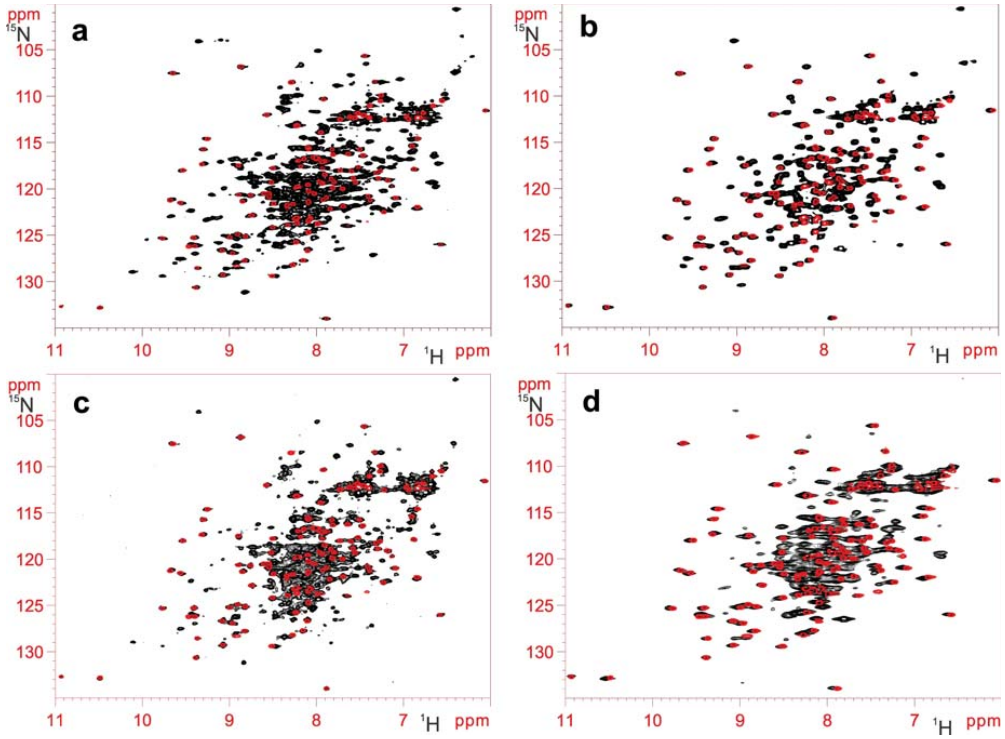

Supplementary Fig. 3. Monitoring by NMR the interaction between different constructs of GRX3 and full-length anamorsin in their apo forms. (**a**) Overlay of ^{1}H-^{15}N HSQC spectra of ^{15}N labeled apo GRX3(Trx-GrxA) (black) and of a 1:1 mixture between ^{15}N labeled apo GRX3(Trx-GrxA) and unlabelled apo anamorsin (red). (**b**) Overlay of ^{1}H-^{15}N HSQC spectra of ^{15}N labeled apo fGRX3 (black) and of a 1:1 mixture between ^{15}N labeled apo fGRX3 and unlabelled apo anamorsin (red). (**c**) Overlay of ^{1}H-^{15}N HSQC spectra of the two mixtures, i.e. 1:1 mixture between ^{15}N labeled apo GRX3(Trx-GrxA) and unlabelled apo anamorsin (black) and 1:1 mixture between ^{15}N labeled apo fGRX3 and unlabelled apo anamorsin (red).

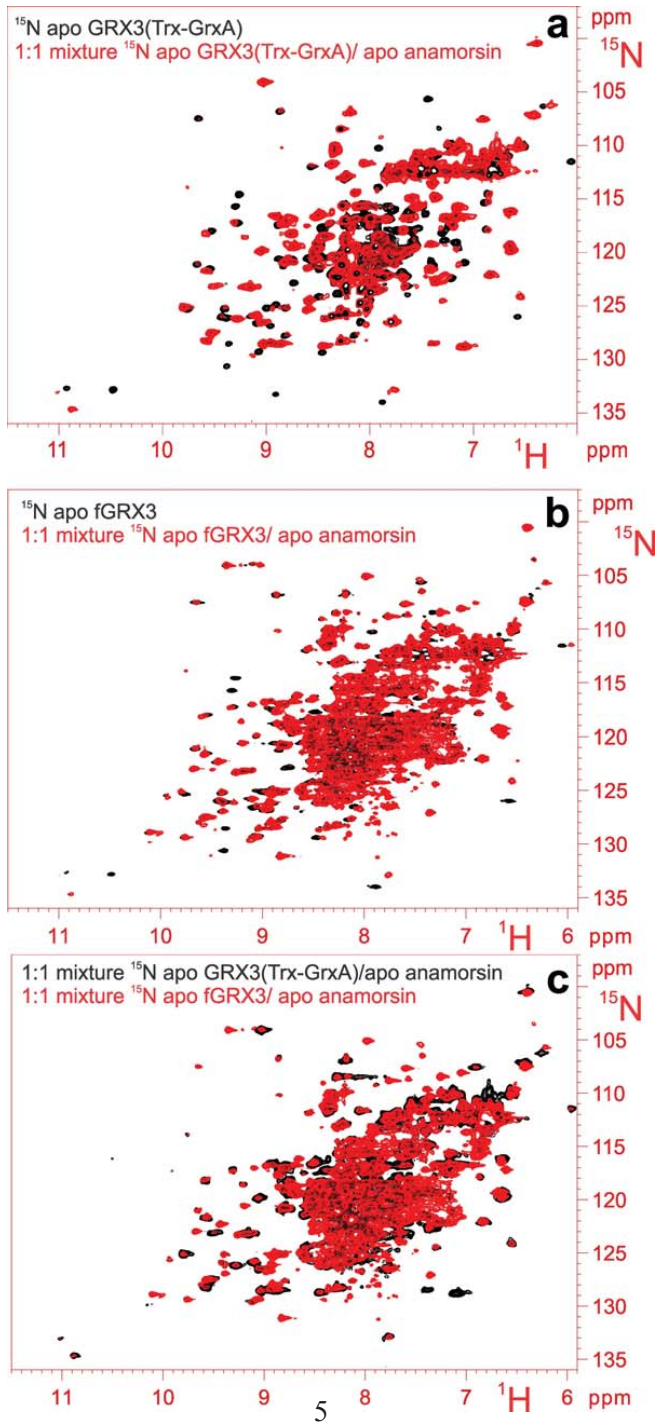

Supplementary Figure 4: NMR analysis of the interaction between different constructs of GRX3 and full-length anamorsin in their apo forms Overlay of ^{1}H-^{15}N HSQC spectral regions of ^{15}N labeled apo GRX3(GrxA/B) (black) and GRX3(TRX) (red) GRX3 with 1:1 mixtures between ^{15}N labeled apo GRX3(Trx-GrxA) and unlabelled apo anamorsin (green), and between ^{15}N labeled apo fGRX3 and unlabelled apo anamorsin (cyano). Arrows indicate chemical shift changes of NHs belonging to the Trx domain, while NHs of GrxA and GrxB domains remain essentially unperturbed.

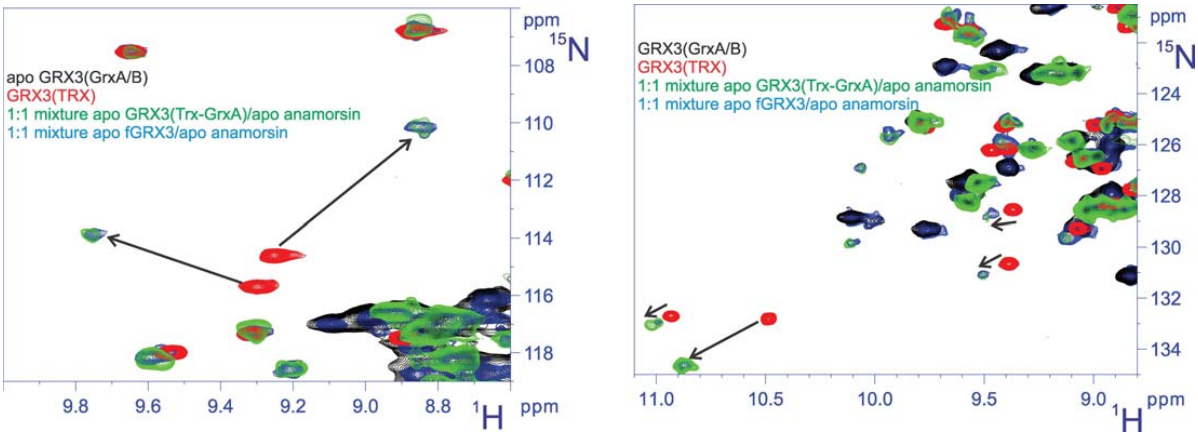

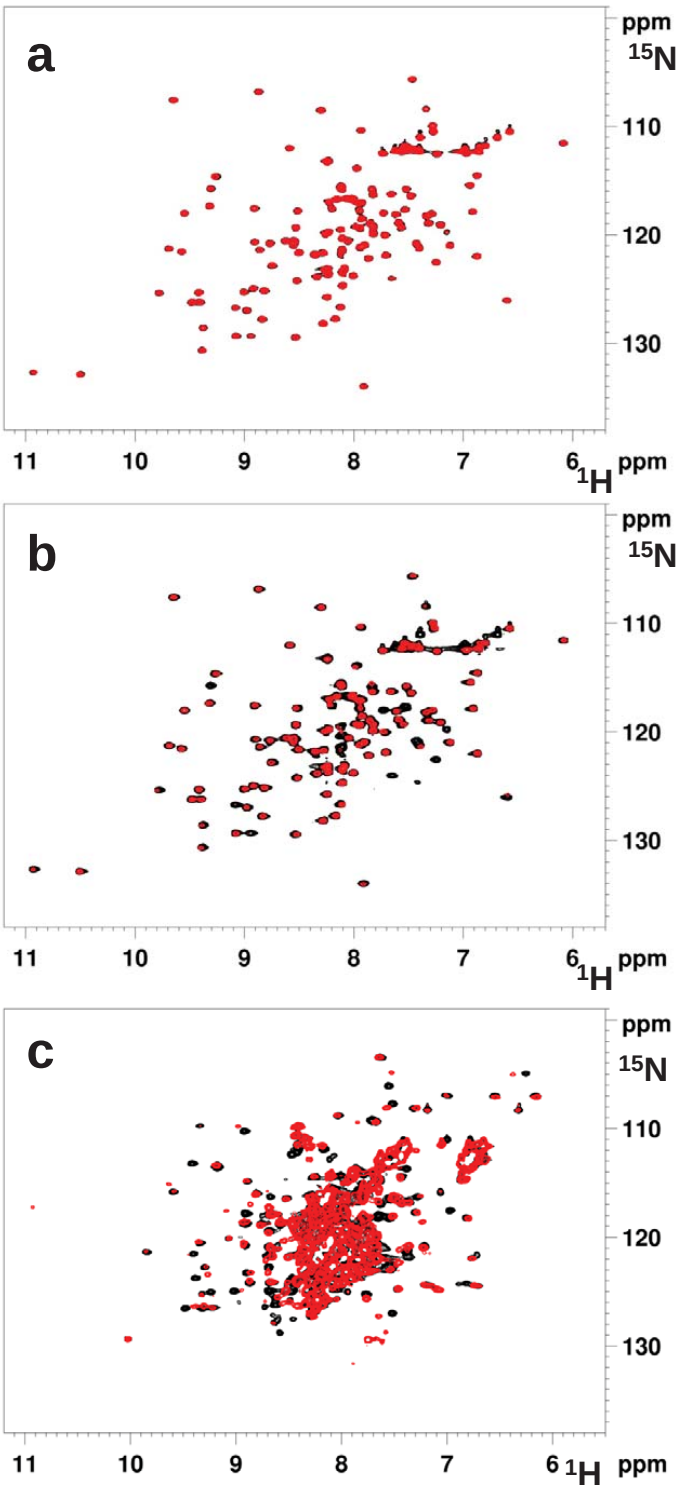

Supplementary Fig. 5. Monitoring by NMR the interaction site of apo anamorsin with the Trx domain of apo GRX3. (**a**) Overlay of ^{1}H-^{15}N HSQC spectra, recorded at 700 MHz and 298 K, of ^{15}N labeled GRX3(Trx) before (black) and after (red) incubation with 1 eq. of the apo form of the CIAPIN1 domain of anamorsin, and (**b**) before and after addition of 1 eq. of the N-domain of anamorsin to this mixture. (**c**) Overlay of ^{1}H-^{15}N HSQC spectra of ^{15}N labeled apo anamorsin before (black) and after (red) incubation with 1 eq. of GRX3(Trx) recorded at 800 MHz and 298 K.

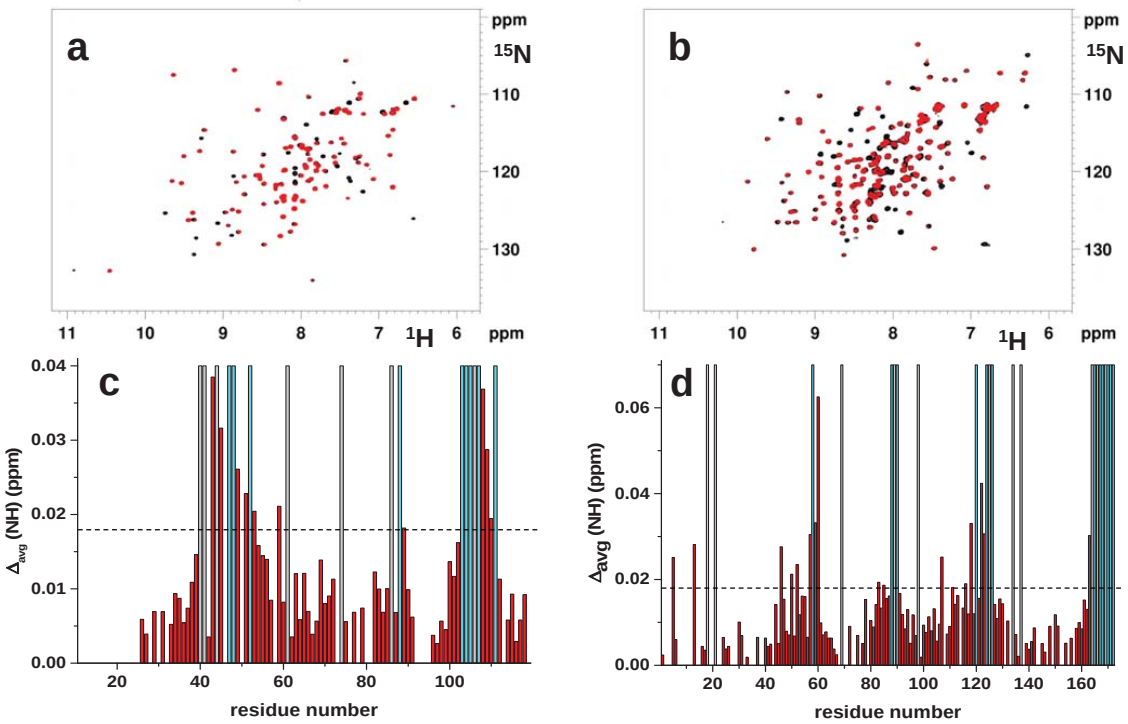

Supplementary Fig. 6. NMR analysis of the protein-protein interaction between the N-terminal domains of GRX3 and anamorsin. Overlay of ^{1}H-^{15}N HSQC spectra of ^{15}N labeled GRX3(Trx) (**a**) and of ^{15}N labeled N-domain of anamorsin (**b**) before (black) and after (red) incubation with 1 eq. of the N-domain of anamorsin and GRX3(Trx), respectively, recorded at 950MHz and 800MHz, respectively. Backbone weighted average chemical shift differences $\Delta_{avg}(HN)$ (i.e. $((\Delta H)^2 + (\Delta N/5)^2)/2)^{1/2}$, where ΔH and ΔN are chemical shift differences for ^{1}H and ^{15}N, respectively) versus residue numbers, observed upon addition of 1 eq. of the unlabelled N-domain of anamorsin to ^{15}N-labeled GRX3(Trx) (**c**), and upon addition of 1 eq. of unlabelled GRX3(Trx) to ^{15}N labeled N-domain of anamorsin (**d**). Gray bars indicate Pro residues and the unassigned backbone NH of Ala 40 of GRX3(Trx), cyano bars indicate backbone NHs which broadened beyond detection. Thresholds of 0.018 ppm (mean value of $\Delta_{avg}(HN)$ plus 1σ, black dashed line) were used in both titrations to identify significant chemical shift differences.

Supplementary Fig. 7. Monitoring by NMR the interaction between [2Fe-2S] cluster-bound forms of GRX3 and apo anamorsin. (**a**) Overlay of ^{1}H-^{15}N HSQC spectra of a 1:1 mixture of ^{15}N labeled [2Fe-2S]-GRX3(Trx-GrxA)$_2$/unlabeled apo anamorsin (red) and a 1:1 mixture of ^{15}N labeled apo GRX3(Trx-GrxA)/unlabeled apo anamorsin (black). (**b**) Overlay of ^{1}H-^{15}N HSQC spectra of a 1:1 mixture of ^{15}N labeled [2Fe-2S]$_2$-fGRX3$_2$/unlabeled apo anamorsin (red) and a 1:1 mixture of ^{15}N labeled apo fGRX3/unlabeled apo anamorsin (black).

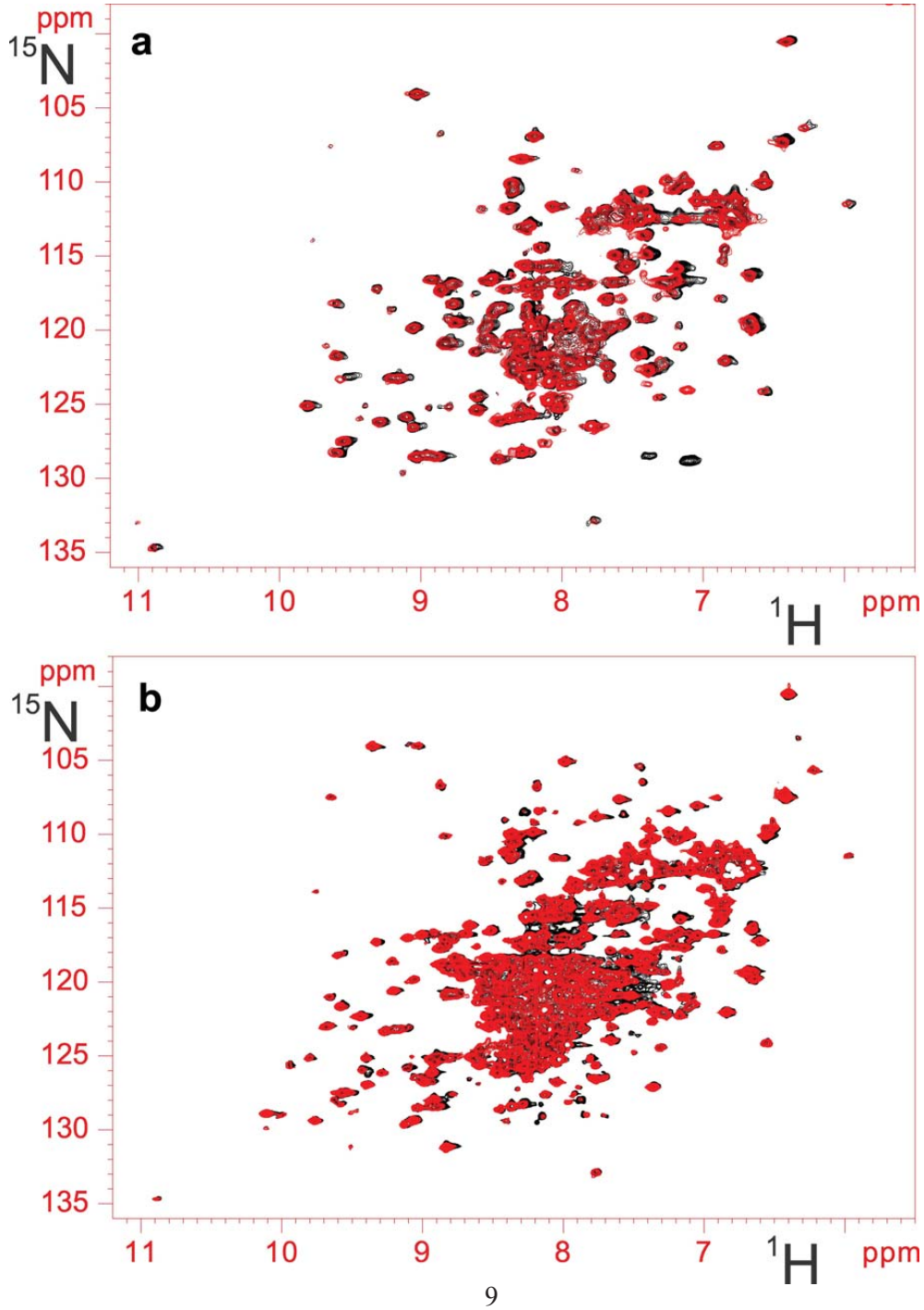

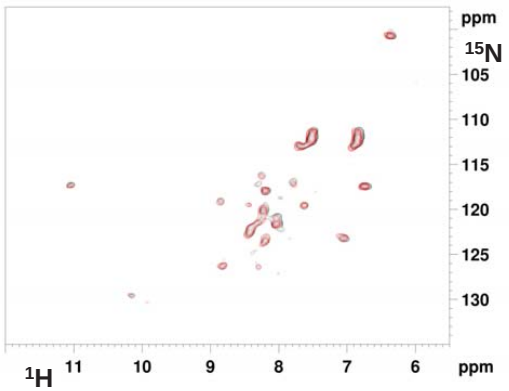

Supplementary Fig. 8. Paramagnetic NMR spectra to monitor cluster transfer from [2Fe-2S]-GRX3(Trx-GrxA)$_2$ to apo anamorsin. Overlay of paramagnetic IR-^{15}N-HSQC-AP spectra of a ~1:1 apo anamorsin/[2Fe-2S]-GRX3(Trx-GrxA)$_2$ mixture (black) and of [2Fe-2S]- anamorsin (red) recorded at 700MHz and 311K.

5.2. A new tool for NMR[3]

As mentioned, a crucial factor for the understanding of structure-function relationships in metalloproteins is the identification of NMR signals from residues surrounding the metal cofactor. When the latter is paramagnetic, the NMR information in the proximity of the metal center may be scarce, because fast nuclear relaxation quenches signal intensity and coherence transfer efficiency. To identify residues at a short distance from a paramagnetic center, we developed a modified version of the ^{15}N-HSQC experiment where

- is added an inversion recovery filter prior to HSQC,
- the INEPT period has been optimized according to fast relaxation of interested spins,
- the inverse INEPT has been eliminated and signals acquired as antiphase doublets.

Large contributions to relaxation and small contributions to chemical shift represent the most challenging situation for resonance assignment. Unfortunately, some of the metal cofactors that play a fundamental role in metalloproteins have negligible magnetic susceptibility anisotropy and, therefore, belong to this category[4,5]. In iron-sulfur containing proteins ((Fe-S) proteins, hereafter), relatively long electron relaxation times and a highly symmetric electronic environment around iron ions give rise to efficient nuclear relaxation and negligible hyperfine shifts for resonances of nuclei not belonging to iron bound residues but in spatial proximity to the cluster. The magnetic coupling between iron ions renders (Fe-S) clusters less paramagnetic than isolated, tetra coordinated iron ions[6]; however the extent

of magnetic coupling is difficult to predict ‘‘a priori’’ and may vary even for structurally homologous proteins[7,8]. An understanding of the structural properties of residues in the proximity of the cluster is crucial for the elucidation of (Fe-S) proteins structure-function relationships. NMR methodologies need to be developed in order to detect signals that, on one hand cannot be identified in 1D NMR experiments because they are overwhelmed from the bulk diamagnetic envelope and, on the other hand, cannot be observed in conventional double and triple resonance experiments because coherence transfer and NOEs are quenched due to fast relaxation. So for testing this modified pulse sequence of a ^{1}H-^{15}N HSQC, we selected the c-terminal part of anamorsin. Experiments were recorded on a 11.7 T Bruker AVANCE 500 MHz equipped with a triple resonance, inverse detection, cryoprobe (TXI). All experiments were recorded using the same overall experimental time. Standard ^{15}N-HSQC experiments were recorded using Watergate and flip-back pulses to suppress solvent signal. 96 scans were recorded over 256 increments, with 1.1 s as recycle delay. For IR-^{15}N-HSQC-AP experiments, 2,048 scans were collected over 100 increments (t1max= 24.7 ms), using an INEPT transfer period of 833 us. Acquisition time, recycle delay and inversion recovery (IR) delay were 20, 55 and 50 ms, respectively. T_1 measurements were obtained from a series of ten IR-^{15}N-HSQC-AP experiments recorded using IR delays of 50, 35, 25, 15, 10, 7, 5, 3, 2, 1 ms. The pulse sequence of the IR ^{15}N-HSQC, antiphase detected experiment (IR-^{15}N-HSQC-AP) is reported in **Fig.34**.

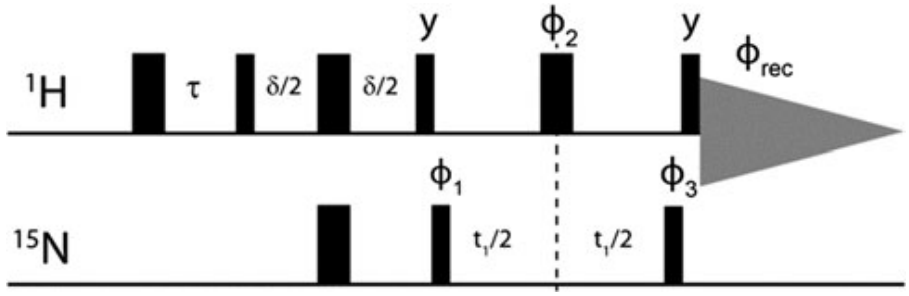

Figure 34. Pulse scheme of IR-^{15}N-HSQC-AP. Narrow and wide symbols stand for 90° and 180° pulses, respectively. The pulses were applied along the x axis unless noted differently. The phase cycling employed is as follows: ϕ_1 = (x,-x) ϕ_2 = (x,x,-x,-x) ϕ_3= (x,x,x,x,-x,-x,-x,-x) ϕ_{rec} = (x,-x,x,-x,-x,x,-x,x). Quadrature in F1 is obtained via States-TPPI of /1

At variance with conventional ^{15}N-HSQC experiments, ^{1}H excitation has been accomplished via an IR building block. IR discriminates nuclear spin magnetizations according to their T_1 relaxation times: a suitable choice of the interpulse delay s causes a sign discrimination between fast relaxing signals and slow relaxing signals[9,10]. When IR is combined with a short duty cycle, the intensity of diamagnetic signals is significantly suppressed, and the paramagnetic ^{1}H resonances that are usually overwhelmed by the bulk envelope of diamagnetic signals can be observed. In ^{15}N-HSQC experiments, the loss of magnetization during coherence transfer steps is, of course, another factor that modulates signal intensity. To circumvent the problem, the INEPT period can be shortened according to T_2 relaxation properties of signals of interest[20]. When the overall INEPT period is shortened down to 1.5 ms, coherence transfer efficiency of 57, 37 and 17 % are recovered for signals characterized by T_2 values of 5, 2 and 1 ms, respectively, while the efficiency of coherence transfer from nuclei that experience a smaller hyperfine interaction is about 75%. The most critical step of a standard ^{15}N-HSQC experiment is the inverse INEPT block, during which coherences are

back converted into observable, in phase Hy. When both forward and backward INEPT steps are used, a signal with T_2 = 1 ms (Dm ca. 300 Hz) will exhibit, under the very best experimental conditions, an overall transfer efficiency of 4%. As a consequence, a reduction of the INEPT period without any pulse sequence modification allows one only to detect HN connectivities involving ^{1}H resonances ≤ 250 Hz linewidth and fails at larger linewidths. To overcome the problem, we removed the inverse INEPT refocusing step and we acquired the signal as a doublet, antiphase component without 15N decoupling during acquisition. The IR-^{15}N-HSQC-AP experiment is not only useful to identify previously undetected signals, but also provides metal-to proton distances which, in the proximity of the prosthetic group, are the most valuable structural constraint[11] The CIAPIN1 domain of the human protein anamorsin[12,13] is a challenging system to test the sequence presented above. It is a 108 amino acid domain that binds a $[2Fe\text{-}2S]^{2+}$ cluster per molecule. The CIAPIN1 domain is largely unstructured without significant tertiary structure organization (**Fig.35**).

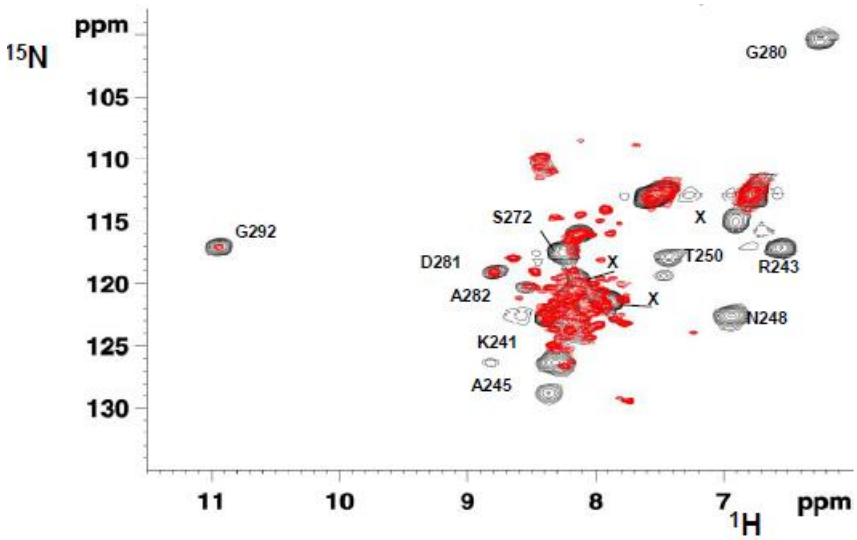

Figure 35 Overlay of a standard ^{15}N-HSQC (red) and IR-^{15}NHSQC- AP (black) experiments acquired on 500 MHz at 298 K on the $[2Fe\text{-}2S]^{2+}$-CIAPIN1 domain.

$[2Fe\text{-}2S]^{2+}$ clusters are expected to induce minimal hyperfine shift and sizable hyperfine. nuclear relaxation on 1H spins that do not belong to metal coordinating cysteine residues but are within a, roughly, 10 A° distance from each of the two iron ions. Consistent with expectations, the ^{15}N-HSQC spectrum of the protein, recorded under standard conditions, shows only 71 out of 108 residues. Their assignment was performed via conventional double and triple resonance experiments[12]. As shown in **Fig. 35** when IR-^{15}N-HSQC-AP experiment was performed, 10 additional HN signals, completely absent in previous experiments, are now observed. Furthermore, three HN signals, barely detectable in conventional experiments, significantly increased their intensity. The IR-^{15}N-HSQC-AP experiment selectively identifies HN groups from the environment of the paramagnetic center that experience significant paramagnetic relaxation and almost negligible contributions to chemical shift. In particular, we have shown that in the case of proteins involved in the iron-sulfur protein biogenesis, the IR-^{15}N-HSQC-AP experiment substantially contributes to decrease, and eventually abolish, the blind sphere around the metal center that typically escape routine NMR investigation.

J Biomol NMR
DOI 10.1007/s10858-013-9810-2

ARTICLE

The IR-^{15}N-HSQC-AP experiment: a new tool for NMR spectroscopy of paramagnetic molecules

Simone Ciofi-Baffoni · Angelo Gallo · Riccardo Muzzioli · Mario Piccioli

Received: 29 October 2013 / Accepted: 27 December 2013

Abstract A crucial factor for the understanding of structure-function relationships in metalloproteins is the identification of NMR signals from residues surrounding the metal cofactor. When the latter is paramagnetic, the NMR information in the proximity of the metal center may be scarce, because fast nuclear relaxation quenches signal intensity and coherence transfer efficiency. To identify residues at a short distance from a paramagnetic center, we developed a modified version of the ^{15}N-HSQC experiment where (1) an inversion recovery filter is added prior to HSQC, (2) the INEPT period has been optimized according to fast relaxation of interested spins, (3) the inverse INEPT has been eliminated and signals acquired as antiphase doublets. The experiment has been successfully tested on a human [Fe_2S_2] protein which is involved in the biogenesis of iron-sulfur proteins. Thirteen H_N resonances, unobserved with conventional HSQC experiments, could be identified. The structural arrangement of the protein scaffold in the proximity of the Fe/S cluster is fundamental to comprehend the molecular processes responsible for the transfer of Fe/S groups in the iron-sulfur protein assembly machineries.

Keywords Iron-sulfur proteins · Paramagnetic NMR · ^{15}N-HSQC · Pulse sequences · Paramagnetic relaxation · Anamorsin

S. Ciofi-Baffoni · A. Gallo · R. Muzzioli · M. Piccioli (✉)
Magnetic Resonance Center and Department of Chemistry, University of Florence, Via Luigi Sacconi 6, 50019 Sesto Fiorentino, Florence, Italy
e-mail: piccioli@cerm.unifi.it

Introduction

Solution state and solid state NMR spectroscopy of paramagnetic molecules (Knight et al. 2013; Otting 2010; Arnesano et al. 2006) play a fundamental role in the understanding of many biological processes, such as electron transfer (Ubbink 2012), metal homeostasis (Lutsenko 2010; Banci et al. 2010), metal trafficking (Finney and O'Halloran 2003; Banci et al. 2006; Boal and Rosenzweig 2009; Leary et al. 2009). Metalloproteins offer many examples in which structure, function and dynamics have been found to be redox dependent (Fetrow and Baxter 1999; Bertini et al. 1995; Lyons et al. 1996), or to be driven by the coordination chemistry of the metal center (Caillet-Saguy et al. 2012). Paramagnetic probes (Gaponenko et al. 2004; Keizers and Ubbink 2011; Iwahara et al. 2004) have been used for decades to study structure (Yagi et al. 2013), dynamics and solvent accessibility (Bertini et al. 1997) of large biomolecules (Clore and Iwahara 2009), multidomain proteins (Russo et al. 2013; Bertini et al. 2007) and biomolecular complexes (Volkov et al. 2010), in which only sparse information is available via conventional NMR approaches (Bertini et al. 2002; Balayssac et al. 2006; Machonkin et al. 2002).

The wide, and still growing, range of application of paramagnetic NMR depends on the fact that electronic correlation times of metal centers range from 10^{-13} to 10^{-8} s (Bertini et al. 2001b). As a consequence, nuclear relaxation properties of the environment of the metal centers are versatile. The hyperfine interaction affects NMR shifts and linewidths to different extents and, therefore one faces different scenarios depending on the metal ion, on the coordination environment, and on the nucleus investigated. As summarized in Fig. 1, for a ^{1}H spin at a fixed distance from the metal center, calculated contributions (Bertini

Published online: 11 January 2014

et al. 2001b) to nuclear relaxation and chemical shifts range from null to thousands Hz and hundreds of ppm, depending on the paramagnetic probe.

Large contributions to relaxation and small contributions to chemical shift represent the most challenging situation for resonance assignment. Unfortunately, some of the metal cofactors that play a fundamental role in metalloproteins have negligible magnetic susceptibility anisotropy and, therefore, belong to this category (Bertini et al. 1994b; Abriata et al. 2009). When the magnetic susceptibility tensor of the metal cofactor is not affected by efficient spin-orbit coupling mechanisms, hyperfine shifts only arise from unpaired electron spin density delocalized onto the observed nuclear spin, which typically quenches a few chemical bonds away from the metal center, unless spin polarization mechanisms due to the presence of aromatic ligands occurs (Bertini et al. 1994c). However, the electron spin-nuclear spin dipolar coupling still contributes to nuclear relaxation; as a consequence, signals that do not belong to the first coordination sphere but are spatially close to the metal cofactor, exhibit negligible hyperfine shifts but efficient paramagnetic relaxation enhancements (Im et al. 1998; Skjeldal et al. 1991; Mo et al. 1999).

In iron-sulfur containing proteins (Fe/S proteins, hereafter), relatively long electron relaxation times and a highly symmetric electronic environment around iron ions give rise to efficient nuclear relaxation and negligible hyperfine shifts for resonances of nuclei not belonging to iron bound residues but in spatial proximity to the cluster. The magnetic coupling between iron ions renders Fe/S clusters less paramagnetic than isolated, tetra coordinated iron ions (Wilkens et al. 1998); however the extent of magnetic coupling is difficult to predict "a priori" and may vary even for structurally homologous proteins (Bertini et al. 1992; Banci et al. 1993). An understanding of the structural properties of residues in the proximity of the cluster is crucial for the elucidation of Fe/S proteins structure-function relationships. In the past, this has been successfully addressed for small electron transfer proteins such as High Potential Iron-Sulfur Proteins (HiPIP) and Ferredoxins (Fdx) (Lin et al. 2009; Volkman et al. 1999; Bentrop et al. 1996; Bertini et al. 1994a). Recently, our group faced the problem to characterize the functional properties of Fe/S proteins involved into Fe/S cluster biogenesis (Banci et al. 2011, 2013a; b). At variance with HiPIP and Fdx, characterized by rigid structures and high thermodynamic stability, these proteins show flexible structures and various conformational states, particularly in the proximity of the cofactor binding sites, that are driven by the uptake and release of the Fe/S cluster (Markley et al. 2013; Li et al. 2013). NMR methodologies need to be developed in order to detect signals that, on one hand cannot be identified in 1D NMR experiments because they are overwhelmed from the bulk diamagnetic envelope and, on the other hand, cannot be observed in conventional double and triple resonance experiments because coherence transfer and NOEs are quenched due to fast relaxation. We present here a modified version of the ^{15}N-HSQC experiment which enables the identification of residues at a short distance from the Fe/S cluster and applied it to the largely unstructured, C-terminal domain of the human $[Fe_2S_2]$ protein anamorsin.

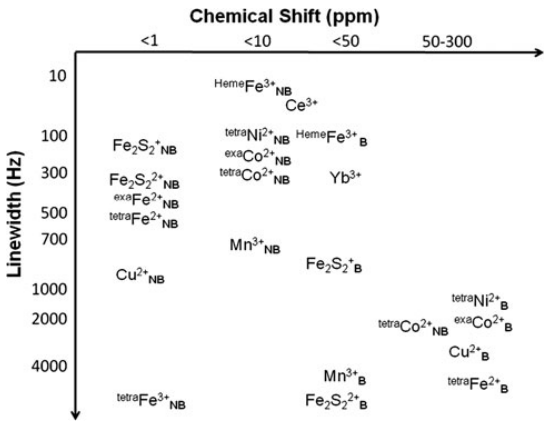

Fig. 1 Expected hyperfine shifts versus expected paramagnetic *line* broadening in ^{1}H resonances for a number of metal centers for directly metal bound (subscript B) and non bound (subscript NB) residues. Tetra and exa *indicate* tetrahedral and octahedral coordination geometries, respectively. Values are estimated by using reported values of electronic relaxation times (Bertini et al. 2001b). For signals from coordinating residues, a 3.5 Å distance from the metal and hyperfine coupling constants ranging 1–4 MHz were considered. For non bound residues, a metal to proton distance of 6 Å was considered. Simulations were performed assuming B_0 = 11.7 T (500 MHz). Scales in both x- and y-axis are arbitrary

Materials and methods

Protein expression and purification

The C-terminal domain of the human protein anamorsin, residues 205-312, named cytokine-induced apoptosis inhibitor 1 (CIAPIN1 domain, hereafter), has been cloned and produced as an independent domain, according to a previously reported methodology (Banci et al. 2013a). This domain was found to bind Fe_2S_2 clusters with two ferric ions ($[Fe_2S_2]^{2+}$, hereafter) (Banci et al. 2011, 2013b).

NMR spectroscopy

Experiments were recorded on a 11.7 T Bruker AVANCE 500 equipped with a triple resonance, inverse detection,

cryoprobe (TXI). All experiments were recorded using the same overall experimental time. Standard ^{15}N-HSQC experiments were recorded using Watergate and flip-back pulses to suppress solvent signal. 96 scans were recorded over 256 increments, with 1.1 s as recycle delay. To collect a fast repetition ^{15}N-HSQC, the GARP4 decoupling scheme was replaced with an adiabatic decoupling that covers 1,500 Hz and uses a 2 ms 180° pulse. 288 scans were recorded over 256 increments with a recycle delay of 350 ms. For IR-^{15}N-HSQC-AP experiments, 2,048 scans were collected over 100 increments (t_{1max}= 24.7 ms), using an INEPT transfer period of 833 us. Acquisition time, recycle delay and inversion recovery (IR) delay were 20, 55 and 50 ms, respectively. T_1 measurements were obtained from a series of ten IR-^{15}N-HSQC-AP experiments recorded using IR delays of 50, 35, 25, 15, 10, 7, 5, 3, 2, 1 ms. Signals characterized by T_1 values longer than 100 ms were measured using a series of experiments using a recycle delay of 350 ms and IR delays of 250, 150, 100, 60, 40, 25, 15, 8, 4 ms.

Results and discussion

The IR-^{15}N-HSQC-AP experiment

The pulse sequence of the IR ^{15}N-HSQC, antiphase detected experiment (IR-^{15}N-HSQC-AP) is reported in Fig. 2. At variance with conventional ^{15}N-HSQC experiments, ^{1}H excitation has been accomplished via an IR building block. IR discriminates nuclear spin magnetizations according to their T_1 relaxation times: a suitable choice of the interpulse delay τ causes a sign discrimination between fast relaxing signals and slow relaxing signals (Gelis et al. 2003; Machonkin et al. 2004). When IR is combined with a short duty cycle, the intensity of diamagnetic signals is significantly suppressed, and the paramagnetic ^{1}H resonances that are usually overwhelmed by the bulk envelope of diamagnetic signals can be observed. In ^{15}N-HSQC experiments, the loss of magnetization during coherence transfer steps is, of course, another factor that modulates signal intensity. Coherence transfer from H_y to $2H_xN_z$ and vice versa competes with relaxation of the $2H_xN_z$ antiphase magnetization which, in a paramagnetic system, is dominated by ^{1}H T_2 relaxation. As shown in Fig. 3, for a ^{1}H signal with T_2 values of 5 ms, about 60% of signal is retained after a standard INEPT transfer step, while only 7% is retained for T_2 values as short as 1 ms. To circumvent the problem, the INEPT period can be shortened according to T_2 relaxation properties of signals of interest (Piccioli and Poggi 2002). When the overall INEPT period is shortened down to 1.5 ms, coherence transfer efficiency of 57, 37 and 17 % are recovered for signals characterized by T_2 values of 5, 2 and 1 ms, respectively, while the efficiency of coherence transfer from nuclei that experience a smaller hyperfine interaction is about 75%. In principle, the hyperfine interaction affects also longitudinal relaxation rates of ^{15}N spins and additional contributions to the relaxation of antiphase H_xN_z magnetization should be considered. However, paramagnetic dipolar relaxation is dependent on the γ^2 of the nucleus and therefore the paramagnetic relaxation experienced by heteronuclear spin can be safely neglected (Bermel et al. 2006). The INEPT approach is useless for ^{1}H resonances with T_2<0.5 ms (Δν ca.> 600 Hz). For the latter case, the coherence transfer pathway never exceeds 10% efficiency and therefore the direct excitation of ^{15}N spins is the best approach (Hsueh et al. 2010).

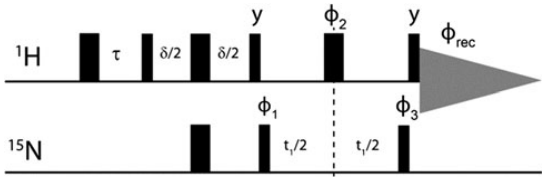

Fig. 2 Pulse scheme of IR-^{15}N-HSQC-AP. Narrow and wide symbols stand for 90° and 180° pulses, respectively. The pulses were applied along the *x* axis unless noted differently. The phase cycling employed is as follows: $\phi_1 = (x,-x)$ $\phi_2 = (x,x,-x,-x)$ $\phi_3 = (x,x,x,x,-x,-x,-x,-x)$ $\phi_{rec} = (x,-x,x,-x,-x,x,-x,x)$. Quadrature in F1 is obtained via States-TPPI of ϕ_1

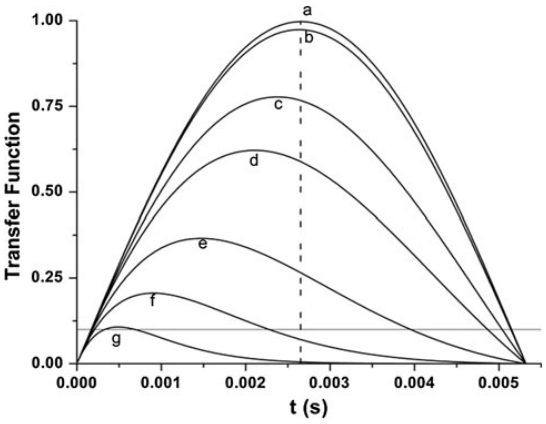

Fig. 3 Efficiency of an INEPT transfer function at different ^{1}H T_2 values: *b* 100 ms, *c* 10 ms, *d* 5 ms, *e* 2 ms, *f* 1 ms, *g* 0.5 ms. Relaxation is neglected in *a*. *Letters* have been drawn at the correspondence of the maximum values for each transfer function. A *dashed line* is shown at the 2.65 ms of INEPT step (94 Hz for ^{1}H-^{15}N J coupling). A *solid line* is shown in correspondence of 10% transfer efficiency

The most critical step of a standard ^{15}N-HSQC experiment is the inverse INEPT block, during which coherences are back converted into observable, in phase Hy. When both forward and backward INEPT steps are used, a signal with T_2 = 1 ms ($\Delta\nu$ ca. 300 Hz) will exhibit, under the very best experimental conditions, an overall transfer efficiency of 4%. As a consequence, a reduction of the INEPT period without any pulse sequence modification allows one only to detect H_N connectivities involving ^{1}H resonances $\leq$250 Hz linewidth and fails at larger linewidths. To overcome the problem, we removed the inverse INEPT refocusing step and we acquired the signal as a doublet, antiphase component without ^{15}N decoupling during acquisition. In this simplified scheme, the critical ^{1}H T_2 relaxation is operative only during t_2 acquisition that should be tuned accordingly. The loss in sensitivity arising from the acquisition of the antiphase component versus an in-phase singlet is partly recovered when the direct acquisition dimension is processed with a 90° phase shift. i.e. the antiphase doublet is processed in dispersion mode. When signal linewidth is larger than doublet separation, the components of in phase doublets partly overlap and cancel signal (Bertini et al. 2005). However, when the doublet is phased in dispersion mode, it gives rise to a "pseudosinglet" originated by the sum of the two dispersive components of the doublet. This contributes to the identification of broad, fast relaxing peaks and also to discriminate signals more severely affected by paramagnetic relaxation with respect to the others.

The IR-^{15}N-HSQC-AP experiment is not only useful to identify previously undetected signals, but also provides metal-to proton distances which, in the proximity of the prosthetic group, are the most valuable structural constraint (Bertini et al. 2001a). Indeed, when a series of IR-^{15}N-HSQC-AP experiments is performed in which the interpulse delay of the IR building block, τ, is arrayed, non selective T_1 values of ^1H_N amide resonances are obtained according to a classical IR ^{1}H experiment where the 90° reading pulse is replaced by the ^{15}N-HSQC-AP block. Assuming that ^{1}H relaxation is dominated by the electron spin-nuclear spin metal centered dipolar contribution, T_1 hyperfine relaxation directly depends on r_{MH}^{-6}.

The case of Fe/S proteins

The CIAPIN1 domain of the human protein anamorsin (Banci et al. 2013b; Banci et al. 2011) is a challenging system to test the sequence presented above. It is a 108 amino acid domain that binds a $[Fe_2S_2]^{2+}$ cluster per molecule (Banci et al. 2013a, b). The CIAPIN1 domain is largely unstructured without significant tertiary structure organization (Fig. 4). $[Fe_2S_2]^{2+}$ clusters are expected to induce minimal hyperfine shift and sizable hyperfine nuclear relaxation on ^{1}H spins that do not belong to metal coordinating cysteine residues but are within a, roughly, 10 Å distance from each of the two iron ions. Consistent with expectations, the ^{15}N-HSQC spectrum of the protein, recorded under standard conditions, shows only 71 out of 108 residues. Their assignment was performed via conventional double and triple resonance experiments (Banci et al. 2013a). About 30% of the resonances remain unobserved due to paramagnetic broadening or exchange contributions. As shown in Fig. 4, when IR-^{15}N-HSQC-AP experiment was performed, 10 additional H_N signals, completely absent in previous experiments, are now observed. Furthermore three H_N signals, barely detectable in conventional experiments, significantly increased their intensity. The repetition of the experiment at different IR delays allowed us, from the analysis of integrated intensity of the paramagnetic ^{1}H-^{15}N resonances, to measure the T_1 values for 12 out of 13 paramagnetic ^{1}H signals, that have been identified in IR-^{15}N-HSQC-AP from nuclei spatially close to the $[Fe_2S_2]^{2+}$ cluster. Four of them had T_1 shorter than 10 ms, four in 10–20 ms range, one 20–50 ms range, and three in the 80–150 ms range. An assignment has been proposed for 10 out of 13 resonances by the analysis of chemical shift values, relaxation rates, and ^{13}C-detected experiments tailored to paramagnetic systems (Banci et al. 2013a).

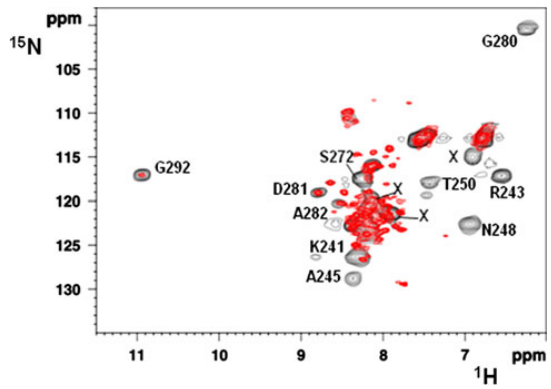

Fig. 4 Overlay of a standard ^{15}N-HSQC (*thin lines*) and IR-^{15}N-HSQC-AP (*thick lines*) experiments acquired on 500 MHz at 298 K on the $[Fe_2S_2]^{2+}$-CIAPIN1 domain. The experimental time for both experiments was ca. 7 h. For the IR-^{15}N-HSQC-AP, acquisition times of 20 and 24 ms were used in t_2 and t_1 acquisition dimensions, respectively, and recycle and IR delays were 55 and 50 ms, respectively. To rule out effects due to short recycle delays, the reference ^{15}N HSQC has been recorded with a 350 ms overall recycle delay. *Peaks* are labeled according to their assignment (Banci et al. 2013a). Unassigned resonances are indicated with X. Signals attributed to D281, A282 and G292 were observed also in the reference experiment but at much lower intensity. For 12 out of 13 *peaks* T_1 values could be obtained. Ten of them have been used as structural constraints

Conclusions

The collection of an exhaustive series of double and triple resonance experiments, in which all parameters have been previously optimized on the basis of reference systems, is nowadays the approach of every NMR laboratory involved in structural biology. Paramagnetic centers cannot be treated with a routine approach and require knowledge of the electronic properties of the metal cofactor of the molecule. We have shown here that fundamental pulse sequence building blocks such as the ^{15}N-HSQC experiment can be easily modified in order to improve the outcome of standard experiments. The IR-^{15}N-HSQC-AP experiment selectively identifies H_N groups from the environment of the paramagnetic center that experience significant paramagnetic relaxation and almost negligible contributions to chemical shift. For the identified H_N resonances, the experiment provides also T_1 relaxation times, which are dependent on the r_{MH}^{-6} on the basis of the Solomon equation (Arnesano et al. 2006) and typically constitute the most precious structural information for metalloprotein structural studies.

This experiment is valuable for those systems in which no pseudocontact shift occurs, such as Cu^{2+} proteins and Fe/S proteins. In particular, we have shown that in the case of proteins involved in the iron-sulfur protein biogenesis, the IR-^{15}N-HSQC-AP experiment substantially contributes to decrease, and eventually abolish, the blind sphere around the metal center that typically escape routine NMR investigation. The structural arrangement of protein scaffold in the proximity of the Fe/S cluster is a fundamental factor to be investigated to comprehend at the molecular level the events responsible of the transfer of Fe/S groups in the iron-sulfur protein assembly machineries.

Acknowledgments Dr Maciej Mikolajczyk is gratefully acknowledged for the production of CIAPIN1 samples. We gratefully acknowledge the "Programmi di Ricerca di Rilevante Interesse Nazionale" (PRIN) (2009FAKHZT_001), POR CREO FESR 2007-20013—Finding "Farmaci innovativi per malattie neurodegenerative", POR CREO FESR 2007-20013—Biovax "Vaccini biotecnologici da genomica strutturale" and Ente Cassa di Risparmio di Firenze for financial support. This work was supported by the European Union ESFRI Instruct Core Centre "Centro di Risonanze Magnetiche" (Italy).

References

Abriata LA, Ledesma GN, Pierattelli R, Vila AJ (2009) Electronic structure of the ground and excited states of the Cu_a site by NMR spectroscopy. J Am Chem Soc 131:1939–1946

Arnesano F, Banci L, Piccioli M (2006) NMR structures of paramagnetic metalloproteins. Q Rev Biophys 38:167–219

Balayssac S, Bertini I, Luchinat C, Parigi G, Piccioli M (2006) ^{13}C direct detected NMR increases the detectability of residual dipolar couplings. J Am Chem Soc 128:15042–15043

Banci L, Bertini I, Ciurli S, Ferretti S, Luchinat C, Piccioli M (1993) The electronic structure of $(Fe_4S_4)^{3+}$ clusters in proteins. An investigation of the oxidized high-potential iron-sulfur protein II from *Ectothiorhodospira vacuolata*. Biochemistry 32:9387–9397

Banci L, Bertini I, Ciofi-Baffoni S, Kandias NG, Spyroulias GA, Su XC, Robinson NJ, Vanarotti M (2006) The delivery of copper for thylakoid import observed by NMR. Proc Natl Acad Sci USA 103:8325

Banci L, Bertini I, Cantini F, Ciofi-Baffoni S (2010) Cellular copper distribution: a mechanistic systems biology approach. Cell Mol Life Sci 67:2563–2589

Banci L, Bertini I, Ciofi-Baffoni S, Boscaro F, Chatzi A, Mikolajczyk M, Tokatlidis K, Winkelmann J (2011) Anamorsin is a 2Fe2S cluster-containing substrate of the Mia40-dependent mitochondrial protein trapping machinery. Chem Biol 18:794–804

Banci L, Bertini I, Calderone V, Ciofi-Baffoni S, Giachetti A, Jaiswal D, Mikolajczyk M, Piccioli M, Winkelmann J (2013a) Molecular view of an electron transfer process essential for iron-sulfur protein biogenesis. Proc Natl Acad Sci USA 110:7136–7141

Banci L, Ciofi-Baffoni S, Mikolajczyk M, Winkelmann J, Bill E and Eirini Pandelia M (2013b) Human anamorsin binds (2Fe.2S) clusters with unique electronic properties. J Biol Inorg Chem 18:883–893

Bentrop D, Bertini I, Luchinat C, Mendes J, Piccioli M, Teixeira M (1996) Paramagnetic NMR of the 7Fe ferredoxin from the hyperthermoacidophilic archaeon *Desulfurolobus ambivalens* reveals structural similarity to other dicluster ferredoxins. Eur J Biochem 236:92–99

Bermel W, Bertini I, Felli IC, Piccioli M, Pierattelli R (2006) ^{13}C-detected protonless NMR spectroscopy of proteins in solution. Progr NMR Spectrosc 48:25–45

Bertini I, Capozzi F, Luchinat C, Piccioli M, Vicens Oliver M (1992) NMR is a unique and necessary step in the investigation of iron-sulfur proteins: the HiPIP from *R. gelatinosus* as an example. Inorg Chim Acta 198–200:483–491

Bertini I, Capozzi F, Luchinat C, Piccioli M, Vila AJ (1994a) The Fe_4S_4 centers in ferredoxins studied through proton and carbon hyperfine coupling. Sequence specific assignments of cysteines in ferredoxins from *Clostridium acidi urici* and *Clostridium pasteurianum*. J Am Chem Soc 116:651–660

Bertini I, Felli IC, Kastrau DHW, Luchinat C, Piccioli M, Viezzoli MS (1994b) Sequence-specific assignment of the ^{1}H and ^{15}N Nuclear Magnetic Resonance spectra of the reduced recombinant high potential iron sulfur protein (HiPIP) I from *Ectothiorhodospira halophila*. Eur J Biochem 225:703–714

Bertini I, Luchinat C, Piccioli M (1994c) Copper zinc superoxide dismutase a paramagnetic protein that provides a unique frame for the NMR investigations. Progr NMR Spectrosc 26:91–141

Bertini I, Eltis LD, Felli IC, Kastrau DHW, Luchinat C, Piccioli M (1995) The solution structure of oxidized HiPIP I from *Ectothiorhodospira halophila*, can NMR probe rearrangements associated to electron transfer processes? Chem Eur J 1:598–607

Bertini I, Dalvit C, Huber JG, Luchinat C, Piccioli M (1997) ePHOGSY experiment on a paramagnetic protein: location of the catalytic water molecule in the heme crevice of the oxidized form of horse heart Cytochrome c. FEBS Lett 415:45–48

Bertini I, Donaire A, Jiménez B, Luchinat C, Parigi G, Piccioli M, Poggi L (2001a) Paramagnetism-based versus classical constraints: an analysis of the solution structure of Ca Ln Calbindin D_{9k}. J Biomol NMR 21:85–98

Bertini I, Luchinat C, Parigi G (2001b) Solution NMR of paramagnetic molecules. Elsevier, Amsterdam

Bertini I, Cavallaro G, Cosenza M, Kümmerle R, Luchinat C, Piccioli M, Poggi L (2002) Cross correlation rates between curie spin and dipole-dipole relaxation in paramagnetic proteins: the case of cerium substituted Calbindin D_{9k}. J Biomol NMR 23:115–125

Bertini I, Jiménez B, Piccioli M (2005) ^{13}C direct detected experiments: optimisation to paramagnetic signals. J Magn Reson 174:125–132

Bertini I, Gupta YK, Luchinat C, Parigi G, Peana M, Sgheri L, Yuan J (2007) Paramagnetism-based NMR restraints provide maximum allowed probabilities for the different conformations of partially independent protein domains. J Am Chem Soc 129:12786–12794

Boal AK, Rosenzweig AC (2009) Structural biology of copper trafficking. Chem Rev 109:4760–4779

Caillet-Saguy C, Piccioli M, Turano P, Lukat-Rodgers G, Wolff N, Rodgers K, Izadi-Pruneyre N, Delepierre M, Lecroisey A (2012) Heme carrier HasA: learning about the role of the iron axial ligands in the heme uptake and release processes. J Biol Chem 287:26932–26943

Clore GM, Iwahara J (2009) Theory, practice, and applications of paramagnetic relaxation enhancement for the characterization of transient low-population states of biological macromolecules and their complexes. Chem Rev 109:4108–4139

Fetrow JS, Baxter SM (1999) Assignment of ^{15}N chemical shifts and ^{15}N relaxation measurements for oxidized and reduced iso-1-cytochrome *c*. Biochemistry 38:4480–4492

Finney LA, O'Halloran TV (2003) Transition metal speciation in the cell: insights from the chemistry of metal ion receptors. Science 300:931–936

Gaponenko V, Sarma SP, Altieri AS, Horita DA, Li J, Byrd RA (2004) Improving the accuracy of NMR structures of large proteins using pseudocontact shifts as long/range restraints. J Biomol NMR 28:205–212

Gelis I, Katsaros N, Luchinat C, Piccioli M, Poggi L (2003) A simple protocol to study blue copper proteins by NMR. Eur J Biochem 270:600–609

Hsueh KL, Westler WM, Markley JL (2010) NMR investigations of the Rieske protein from thermus thermophilus support a coupled proton and electron transfer mechanism. J Am Chem Soc 132:7908–7918

Im S-C, Liu G, Luchinat C, Sykes AG, Bertini I (1998) The solution structure of parsley [2Fe-2S] ferredoxin. Eur J Biochem 258:465–477

Iwahara J, Schwieters CD, Clore GM (2004) Characterization of nonspecific protein-DNA interactions by H-1 paramagnetic relaxation enhancement. J Am Chem Soc 126:12800–12808

Keizers PHJ, Ubbink M (2011) Paramagnetic tagging for protein structure and dynamics analysis. Prog Nucl Magn Reson Spectrosc 58:88–96

Knight MJ, Felli IC, Pierattelli R, Emsley L, Pintacuda G (2013) Magic angle spinning NMR of paramagnetic proteins. Acc Chem Res 46:2108–2116

Leary SC, Winge DR, Cobine PA (2009) "Pulling the plug" on cellular copper: the role of mitochondria in copper export. Biochim Biophys Acta 1793:146–153

Li J, Ding S, Cowan JA (2013) Thermodynamic and structural analysis of human NFU conformational chemistry. Biochemistry 52(29):4904–4913

Lin IJ, Xia B, King DS, Machonkin TE, Westler WM, Markley JL (2009) Hyperfine-Shifted 13C and 15 N NMR signals from clostridium pasteurianum rubredoxin: extensive assignments and quantum chemical verification. J Am Chem Soc 131:15555–15563

Lutsenko S (2010) Human copper homeostasis: a network of interconnected pathways. Curr Opin Chem Biol 14:211–217

Lyons TA, Ratnaswamy G, Pochapsky TC (1996) Redox-dependent dynamics of putidaredoxin characterized by amide proton exchange. Protein Sci 5:627–639

Machonkin TE, Westler WM, Markley JL (2002) ^{13}C-^{13}C 2D NMR: a novel strategy for the study of paramagnetic proteins with slow electronic relaxation times. J Am Chem Soc 124:3204–3205

Machonkin TE, Westler WM, Markley JL (2004) Strategy for the study of paramagnetic proteins with slow electronic relaxation rates by NMR spectroscopy application to oxidized human [2Fe-2S] ferredoxin. J Am Chem Soc 126:5413–5426

Markley JL, Kim JH, Dai Z, Bothe JR, Cai K, Frederick RO, Tonelli M (2013) Metamorphic protein IscU alternates conformations in the course of its role as the scaffold protein for iron-sulfur cluster biosynthesis and delivery. FEBS Lett 587:1172–1179

Mo H, Pochapsky SS, Pochapsky TC (1999) A model for the solution structure of oxidized terpredoxin, a Fe2S2 ferredoxin from Pseudomonas. Biochemistry 38:5666

Otting G (2010) Protein NMR using paramagnetic ions. Annu Rev Biophys 39:387–405

Piccioli M, Poggi L (2002) Tailored HCCH-TOCSY experiment for resonance assignment in the proximity of a paramagnetic center. J Magn Reson 155:236–243

Russo L, Maestre-Martinéz M, Wolff S, Becker S and Griesinger C (2013) Inter-domain dynamics explored by paramagnetic NMR. J Am Chem Soc 135:17111–17120

Skjeldal L, Markley JL, Coghlan VM, Vickery LE (1991) ^{1}H-NMR spectra of vertebrate (2Fe-2S) ferredoxins. Hyperfine resonances suggest different electron delocalization patterns from plant ferredoxins. Biochemistry 30:9078–9083

Ubbink M (2012) Dynamics in transient complexes of redox proteins. Biochem Soc Trans 40:415–418

Volkman BF, Wilkens SJ, Lee AL, Xia B, Westler WM, Berger R, Markley JL (1999) Redox-depedendent magnetic alignment of *Clostridium pasteurianum* rubredoxin: measurement of magnetic susceptibility anisotropy and prediction of pseudocontact shift contributions. J Am Chem Soc 121:4677–4683

Volkov AN, Ubbink M, Van Nuland NAJ (2010) Mapping the encounter state of a transient protein complex by PRE NMR spectroscopy. J Biomol NMR 48:225–236

Wilkens SJ, Xia B, Weinhold F, Markley JL, Westler WM (1998) NMR investigations of clostridium pasteurianum rubredoxin. Origin of hyperfine 1H, 2H, 13C and 15 N NM chemical shfits in iron-sulfur proteins as determined by comparison of experimental data with hybrid density functional calculations. J Am Chem Soc 120:4806–4814

Yagi H, Pilla KB, Maleckis A, Graham B, Huber T and Otting G (2013) Three-dimensional protein fold determination from backbone amide pseudocontact shifts generated by lanthanide tags at multiple sites. Structure 21:883–890

5.3. The role of BOLA2 in the GRX3 dependent Anamorsin maturation pathway[19]

Interaction of apo GRX3 with apo BOLA2. Full-length BOLA2 protein was overexpressed in E. coli cells and purified in its apo form. Analytical gel filtration and ^{15}N NMR relaxation data, which provided a molecular reorientational correlation time of 6.9 ± 0.23 ns, showed that the purified apo protein is monomeric. Purified apo BOLA2 was unable to bind (Fe-S) clusters when a chemical reconstitution approach[14] was applied. To investigate the interaction between the apo forms of GRX3 and BOLA2, chemical shift changes of backbone NHs were followed by $^{1}H-^{15}N$ HSQC NMR experiments upon titration of ^{15}N-labeled apo GRX3 with unlabeled apo BOLA2, and of ^{15}N-labeled apo BOLA2 with unlabeled apo GRX3, in the presence of 5 mM GSH and 5 mM DTT. Chemical shift variations, which were in a fast/intermediate exchange regime on the NMR time scale, were observed in the $^{1}H-^{15}N$ HSQC maps of GRX3 for the backbone NHs of both Grx domains, when increasing amounts of unlabeled BOLA2 were added up to a 1:2 GRX3-BOLA2 molar ratio, while no significant effects were observed on the backbone NHs of the Trx domain of GRX3 (**Fig.36A**).

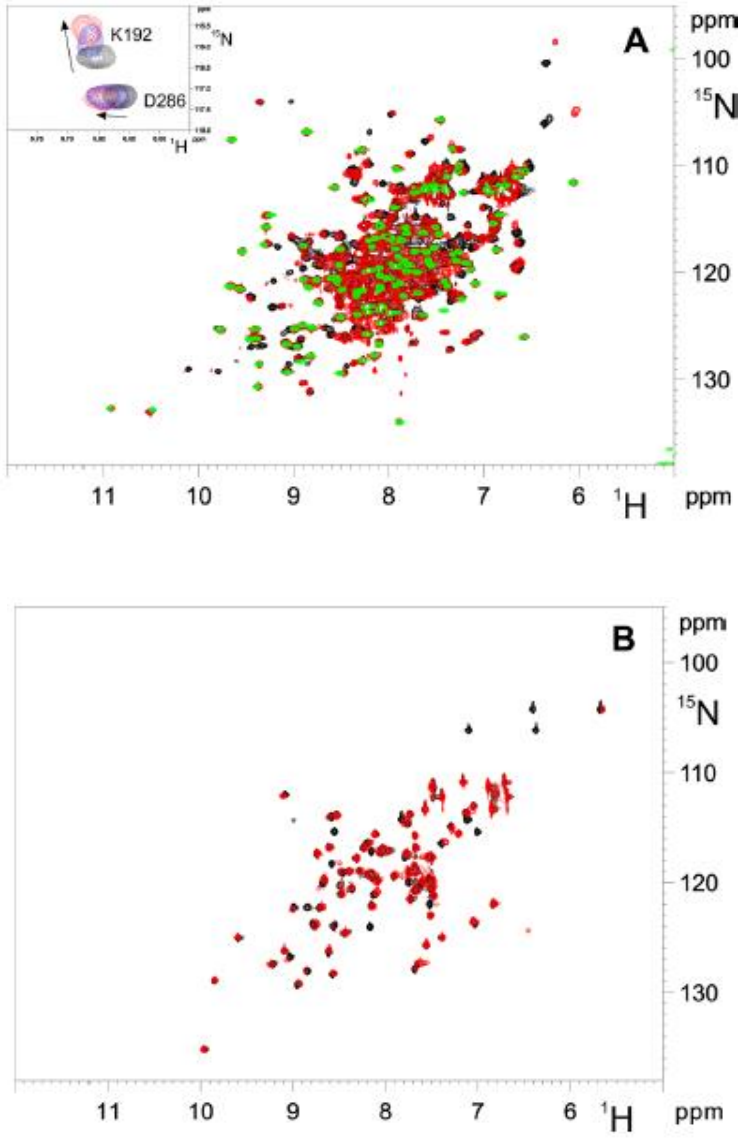

Figure 36. Apo GRX3 interacts with apo BOLA2. (A) Overlay of $^{1}H–^{15}N$ HSQC spectra of ^{15}N-labeled apo GRX3 (black), of ^{15}Nlabeled Trx domain of GRX3 (green), and of a 1:2 mixture of ^{15}Nlabeled apo GRX3 and unlabeled apo BOLA2 (red). (B) Overlay of $^{1}H–^{15}N$ HSQC spectra of ^{15}N-labeled apo BOLA2 (black) and of a 1:2 mixture of unlabeled apo GRX3 and ^{15}N-labeled apo BOLA2 (red).

These chemical shift changes occur simultaneously on both Grx domains, thus indicating that BOLA2 does not have a preferential interaction toward one of the two Grx domains (**Fig.36 A**). Similarly, chemical shift variations in a fast/intermediate exchange regime on the NMR time scale were observed in the $^{1}H-^{15}N$ HSQC maps of BOLA2 when increasing amounts of unlabeled GRX3 were added up to a 1:2 GRX3-BOLA2 molar ratio (**Fig.36 B**). The interaction between apo BOLA2 and apo GRX3 was also followed by analytical gel filtration chromatography, performed on protein mixtures with different apo GRX3 and apo BOLA2 ratios (**Fig.37**). The formation of two peaks was observed by adding apo BOLA2 to apo GRX3 up to a 1:2 GRX3-BOLA2 ratio:

1. a peak with an apparent molecular mass of 70.4 kDa, predominant at 1:1 protein ratio;
2. a peak with an apparent molecular mass of 74.3 kDa, predominant at 1:2 protein ratio.

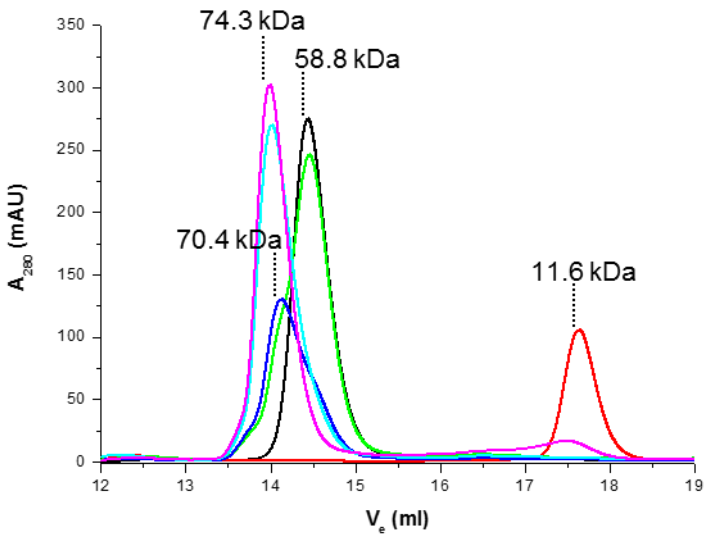

Figure 37. Analytical gel filtration (Superdex 200 10/300 increase column) chromatograms of BOLA2 and GRX3 proteins in their apo states and of their protein mixtures. Black line: apo GRX3; red line: apo BOLA2; green line: 1:0.5 mixture of apo GRX3 and apo BOLA2; blue line: 1:1 mixture of apo GRX3 and apo BOLA2; cyan line: 1:1.5 mixture of apo GRX3 and apo BOLA2; magenta line: 1:2 mixture of apo GRX3 and apo BOLA2.

These results indicated that apo GRX3 forms a heterodimeric complex with apo BOLA2 at the 1:1 protein ratio (the 70.4 kDa value matches indeed with the sum of the apparent molecular masses of apo GRX3 and apo BOLA2), which then evolves, upon addition of a further equivalent of apo BOLA2, to form a species which has an apparent molecular mass (74.3 kDa) intermediate between that of the heterodimeric complex (70.4 kDa) and that of an apo heterotrimeric complex formed by two BOLA2molecules and one GRX3 molecule (82 kDa, obtained by the sum of the apparent molecular masses of apo GRX3 and two molecules of apo BOLA2). The presence of this peak with an intermediate apparent molecular mass can be a

consequence of the applied gel filtration conditions, which determined, indeed, the presence of a fast exchange equilibrium between the heterodimeric and heterotrimeric complexes. Therefore, we performed the analytical gel filtration chromatography using a different column, i.e., Superdex 75 HR 10/30, and it resulted that apo GRX3 protein interacts with apo BOLA2 forming a peak with an apparent molecular mass of 78.8 kDa predominant at 1:2.5 GRX3-BOLA2 protein ratio. This value essentially corresponds to the sum of the apparent molecular masses of apo GRX3 (52.7 kDa) and two molecules of apo BOLA2 (11.0 kDa) (Fig.38), thus definitively indicating the formation of the apo GRX3-$BOLA2_2$ heterotrimeric complex.

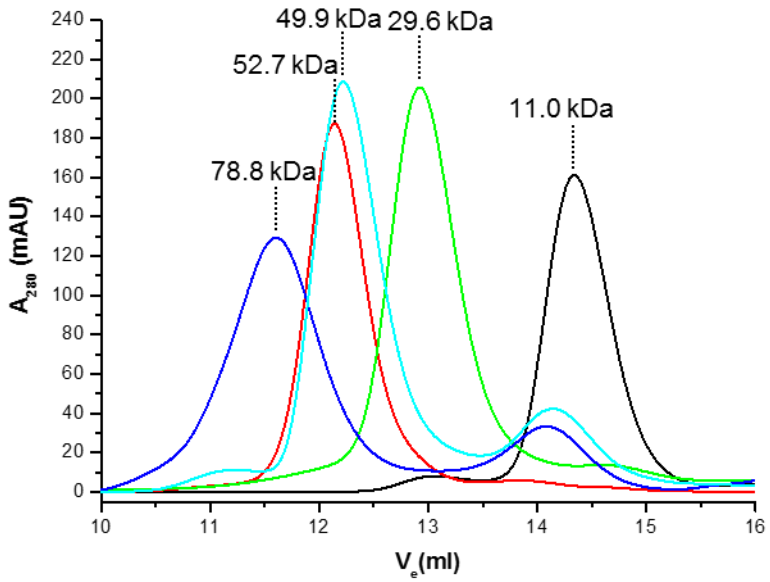

Figure 38. Analytical gel filtration (Superdex 75 HR 10/30 column) chromatograms of isolated BOLA2, GRX3(GrxA/B) and GRX3 proteins in their apo states and of their protein mixtures. Black line: apo BOLA2; red line: apo GRX3; green line: apo GRX3(GrxA/B); cyan line: 1:2.5 mixture of apo GRX3(GrxA/B) and apo BOLA2; blue: 1:2.5 mixture of apo GRX3 and apo BOLA2.

Since the Trx domain is not involved in the interaction between apo BOLA2 and apo GRX3, we produced a two domains construct containing the GrxA and GrxB domains only, (GRX3(GrxA/B)), to map, by solution NMR, the residues involved in the formation of the heterotrimeric complex. With this shorter construct, the chemical shift data analysis was indeed simplified by the reduction of NMR signal overlap and broadening due to the reduced protein size The $^{1}H–^{15}N$ HSQC signals of the final protein mixture, i.e., 1:2 ^{15}N-labeled apo GRX3(GrxA/B)-apo BOLA2, well superimposed with the corresponding signals of a 1:2 apo ^{15}N labeled GRX3-apo BOLA2 mixture, indicating that the same complex involving the same interacting region was present in solution in the two mixtures, and confirming that Trx domain has no specific role in the protein−protein recognition between apo GRX3 and apo BOLA2. Comparing the $^{1}H–^{15}N$ HSQC map of the final apo GRX3(GrxA/B)-apo ^{15}N-labeled BOLA2 mixture with that of ^{15}N-labeled BOLA2 (**Fig.39**), 15 signals of BOLA2 experienced significant chemical shift variations and two NH signals broadened beyond detection.

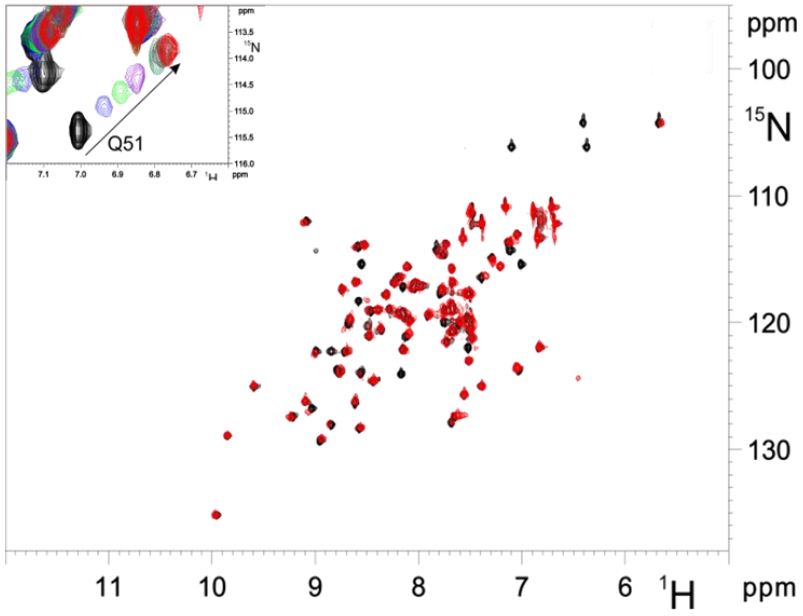

Figure 39. Overlay of $^{1}H–^{15}N$ HSQC spectra of ^{15}N-labeled apo BOLA2 (black) and of a 2:1 mixture of ^{15}N-labeled apo BOLA2 and unlabeled apo GRX3(GrxA/B) (red). In the inset, a zoom of $^{1}H–^{15}N$ HSQC spectra on the Q51 backbone NH signal is reported for ^{15}N labeled apo BOLA2 (black) and for the 0.1:1 (blue), 0.15:1 (green), 0.25:1 (violet), 0.5:1 (dark green), 0.75:1 (gray), 1:1 (brown), and 2:1 (red) mixtures of unlabeled apo GRX3(GrxA/B)

In the reverse titration, when detecting ^{15}N-labeled GRX3-(GrxA/B), 15 NH signals broadened beyond detection and 21 NH signals experienced chemical shift variations in the $^{1}H–^{15}N$ HSQC spectrum of the final 1:2 GRX3(GrxA/B)-BOLA2 mixture once compared with that of ^{15}N-labeled GRX3(GrxA/B). Once the affected residues are mapped on the structural model of apo BOLA2 (calculated with MODELER 9.15 software using the solution structure of apo BOLA2 from Mus musculus[21] as template with a 87% sequence identity) and on the crystal structures of the apo form of the single GrxA (PDB ID 3ZYW) and GrxB (PDB ID 2YAN) domains of GRX3, well-defined interacting regions were identified on both proteins. On

BOLA2 side, it comprises helix α3 and the following strand β3, containing His 68, a ligand of the $[2Fe\text{-}2S]^{2+}$ cluster[15]. On each GrxA and GrxB domain, the interacting surface involves helices α2 and α3, strand β4, and the surrounding loops and comprises the Cys ligand of the $[2Fe\text{-}2S]^{2+}$ bound cluster21. The analytical gel filtration data collected with a Superdex 75 HR 10/30 column, which showed the formation of a peak with an apparent molecular mass of 49.9 kDa in the chromatogram of the protein mixture, which essentially corresponds to the sum of the apparent molecular masses of apo GRX3(GrxA/B) (29.6 kDa) and two molecules of apo BOLA2 (11.1 kDa). The interaction of apo BOLA2 with the holo-dimeric form of GRX3, i.e., $[2Fe\text{-}2S]_2$ $GRX3_2$, was characterized by UV−vis, CD, EPR, NMR, and analytical gel filtration. Upon stepwise additions of apo BOLA2 to $[2Fe\text{-}2S]_2$ $GRX3_2$, the absorbance peaks typical of the oxidized $[2Fe\text{-}2S]^{2+}$ clusters bound to GRX3 disappeared in the UV−vis and CD spectra and new absorbance peaks appeared. The final spectra (**Fig.40 A, B)** at a 1:4 $[2Fe\text{-}2S]_2$ $GRX3_2$-BOLA2 ratio are very similar to that of the holo complex obtained by chemically reconstituting apo GRX3-$BOLA2_2$ with two $[2Fe\text{-}2S]^{2+}$ clusters ($[2Fe\text{-}2S]_2$ GRX3-$BOLA2_2$, hereafter), as assessed by iron and acid-labile sulfide chemical analysis (Fe and acid-labile S values, reported as mol Fe or S per mol of trimer, are 3.8 ± 0.1 and 3.9 ± 0.1, respectively).

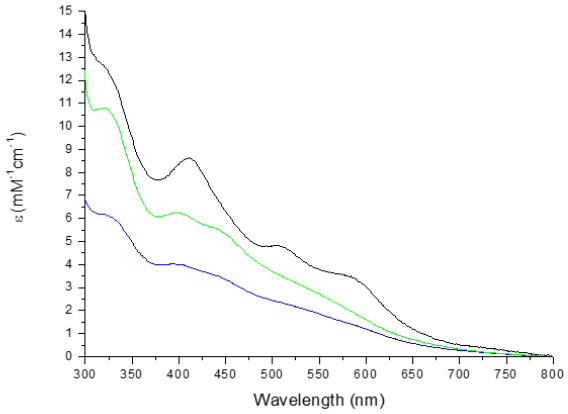

Figure 40. Formation of the $[2Fe\text{-}2S]_2$ GRX3-$BOLA2_2$ complex from the interaction between $[2Fe\text{-}2S]_2$ GRX3 and apo BOLA2. (**A**) UV−vis of $[2Fe\text{-}2S]_2$ $GRX3_2$ (black line) the 1:4 [2Fe-2S]2 GRX32-apo BOLA2 mixture (blue line), and of chemically reconstituted [2Fe- $2S]_2$ GRX3-$BOLA2_2$ (green line).

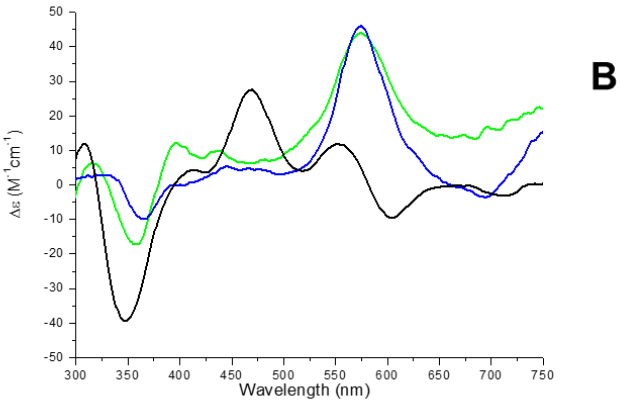

Figure 40. Formation of the $[2Fe\text{-}2S]_2$ GRX3-$BOLA2_2$ complex from the interaction between $[2Fe\text{-}2S]_2$ $GRX3_2$ and apo BOLA2. (**B**) CD spectra of $[2Fe\text{-}2S]_2$ $GRX3_2$ (black line), of the 1:4 $[2Fe\text{-}2S]_2$ $GRX3_2$-apo BOLA2 mixture (blue line), and of chemically reconstituted $[2Fe\text{-}2S]_2$ GRX3-$BOLA2_2$ (green line).

The 1:4 protein−protein ratio is needed to fully saturate the four Grx domains present in the dimeric [2Fe-2S]$_2$ GRX3$_2$ complex with BOLA2 molecules. The final mixture containing [2Fe-2S]$_2$ GRX3$_2$ and apo BOLA2 at a 1:4 molar ratio was EPR silent, as expected for the presence of a S = 0 ground state of oxidized [2Fe-2S]$^{2+}$ clusters. Upon chemical reduction with sodium dithionite, the EPR signal of a reduced [2Fe-2S]$^{+}$ protein-bound cluster is observed with g values of 2.01, 1.91, and ∼1.87 (g_{av} ∼ 1.93), which are the same as those observed on the chemically reconstituted heterotrimeric [2Fe-2S]$_2$ GRX3-BOLA2$_2$ complex upon sodium dithionite reduction. Analytical gel filtration chromatography, performed with a Superdex 75 HR 10/30 column on the same final mixture, showed the presence of a main peak with an apparent molecular mass of 73.2 kDa, which is very close to the sum of the apparent molecular masses of apo GRX3 (52.7 kDa) and two molecules of apo BOLA2(11.1 kDa) (**Fig.40 C**). These results indicate that [2Fe-2S]$_2$ GRX3$_2$ interacts with apo BOLA2 to form, in the final protein mixture, a GRX3-BOLA2$_2$ heterotrimeric complex that binds [2Fe-2S]$^{2+}$ cluster(s). Holo complex formation between [2Fe-2S]$_2$ GRX3$_2$ and apo BOLA2 was also followed by NMR, performing ^{1}H−^{15}N HSQC spectra on ^{15}N-labeled [2Fe-2S]$_2$ GRX3$_2$ titrated with unlabeled apo BOLA2 up to a protein−protein ratio of 1:4 and vice versa on ^{15}N-labeled BOLA2 titrated with unlabeled [2Fe-2S]$_2$ GRX3$_2$ up to a 4:1 protein−protein ratio.

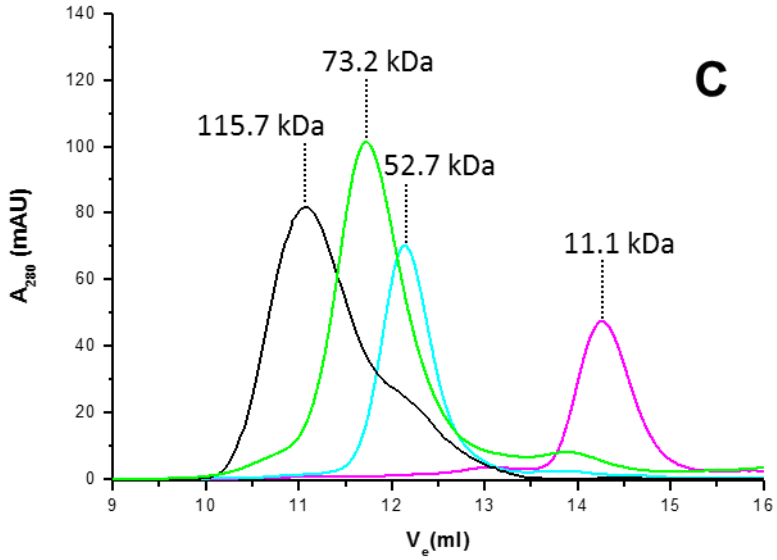

Figure 40. Formation of the $[2Fe\text{-}2S]_2$ GRX3-BOLA2$_2$ complex from the interaction between $[2Fe\text{-}2S]_2$ GRX3$_2$ and apo BOLA2. (**C**) Analytical gel filtration (Superdex 75 HR 10/30 column) chromatograms of BOLA2 (magenta) and GRX3 (cyan) proteins in their apo states, of $[2Fe\text{-}2S]_2$ GRX3$_2$ complex (black), and of a 1:4 $[2Fe\text{-}2S]_2$ GRX3$_2$-apo BOLA2 mixture (green).

In the final mixture of the first titration, the NH signals of GRX3 affected by BOLA2 additions belong to residues of both Grx domains, while those of the Trx domain remain unperturbed. In the $^{1}H–^{15}N$ HSQC NMR spectra acquired throughout the titration steps, a decrease in the intensity of some backbone NH signals of $[2Fe\text{-}2S]_2$ GRX3$_2$ (located more than 10 Å away from the paramagnetic $[2Fe\text{-}2S]^{2+}$ cluster and therefore only affected by BOLA2−GRX3 interaction) was observed, with the concomitant appearance of new backbone NH signals. This indicates the formation of a new species in solution in slow exchange, on the NMR time scale, with the $[2Fe\text{-}2S]_2$ GRX3$_2$ species. This species has chemical shifts slightly different from those

of the heterotrimeric complex formed by two apo BOLA2 molecules and an apo GRX3 molecule. In the final mixture, the NH signals of the $[2Fe\text{-}2S]_2$ $GRX3_2$ species fully disappeared in favor of the new NH signals, indicating the complete consumption of $[2Fe\text{-}2S]_2$ $GRX3_2$, which therefore completely evolves to the new species. In the reverse titration, upon addition of unlabeled $[2Fe\text{-}2S]_2$ $GRX3_2$, some backbone NHs of ^{15}N-labeled BOLA2 broaden beyond detection, and others display chemical shift changes in a slow exchange regime on the NMR time. The residues undergoing such spectral changes are essentially the same as those involved in the apo−apo interaction, indicating that the interaction region is the same in both apo and holo GRX3−BOLA2 interactions. Overall, the spectroscopic and gel filtration data indicate:

1. a complete conversion of the homodimeric $[2Fe\text{-}2S]_2$ $GRX3_2$ into a GRX3-$BOLA2_2$ heterotrimeric complex that contains $[2Fe\text{-}2S]^{2+}$ cluster(s)
2. the GrxA and GrxB domains of GRX3 interact with two BolA2molecules, while Trx domain is not involved in such interaction.

Two possible scenarios can occur at the 1:4 $[2Fe\text{-}2S]_2$ $GRX3_2$-BOLA2ratio, i.e., the formation of a heterotrimeric GRX3-$BOLA2_2$ complex containing two $[2Fe\text{-}2S]^{2+}$ clusters together with the formation of a heterotrimeric apo GRX3-apo $BOLA2_2$ complex, or the formation of two heterotrimeric GRX3-$BolA2_2$ complexes each containing only one $[2Fe\text{-}2S]^{2+}$ cluster. The two scenarios result from two possible occurring molecular mechanisms, A and B shown in **Scheme 1**.

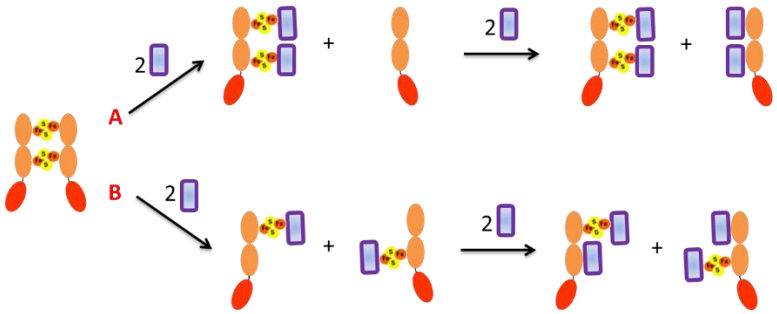

Scheme 1 Possible Solution Equilibria upon Reaction of $[2Fe\text{-}2S]_2$ $GRX3_2$ With apo BOLA2 up to a 1:4 Ratio

The key experimental evidence, that would allow us to provide information on whether a favorite mechanism between A and B is operative, is the detection of the formation of the apo free GRX3 form, which is observed indeed in the A mechanism only (**Scheme 1**). Analytical gel filtration was therefore performed on $[2Fe\text{-}2S]_2$ $GRX3_2$-apo BOLA2 protein mixtures at different protein:protein ratios, using a Superdex 75 HR 10/30 column to investigate the possible presence of free apo GRX3.

These gel filtration analysis showed:

1. the presence of a main peak with an apparent molecular mass which increases from 68.0 to 73.2 kDa upon addition of apo BOLA2;
2. the presence, only for $[2Fe\text{-}2S]_2$ $GRX3_2$-apo BOLA2 ratios >1:4, of a peak with the apparent molecular mass similar to that of apo BOLA2;
3. no formation of a peak with the apparent molecular mass of apo GRX3 at any investigated protein:protein ratio (**Fig.41**).

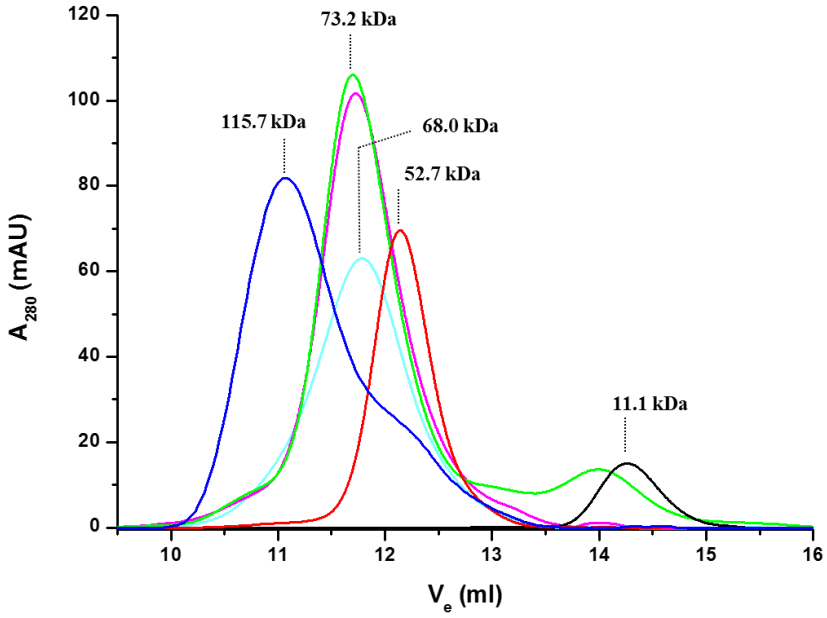

Figure 41. Analytical gel filtration chromatograms of BOLA2 (black) and GRX3 (red) proteins in their apo states, of $[2Fe\text{-}2S]_2$ $GRX3_2$ (blue) and of a 1:2 (cyan), 1:4 (magenta), 1:6 (green) $[2Fe\text{-}2S]_2$ $GRX3_2$-apo BOLA2 mixtures (Superdex 75 HR 10/30 column).

The analytical gel filtration chromatography was also performed at higher resolution with a Superdex 200 10/300 increase column on protein mixtures at substoichiometric $[2Fe\text{-}2S]_2$ $GRX3_2$-apo BOLA2 ratios of 1:0.25, 1:0.5, and 1:1 (**Fig.42**). It was observed the concurrent formation of:

1. the 1:1 heterodimeric complex, corresponding to the peak with an apparent molecular mass of 71.3 kDa, which is indeed very close to the sum of the apparent molecular masses of one molecule of apo BOLA2 and one molecule of apo GRX3 (i.e.,70.4 kDa), and

2. of the heterotrimeric complex, corresponding to the peak with an apparent molecular mass of 87.4 kDa, which is indeed close to the sum of the apparent molecular masses of two apo BOLA2molecules and one molecule of apo GRX3 (i.e., 82.0 kDa).

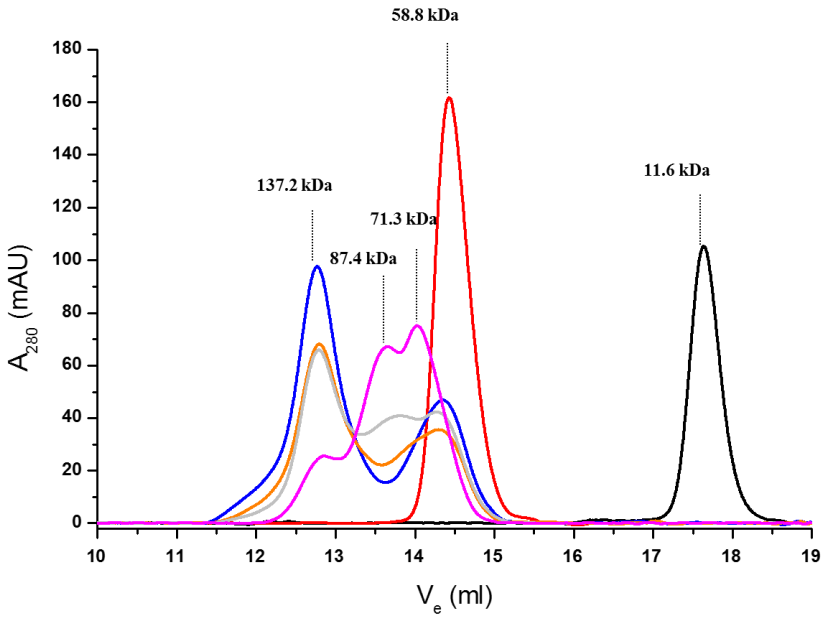

Figure 42.BOLA2 (black) and GRX3 (red) proteins in their apo states, of $[2Fe\text{-}2S]_2$ $GRX3_2$ (blue) and of a 1:0.25 (orange), 1:0.5 (light gray), 1:1 (light magenta) $[2Fe\text{-}2S]_2$ $GRX3_2$-apo BOLA2 mixtures (Superdex 200 10/300 increase column).

The peak of apo GRX3, which is always present at a low percentage in the chemically reconstituted $[2Fe\text{-}2S]_2$ $GRX3_2$ sample, does not increase in its intensity upon BOLA2 substoichiometric additions (**Fig.42**), as expected if the A mechanism was the favored process. From these gel filtration data, we can conclude that the B mechanism is the preferential occurring process. Cluster transfer from $[2Fe\text{-}2S]_2$ GRX3- $BOLA2_2$ to apo anamorsin was

followed by UV−vis, CD spectroscopy, and analytical gel filtration. Once the chemically reconstituted $[2Fe\text{-}2S]_2$ GRX3- $BOLA2_2$ heterotrimeric complex was titrated with apo anamorsin up to a 1:1 protein- protein ratio, in the UV−vis and CD spectra the absorbance peaks typical of $[2Fe\text{-}2S]_2$ GRX3-$BOLA2_2$ disappeared and the absorbance peaks typical of the $[2Fe\text{-}2S]^{2+}$ cluster-bound form of anamorsin ([2Fe-2S] anamorsin)[16,17] appeared (**Fig.43**).

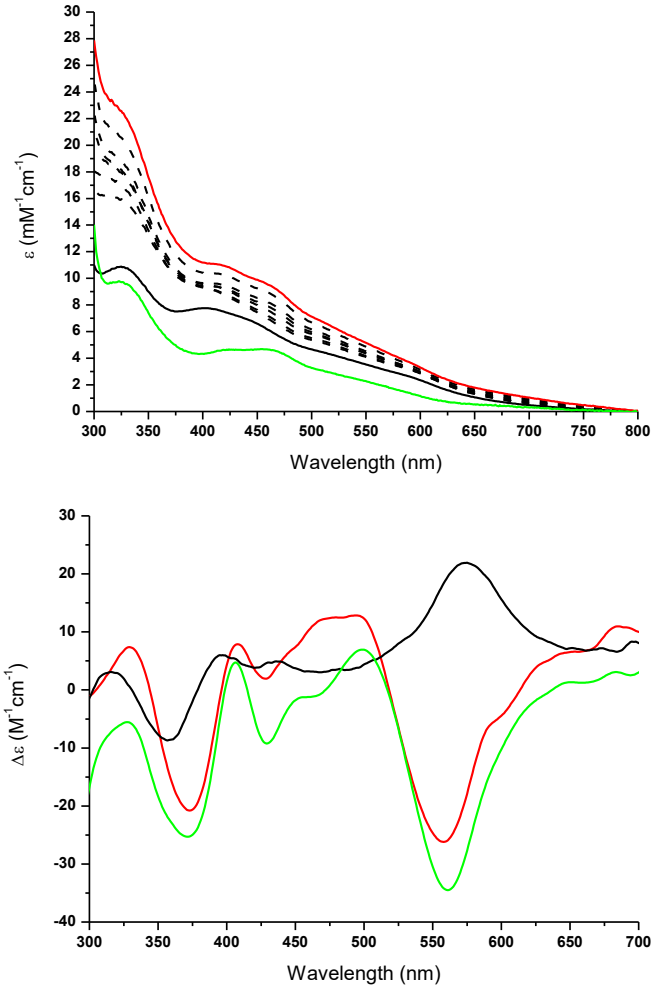

Figure 43. (up) UV−vis spectra of $[2Fe\text{-}2S]_2$ GRX3-$BOLA2_2$ (black line) titrated with 0.1, 0.2, 0.3, 0.4, 0.5, 0.6, 0.8 equiv of apo anamorsin (black dashed lines). (down) CD spectra acquired to follow cluster transfer from $[2Fe\text{-}2S]_2$ GRX3-$BOLA2_2$ to apo anamorsin. Black line: chemically reconstituted $[2Fe\text{-}2S]_2$ GRX3-$BOLA2_2$; green line: [2Fe-2S] anamorsin; red line: 1:1 mixture of $[2Fe\text{-}2S]_2$ GRX3-$BOLA2_2$ and apo anamorsin.

The CD spectrum of the final 1:1 mixture essentially corresponds to that of [2Fe-2S] anamorsin, being clearly distinguishable from that of $[2Fe\text{-}2S]_2$ GRX3-$BOLA2_2$.

Analytical gel filtration chromatography performed with Superdex 75 HR 10/30 column on the final 1:1 mixture showed the presence of a main peak with an apparent molecular mass of 128.2 kDa, which essentially corresponds to the sum of the apparent molecular masses of $[2Fe\text{-}2S]_2$ GRX3-$BOLA2_2$(73.2 kDa) and apo anamorsin (52.0 kDa) (Figure).

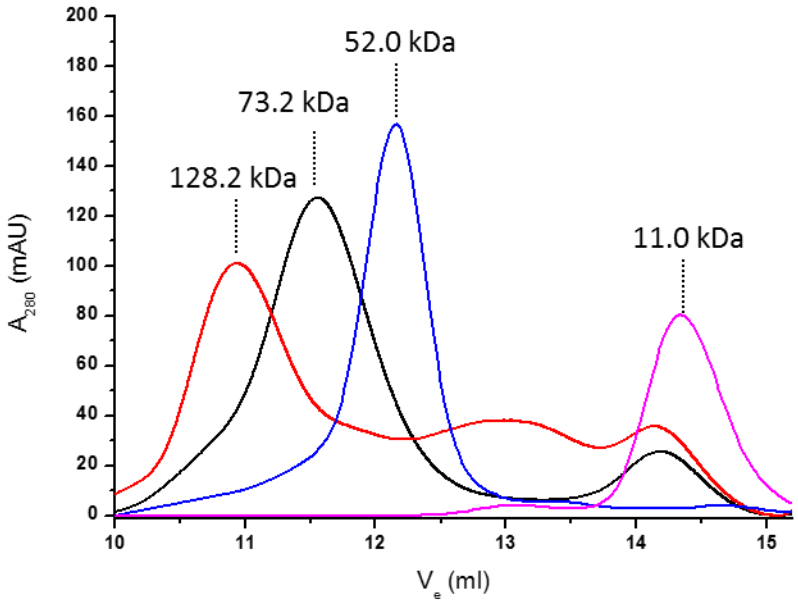

Figure 44. Analytical gel filtration (75 HR 10/30 column) chromatograms of BOLA2 (magenta) and anamorsin (blue) proteins in their apo states, of $[2Fe\text{-}2S]_2$ GRX3-$BOLA2_2$ (black), and of a 1:1 mixture between $[2Fe\text{-}2S]_2$ GRX3- $BOLA2_2$ and apo anamorsin (red).

Overall, the data showed that (i) both $[2Fe\text{-}2S]^{2+}$ cluster are completely transferred from $[2Fe\text{-}2S]_2$ GRX3-$BOLA2_2$ to apo anamorsin and (ii) the final product is a complex formed by an apo GRX3 molecule, two apo

BolA2molecules and a [2Fe-2S] anamorsin molecule (GRX3-BOLA2$_2$-[2Fe-2S] anamorsin, hereafter). Moreover, by gel filtrating a 1:1 mixture of apo GRX3(GrxA/B)-BOLA2$_2$and [2Fe-2S] anamorsin, a peak corresponding to a ternary complex formed by GRX3(GrxA/B), BolA2, and anamorsin is not observed. This demonstrates that, in the final GRX3-BOLA2$_2$-[2Fe-2S] anamorsin complex, the interaction between apo GRX3−BOLA2$_2$and [2Fe-2S] anamorsin depends on the presence of the Trx domain of GRX3. We had previously shown that the Trx domain of GRX3 interacts with the N-terminal domain of anamorsin mediating the cluster transfer between the two proteins[18]. Here we show that the Trx domain, in addition of being essential for the complex formation between anamorsin and GRX3-BOLA2$_2$ in the GRX3-BOLA2$_2$-[2Fe-2S] anamorsin complex, maintains the same conformational freedom as it has in the homodimeric [2Fe-2S]$_2$ GRX3$_2$ complex. So the cluster transfer mechanism previously reported for [2Fe-2S]$_2$ GRX3$_2$[18] is also operative in the [2Fe-2S]$_2$ GRX3−BOLA2$_2$-apo anamorsin interaction, i.e., the protein recognition, specifically occurring between the N-terminal domains of the two proteins, plays a role in the cluster transfer process.

This data showed that apo BOLA2 and the Grx domains of apo GRX3 significantly and specifically interact forming an apo heterotrimeric complex composed by a GRX3 molecule and two BOLA2 molecules. This complex can bind two [2Fe-2S]$^{2+}$ clusters upon chemical reconstitution. The same cluster content was achieved in the heterotrimeric complex obtained by co-expressing in E. coli cells human BOLA2 and a construct of GRX3 containing only the two Grx domains[15].A heterotrimeric GRX3-BolA2$_2$complex was also obtained by mixing in vitro [2Fe-2S]$_2$ GRX3$_2$ with apo BOLA2. Both complexes, i.e., the homodimeric GRX3 and the heterotrimeric GRX3-BOLA2$_2$ complexes containing two [2Fe-2S]$^{2+}$

clusters, can thus be active players, at the cellular level, for maturing anamorsin. The present data also suggest that the mechanism of cluster transfer relying on the interaction between the N-terminal domains of anamorsin and GRX3[18] is common to both cluster transfer processes, i.e., from $[2Fe\text{-}2S]_2$ $GRX3_2$ to apo anamorsin and from $[2Fe\text{-}2S]_2$ GRX3-$BOLA2_2$ to apo anamorsin.

JACS
JOURNAL OF THE AMERICAN CHEMICAL SOCIETY

Article

pubs.acs.org/JACS

Elucidating the Molecular Function of Human BOLA2 in GRX3-Dependent Anamorsin Maturation Pathway

Lucia Banci,*[,†,‡] Francesca Camponeschi,[†,‡] Simone Ciofi-Baffoni,*[,†,‡] and Riccardo Muzzioli[†,‡]

[†]Magnetic Resonance Center CERM, University of Florence, Via Luigi Sacconi 6, 50019, Sesto Fiorentino, Florence, Italy
[‡]Department of Chemistry, University of Florence, Via della Lastruccia 3, 50019 Sesto Fiorentino, Florence, Italy

Supporting Information

ABSTRACT: In eukaryotes, the interaction between members of the monothiol glutaredoxin family and members of the BolA-like protein family has been involved in iron metabolism. To investigate the still unknown functional role of the interaction between human glutaredoxin-3 (GRX3) and its protein partner BOLA2, we characterized at the atomic level the interaction of apo BOLA2 with the apo and holo states of GRX3 and studied the role of BOLA2 in the GRX3-dependent anamorsin maturation pathway. From these studies, it emerged that apo GRX3 and apo BOLA2 form a heterotrimeric complex, composed by two BOLA2 molecules and one GRX3 molecule. This complex is able to bind two $[2Fe\text{-}2S]^{2+}$ clusters, each being bridged between a BOLA2 molecule and a monothiol glutaredoxin domain of GRX3, and to transfer both $[2Fe\text{-}2S]^{2+}$ clusters to apo anamorsin producing its mature holo state. Collectively, the data suggest that the heterotrimeric complex can work as a $[2Fe\text{-}2S]^{2+}$ cluster transfer component in cytosolic Fe/S protein maturation pathways.

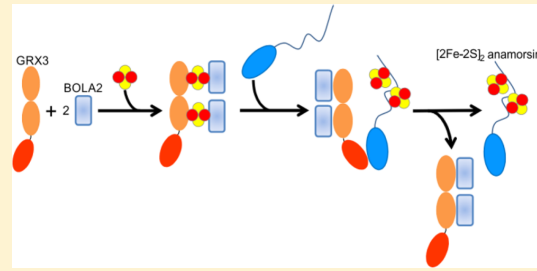

INTRODUCTION

In eukaryotes, the biosynthetic pathways responsible for the maturation of Fe/S proteins is a complex, multistep process involving more than 30 different proteins.[1] As a result, atomic level studies are vital to fully unravel the molecular function of each single player in the Fe/S protein maturation process. In this work, we characterized at the atomic level the interaction between human glutaredoxin-3 (GRX3) and its protein partner BOLA2 and identified a possible role for BOLA2 in the GRX3-dependent anamorsin maturation pathway.

The functional role of eukaryotic monothiol glutaredoxins (Grx) has been largely studied in *Saccharomyces cerevisiae*, which encodes three CysGlyPheSer(CGFS)-type monothiol Grx homologues, Grx3, Grx4, and Grx5.[2−4] Grx5 is a single domain protein, located in the mitochondrial matrix, which binds a [2Fe-2S] cluster ligated by two protein molecules, each providing a cysteine ligand, and by two glutathione molecules, each providing a further cysteine ligand.[5,6] Grx5 has been shown to participate in the mitochondrial iron−sulfur (Fe/S) cluster (ISC) assembly machinery, acting, in its holo-homodimeric state, as a donator of a [2Fe-2S] cluster to partner apo-proteins.[7,8] Grx3 and Grx4 are located in the cytoplasm, and each consists of a N-terminal thioredoxin (Trx) domain, with no Trx-related activity,[9,10] and of a glutaredoxin domain capable of binding a [2Fe-2S] cluster through protein dimerization and glutathione binding,[11] in the same way as Grx5 does. Grx3 and Grx4 have been linked to iron regulation through their binding to the transcriptional activator Aft1/2, which regulates iron uptake in yeast.[12−14] Specifically, to perform this regulatory function, Grx3 (or Grx4) needs to be complexed with the BolA-like protein Fra2, forming a [2Fe-2S]-bridged heterodimeric complex,[11,15] which, at variance with the holo-homodimeric species, can transfer the cluster to the iron-responsive transcription factor Aft2.[16] Based on this information on yeast, holo-heterodimeric Grx/BolA complexes have been generally linked to iron homeostasis regulation, while holo-homodimeric Grx complexes have been related to Fe/S protein biogenesis.[17] Recently, it has been also shown that double depletion of yeast Grx3/4 specifically impaired all iron-requiring reactions in the cytosol, in mitochondria, and in the nucleus, including the synthesis of Fe/S clusters, of heme, and of di-iron centers.[9] These data suggest that holo-homodimeric cytoplasmatic Grxs species can also function in intracellular iron trafficking.

In humans, two monothiol Grxs are present, GRX3 and GRX5.[2,18] GRX5 is located in mitochondria essentially performing the same function as the yeast Grx5 homologue, i.e., it acts as a [2Fe-2S] cluster transfer protein in the ISC machinery.[19,20] GRX3 consists of three domains: one N-terminal Trx domain and two Grx domains, each able to bind a glutathione-coordinated [2Fe-2S] cluster via protein dimerization.[21,22] GRX3 is located in the cytosol, and similarly to what was found for yeast Grx3/Grx4, the molecular function of its holo-homodimeric state ($[2Fe\text{-}2S]_2$ $GRX3_2$) has been associated with intracellular iron trafficking, being responsible

Received: October 9, 2015
Published: November 27, 2015

DOI: 10.1021/jacs.5b10592
J. Am. Chem. Soc. 2015, 137, 16133−16143

for iron redistribution to virtually all iron-binding proteins or iron-dependent pathways in the cell.[23] Recently, we proposed that human GRX3 is an active component of the cytosolic Fe/S cluster assembly (CIA) machinery, as its homodimeric [2Fe-2S]$_2$ GRX3$_2$ form is able to mature the cytosolic [2Fe-2S]-binding protein anamorsin, an essential component of the CIA machinery.[24] The CIA machinery is responsible for the maturation of cytosolic and nuclear Fe/S proteins performing key functions in metabolic catalysis, iron regulation, protein translation, DNA synthesis, and DNA repair.[25,26] Therefore, the cellular function of GRX3 in maturing the CIA component anamorsin indirectly affects several crucial life processes.

Similarly to yeast, GRX3 can form a holo-hetero complex with a BolA-like protein, the cytosolic BOLA2.[21] However, while the yeast Grx3/4 forms a [2Fe-2S]-bridged heterodimer with a Fra2 molecule, the human GRX3 forms a [2Fe-2S]-bridged heterotrimer with two BOLA2 molecules ([2Fe-2S]$_2$ GRX3-BOLA2$_2$). Since there is no human ortholog of the transcription factor Aft1, being indeed cellular iron homeostasis in humans regulated at the RNA-level by the Iron Regulatory Proteins 1 and 2,[27] [2Fe-2S]$_2$ GRX3-BOLA2$_2$ heterotrimers cannot be involved in the same [2Fe-2S] cluster transfer pathway found in yeast to regulate iron homeostasis. Although other functions of the [2Fe-2S]$_2$ GRX3-BOLA2$_2$ heterotrimer in human cells might be possible, it seems conceivable that this complex takes a role in iron metabolism given that (i) [2Fe-2S]-bridged Grx3−BolA2 interaction is conserved from *S. cerevisiae* to humans,[17] (ii) human GRX3 binds iron *in vivo*,[22] and (iii) human GRX3 partially rescues the growth defects and iron accumulation in the *S. cerevisiae grx3Δgrx4Δ* mutant, suggesting that human GRX3 partially can complement the functions of yeast Grx3 and Grx4 in iron homeostasis.[28]

In this work we have characterized *in vitro* the interaction of apo BOLA2 with the apo and holo states of GRX3 and investigated the role of BOLA2 in the GRX3-dependent anamorsin maturation pathway.

EXPERIMENTAL SECTION

Protein Production. The cDNA coding for human BOLA2 (UniProtKB/Swiss-Prot: Q9H3K6) was acquired from Life technologies. BOLA2 gene was amplified by PCR and subsequently inserted into the pET21a vector using the restriction enzymes NdeI and BanHI. BL21(DE3) gold competent *Escherichia coli* cells (Stratagene, La Jolla, CA) were transformed with the obtained plasmid, and cells were grown in LB or minimal media (with $(^{15}NH_4)_2SO_4$ and/or [^{13}C]-glucose) containing 1 mM ampicillin at 37 °C under vigorous shaking up to a cell OD_{600} of 0.6. Protein expression was induced by adding 0.5 mM IPTG, and cells were grown for 4 h at 25 °C. Cells were harvested by centrifugation at 7500*g* and resuspended in lysis buffer (25 mM MES pH 6 containing 0.01 mg/mL DNAase, 0.01 mg/mL lysozyme, 1 mM $MgSO_4$, 0.5 mM EDTA, and 5 mM DTT). Cell disruption was performed on ice by sonication, and the soluble extract, obtained by ultracentrifugation at 40000*g*, was loaded on HiTrap SP FF column (GE Healthcare). BOLA2 protein was eluted with 25 mM MES pH 6, 1 M NaCl and 5 mM DTT, concentrated with Amicon Ultra-15 Centrifugal Filter Units with a MWCO of 3 kDa (Millipore), and the buffer exchanged by PD10 desalting column in 50 mM phosphate buffer pH 7, 5 mM DTT and 5 mM GSH.

Various constructs of human GRX3 (full-length protein, Trx, and GRX3(GrxA/B) constructs in their apo and/or [2Fe-2S]-bound forms) were obtained following previously reported procedures.[24] [2Fe-2S]$_2$ GRX3$_2$ was obtained by chemical reconstitution following a previously reported procedure.[24]

Biochemical and UV−vis, CD, EPR Spectroscopic Methods. The aggregation state of isolated apo and holo proteins and of protein mixtures was analyzed using analytical gel filtration on Superdex 75 HR 10/30 and Superdex 200 10/300 increase columns (Amersham Bioscience), calibrated with gel filtration marker calibration kit, 6500−66000 Da (Sigma-Aldrich), to obtain the apparent molecular masses of the detected species. Purified samples in degassed phosphate buffer 50 mM pH 7, 5 mM DTT, and 5 mM GSH were loaded on the column pre-equilibrated with degassed 50 mM phosphate buffer pH 7, 5 mM GSH, and 5 mM DTT. Elution profiles were recorded at 280 nm with a flow rate of 0.5 mL/min for Superdex 75 HR 10/30 column and 0.75 mL/min for Superdex 200 10/300 increase column.

UV−vis and CD spectra were anaerobically acquired on a Cary 50 Eclipse spectrophotometer and JASCO J-810 spectropolarimeter, respectively, in degassed 50 mM phosphate buffer pH 7, 5 mM GSH, and 5 mM DTT.

EPR spectra of the 1:4 [2Fe-2S]$_2$ GRX3$_2$-apo BOLA2 mixture and of the chemically reconstituted [2Fe-2S]$_2$ GRX3-BOLA2$_2$ heterotrimeric complex were recorded after the anaerobic reduction of the cluster by stoichiometric addition of sodium dithionite and immediate freezing of the protein solution in liquid nitrogen. EPR spectra were acquired in degassed 50 mM phosphate buffer pH 7, 5 mM GSH, 5 mM DTT, and 10% glycerol at 45 K, using a Bruker Elexsys E500 spectrometer working at a microwave frequency of ca. 9.45 GHz, equipped with a SHQ cavity and a continuous flow He cryostat (ESR900, Oxford instruments) for temperature control. Acquisition parameters were as following: microwave frequency, 9.640928 GHz; microwave power, 5 mW; modulation frequency, 100 kHz; modulation amplitude, 2.0 G; acquisition time constant, 163.84 ms; number of points 1024; number of scans 8; field range 500−6000 G or 2300−4300 G.

The iron and inorganic sulfur content and the protein concentration were estimated following standard chemical assays as already reported.[29]

NMR Spectroscopy. Standard ^{1}H-detected triple-resonance NMR experiments for backbone resonance assignment were recorded on 1 mM ^{13}C, ^{15}N-labeled samples (apo forms of GRX3(GrxA/B) and BOLA2) in degassed 50 mM phosphate buffer pH 7, 5 mM DTT, and 5 mM GSH at 298 K, using Bruker AVANCE 500 and 700 MHz spectrometers. ^{15}N heteronuclear relaxation experiments were performed on ^{15}N-labeled apo BOLA2 and on ^{15}N-labeled apo GRX3(GrxA/B) in the presence and in the absence of 2 equiv of unlabeled apo BOLA2, in degassed 50 mM phosphate buffer pH 7, 5 mM DTT, and 5 mM GSH at 298 K, to measure ^{15}N backbone longitudinal (R_1) and transverse (R_2) relaxation rates and heteronuclear ^{15}N{^{1}H} NOEs. All NMR data were processed using the Topspin software package and were analyzed with the program CARA.

An apparent dissociation constant (K_d) for the interaction between apo GRX3(GrxA/B) and apo BOLA2 proteins, in degassed 50 mM phosphate buffer pH 7, 5 mM DTT at 298 K, was obtained by plotting the average chemical shift differences δ_{av} (i.e., $(((\Delta H)^2 + (\Delta N/5)^2)/2)^{1/2}$, where ΔH and ΔN are chemical shift differences for backbone amide ^{1}H and ^{15}N nuclei, respectively) of five well-resolved backbone NH signals of ^{15}N-labeled GRX3(GrxA/B) and of six well resolved backbone NH signals of ^{15}N-labeled BOLA2, as a function of BOLA2 and GRX3(GrxA/B) concentrations, respectively. These data were then fitted to a simple two-component model and averaged to obtain the final K_d value.[30,31]

Protein−Protein Interaction and Cluster Transfer. Apo GRX3 (or apo GRX3(GrxA/B))-apo BOLA2 interaction was investigated by ^{1}H−^{15}N HSQC NMR spectra, titrating ^{15}N-labeled apo forms of GRX3 or GRX3(GrxA/B) with unlabeled apo BOLA2, and ^{15}N-labeled apo BOLA2 with unlabeled apo forms of GRX3 or GRX3(GrxA/B), in degassed 50 mM phosphate buffer pH 7, 5 mM GSH, and 5 mM DTT containing 10% (v/v) D_2O at 298 K. Spectral changes were monitored upon the addition of increasing amounts of the unlabeled partner. NMR data were analyzed with CARA program and plotted following standard procedures.

To follow changes in cluster coordination upon interaction between [2Fe-2S]$_2$ GRX3$_2$ and apo BOLA2, [2Fe-2S]$_2$ GRX3$_2$ was incubated under anaerobic conditions with increasing concentrations of apo BOLA2 up to a 1:4 protein ratio, in degassed 50 mM phosphate buffer

DOI: 10.1021/jacs.5b10592
J. Am. Chem. Soc. 2015, 137, 16133−16143

pH 7, 5 mM GSH, and 5 mM DTT. UV−vis, EPR, and CD spectra were then recorded as described above and compared with those collected on a $[2Fe\text{-}2S]_2$ GRX3-BOLA2$_2$ complex, which was obtained by chemically reconstituting a 1:2.5 apo GRX3-apo BOLA2 mixture following a previously reported procedure.[24] Protein−protein interaction between $[2Fe\text{-}2S]_2$ GRX3$_2$ and apo BOLA2 was investigated by $^1H-^{15}N$ HSQC NMR spectra performed on ^{15}N-labeled $[2Fe\text{-}2S]_2$ GRX3$_2$ titrated with unlabeled apo BOLA2 and on ^{15}N-labeled apo BOLA2 titrated with unlabeled $[2Fe\text{-}2S]_2$ GRX3$_2$. Spectral changes were monitored and analyzed upon the addition of increasing amounts of the unlabeled partner.

The chemically reconstituted $[2Fe\text{-}2S]_2$ GRX3-BOLA2$_2$ complex was titrated under anaerobic conditions with increasing concentrations of apo anamorsin up to a 1:1 protein ratio in degassed 50 mM phosphate buffer pH 7, 5 mM GSH, and 5 mM DTT. Cluster transfer and the protein−protein interaction were followed by UV−vis and CD spectroscopy and analytical gel filtration chromatography, respectively.

RESULTS

Interaction of apo GRX3 with apo BOLA2. Full-length BOLA2 protein was overexpressed in *E. coli* cells and purified in its apo form. Analytical gel filtration and ^{15}N NMR relaxation data (Supporting Information Figure S1), which provided an molecular reorientational correlation time of 6.9 ± 0.23 ns, showed that the purified apo protein is monomeric. Purified apo BOLA2 was unable to bind Fe/S clusters when a chemical reconstitution approach[29] was applied.

To investigate the interaction between the apo forms of GRX3 and BOLA2, chemical shift changes of backbone NHs were followed by $^1H-^{15}N$ HSQC NMR experiments upon titration of ^{15}N-labeled apo GRX3 with unlabeled apo BOLA2, and of ^{15}N-labeled apo BOLA2 with unlabeled apo GRX3, in the presence of 5 mM GSH and 5 mM DTT. Chemical shift variations, which were in a fast/intermediate exchange regime on the NMR time scale, were observed in the $^1H-^{15}N$ HSQC maps of GRX3 for the backbone NHs of both Grx domains, when increasing amounts of unlabeled BOLA2 were added up to a 1:2 GRX3-BOLA2 molar ratio, while no significant effects were observed on the backbone NHs of the Trx domain of GRX3 (Figure 1A). These chemical shift changes occur simultaneously on both Grx domains, thus indicating that BOLA2 does not have a preferential interaction toward one of the two Grx domains (Figure 1A, inset). Similarly, chemical shift variations in a fast/intermediate exchange regime on the NMR time scale were observed in the $^1H-^{15}N$ HSQC maps of BOLA2 when increasing amounts of unlabeled GRX3 were added up to a 1:2 GRX3-BOLA2 molar ratio (Figure 1B).

The interaction between apo BOLA2 and apo GRX3 was also followed by analytical gel filtration chromatography, performed on protein mixtures with different apo GRX3 and apo BOLA2 ratios (Figure 2A). The formation of two peaks was observed by adding apo BOLA2 to apo GRX3 up to a 1:2 GRX3-BOLA2 ratio: (i) a peak with an apparent molecular mass of 70.4 kDa, predominant at 1:1 protein ratio; (ii) a peak with an apparent molecular mass of 74.3 kDa, predominant at 1:2 protein ratio (Figure 2A). These results indicated that apo GRX3 forms a heterodimeric complex with apo BOLA2 at the 1:1 protein ratio (the 70.4 kDa value matches indeed with the sum of the apparent molecular masses of apo GRX3 and apo BOLA2), which then evolves, upon addition of a further equivalent of apo BOLA2, to form a species which has an apparent molecular mass (74.3 kDa) intermediate between that of the heterodimeric complex (70.4 kDa) and that of an apo heterotrimeric complex formed by two BOLA2 molecules and one GRX3 molecule (82 kDa, obtained by the sum of the apparent molecular masses of apo GRX3 and two molecules of apo BOLA2). The presence of this peak with an intermediate apparent molecular mass can be a consequence of the applied gel filtration conditions, which determined, indeed, the presence of a fast exchange equilibrium between the heterodimeric and heterotrimeric complexes. Therefore, we performed the analytical gel filtration chromatography using a different column, i.e., Superdex 75 HR 10/30, and it resulted that apo GRX3 protein interacts with apo BOLA2 forming a peak with an apparent molecular mass of 76.8 kDa predominant at 1:2.5 GRX3-BOLA2 protein ratio (Figure 2B). This value essentially corresponds to the sum of the apparent molecular masses of apo GRX3 (52.7 kDa) and two molecules of apo BOLA2 (11.1 kDa) (Figure 2B), thus definitively indicating the formation of the apo GRX3-BOLA2$_2$ heterotrimeric complex.

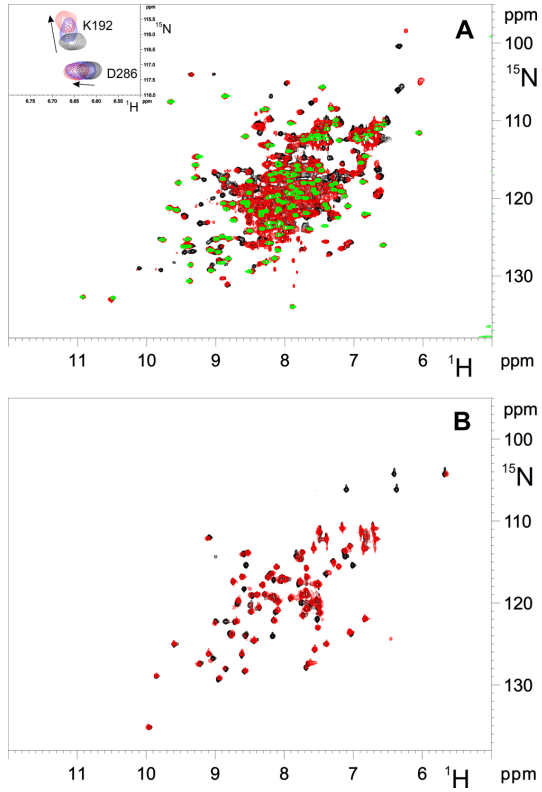

Figure 1. Apo GRX3 interacts with apo BOLA2. (A) Overlay of $^1H-^{15}N$ HSQC spectra of ^{15}N-labeled apo GRX3 (black), of ^{15}N-labeled Trx domain of GRX3 (green), and of a 1:2 mixture of ^{15}N-labeled apo GRX3 and unlabeled apo BOLA2 (red). The chemical shift changes of two backbone NHs belonging to GrxA and GrxB domains, K192 and D286, respectively, are reported in the inset for ^{15}N-labeled apo GRX3 (black), for 1:1 (blue) and 1:2 (red) mixtures of ^{15}N-labeled apo GRX3 and unlabeled apo BOLA2. (B) Overlay of $^1H-^{15}N$ HSQC spectra of ^{15}N-labeled apo BOLA2 (black) and of a 1:2 mixture of unlabeled apo GRX3 and ^{15}N-labeled apo BOLA2 (red).

DOI: 10.1021/jacs.5b10592
J. Am. Chem. Soc. 2015, 137, 16133−16143

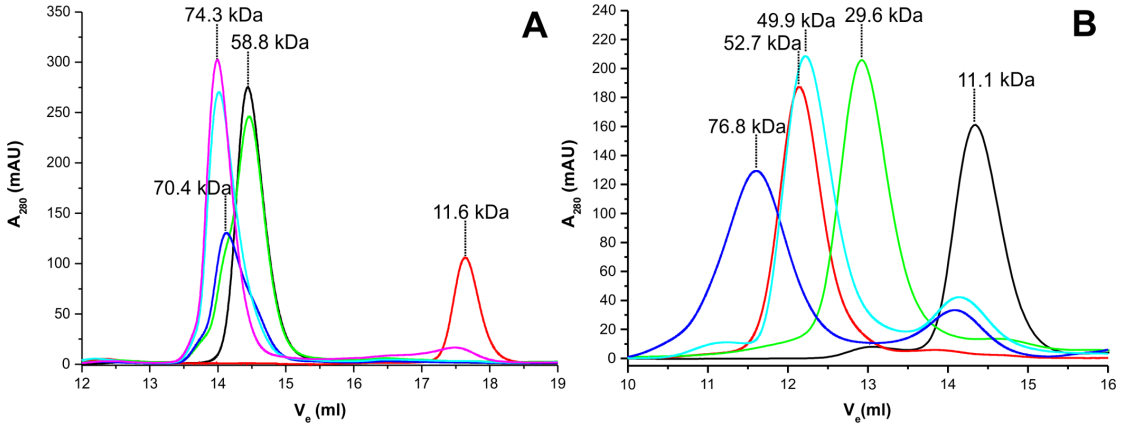

Figure 2. Apo GRX3 and apo BOLA2 form a heterotrimeric 1:2 complex. (A) Analytical gel filtration (Superdex 200 10/300 increase column) chromatograms of BOLA2 and GRX3 proteins in their apo states and of their protein mixtures. Black line: apo GRX3; red line: apo BOLA2; green line: 1:0.5 mixture of apo GRX3 and apo BOLA2; blue line: 1:1 mixture of apo GRX3 and apo BOLA2; cyan line: 1:1.5 mixture of apo GRX3 and apo BOLA2; magenta line: 1:2 mixture of apo GRX3 and apo BOLA2. The apparent molecular masses are reported at the top of each chromatographic peak. (B) Analytical gel filtration (Superdex 75 HR 10/30 column) chromatograms of isolated BOLA2, GRX3(GrxA/B) and GRX3 proteins in their apo states and of their protein mixtures. Black line: apo BOLA2; red line: apo GRX3; green line: apo GRX3(GrxA/B); cyan line: 1:2.5 mixture of apo GRX3(GrxA/B) and apo BOLA2; blue: 1:2.5 mixture of apo GRX3 and apo BOLA2. The apparent molecular masses are reported at the top of each chromatographic peak.

Since the Trx domain is not involved in the interaction between apo BOLA2 and apo GRX3, we produced a two-domain construct containing the GrxA and GrxB domains only, (GRX3(GrxA/B)), to map, by solution NMR, the residues involved in the formation of the heterotrimeric complex. With this shorter construct, the chemical shift data analysis was indeed simplified by the reduction of NMR signal overlap and broadening due to the reduced protein size. We titrated ^{15}N-labeled BOLA2 with unlabeled GRX3(GrxA/B) and ^{15}N-labeled GRX3(GrxA/B) with unlabeled BOLA2 and followed the chemical shift changes of backbone NHs via ^{1}H−^{15}N HSQC experiments. Chemical shift variations are in a fast/intermediate exchange regime on the NMR time scale in both titrations, as it occurs for the apo GRX3−apo BOLA2 interaction. By fitting the chemical shifts to a simple two-component model,[30,31] an apparent dissociation constant of 25 ± 15 μM was obtained (Figure 3A,B insets).

The ^{1}H−^{15}N HSQC signals of the final protein mixture, i.e., 1:2 ^{15}N-labeled apo GRX3(GrxA/B)-apo BOLA2, well superimposed with the corresponding signals of a 1:2 apo ^{15}N-labeled GRX3-apo BOLA2 mixture, indicating that the same complex involving the same interacting region was present in solution in the two mixtures, and confirming that Trx domain has no specific role in the protein−protein recognition between apo GRX3 and apo BOLA2 (Supporting Information Figure S2). Comparing the ^{1}H−^{15}N HSQC map of the final apo GRX3(GrxA/B)-apo ^{15}N-labeled BOLA2 mixture with that of ^{15}N-labeled BOLA2 (Figure 3B), 15 signals of BOLA2 experienced significant chemical shift variations and two NH signals broadened beyond detection (Figure 4A).

In the reverse titration, when detecting ^{15}N-labeled GRX3-(GrxA/B) (Figure 3B), 15 NH signals broadened beyond detection and 21 NH signals experienced chemical shift variations in the ^{1}H−^{15}N HSQC spectrum of the final 1:2 GRX3(GrxA/B)-BOLA2 mixture once compared with that of ^{15}N-labeled GRX3(GrxA/B) (Figure 4B).

Once the affected residues are mapped on the structural model of apo BOLA2 (calculated with MODELER 9.15 software using the solution structure of apo BOLA2 from *Mus musculus*[32] as template with a 87% sequence identity) and on the crystal structures of the apo form of the single GrxA (PDB ID 3ZYW) and GrxB (PDB ID 2YAN) domains of GRX3, well-defined interacting regions were identified on both proteins. On BOLA2 side, it comprises helix α3 and the following strand β3, containing His 68, a ligand of the [2Fe-2S]$^{2+}$ cluster[21] (Figure 4A). On each GrxA and GrxB domain, the interacting surface involves helices α2 and α3, strand β4, and the surrounding loops and comprises the Cys ligand of the [2Fe-2S]$^{2+}$ bound cluster[21] (Figure 4B).

^{15}N backbone NMR relaxation experiments, performed on ^{15}N-labeled apo GRX3(GrxA/B) in absence or in the presence of 2 equiv of apo BOLA2, showed an increase in the molecular reorientational correlation time from 12.0 ± 1.2 ns (consistent with a monomeric state of GRX3(GrxA/B) in solution) to 27.7 ± 4.5 ns. This increase is consistent with the formation of a 1:2 GRX3(GrxA/B)-BOLA2 protein complex, being the molecular reorientational correlation time of apo BOLA2 6.9 ± 0.23 ns. This result is in agreement with the analytical gel filtration data collected with a Superdex 75 HR 10/30 column (Figure 2B), which showed the formation of a peak with an apparent molecular mass of 49.9 kDa in the chromatogram of the protein mixture, which essentially corresponds to the sum of the apparent molecular masses of apo GRX3(GrxA/B) (29.6 kDa) and two molecules of apo BOLA2 (11.1 kDa).

Interaction of [2Fe-2S]$_2$ GRX3$_2$ with apo BOLA2. The interaction of apo BOLA2 with the holo-dimeric form of GRX3, i.e., [2Fe-2S]$_2$ GRX3$_2$, was characterized by UV−vis, CD, EPR, NMR, and analytical gel filtration. Upon stepwise additions of apo BOLA2 to [2Fe-2S]$_2$ GRX3$_2$, the absorbance peaks typical of the oxidized [2Fe-2S]$^{2+}$ clusters bound to GRX3 disappeared in the UV−vis and CD spectra and new absorbance peaks appeared. The final spectra (Figure 5A,B) at a

DOI: 10.1021/jacs.5b10592
J. Am. Chem. Soc. 2015, 137, 16133−16143

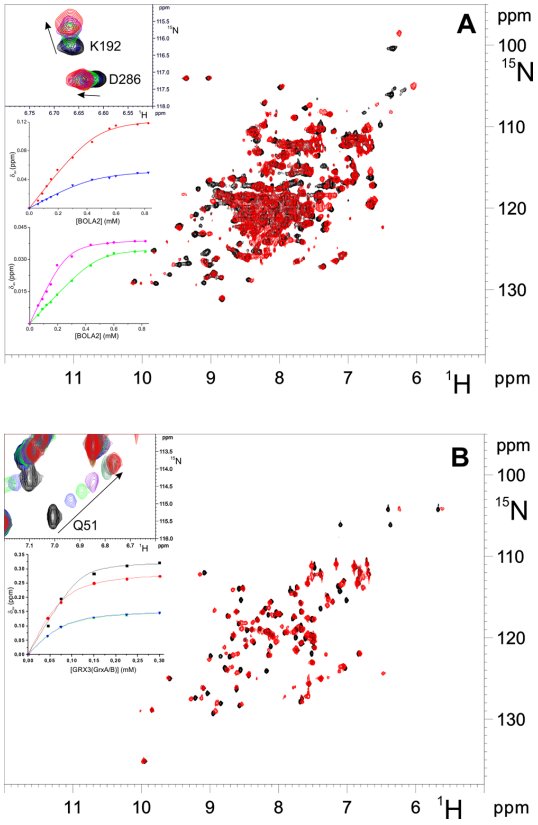

Figure 3. GrxA and GrxB domains interact with apo BOLA2. (A) Overlay of ^{1}H−^{15}N HSQC spectra of ^{15}N-labeled apo GRX3(GrxA/B) (black) and of a 1:2 mixture of ^{15}N-labeled apo GRX3(GrxA/B) and unlabeled apo BOLA2 (red). In the inset, a zoom of ^{1}H−^{15}N HSQC spectra on the K192 and D286 backbone NH signals is reported for ^{15}N-labeled apo GRX3(GrxA/B) (black) and for 1:0.5 (blue), 1:1 (green), 1:1.5 (violet), and 1:2 (red) mixtures of ^{15}N-labeled apo GRX3(GrxA/B) and unlabeled apo BOLA2. The inset also shows the δ_{av} changes measured for T199 (red circles) and Q202 (blue triangles) in the GrxA domain of GRX3(GrxA/B) and of K245 (green squares) and F263 (magenta circles) in the GrxB domain of GRX3(GrxA/B) as a function of apo BOLA2 concentration. Solid lines show the fitting curves. (B) Overlay of ^{1}H−^{15}N HSQC spectra of ^{15}N-labeled apo BOLA2 (black) and of a 2:1 mixture of ^{15}N-labeled apo BOLA2 and unlabeled apo GRX3(GrxA/B) (red). In the inset, a zoom of ^{1}H−^{15}N HSQC spectra on the Q51 backbone NH signal is reported for ^{15}N-labeled apo BOLA2 (black) and for the 0.1:1 (blue), 0.15:1 (green), 0.25:1 (violet), 0.5:1 (dark green), 0.75:1 (gray), 1:1 (brown), and 2:1 (red) mixtures of unlabeled apo GRX3(GrxA/B) and ^{15}N-labeled apo BOLA2. The inset also shows the δ_{av} changes measured for the L50 (black squares), Q51 (red circles), V56 (green up triangles), and N57 (blue down triangles) residues of BOLA2 as a function of apo GRX3(GrxA/B) concentration. Solid lines show the fitting curves.

1:4 $[2Fe\text{-}2S]_2$ $GRX3_2$-BOLA2 ratio are very similar to that of the holo complex obtained by chemically reconstituting apo GRX3-$BOLA2_2$ with two $[2Fe\text{-}2S]^{2+}$ clusters ($[2Fe\text{-}2S]_2$ GRX3-$BOLA2_2$, hereafter), as assessed by iron and acid-labile sulfide chemical analysis (Fe and acid-labile *S* values, reported as mol Fe or S per mol of trimer, are 3.8 ± 0.1 and 3.9 ± 0.1, respectively).

The 1:4 protein−protein ratio is needed to fully saturate the four Grx domains present in the dimeric $[2Fe\text{-}2S]_2$ $GRX3_2$ complex with BOLA2 molecules. The final mixture containing $[2Fe\text{-}2S]_2$ $GRX3_2$ and apo BOLA2 at a 1:4 molar ratio was EPR silent, as expected for the presence of a $S = 0$ ground state of oxidized $[2Fe\text{-}2S]^{2+}$ clusters. Upon chemical reduction with sodium dithionite, the EPR signal of a reduced $[2Fe\text{-}2S]^{+}$ protein-bound cluster is observed with *g* values of 2.01, 1.91, and ∼1.87 ($g_{av} \sim 1.93$), which are the same as those observed on the chemically reconstituted heterotrimeric $[2Fe\text{-}2S]_2$ GRX3-$BOLA2_2$ complex upon sodium dithionite reduction (Supporting Information Figure S3). Analytical gel filtration chromatography, performed with a Superdex 75 HR 10/30 column on the same final mixture, showed the presence of a main peak with an apparent molecular mass of 73.2 kDa, which is very close to the sum of the apparent molecular masses of apo GRX3 (52.7 kDa) and two molecules of apo BOLA2 (11.1 kDa) (Figure 5C). These results indicate that $[2Fe\text{-}2S]_2$ $GRX3_2$ interacts with apo BOLA2 to form, in the final protein mixture, a GRX3-$BOLA2_2$ heterotrimeric complex that binds $[2Fe\text{-}2S]^{2+}$ cluster(s). The EPR, UV−vis, CD, and analytical gel filtration data collected on this final mixture mirror the data previously obtained on a $[2Fe\text{-}2S]_2$ GRX3(GrxA/B)-$BOLA2_2$ complex produced by coexpressing human BOLA2 and GRX3(GrxA/B) in *E. coli* cells.[21] This indicates that the same type of cluster is bound to the heterotrimeric complex regardless of following different holo protein production approaches, i.e., chemical reconstitution vs *in vitro* and *in cell* Fe−S metalation, as well as different protein constructs, i.e. full-length protein vs a GrxA/GrxB domain construct.

Holo complex formation between $[2Fe\text{-}2S]_2$ $GRX3_2$ and apo BOLA2 was also followed by NMR, performing ^{1}H−^{15}N HSQC spectra on ^{15}N-labeled $[2Fe\text{-}2S]_2$ $GRX3_2$ titrated with unlabeled apo BOLA2 up to a protein−protein ratio of 1:4 and vice versa on ^{15}N-labeled BOLA2 titrated with unlabeled $[2Fe\text{-}2S]_2$ $GRX3_2$ up to a 4:1 protein−protein ratio. In the final mixture of the first titration, the NH signals of GRX3 affected by BOLA2 additions belong to residues of both Grx domains, while those of the Trx domain remain unperturbed. In the ^{1}H−^{15}N HSQC NMR spectra acquired throughout the titration steps (Figure 5D), a decrease in the intensity of some backbone NH signals of $[2Fe\text{-}2S]_2$ $GRX3_2$ (located more than 10 Å away from the paramagnetic $[2Fe\text{-}2S]^{2+}$ cluster and therefore only affected by BOLA2−GRX3 interaction) was observed, with the concomitant appearance of new backbone NH signals. This indicates the formation of a new species in solution in slow exchange, on the NMR time scale, with the $[2Fe\text{-}2S]_2$ $GRX3_2$ species (Figure 5D). This species has chemical shifts slightly different from those of the heterotrimeric complex formed by two apo BOLA2 molecules and an apo GRX3 molecule. In the final mixture, the NH signals of the $[2Fe\text{-}2S]_2$ $GRX3_2$ species fully disappeared in favor of the new NH signals, indicating the complete consumption of $[2Fe\text{-}2S]_2$ $GRX3_2$, which therefore completely evolves to the new species (Figure 5D). In the reverse titration, upon addition of unlabeled $[2Fe\text{-}2S]_2$ $GRX3_2$, some backbone NHs of ^{15}N-labeled BOLA2 broaden beyond detection, and others display chemical shift changes in a slow exchange regime on the NMR time scale (Figure 5D). The residues undergoing such spectral changes are essentially the same as those involved in the apo−apo interaction, indicating that the interaction region is the same in both apo and holo

DOI: 10.1021/jacs.5b10592
J. Am. Chem. Soc. 2015, 137, 16133−16143

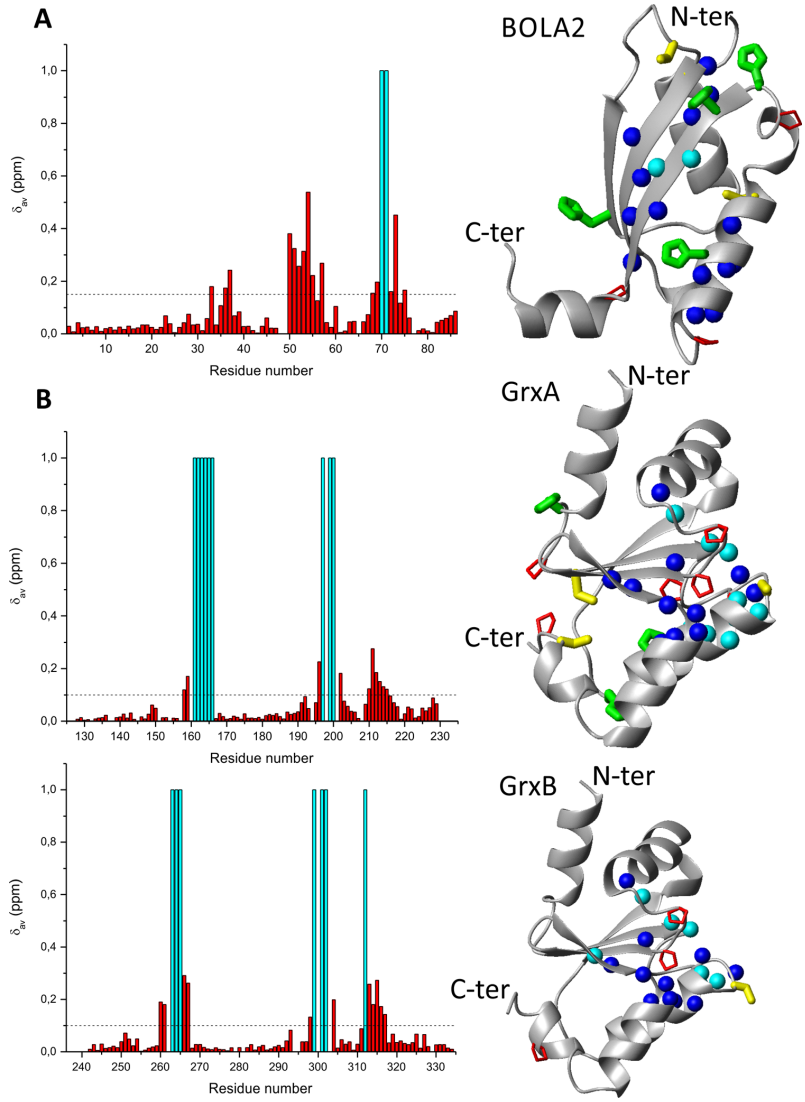

Figure 4. Mapping the interaction surfaces between BOLA2 and each GrxA and GrxB domain in the apo heterotrimeric complex. The left panels show backbone weighted average chemical shift differences δ_{av} for BOLA2 residues, observed upon addition of unlabeled apo GRX3(GrxA/B) to ^{15}N-labeled apo BOLA2 up to a 2:1 BOLA2-GRX3(GrxA/B) ratio (A) and for GRX3(GrxA/B) residues observed upon addition of 2 equiv of unlabeled apo BOLA2 to ^{15}N-labeled apo GRX3(GrxA/B) (B). A threshold of 0.15 ppm (mean value of δ_{av} plus 1σ, black dashed line) for BOLA2 and of 0.10 ppm for GRX3(GrxA/B) were used to identify significant chemical shift differences. Cyan bars identify residues whose backbone NHs broaden beyond detection upon complex formation. The δ_{av} value for Pro residues was arbitrarily set to zero. The right panels show backbone NHs experiencing significant chemical shift differences in the ^{1}H−^{15}N HSQC spectra upon the formation of the heterotrimeric apo GRX3(GrxA/B)-BOLA2$_2$ complex mapped as blue and cyan spheres on a structural model of apo BOLA2 (A) and on the crystal structure of GrxA (PDB ID 3ZYW) and GrxB (PDB ID 2YAN) domains of apo GRX3 (B). Blue spheres identify NHs showing significant chemical shift variations, and cyan spheres identify backbone NHs broaden beyond detection. Side-chains of His, Cys, and Pro residues are in green, yellow and red, respectively.

GRX3−BOLA2 interactions. Overall, the spectroscopic and gel filtration data indicate: (i) a complete conversion of the homodimeric [2Fe-2S]$_2$ GRX3$_2$ into a GRX3-BOLA2$_2$ heterotrimeric complex that contains [2Fe-2S]$^{2+}$ cluster(s); and (ii) similarly to what we found for the apo/apo heterotrimeric complex, the GrxA and GrxB domains of GRX3 interact with two BOLA2 molecules, while Trx domain is not involved in such interaction.

Two possible scenarios can occur at the 1:4 [2Fe-2S]$_2$ GRX3$_2$-BOLA2 ratio, i.e., the formation of a heterotrimeric GRX3-BOLA2$_2$ complex containing two [2Fe-2S]$^{2+}$ clusters together with the formation of a heterotrimeric apo GRX3-apo BOLA2$_2$ complex, or the formation of two heterotrimeric

DOI: 10.1021/jacs.5b10592
J. Am. Chem. Soc. 2015, 137, 16133−16143

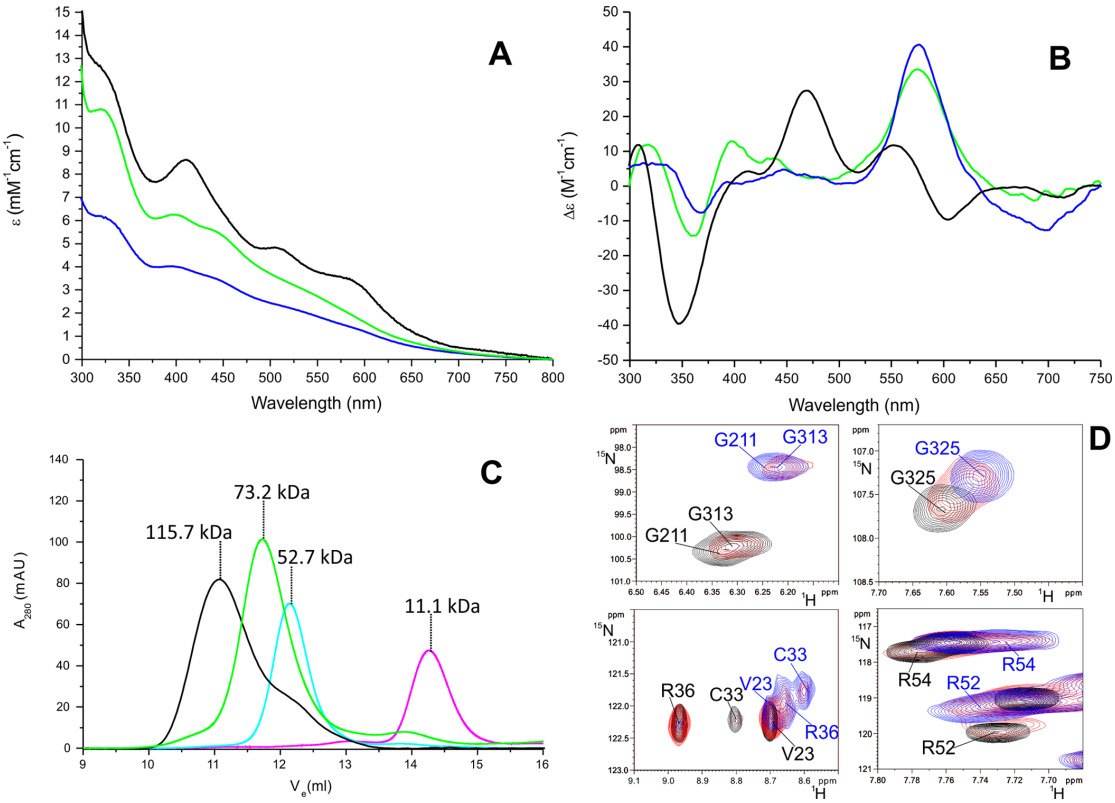

Figure 5. Formation of the [2Fe-2S] GRX3-BOLA2$_2$ complex from the interaction between [2Fe-2S]$_2$ GRX3$_2$ and apo BOLA2. (A) UV−vis and (B) CD spectra of [2Fe-2S]$_2$ GRX3$_2$ (black line), of the 1:4 [2Fe-2S]$_2$ GRX3$_2$-apo BOLA2 mixture (blue line), and of chemically reconstituted [2Fe-2S]$_2$ GRX3-BOLA2$_2$ (green line). (C) Analytical gel filtration (Superdex 75 HR 10/30 column) chromatograms of BOLA2 (magenta) and GRX3 (cyan) proteins in their apo states, of [2Fe-2S]$_2$ GRX3$_2$ complex (black), and of a 1:4 [2Fe-2S]$_2$ GRX3$_2$-apo BOLA2 mixture (green). The apparent molecular masses are reported at the top of each chromatographic peak. (D) In the upper panels, the overlay of ^{1}H−^{15}N HSQC spectral regions of ^{15}N-labeled [2Fe-2S]$_2$ GRX3$_2$ (black) and of 1:2 (red) and 1:4 (blue) ^{15}N-labeled [2Fe-2S]$_2$ GRX3$_2$/unlabeled apo BOLA2 mixtures. In the lower panels, the overlay of ^{1}H−^{15}N HSQC spectral regions of ^{15}N-labeled apo BOLA2 (black) and of 2:1 (red) and 4:1 (blue) ^{15}N-labeled apo BOLA2-unlabeled [2Fe-2S]$_2$ GRX3$_2$ mixtures.

GRX3-BOLA2$_2$ complexes each containing only one [2Fe-2S]$^{2+}$ cluster. The two scenarios result from two possible occurring molecular mechanisms, A and B shown in Scheme 1.

The key experimental evidence, that would allow us to provide information on whether a favorite mechanism between A and B is operative, is the detection of the formation of the apo free GRX3 form, which is observed indeed in the A mechanism only (Scheme 1). Analytical gel filtration was therefore performed on [2Fe-2S]$_2$ GRX3$_2$-apo BOLA2 protein mixtures at different protein:protein ratios, using a Superdex 75 HR 10/30 column to investigate the possible presence of free apo GRX3. These gel filtration analysis showed: (i) the presence of a main peak with an apparent molecular mass which increases from 68.0 to 73.2 kDa upon addition of apo BOLA2; (ii) the presence, only for [2Fe-2S]$_2$ GRX3$_2$-apo BOLA2 ratios >1:4, of a peak with the apparent molecular mass similar to that of apo BOLA2; and (iii) no formation of a peak with the apparent molecular mass of apo GRX3 at any investigated protein:protein ratio (Figure 6A).

The analytical gel filtration chromatography was also performed at higher resolution with a Superdex 200 10/300 increase column on protein mixtures at substoichiometric [2Fe-2S]$_2$ GRX3$_2$-apo BOLA2 ratios of 1:0.25, 1:0.5, and 1:1 (Figure 6B). It was observed the concurrent formation of (i) the 1:1 heterodimeric complex, corresponding to the peak with an apparent molecular mass of 71.3 kDa, which is indeed very close to the sum of the apparent molecular masses of one molecule of apo BOLA2 and one molecule of apo GRX3 (i.e., 70.4 kDa), and (ii) of the heterotrimeric complex, corresponding to the peak with an apparent molecular mass of 87.4 kDa, which is indeed close to the sum of the apparent molecular masses of two apo BOLA2 molecules and one molecule of apo GRX3 (i.e., 82.0 kDa). The peak of apo GRX3, which is always present at a low percentage in the chemically reconstituted [2Fe-2S]$_2$ GRX3$_2$ sample, does not increase in its intensity upon BOLA2 substoichiometric additions (Figure 6B), as expected if the A mechanism was the favored process. From these gel filtration data we therefore conclude that the B mechanism is the preferential occurring process.

[2Fe-2S]$_2$ GRX3-BOLA2$_2$ Complex Transfers [2Fe-2S]$^{2+}$ Clusters to apo Anamorsin. Cluster transfer from [2Fe-2S]$_2$ GRX3-BOLA2$_2$ to apo anamorsin was followed by UV−vis, CD

DOI: 10.1021/jacs.5b10592
J. Am. Chem. Soc. 2015, 137, 16133−16143

Scheme 1. Possible Solution Equilibria upon Reaction of $[2Fe\text{-}2S]_2$ $GRX3_2$ With apo BOLA2 up to a 1:4 Ratio[a]

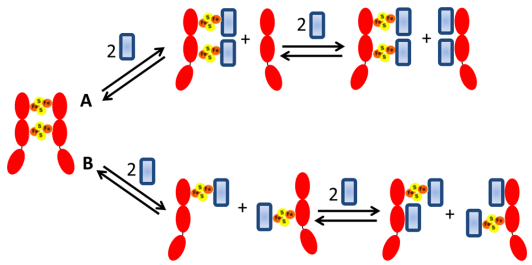

[a](A) Two molecules of apo BOLA2 (in blue) interact with a $[2Fe\text{-}2S]_2$ $GRX3_2$ molecule (GRX3 molecules are in red) to form a heterotrimeric GRX3-$BOLA2_2$ complex that binds two $[2Fe\text{-}2S]^{2+}$ clusters and an apo GRX3 molecule. The further addition of 2 equiv of apo BOLA2 determines the formation of an apo heterotrimeric GRX3-$BOLA2_2$ complex. (B) Two distinct heterodimeric GRX3-BOLA2 complexes, containing one $[2Fe\text{-}2S]^{2+}$ cluster each, are first formed. Then, the further addition of 2 equiv of apo BOLA2 determines the formation of two distinct heterotrimeric GRX3-$BOLA2_2$ complexes still containing one $[2Fe\text{-}2S]^{2+}$ cluster each.

spectroscopy, and analytical gel filtration. Once the chemically reconstituted $[2Fe\text{-}2S]_2$ GRX3-$BOLA2_2$ heterotrimeric complex was titrated with apo anamorsin up to a 1:1 protein–protein ratio, in the UV–vis and CD spectra the absorbance peaks typical of $[2Fe\text{-}2S]_2$ GRX3-$BOLA2_2$ disappeared and the absorbance peaks typical of the $[2Fe\text{-}2S]^{2+}$ cluster-bound form of anamorsin ($[2Fe\text{-}2S]$ anamorsin)[29,33] appeared (Figure 7A,B). The CD spectrum of the final 1:1 mixture essentially corresponds to that of $[2Fe\text{-}2S]$ anamorsin, being clearly distinguishable from that of $[2Fe\text{-}2S]_2$ GRX3-$BOLA2_2$. Analytical gel filtration chromatography performed with Superdex 75 HR 10/30 column on the final 1:1 mixture showed the presence of a main peak with an apparent molecular mass of 128.2 kDa, which essentially corresponds to the sum of the apparent molecular masses of $[2Fe\text{-}2S]_2$ GRX3-$BOLA2_2$ (73.2 kDa) and apo anamorsin (52.0 kDa) (Figure 7C). Overall, the data showed that (i) both $[2Fe\text{-}2S]^{2+}$ cluster are completely transferred from $[2Fe\text{-}2S]_2$ GRX3-$BOLA2_2$ to apo anamorsin and (ii) the final product is a complex formed by an apo GRX3 molecule, two apo BOLA2 molecules and a $[2Fe\text{-}2S]$ anamorsin molecule (GRX3-$BOLA2_2$-$[2Fe\text{-}2S]$ anamorsin, hereafter).

Moreover, by gel filtrating a 1:1 mixture of apo GRX3(GrxA/B)-$BOLA2_2$ and $[2Fe\text{-}2S]$ anamorsin, a peak corresponding to a ternary complex formed by GRX3(GrxA/B), BOLA2, and anamorsin is not observed (Supporting Information Figure S4), at variance to what detected in the 1:1 GRX3-$BOLA2_2$-$[2Fe\text{-}2S]$ anamorsin mixture, where the corresponding ternary complex is formed (Figure 7C). This demonstrates that, in the final GRX3-$BOLA2_2$-$[2Fe\text{-}2S]$ anamorsin complex, the interaction between apo GRX3–$BOLA2_2$ and $[2Fe\text{-}2S]$ anamorsin depends on the presence of the Trx domain of GRX3. We had previously shown that the Trx domain of GRX3 interacts with the N-terminal domain of anamorsin mediating the cluster transfer between the two proteins.[24] Here we show that the Trx domain, in addition of being essential for the complex formation between anamorsin and GRX3-$BOLA2_2$ in the GRX3-$BOLA2_2$-$[2Fe\text{-}2S]$ anamorsin complex, maintains the same conformational freedom as it has in the homodimeric $[2Fe\text{-}2S]_2$ $GRX3_2$ complex. Therefore, we propose that the cluster transfer mechanism previously reported for $[2Fe\text{-}2S]_2$ $GRX3_2$[24] is also operative in the $[2Fe\text{-}2S]_2$ GRX3–$BOLA2_2$-apo anamorsin interaction, i.e., the protein recognition, specifically occurring between the N-terminal domains of the two proteins, plays a role in the cluster transfer process.

DISCUSSION

BolA-like proteins have recently emerged as novel players in iron metabolism, being involved, on the basis of genetic and biochemical studies, in intracellular iron regulation pathways and in the maturation of Fe/S cluster-containing proteins.[3,17,34] Specifically, a role for the cytosolic *S. cerevisiae* BolA2 (usually

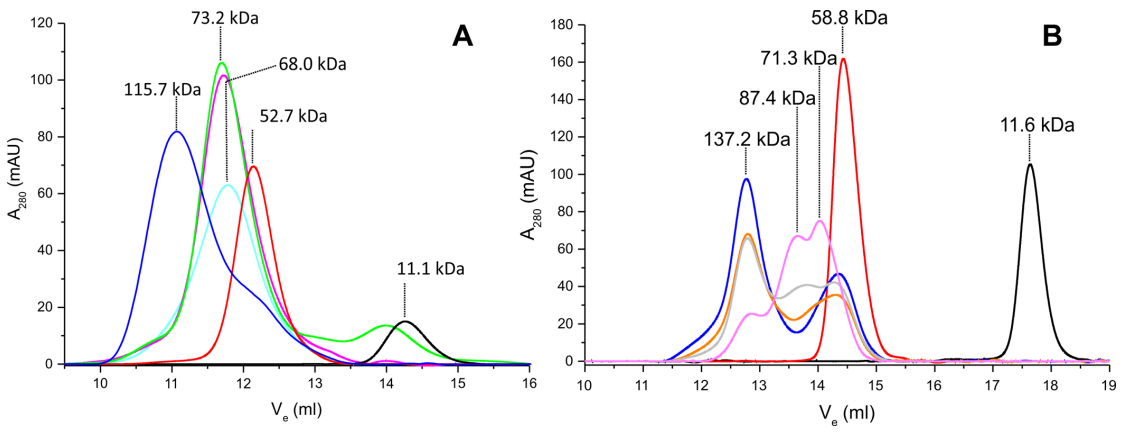

Figure 6. The formation of apo GRX3 is not observed upon the interaction of $[2Fe\text{-}2S]_2$ $GRX3_2$ with apo BOLA2. Analytical gel filtration chromatograms of (A) BOLA2 (black) and GRX3 (red) proteins in their apo states, of $[2Fe\text{-}2S]_2$ $GRX3_2$ (blue) and of a 1:2 (cyan), 1:4 (magenta), 1:6 (green) $[2Fe\text{-}2S]_2$ $GRX3_2$-apo BOLA2 mixtures (Superdex 75 HR 10/30 column), and of (B) BOLA2 (black) and GRX3 (red) proteins in their apo states, of $[2Fe\text{-}2S]_2$ $GRX3_2$ (blue) and of a 1:0.25 (orange), 1:0.5 (light gray), 1:1 (light magenta) $[2Fe\text{-}2S]_2$ $GRX3_2$-apo BOLA2 mixtures (Superdex 200 10/300 increase column). The apparent molecular masses are reported at the top of each chromatographic peak.

DOI: 10.1021/jacs.5b10592
J. Am. Chem. Soc. 2015, 137, 16133–16143

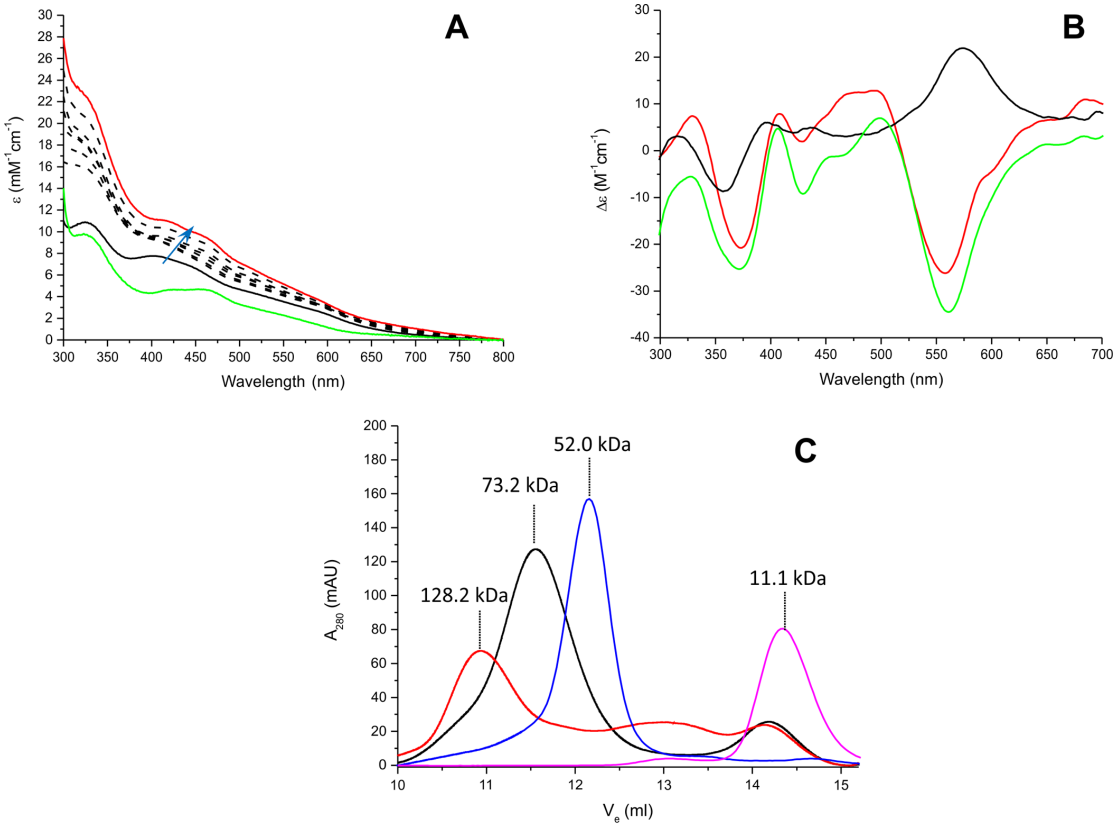

Figure 7. $[2Fe\text{-}2S]_2$ GRX3-BOLA2$_2$ transfers its clusters to apo anamorsin upon complex formation. (A) UV−vis spectra of $[2Fe\text{-}2S]_2$ GRX3-BOLA2$_2$ (black line) titrated with 0.1, 0.2, 0.3, 0.4, 0.5, 0.6, 0.8 equiv of apo anamorsin (black dashed lines). The arrow indicates the direction of the change in intensity and wavelength of the absorbance peaks with the increase of apo anamorsin concentration. The UV−vis spectra of the final 1:1 protein mixture and of $[2Fe\text{-}2S]$ anamorsin are shown as red and green lines, respectively. (B) CD spectra acquired to follow cluster transfer from $[2Fe\text{-}2S]_2$ GRX3-BOLA2$_2$ to apo anamorsin. Black line: chemically reconstituted $[2Fe\text{-}2S]_2$ GRX3-BOLA2$_2$; green line: $[2Fe\text{-}2S]$ anamorsin; red line: 1:1 mixture of $[2Fe\text{-}2S]_2$ GRX3-BOLA2$_2$ and apo anamorsin. (C) Analytical gel filtration (75 HR 10/30 column) chromatograms of BOLA2 (magenta) and anamorsin (blue) proteins in their apo states, of $[2Fe\text{-}2S]_2$ GRX3-BOLA2$_2$ (black), and of a 1:1 mixture between $[2Fe\text{-}2S]_2$ GRX3-BOLA2$_2$ and apo anamorsin (red). The apparent molecular masses are reported at the top of each chromatographic peak.

named Fra2) in iron regulation[14,16,35] and for the mitochondrial human BOLA3 in the production of the lipoate-containing 2-oxoacid dehydrogenases and in the assembly of the respiratory chain complexes[36] has been established. However, there are no studies exploring analogous functions for BolA homologues in *S. cerevisiae* and humans. In particular, since the Fra2-dependent, iron signaling pathway described in *S. cerevisiae* is not conserved in humans,[27] a homologous regulatory function of BOLA2 in human cells can be excluded.

In this work we have investigated by *in vitro* studies the role of the GRX3−BOLA2 interaction in cytoplasmic Fe/S protein biogenesis, i.e., in the CIA pathway, being inspired (i) by the general accepted view that BOLA2 protein is involved in human iron metabolism once interacting with its protein partner GRX3;[17,37] (ii) by knowing that human BOLA2 forms *in vitro* a $[2Fe\text{-}2S]$-bridged hetero complex with each monothiol Grx domain of GRX3;[21] and (iii) by our recent finding that the holo form of GRX3 is capable to mature the cytosolic Fe/S protein anamorsin, thus proposing GRX3 as a component of the CIA machinery.[24]

Our data showed that apo BOLA2 and the Grx domains of apo GRX3 significantly and specifically interact forming an apo heterotrimeric complex composed by a GRX3 molecule and two BOLA2 molecules. This complex is able to bind two $[2Fe\text{-}2S]^{2+}$ clusters upon chemical reconstitution. The same cluster content was achieved in the heterotrimeric complex obtained by co-expressing in *E. coli* cells human BOLA2 and a construct of GRX3 containing only the two Grx domains.[21] A heterotrimeric GRX3-BOLA2$_2$ complex was also obtained by mixing *in vitro* $[2Fe\text{-}2S]_2$ GRX3$_2$ with apo BOLA2. However, in this case the formed heterotrimeric GRX3-BOLA2$_2$ complex contains only one $[2Fe\text{-}2S]^{2+}$ cluster per complex. These data indicate that a heterotrimeric GRX3-BOLA2$_2$ complex containing two $[2Fe\text{-}2S]^{2+}$ clusters can be formed in one-step process only by inserting two $[2Fe\text{-}2S]^{2+}$ clusters in an apo heterotrimeric GRX3-BOLA2$_2$ complex. Therefore, it is reasonable to suggest that the apo heterotrimeric GRX3-BOLA2$_2$ complex, similarly to apo GRX3 alone,[24] might be a physiologically relevant species that receives two $[2Fe\text{-}2S]^{2+}$ clusters in the cytoplasm from a still unknown protein partner.

DOI: 10.1021/jacs.5b10592
J. Am. Chem. Soc. 2015, 137, 16133−16143

In support of this, our data showed that, similarly to what observed for the holo homodimeric form of GRX3 containing two $[2Fe\text{-}2S]^{2+}$ clusters,[24] the heterotrimeric complex containing two $[2Fe\text{-}2S]^{2+}$ clusters matures the CIA machinery component anamorsin by transferring both clusters to the CIAPIN1 domain of apo anamorsin to generate $[2Fe\text{-}2S]$ anamorsin. Both complexes, i.e., the homodimeric GRX3 and the heterotrimeric GRX3-BOLA2$_2$ complexes containing two $[2Fe\text{-}2S]^{2+}$ clusters, can thus be active players, at the cellular level, for maturing anamorsin. The present data also suggest that the mechanism of cluster transfer relying on the interaction between the N-terminal domains of anamorsin and GRX3[24] is common to both cluster transfer processes, i.e., from $[2Fe\text{-}2S]_2$ GRX3$_2$ to apo anamorsin and from $[2Fe\text{-}2S]_2$ GRX3-BOLA2$_2$ to apo anamorsin.

Now, the arising question is whether and how the cells can select the homodimeric $[2Fe\text{-}2S]_2$ GRX3$_2$ vs the heterotrimeric $[2Fe\text{-}2S]_2$ GRX3-BOLA2$_2$ complex to mature anamorsin. Assuming that the interaction between apo BOLA2 and apo GRX3 is physiologically relevant, the relative cellular levels of GRX3 and BOLA2, which can be regulated by cellular conditions (i.e., aerobic vs anaerobic cellular growth, oxidative stress, etc.), should select which of the two complexes mature anamorsin. The sensitivity of Fe/S protein biogenesis pathways toward oxygen and/or oxidative stress has been observed for members of both bacterial and eukaryotic Fe/S cluster assembly machineries.[38−42] Recently, two new CIA yeast proteins were found to be specifically involved in the maturation of the ribosome-associated ABC protein Rli1, and this function is fundamental under oxidative stress cellular conditions, as in the absence of oxygen these factors can be overcome to some extent without losing cell viability.[43] It might be possible therefore that the homodimeric $[2Fe\text{-}2S]_2$ GRX3$_2$ complex is operative in normal cellular conditions, while the heterotrimeric $[2Fe\text{-}2S]_2$ GRX3-BOLA2$_2$ complex works under oxidative stress. Consistently with this possible model, bacterial BolA proteins have been observed to be specifically required under aerobic and oxidative stress conditions. For instance, in *E. coli* BolA protein is upregulated under oxidative stress conditions,[44] and in bacterial operons, BolA tends to occur not only with a monothiol glutaredoxin, but also with proteins involved in defense against oxidative stress.[45] Also in eukaryotic genomes, the presence of BOLAs strongly correlates with an aerobic metabolism.[46] Last but not least, $[2Fe\text{-}2S]_2$ GRX3-BOLA2$_2$ complex is stable in air, while the homodimeric $[2Fe\text{-}2S]_2$ GRX3$_2$ is oxidatively labile and is gradually degraded in air over a period of ∼1 h.[21] Thus, BOLA2 binding to GRX3 stabilizes $[2Fe\text{-}2S]^{2+}$ clusters against oxidative degradation, similarly to what was observed in the yeast $[2Fe\text{-}2S]^{2+}$ Fra2-Grx3/4 complexes.[11]

CONCLUSION

In conclusion, we propose that the GRX3−BOLA2 interaction might have a role in the CIA pathway. GRX3 and BOLA2 form indeed an apo complex composed by two molecules of BOLA2 bound to a molecule of GRX3. This species, upon binding two $[2Fe\text{-}2S]^{2+}$ clusters, is able to transfer both of them to anamorsin, thus maturing it in one-step process, similarly to what we already showed for the holo homodimeric GRX3 form.[24] The $[2Fe\text{-}2S]^{2+}$ cluster bound forms of GRX3 and GRX3-BOLA2$_2$ might thus act as $[2Fe\text{-}2S]^{2+}$ cluster transfer components in the cytosol, in a similar way as monothiol glutaredoxins do in mitochondria.[7,19,47,48]

ASSOCIATED CONTENT

Supporting Information

The Supporting Information is available free of charge on the ACS Publications website at DOI: 10.1021/jacs.5b10592.

Four figures reporting: ^{15}N backbone amide relaxation parameters of apo BOLA2; an overlay of $^{1}H-^{15}N$ HSQC spectra of different constructs of apo GRX3 in the presence or absence of apo BOLA2; EPR spectra of $[2Fe\text{-}2S]_2$ GRX3-BOLA2$_2$ complexes obtained by chemical reconstitution and by mixing $[2Fe\text{-}2S]_2$ GRX3$_2$ with apo BOLA2; gel filtration of a 1:1 mixture of apo GRX3(GrxA/B)-BOLA2$_2$ and $[2Fe\text{-}2S]$ anamorsin (PDF)

AUTHOR INFORMATION

Corresponding Authors

*banci@cerm.unifi.it

*ciofi@cerm.unifi.it

Notes

The authors declare no competing financial interest.

ACKNOWLEDGMENTS

We thank Angelo Gallo (CERM) for assistance in recording the EPR spectra. This work was supported by Ente Cassa di Risparmio (grant ID no. 2013/7201) and by the European Integrated Structural Biology Infrastructure (INSTRUCT), which is part of the European Strategy Forum on Research Infrastructures and supported by national member subscriptions.

REFERENCES

(1) Lill, R. *Nature* **2009**, *460*, 831−838.

(2) Herrero, E.; de la Torre-Ruiz, M. A. *Cell. Mol. Life Sci.* **2007**, *64*, 1518−1530.

(3) Couturier, J.; Przybyla-Toscano, J.; Roret, T.; Didierjean, C.; Rouhier, N. *Biochim. Biophys. Acta, Mol. Cell Res.* **2015**, *1853*, 1513−1527.

(4) Rouhier, N.; Couturier, J.; Johnson, M. K.; Jacquot, J. P. *Trends Biochem. Sci.* **2010**, *35*, 43−52.

(5) Picciocchi, A.; Saguez, C.; Boussac, A.; Cassier-Chauvat, C.; Chauvat, F. *Biochemistry* **2007**, *46*, 15018−15026.

(6) Johansson, C.; Roos, A. K.; Montano, S. J.; Sengupta, R.; Filippakopoulos, P.; Guo, K.; von Delft, F.; Holmgren, A.; Oppermann, U.; Kavanagh, K. L. *Biochem. J.* **2011**, *433*, 303−311.

(7) Uzarska, M. A.; Dutkiewicz, R.; Freibert, S. A.; Lill, R.; Muhlenhoff, U. *Mol. Biol. Cell* **2013**, *24*, 1830−1841.

(8) Muhlenhoff, U.; Gerber, J.; Richhardt, N.; Lill, R. *EMBO J.* **2003**, *22*, 4815−4825.

(9) Muhlenhoff, U.; Molik, S.; Godoy, J. R.; Uzarska, M. A.; Richter, N.; Seubert, A.; Zhang, Y.; Stubbe, J.; Pierrel, F.; Herrero, E.; Lillig, C. H.; Lill, R. *Cell Metab.* **2010**, *12*, 373−385.

(10) Hoffmann, B.; Uzarska, M. A.; Berndt, C.; Godoy, J. R.; Haunhorst, P.; Lillig, C. H.; Lill, R.; Muhlenhoff, U. *Antioxid. Redox Signaling* **2011**, *15*, 19−30.

(11) Li, H.; Mapolelo, D. T.; Dingra, N. N.; Naik, S. G.; Lees, N. S.; Hoffman, B. M.; Riggs-Gelasco, P. J.; Huynh, B. H.; Johnson, M. K.; Outten, C. E. *Biochemistry* **2009**, *48*, 9569−9581.

(12) Ojeda, L.; Keller, G.; Muhlenhoff, U.; Rutherford, J. C.; Lill, R.; Winge, D. R. *J. Biol. Chem.* **2006**, *281*, 17661−17669.

(13) Pujol-Carrion, N.; Belli, G.; Herrero, E.; Nogues, A.; de la Torre-Ruiz, M. A. *J. Cell Sci.* **2006**, *119*, 4554−4564.

(14) Kumanovics, A.; Chen, O. S.; Li, L.; Bagley, D.; Adkins, E. M.; Lin, H.; Dingra, N. N.; Outten, C. E.; Keller, G.; Winge, D.; Ward, D. M.; Kaplan, J. *J. Biol. Chem.* **2008**, *283*, 10276−10286.

DOI: 10.1021/jacs.5b10592
J. Am. Chem. Soc. 2015, 137, 16133−16143

(15) Li, H.; Mapolelo, D. T.; Dingra, N. N.; Keller, G.; Riggs-Gelasco, P. J.; Winge, D. R.; Johnson, M. K.; Outten, C. E. *J. Biol. Chem.* **2011**, *286*, 867−876.
(16) Poor, C. B.; Wegner, S. V.; Li, H.; Dlouhy, A. C.; Schuermann, J. P.; Sanishvili, R.; Hinshaw, J. R.; Riggs-Gelasco, P. J.; Outten, C. E.; He, C. *Proc. Natl. Acad. Sci. U. S. A.* **2014**, *111*, 4043−4048.
(17) Li, H.; Outten, C. E. *Biochemistry* **2012**, *51*, 4377−4389.
(18) Vilella, F.; Alves, R.; Rodriguez-Manzaneque, M. T.; Belli, G.; Swaminathan, S.; Sunnerhagen, P.; Herrero, E. *Comp. Funct. Genomics* **2004**, *5*, 328−341.
(19) Banci, L.; Brancaccio, D.; Ciofi-Baffoni, S.; Del Conte, R.; Gadepalli, R.; Mikolajczyk, M.; Neri, S.; Piccioli, M.; Winkelmann, J. *Proc. Natl. Acad. Sci. U. S. A.* **2014**, *111*, 6203−6208.
(20) Lill, R.; Hoffmann, B.; Molik, S.; Pierik, A. J.; Rietzschel, N.; Stehling, O.; Uzarska, M. A.; Webert, H.; Wilbrecht, C.; Muhlenhoff, U. *Biochim. Biophys. Acta, Mol. Cell Res.* **2012**, *1823*, 1491−1508.
(21) Li, H.; Mapolelo, D. T.; Randeniya, S.; Johnson, M. K.; Outten, C. E. *Biochemistry* **2012**, *51*, 1687−1696.
(22) Haunhorst, P.; Berndt, C.; Eitner, S.; Godoy, J. R.; Lillig, C. H. *Biochem. Biophys. Res. Commun.* **2010**, *394*, 372−376.
(23) Haunhorst, P.; Hanschmann, E. M.; Brautigam, L.; Stehling, O.; Hoffmann, B.; Muhlenhoff, U.; Lill, R.; Berndt, C.; Lillig, C. H. *Mol. Biol. Cell* **2013**, *24*, 1895−1903.
(24) Banci, L.; Ciofi-Baffoni, S.; Gajda, K.; Muzzioli, R.; Peruzzini, R.; Winkelmann, J. *Nat. Chem. Biol.* **2015**, *11*, 772−778.
(25) Lill, R.; Dutkiewicz, R.; Freibert, S. A.; Heidenreich, T.; Mascarenhas, J.; Netz, D. J.; Paul, V. D.; Pierik, A. J.; Richter, N.; Stumpfig, M.; Srinivasan, V.; Stehling, O.; Muhlenhoff, U. *Eur. J. Cell Biol.* **2015**, *94*, 280−291.
(26) Paul, V. D.; Lill, R. *Biochim. Biophys. Acta, Mol. Cell Res.* **2015**, *1853*, 1528−1539.
(27) Rouault, T. A. *Nat. Chem. Biol.* **2006**, *2*, 406−414.
(28) Cheng, N. H.; Zhang, W.; Chen, W. Q.; Jin, J.; Cui, X.; Butte, N. F.; Chan, L.; Hirschi, K. D. *FEBS J.* **2011**, *278*, 2525−2539.
(29) Banci, L.; Bertini, I.; Ciofi-Baffoni, S.; Boscaro, F.; Chatzi, A.; Mikolajczyk, M.; Tokatlidis, K.; Winkelmann, J. *Chem. Biol.* **2011**, *18*, 794−804.
(30) Lian, L. Y.; Roberts, G. C. K. *NMR of Macromolecules. A Practical Approach*; Oxford University Press: Oxford, 1993; pp 153−182.
(31) Williamson, M. P. *Prog. Nucl. Magn. Reson. Spectrosc.* **2013**, *73*, 1−16.
(32) Kasai, T.; Inoue, M.; Koshiba, S.; Yabuki, T.; Aoki, M.; Nunokawa, E.; Seki, E.; Matsuda, T.; Matsuda, N.; Tomo, Y.; Shirouzu, M.; Terada, T.; Obayashi, N.; Hamana, H.; Shinya, N.; Tatsuguchi, A.; Yasuda, S.; Yoshida, M.; Hirota, H.; Matsuo, Y.; Tani, K.; Suzuki, H.; Arakawa, T.; Carninci, P.; Kawai, J.; Hayashizaki, Y.; Kigawa, T.; Yokoyama, S. *Protein Sci.* **2004**, *13*, 545−548.
(33) Banci, L.; Ciofi-Baffoni, S.; Mikolajczyk, M.; Winkelmann, J.; Bill, E.; Pandelia, M. E. *JBIC, J. Biol. Inorg. Chem.* **2013**, *18*, 883−893.
(34) Dhalleine, T.; Rouhier, N.; Couturier, J. *Plant Signaling Behav.* **2014**, *9*, e28564.
(35) Lesuisse, E.; Knight, S. A.; Courel, M.; Santos, R.; Camadro, J. M.; Dancis, A. *Genetics* **2005**, *169*, 107−122.
(36) Cameron, J. M.; Janer, A.; Levandovskiy, V.; MacKay, N.; Rouault, T. A.; Tong, W. H.; Ogilvie, I.; Shoubridge, E. A.; Robinson, B. H. *Am. J. Hum. Genet.* **2011**, *89*, 486−495.
(37) Couturier, J.; Przybyla-Toscano, J.; Roret, T.; Didierjean, C.; Rouhier, N. *Biochim. Biophys. Acta, Mol. Cell Res.* **2015**, *1853*, 1513−1527.
(38) Johnson, D. C.; Unciuleac, M. C.; Dean, D. R. *J. Bacteriol.* **2006**, *188*, 7551−7561.
(39) Tan, G.; Lu, J.; Bitoun, J. P.; Huang, H.; Ding, H. *Biochem. J.* **2009**, *420*, 463−472.
(40) Angelini, S.; Gerez, C.; Ollagnier-de, C. S.; Sanakis, Y.; Fontecave, M.; Barras, F.; Py, B. *J. Biol. Chem.* **2008**, *283*, 14084−14091.
(41) Bandyopadhyay, S.; Naik, S. G.; O'Carroll, I. P.; Huynh, B. H.; Dean, D. R.; Johnson, M. K.; Dos Santos, P. C. *J. Biol. Chem.* **2008**, *283*, 14092−14099.
(42) Py, B.; Gerez, C.; Angelini, S.; Planel, R.; Vinella, D.; Loiseau, L.; Talla, E.; Brochier-Armanet, C.; Garcia, S. R.; Latour, J. M.; Ollagnier-de, C. S.; Fontecave, M.; Barras, F. *Mol. Microbiol.* **2012**, *86*, 155−171.
(43) Paul, V. D.; Muhlenhoff, U.; Stumpfig, M.; Seebacher, J.; Kugler, K. G.; Renicke, C.; Taxis, C.; Gavin, A. C.; Pierik, A. J.; Lill, R. *eLife* **2015**, *4*, e08231.
(44) Santos, J. M.; Freire, P.; Vicente, M.; Arraiano, C. M. *Mol. Microbiol.* **1999**, *32*, 789−798.
(45) Huynen, M. A.; Spronk, C. A.; Gabaldon, T.; Snel, B. *FEBS Lett.* **2005**, *579*, 591−596.
(46) Willems, P.; Wanschers, B. F.; Esseling, J.; Szklarczyk, R.; Kudla, U.; Duarte, I.; Forkink, M.; Nooteboom, M.; Swarts, H.; Gloerich, J.; Nijtmans, L.; Koopman, W.; Huynen, M. A. *Antioxid. Redox Signaling* **2013**, *18*, 129−138.
(47) Brancaccio, D.; Gallo, A.; Mikolajczyk, M.; Zovo, K.; Palumaa, P.; Novellino, E.; Piccioli, M.; Ciofi-Baffoni, S.; Banci, L. *J. Am. Chem. Soc.* **2014**, *136*, 16240−16250.
(48) Muhlenhoff, U.; Gerber, J.; Richhardt, N.; Lill, R. *EMBO J.* **2003**, *22*, 4815−4825.

DOI: 10.1021/jacs.5b10592
J. Am. Chem. Soc. 2015, 137, 16133−16143

Supplementary Information

Elucidating the molecular function of human BOLA2 in GRX3-dependent anamorsin maturation pathway

Lucia Banci*[,†,‡], Francesca Camponeschi[†,‡], Simone Ciofi-Baffoni*[,†,‡], Riccardo Muzzioli[†,‡]

[†]Magnetic Resonance Center CERM, University of Florence, Via Luigi Sacconi 6, 50019, Sesto Fiorentino, Florence, Italy

[‡]Department of Chemistry, University of Florence, Via della Lastruccia 3, 50019 Sesto Fiorentino, Florence, Italy

*Corresponding Authors: banci@cerm.unifi.it, ciofi@cerm.unifi.it

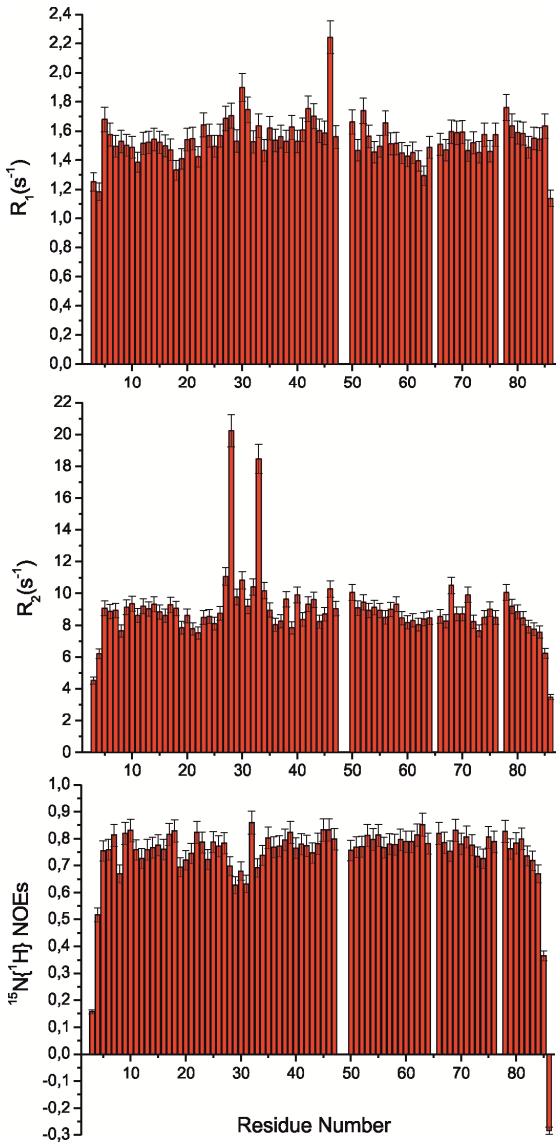

Figure S1. ^{15}N backbone amide relaxation parameters of apo BOLA2. ^{15}N R_1, R_2, and ^{15}N{^{1}H} NOE values versus residue number of apo BOLA2 obtained at 600 MHz and 298 K. Missing bars indicate Pro residues and the not observable backbone NHs of Met 1, Glu 2, Leu 49.

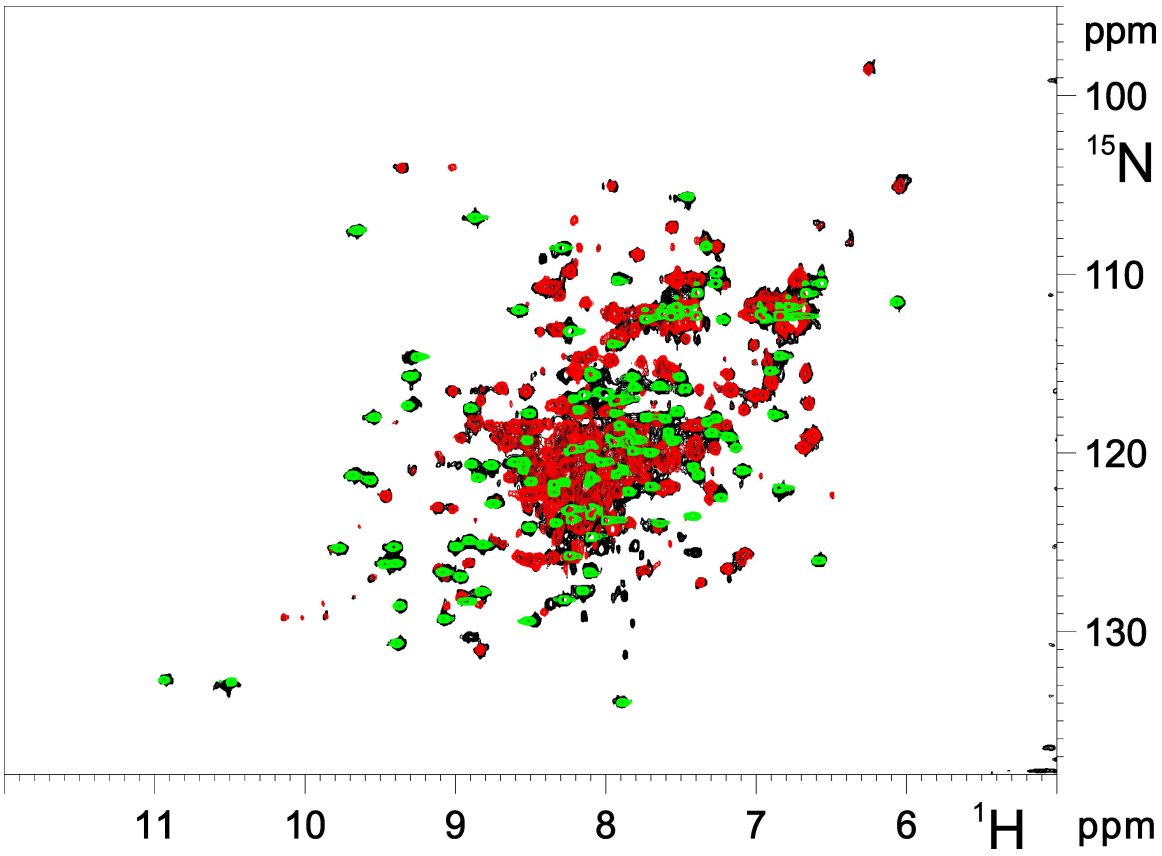

Figure S2. Apo GRX3 interacts with apo BOLA2 as the apo GRX3(GrxA/B) construct does. Overlay of ^{1}H-^{15}N HSQC spectra of a 1:2 mixture between ^{15}N labeled apo GRX3 and unlabelled apo BOLA2 (black), of a 1:2 mixture between ^{15}N labeled apo GRX3(GrxA/B) and unlabelled apo BOLA2 (red), and of ^{15}N labeled Trx domain of GRX3 (green).

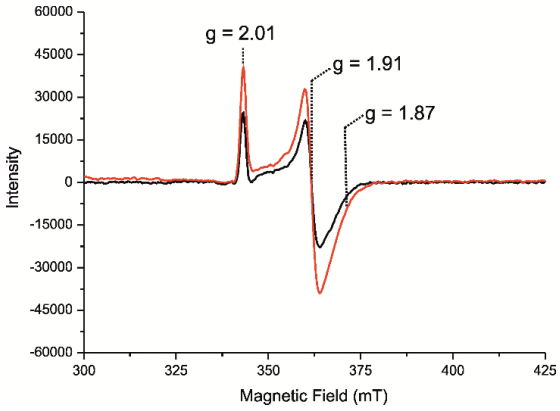

Figure S3. EPR spectra monitoring cluster properties upon GRX3 and BOLA2 interaction. EPR spectra at 45 K obtained mixing $[2Fe\text{-}2S]_2$ $GRX3_2$ and apo BOLA2 in a 1:4 ratio (black) and chemically reconstituting the heterotrimeric apo GRX3/$BOLA2_2$ complex (red), after anaerobic reduction with stoichiometric sodium dithionite and rapid freezing in 50 mM phosphate, 5 mM GSH, 5 mM DTT buffer at pH 7, 10% glycerol. The g-values are indicated.

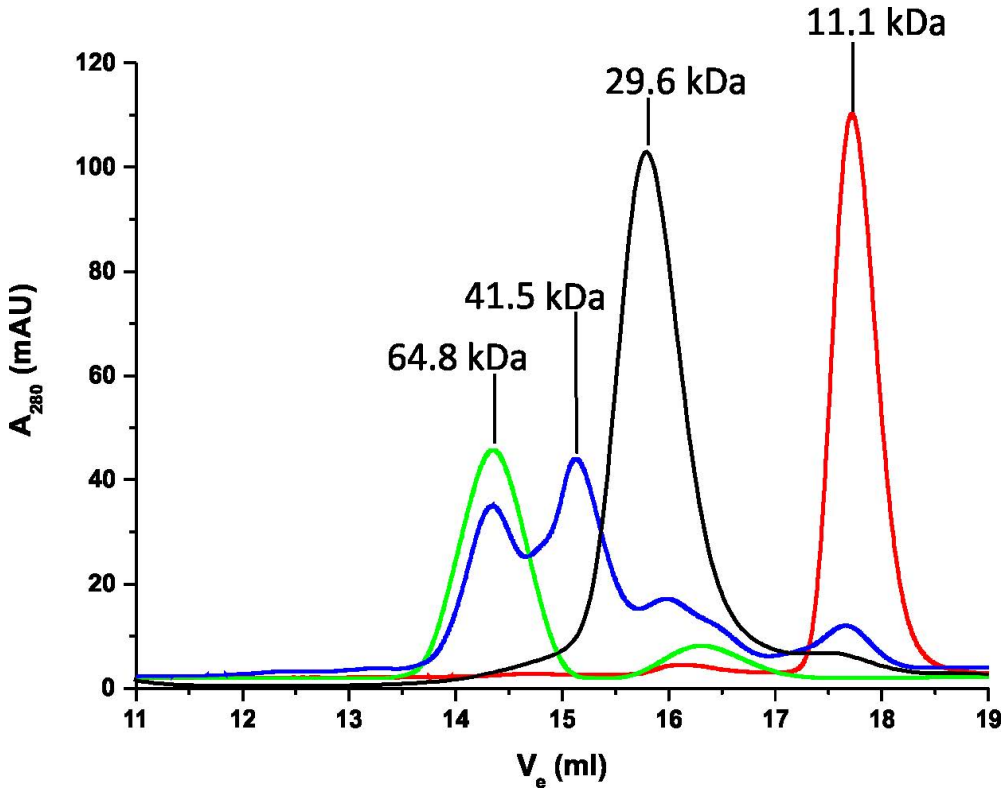

Figure S4. The Trx domain of GRX3 is essential for complex formation between GRX3-BOLA2$_2$ and anamorsin. Analytical gel filtration (Superdex 200 10/300 increase column) chromatograms of apo BOLA2 (red) and [2Fe-2S] anamorsin (green), of apo GRX3(GrxA/B) (black) and of a 1:1 mixture between apo GRX3(GrxA/B)-BOLA2$_2$ and [2Fe-2S] anamorsin (blue). The apparent molecular masses are reported at the top of each chromatographic peak.

5.4. Lipoyl Sinthase (LIAS)

The gene, optimized for the *E. coli* expression, were inserted in a pENTR like vector for the recombination reaction in different expression vectors using the gateway® technology. We selected these vectors:

- pDest His-MBP
- pDest 14
- pDest 17
- pETG 20A
- pETG 30A
- pTH34
- pCold 12-Hit tag.

After the recombination reaction, different *E. coli* strains and different temperatures were screened for check the expression levels. I performed the expression test combining all the plasmid in three *E. coli* strains (BL21 (DE3), BL21 (DE3) Rosetta Plyss, BL21 (DE3)RIPL codon^{+}) at three temperature after induction; 17°C, 25°C and 37°C (**Fig.45**). After the expression tests, the best condition was selected for the protein purification protocol set-up. The protein was purified in anaerobic condition and I obtain the protein in the holo form binding two [4Fe-4S] clusters.

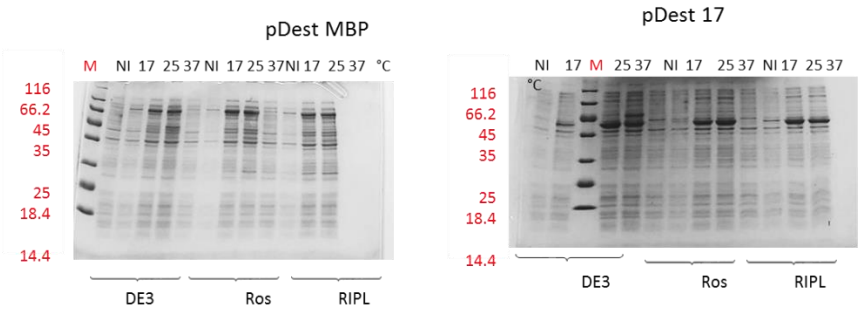

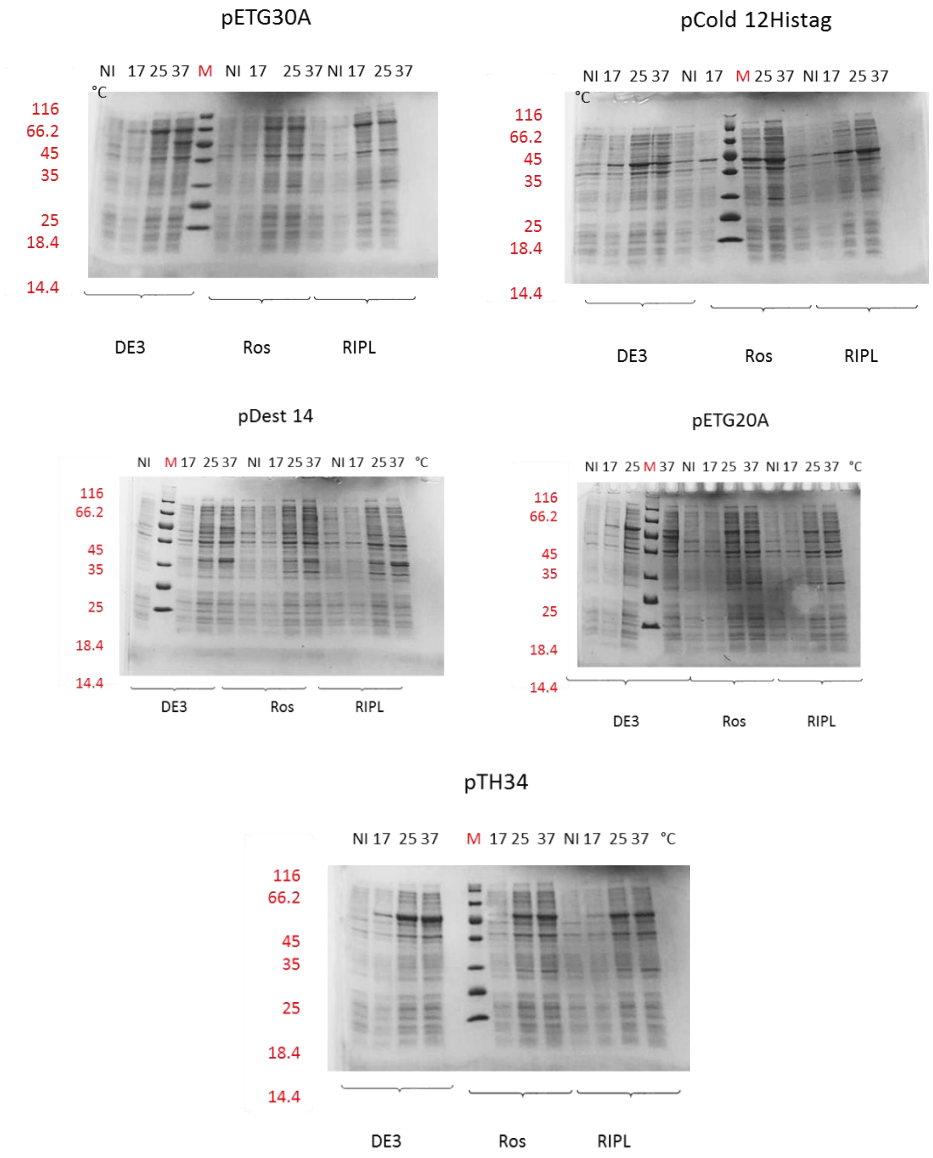

Figure 45. SDS-PAGE gel of the expression test of the different conditions for LIAS

Before continue with the characterization, we need to know the exact molecular weight to confirm the presence of our protein. A MALDI spectrum was acquired providing the exact mass of the LIAS (**Fig.46**)

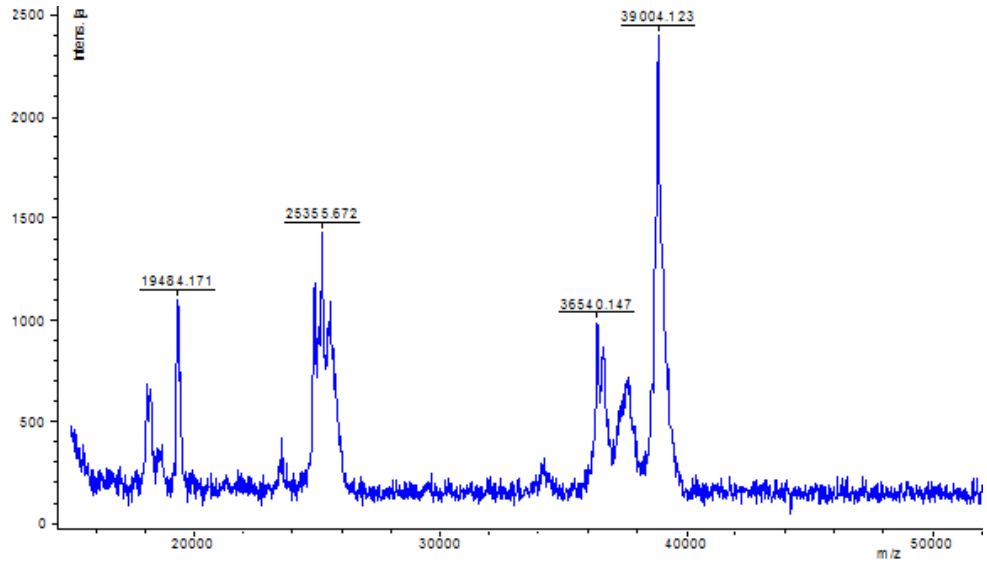

Figure 46. MALDI spectra of the LIAS as purified from cells.

Analytical gel filtration analysis was then performed to evaluate the aggregations state of the protein. By performing a calibration curve with MW standards ranging from 6000 Da to 66000 Da, LIAS runs (**Fig.47**) with an apparent molecular mass of 41.3 kDa, which nicely matches with the theoretical mass of a monomeric protein , i.e. 39 kDa.

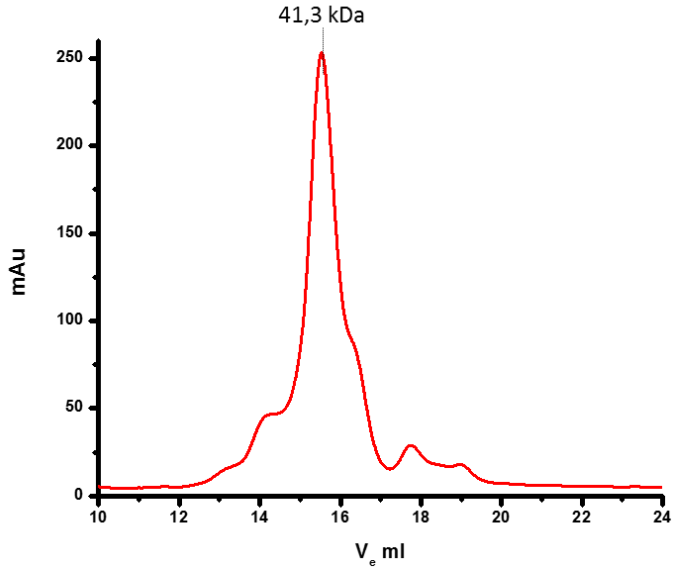

Figure 47. Analytical gel filtration of LIAS

For the spectroscopic characterization of holo-LIAS, Uv-Vis and CD spectra were acquired. Uv-Vis spectrum showed the presence of a characteristic band of a [4Fe-4S] cluster at about 410 nm (**Fig.48**).

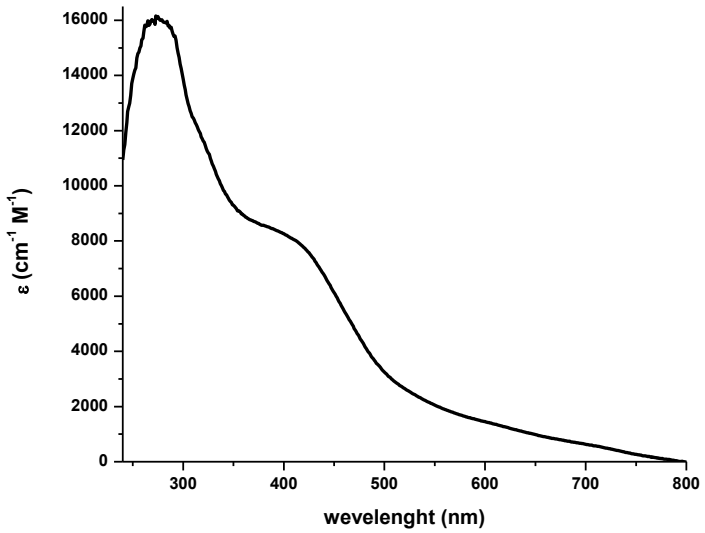

Figure 48. Uv visible spectra of holo LIAS

The far-UV (ultraviolet) CD spectrum of holo LIAS showed a characteristic peak at 209 nm and 225 nm characteristic of a majority composition of α helices as secondary structure elements (**Fig.49**).

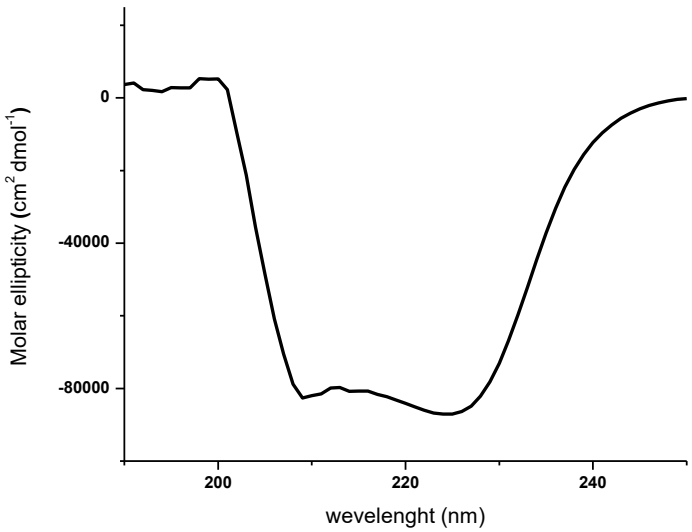

Figure 49. CD spectra in the Uv region

We are now working on the characterization of the metal center via paramagnetic NMR following the chemical shifts of the Hβ of the cysteine ligands. A mono dimensional paramagnetic NMR spectrum with short acquisition time for observe these paramagnetic peaks was acquired andtemperature temperature dependence of the detected proton signals has been performed to understand the magnetic behavior of this system. As we can see in **Fig.50**, we observed chemical shift of the peak at 18.2 ppm (at 298 K) to 17.5 ppm (at 286K). This high field shift is compatible with an anti-curie behavior, where the paramagnetism derived from the excited state.

This trend is compatible with the presence of an oxidized $[4Fe\text{-}4S]^{2+}$ cluster with $S = 0$.

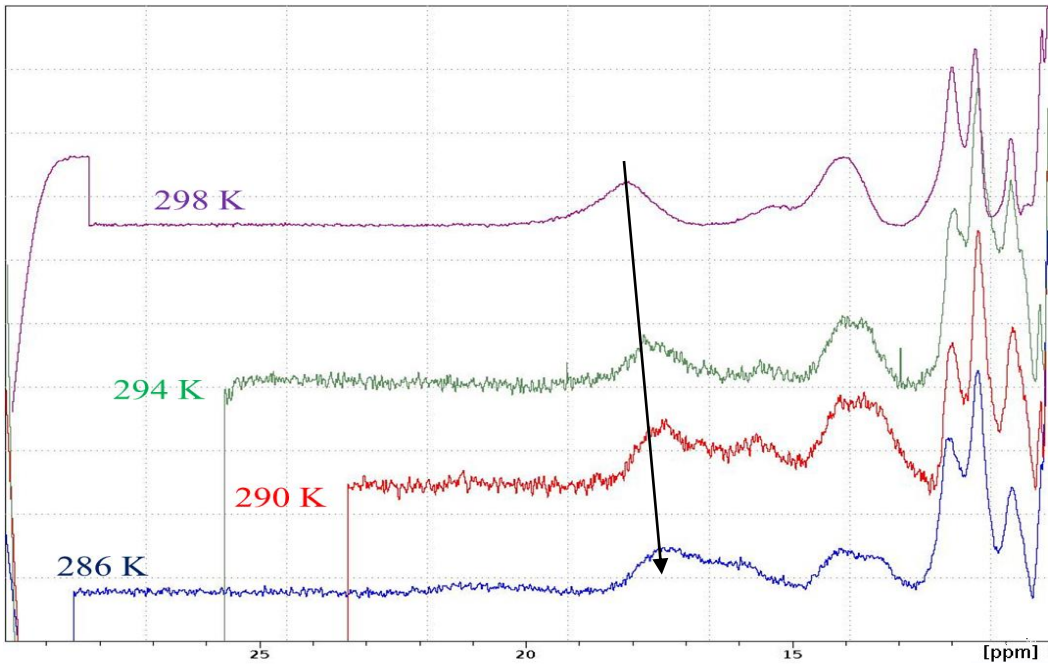

Figure 50. Chemical shift variation of a para-NMR peak of $[4Fe\text{-}4S]^{2+}$ LIAS

We followed the same peak for monitoring the stability of the $[4Fe\text{-}4S]^{2+}$ cluster under thermal denaturation process. We acquire the same set of experiments upon increasing the temperature to follow the degradation of the coordination sphere of this cluster of LIAS (**Fig.51**).

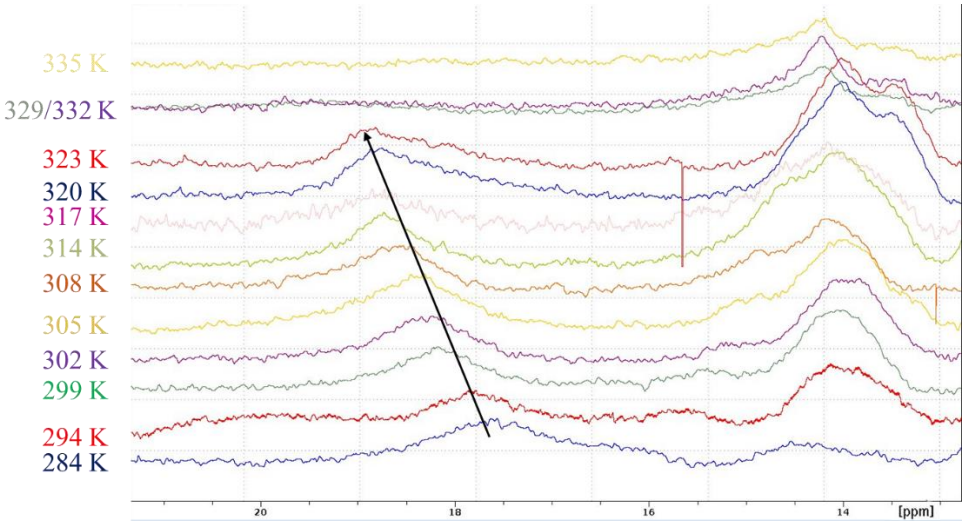

Figure 51. Intensity and chemical shift variation of LIAS after thermal sfolding.

We can see that the cluster is stable until 317 K (43.85 °C); after this temperature, we saw a loss of intensity of the peak. Also, raising the temperature, the signal continues to show an anti-curie behavior typical of a $[4Fe\text{-}4S]^{2+}$ with $S = 0$.

Further studies on LIAS and on the two metal binding sites mutants, now under investigation, will allow us to obtain more information on the cluster binding sites to better understand the relationship between structure and function.

References

1. Dominguez, C., Boelens, R. & Bonvin, A.M. HADDOCK: a protein-protein docking approach based on biochemical or biophysical information. J. Am. Chem. Soc. 125, 1731–1737 (2003).
2. Banci, L. et al. Human anamorsin binds [2Fe-2S] clusters with unique electronic properties. J. Biol. Inorg. Chem. 18, 883–893 (2013).
3. Ciofi-Baffoni, S., Gallo, A., Muzzioli, R. & Piccioli, M. The IR-15N-HSQC-AP experiment: a new tool for NMR spectroscopy of paramagnetic molecules. J. Biomol. NMR 58, 123–128 (2014).
4. Bertini I, Capozzi F, Luchinat C, Piccioli M, Vila AJ (1994a) The Fe4S4 centers in ferredoxins studied through proton and carbon hyperfine coupling. Sequence specific assignments of cysteines in ferredoxins from Clostridium acidi urici and Clostridium pasteurianum. J Am Chem Soc 116:651–660
5. Abriata LA, Ledesma GN, Pierattelli R, Vila AJ (2009) Electronic structure of the ground and excited states of the Cua site by NMR spectroscopy. J Am Chem Soc 131:1939–1946
6. Wilkens SJ, Xia B, Weinhold F, Markley JL, Westler WM (1998) NMR investigations of clostridium pasteurianum rubredoxin. Origin of hyperfine ^{1}H, ^{2}H, ^{13}C and ^{15}N
NMR chemical shfits in iron-sulfur proteins as determined by comparison of experimental
data with hybrid density functional calculations. J Am Chem Soc 120:4806–4814
7. Bertini I, Capozzi F, Luchinat C, Piccioli M, Vicens Oliver M (1992) NMR is a unique and necessary step in the investigation of ironsulfur proteins: the HiPIP from R. gelatinosus as an example. Inorg Chim Acta 198–200:483–491

8. Banci L, Bertini I, Ciurli S, Ferretti S, Luchinat C, Piccioli M (1993) The electronic structure of (Fe4S4)3? clusters in proteins. An investigation of the oxidized high-potential iron-sulfur protein II from Ectothiorhodospira vacuolata. Biochemistry 32:9387–9397

9. Gelis I, Katsaros N, Luchinat C, Piccioli M, Poggi L (2003) A simple protocol to study blue copper proteins by NMR. Eur J Biochem 270:600–609

10. Machonkin TE, Westler WM, Markley JL (2004) Strategy for the study of paramagnetic proteins with slow electronic relaxation rates by NMR spectroscopy application to oxidized human [2Fe-2S] ferredoxin. J Am Chem Soc 126:5413–5426

11. Bertini I, Donaire A, Jime´nez B, Luchinat C, Parigi G, Piccioli M, Poggi L (2001a) Paramagnetism-based versus classical constraints: an analysis of the solution structure of Ca Ln Calbindin D9k. J Biomol NMR 21:85–98

12. Banci L, Bertini I, Calderone V, Ciofi-Baffoni S, Giachetti A, Jaiswal D, Mikolajczyk M, Piccioli M, Winkelmann J (2013a) Molecular view of an electron transfer process essential for iron-sulfur protein biogenesis. Proc Natl Acad Sci USA 110:7136–7141

13. Banci L, Ciofi-Baffoni S, Mikolajczyk M, Winkelmann J, Bill E and Eirini Pandelia M (2013) Human anamorsin binds (2Fe.2S) clusters with unique electronic properties. J Biol Inorg Chem 18:883–893

14. Banci, L.; Bertini, I.; Ciofi-Baffoni, S.; Boscaro, F.; Chatzi, A.; Mikolajczyk, M.; Tokatlidis, K.; Winkelmann, J. Chem. Biol. 2011, 18, 794−804

15. Li, H.; Mapolelo, D. T.; Randeniya, S.; Johnson, M. K.; Outten,C. E. Biochemistry 2012, 51, 1687−1696.

16. Banci, L.; Bertini, I.; Ciofi-Baffoni, S.; Boscaro, F.; Chatzi, A.; Mikolajczyk, M.; Tokatlidis, K.; Winkelmann, J. Chem. Biol. 2011, 18,

794−804.

17. Banci, L.; Ciofi-Baffoni, S.; Mikolajczyk, M.; Winkelmann, J.; ill, E.; Pandelia, M. E. JBIC, J. Biol. Inorg. Chem. 2013, 18, 883−893.
18. Banci, L.; Ciofi-Baffoni, S.; Gajda, K.; Muzzioli, R.; Peruzzini, R.; Winkelmann, J. Nat. Chem. Biol. 2015, 11, 772−778.
19. Banci L, Camponeschi F, Ciofi-Baffoni S, Muzzioli R. Elucidating the Molecular Function of Human BOLA2 in GRX3-Dependent Anamorsin Maturation Pathway. J Am Chem Soc. 2015 Dec 30;137(51):16133-43.
20. Piccioli M, Poggi L (2002) Tailored HCCH-TOCSY experiment for resonance assignment in the proximity of a paramagnetic center. J Magn Reson 155:236–243
21. Kasai, T.; Inoue, M.; Koshiba, S.; Yabuki, T.; Aoki, M.; Nunokawa, E.; Seki, E.; Matsuda, T.; Matsuda, N.; Tomo, Y.; Shirouzu, M.; Terada, T.; Obayashi, N.; Hamana, H.; Shinya, N.; Tatsuguchi, A.; Yasuda, S.; Yoshida, M.; Hirota, H.; Matsuo, Y.; Tani,K.; Suzuki, H.; Arakawa, T.; Carninci, P.; Kawai, J.; Hayashizaki, Y.; Kigawa, T.; Yokoyama, S. Protein Sci. 2004, 13, 545−548.

-Chapter 6-

CONCLUSION AND FUTURE PROSPECTIVE

6.1. Conclusion and future prospective

Iron sulfur cluster cofactors play a central role in a lot of a cellular processes, from cellular respiration to DNA maintenance. Because of their importance the processes that lead to the biogenesis of these cofactors are conserved in all living organisms and strongly regulated to avoid anomalies. The list of diseases attributable to defects in (Fe-S) protein biogenesis is growing. Mutations or malfunctions in the proteins responsible of the maturation processes of (Fe-S) proteins cause severe disease and mortality in early infancy, and there is no evidence of significant tissue specificity.
During the three years of my PhD program, I focused my attention on the expression, purification and characterization of cytosolic human proteins that have been implicated in iron metabolism but whose functions, at the beginning of my PhD, were still not clearly defined. I characterized these proteins at a structural and biochemical level, as well as investigated their interactions with protein partners. The results obtained by these studies contribute to define the cytosolic Fe-S protein maturation pathways at atomic resolution. Specifically, I showed that the cytosolic monothiol glutaredoxin in its holo form, i.e. $[2Fe\text{-}2S]_2$-$GRX3_2$, can interact with the apo form of anamorsin forming a stable heterodimeric 1:1 complex via a specific recognition occurring between the N-terminal domains of the two proteins. Upon protein-protein interaction, the two[2Fe-2S] clusters bound to GRX3 are transferred from the GRX3 to anamorsin in a specific manner. This study allows to propose for the first time that GRX3 is a component of the CIA machinery since it is involved in the maturation pathway of anamorsin, which, in turn, responsible of the maturation of all cytosolic [4Fe-4S] proteins. Following this research line, the interaction between GRX3 and

another cytosolic protein, which is a protein partner of GRX3 (human BOLA2), but whose function was still undefined, was characterized. The protein was recombinantly produced and then its interaction with both apo and holo forms of GRX3 investigated. From this studies it emerges that a stable heterotrimer is formed between a GRX3 molecule and two BOLA2 with two [2Fe-2S] clusters shared by each of the two monothiol glutaredoxin domains of GRX3 and BOLA2. Since BOLA2 is not interact with the N-terminal domain of GRX3, this heterotrimer is still able to interact with the apo form of anamorsin upon N-terminal domains recognition and transferred the two clusters to anamorsin.

The study of these (Fe-S) proteins give us the possibility also to improve paramagnetic NMR-based tools aimed at characterizing (Fe-S) clusters. The latter represent the most challenging situation for NMR signal detection and resonance assignment of the residues close to the cluster, as a consequence of large contributions to relaxation and small contributions to chemical shift of this paramagnetic center. Thus, to detect NMR signals of residues in the proximity of the metal center, we developed a modified version of the ^{1}H-^{15}N-HSQC experiment where (1) an inversion recovery filter is added prior to HSQC, (2) the INEPT period has been optimized according to fast relaxation of interested spins, (3) the inverse INEPT has been eliminated and signals acquired as antiphase doublets. by applying this sequence to anamorsin, we were able to recover and assign thirteen HN resonances, unobserved with conventional HSQC experiments. This NMR experiment, named IR- ^{15}N HSQC-AP, selectively identifies HN groups from the environment of the paramagnetic center that experience significant paramagnetic relaxation and almost negligible contributions to chemical shift, and it is therefore a valuable tool for those systems in which no pseudocontact shift occurs, such as Cu^{2+} proteins and (Fe-S) proteins.

In the last year of the PhD program, I focused my attention to the human LIAS protein, a crucial enzyme in the matrix of mitochondria that catalyzes the maturation of the lipoyl cofactor. Considering that several mutations of the LIAS gene are involved in severe pathologies, we decided to express and purify this protein. An optimized expression protocol for the wild-type LIAS protein and for two mutants able to "switch off" one or the other of the two [4Fe-4S] clusters bound to the wild-type protein are now concluded. We are performing crystal screenings for the structural studies, and we characterized the metal center by Uv-vis, CD and EPR spectroscopies. On this system we are also investigating the metal [4Fe-4S] centers via paramagnetic NMR for obtaining structural information provided by the chemical shifts and the relaxation times of the paramagnetic signals.

The (Fe-S) protein biogenesis pathways involve several proteins and processes that still need to be characterized. Bioinformatics studies on the genomes suggest several new proteins that can be add to the list of all the proteins involved in these pathways in both mitochondria and cytosol.

We need to go ahead with the structural characterization of LIAS to obtain more information about the two metal site. Indeed, the structure of this protein will be an important goal due its crucial role in humans and its close relationship with human diseases. The importance of LIAS also relies on the possibility of studying the interaction of LIAS with the mitochondrial protein NFU1, a member of the ISC assembly machinery which is already available in our lab. This studies will provide information on the maturation process of LIAS and on the role of NFU1 in the ISC assembly machinery as this is still not clearly defined.

Finally, going back to the cytosol, we need to study the tetramer formed by Nubp1-Nubp2 to better understand:

1. The structure of the tetramer, since no data are available.
2. Whether the holo form of GRX3 can provide its clusters to assemble the scaffold [4Fe-4S] cluster on the tetramer
3. The role of the electron transfer process driven by anamorsin/Ndor1 in the formation of the scaffold [4Fe-4S] cluster bound to the tetramer.